UAB
Universitat Autònoma de Barcelona

Advancing the Hazard Assessment of Nanoplastic Exposure under Environmentally Realistic Conditions Using Human In Vitro Models

Herlem Michelle Morataya Reyes

Universitat Autònoma de Barcelona

Facultat de Biociències

Departament de Genètica i de Microbiologia

Grup de Mutagènesi

Advancing the Hazard Assessment of Nanoplastic Exposure under Environmentally Realistic Conditions Using Human *In Vitro* Models

DOCTORAL DISSERTATION

Herlem Michelle Morataya Reyes

2026

Universitat Autònoma de Barcelona

Facultat de Biociències

Departament de Genètica i de Microbiologia

Grup de Mutagènesi

Advancing the Hazard Assessment of Nanoplastic Exposure under Environmentally Realistic Conditions Using Human *In Vitro* Models

Dissertation respectfully submitted by

Herlem Michelle Morataya Reyes

To Universitat Autònoma de Barcelona in partial fulfillment of the requirements for the degree of Doctor of Philosophy, as per the Doctorate Program in Genetics

Under the supervision of Dra. Alba Hernández Bonilla and Dr. Massimo Bogliolo

Dra. Alba Hernández Bonilla

Dr. Massimo Bogliolo

Herlem Michelle Morataya Reyes

AGRADECIMIENTOS

La realización de esta tesis doctoral ha sido un camino largo y exigente, pero satisfactorio y transformador. Ningún logro en este recorrido ha sido individual, y por ello quiero expresar mi más sincero agradecimiento a quienes han formado parte de este proceso.

En primer lugar, quiero agradecer a Alba y Ricard por su guía científica, su acompañamiento y su confianza a lo largo de estos años. Gracias por animarme a hacer preguntas más profundas, a trabajar buscando la excelencia y a sostener el pensamiento crítico incluso cuando los resultados no eran los esperados. Su exigencia y apoyo han sido fundamentales para mi crecimiento como investigadora y como persona. Al mismo tiempo, agradecer a Massimo por actuar como conexión con el grupo de Mutagénesis y por su confianza en mi trabajo desde los días en Sant Pau.

A mis compañeros de laboratorio, en especial a quienes me acompañaron desde el inicio de este viaje: Aliro, Joan, Gooya, Javi, Lourdes, Ali (Siuuu!). Gracias por su presencia día a día, por las discusiones científicas (y las no tan científicas), por compartir tiempo en cultivos y citometría, frustraciones y éxitos, cafelitos y abracitos. Mil gracias también a Gloria y a Cristian, que con su experiencia y disposición mantienen el laboratorio en movimiento. Juntos somos una prueba de que la ciencia se construye en equipo, y haber formado parte de este grupo ha sido un privilegio.

A la Generalitat de Catalunya, por medio de la AGAUR, y la Universitat Autònoma de Barcelona que han hecho posible esta etapa, gracias por el entorno académico, los recursos y las oportunidades de formación que me han permitido desarrollar este proyecto doctoral.

Finalmente, y de forma muy especial, a mi familia. A Herlem, Douglas, Diego y mis abuelos ♡, que siempre han creído en mí y me han apoyado para crecer profesionalmente, incluso cuando significara estar lejos de casa. Han apoyado desde el inicio a la Miche que no siempre seguía el camino más fácil o tradicional, pero que sabía que su familia siempre estaría ahí para abrazarla. To Ahmad, thank you for believing in me, for standing by my side through every challenge, and for constantly encouraging me to become the best version of myself. Gracias por el apoyo incondicional, por la paciencia en los momentos de estrés, por creer en mí incluso cuando yo dudaba. Esta Tesis también es de todos ustedes.

Y, en un plano más íntimo, esta Tesis es también un pequeño homenaje a mi yo de niña: a su curiosidad inagotable, a sus preguntas constantes sobre cómo funciona el mundo

y a esa fascinación por la ciencia que empezó mucho antes de saber qué significaba hacer un doctorado. Este logro es un paso más en el camino de hacerla feliz y honrar aquella curiosidad que nunca dejó de crecer.

"*What you do makes a difference, and you have to decide what kind of difference you want to make*."

Jane Goodall

ABSTRACT

The exponential growth of global plastic production has led to the accumulation of plastic waste across the environment, which progressively degrades into smaller particles called micro- and nanoplastics (MNPLs). Among these, nanoplastics (NPLS) represent the smallest and most reactive fraction, able to interact with biological systems, which leads to their recognition as contaminants of emerging concern. These particles have been detected in environmental and human biological samples, including blood, stool, lung, and placental tissue, confirming continuous human exposure. Despite growing concern, the assessment of potential human health effects of exposure to MNPLs remains limited by the predominant use of non-representative test materials, acute-exposure experimental designs, and single-contaminant models that fail to reflect the environmentally realistic exposure conditions.

This PhD Thesis aims to advance knowledge of the biological effects induced by nanoplastic exposure in human cell models by addressing current research needs regarding material realism, exposure duration, and exposure complexity. Using human-derived *in vitro* systems representative of key target tissues, including hepatic (HuH-7), immune (THP-1), and bronchial epithelial (BEAS-2B) cells, this work evaluates how physicochemical characteristics of nanoplastics, chemical additives, long-term exposure, and co-exposure scenarios modulate cellular responses relevant to human hazard assessment. In this context, this Thesis is structured around four peer-reviewed studies, each presented as a chapter addressing a specific objective.

In Chapter 1, the influence of polymer identity and physicochemical properties on cellular internalization dynamics and short-term biological effects was investigated using polystyrene (PS), polyethylene terephthalate (PET), and polylactic acid (PLA) nanoplastics in HuH-7 cells. Although all particle types were internalized, pristine and functionalized PS nanoplastics showed no significant biological effects, while realistic PET- and PLA-derived nanoplastics induced oxidative stress, DNA damage, and cytokine release. These findings demonstrate that cellular uptake alone does not predict toxicity and that polymer composition and surface properties are key drivers of early biological responses.

Chapter 2 evaluated the role of chemical additives using PET nanoplastics derived from opaque consumer bottles containing titanium dioxide (TiO_2). In THP-1 cell model, PET(Ti)-NPLs modulated genotoxic responses compared with PET-only particles, highlighting the contribution of additives to nanoplastic bioactivity. The incorporation of

titanium as a measurable tracer also allowed improvement of exposure characterization and dosimetry, addressing a critical methodological challenge in nanoplastic toxicology.

The impact of exposure duration was studied in Chapter 3 by comparing acute and long-term exposure to PET(Ti)-NPLs in BEAS-2B cells. Acute exposure induced temporary oxidative stress, DNA damage, and moderate cytokine signaling consistent with an acute stress response. In contrast, after exposure for up to 15 weeks, genomic instability, sustained inflammatory signaling, and phenotypic remodeling, including increased migration and invasion capacity, were observed. These findings demonstrate that the long-term exposure approach reveals different biological outcomes that are not predictable from short-term assays alone.

For Chapter 4, exposure complexity was addressed by examining long-term co-exposure to PET nanoplastics and cigarette smoke condensate (CSC), a relevant environmental co-contaminant. When compared to single-agent exposure, co-exposure in BEAS-2B cells significantly exacerbated DNA damage, promoted transformation-related phenotypes, and induced transcriptomic changes associated with oxidative stress adaptation, extracellular matrix remodeling, and carcinogenesis-related pathways. These results present nanoplastics as modulators of the biological effects of co-contaminants, generating responses that cannot be inferred from single-agent exposures.

Collectively, the findings of this Thesis demonstrate that nanoplastics are biologically active materials capable of inducing oxidative, genotoxic, and inflammatory responses at sub-cytotoxic concentrations in human-relevant models. The biological impact of nanoplastic exposure is strongly shaped by material realism, exposure duration, and exposure complexity. Acute exposure primarily elicits initial temporary stress responses, while long-term and co-exposure scenarios drive persistent inflammation, genomic instability, and phenotypic alterations associated with disease-relevant processes. By integrating realistic nanoplastic materials, long-term exposure paradigms, and mixture conditions within human cell-based models, this work presents mechanistically informed evidence aligned with New Approach Methodologies and research needs, contributing to the advancement of nanoplastic hazard assessment under environmentally relevant conditions.

ABBREVIATION LIST

AOP:	Adverse Outcome Pathway
Bt:	Billion tons
EMT:	Epithelial to mesenchymal transition
KEs:	Key events
MIEs:	Molecular initiating events
MNPLS:	Micro and nanoplastics
MPLs:	Microplastics
Mt:	Million tons
NAMs:	New Approach Methodologies
NGRA:	Next Generation Risk Assessment
NPLs:	Nanoplastics
OECD:	Organisation for Economic Co-operation and Development
PE:	Polyethylene
PET:	Polyethylene terephthalate
PLA:	Polylactic acid
PP:	Polypropylene
PS:	Polystyrene
PU:	Polyurethane
PVC:	Polyvinyl chloride
ROS:	Reactive oxygen species
TiO_2:	Titanium dioxide
UV:	Ultraviolet

INDEX

1. INTRODUCTION

1. INTRODUCTION

1.1. Plastics: Micro- and Nanoplastics as Emerging Contaminants

1.1.1. Plastics: Global Production and Environmental Release

Plastics are synthetic materials composed primarily of carbon- and hydrogen-based polymers which are built from repeating monomer units that can be shaped into numerous solid configurations. These materials frequently include additives and plasticizers to improve their functional, mechanical, physical, and chemical properties for specific applications (Catalan et al., 2025).

Although the earliest synthetic polymers such as bakelite were developed in the early 1900s, large-scale production started after World War II, driven by advances in petrochemical synthesis and the demand for inexpensive, lightweight materials (Stanley et al., 2025). Since then, the amount of plastic produced worldwide has grown from about 2 million tons (Mt) in 1950 to over 400 Mt in 2022, with projections to reach up to 600 Mt by 2025 and potentially double by 2050 (El-Rayes et al., 2023). This rise is attributed to the functional properties of plastics, such as their lightweight nature, flexibility, versatility, functionality, and low production costs, in addition to the availability of a broad range of polymers and additives that allow for their customization (Khan and Jia, 2023).

According to the Organisation for Economic Co-operation and Development's (OECD) Global Plastics Outlook (2022), plastics production and use are dominated by a few polymer classes. Packaging alone accounts for 40% of total plastic demand, followed by construction (12%), textiles (11%), consumer goods (10%), transport (9%), and electronics (7%). The most widely produced polymers are polyethylene (PE; ~29%), polypropylene (PP; ~19%), polyvinyl chloride (PVC; ~12%), polyethylene terephthalate (PET; ~10%), polyurethane (PU; ~7%), and polystyrene (PS; ~6%) (Geyer et al., 2017; Wagner et al., 2024). Each polymer type has a distinct lifespan. Packaging plastics are typically used for less than one year, whereas construction materials can persist for decades.

However, the same durability that makes plastic useful also results in its persistence as waste. Sorting and recycling plastics is technically challenging and economically unattractive. The number of plastic types is high, and they are often mixed with additives, which tend to result in lower quality and limited applications compared to virgin plastics, further reducing demand (Singh and Walker, 2024). As of 2015, an estimated 8.3 billion tons (Bt) of virgin plastics had been produced globally, generating 6.3 Mt of waste. Of this waste, only about 9% of plastic waste had been recycled, and 19% was permanently

eliminated by incineration, leaving the majority to accumulate in landfills or the environment, leading to widespread contamination (Geyer et al., 2017; OECD, 2022).

Environmental leakage occurs throughout the entire plastic life cycle, from raw material production and product use to waste mismanagement. When plastics enter the environment, they can undergo ageing and degradation processes that change their physicochemical properties, such as mechanical forces, weathering, UV radiation, and microbial interaction (Li et al., 2022). Consequently, they fragment into smaller particles, leading to the formation of microplastics and nanoplastics (MNPLs), particles that can disperse throughout ecosystems and thus represent a major emerging contaminant (Thompson et al., 2024). The OECD (2022) estimates that 22 Mt of plastics enter the environment annually, with macroplastics dominating terrestrial leakage while microplastics represent 35% of total emissions to the oceans. Although high-income nations contribute through diffuse microplastic emissions from wastewater and road runoff, low- and middle-income countries account for most uncontrolled releases due to limited collection and recycling infrastructure.

1.1.2. Environmental Degradation of Plastics into Micro- and Nanoplastics

When plastics are released into the environment, they experience a process called degradation: a sequential breaking down of the polymeric materials into smaller pieces (Avio et al., 2017; Catalan et al., 2025). This process is the fundamental route for the formation of micro- and nanoplastics, the smallest and most reactive fractions of plastic pollution. According to size-based classifications, microplastics (MPLs) are defined as plastic particles smaller than 5 mm in their longest dimension, while nanoplastics (NPLs) refer to particles with a size below 1 μm resulting from the further breakdown of MPLs (Alqahtani et al., 2023). The transition from macro- to micro- and eventually nanoplastic involves continuous fragmentation driven by multiple environmental factors, including UV radiation, mechanical abrasion, thermal stress, and microbial activity, which together alter the polymer's surface chemistry, molecular weight, and crystallinity (Figure 1) (Li et al., 2022; Pradel et al., 2023).

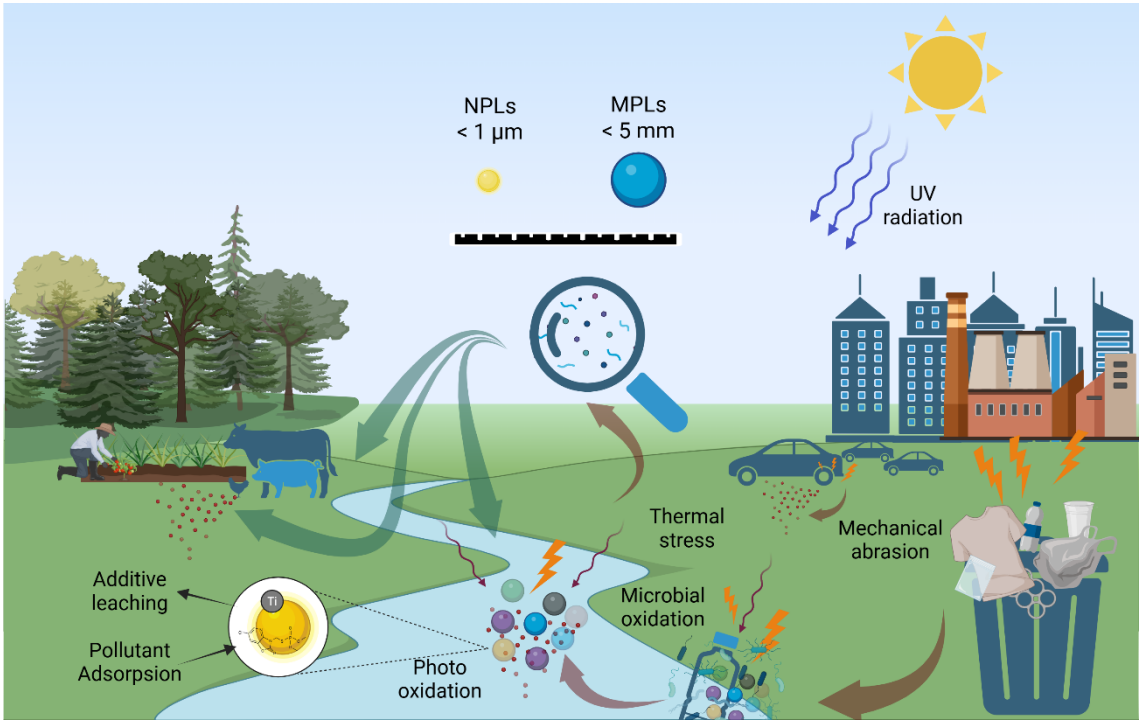

Figure 1: Environmental origin, transformation, and key properties of micro and nanoplastics (MNPLs). The diagram illustrates the primary sources of plastic pollution and the key environmental degradation pathways, including UV radiation, mechanical abrasion, and oxidation, that fragment macroplastics into microplastics (MPLs) and nanoplastics (NPLs). The figure also highlights two critical properties relevant to toxicology: the leaching of chemical additives from the polymer matrix and the adsorption of environmental pollutants onto the particle surface, which facilitates their transport.

Based on their origin, MNPLs are classified into primary and secondary MNPLs. Primary MNPLs are intentionally engineered at the micro- or nanoscale for industrial and consumer applications such as microbeads in cosmetics, synthetic textile fibers, industrial abrasives, and pre-production pellets (Domenech et al., 2023). Secondary MNPLs, in contrast, are generated from the fragmentation and ageing of larger plastic debris and constitute the predominant source of environmental MNPLs pollution (Crosset-Perrotin et al., 2025). This distinction is relevant because the degradation process modifies particle morphology, surface chemistry, and polymer integrity, producing materials that differ markedly from their parent plastics.

Environmental degradation pathways vary by ecosystem. In terrestrial systems, thermal cycling, soil abrasion, and microbial oxidation play major roles; agricultural films, tire wear particles, and littered packaging are mechanically broken down, while microbial biofilms can catalyze polymer oxidation (Li et al., 2022). In aquatic environments, UV-induced photo-oxidation is a dominant mechanism. Sunlight penetration initiates radical chain reactions that form carbonyl and hydroxyl groups, embrittling the polymer surface, while waving action and sediment friction fragment the weakened plastic into micro- and

nanosized debris. In the atmosphere, temperature fluctuations and UV exposure facilitate the generation of airborne MNPLs, while oxidation accelerates surface ageing (Dris et al., 2016; Le et al., 2023).

These differing origins and pathways result in particles with distinct characteristics. Primary MNPLs, engineered via bottom-up polymerization, are often spherical and monodisperse (Alqahtani et al., 2023). On the contrary, secondary MNPLs, generated via a top-down fragmentation, are typically polydisperse, irregularly shaped, and have rough surfaces (Schröter and Ventura, 2022). During environmental ageing, photo-oxidation, hydrolysis, and mechanical abrasion introduce oxygenated functional groups and surface defects. This increases surface roughness, reactivity, and the capacity to absorb environmental pollutants (Li et al., 2022; Pradel et al., 2023).

The chemical composition of environmental MNPLs adds another layer of complexity. These particles comprise diverse polymers, most abundantly PE, PP, PVC, PS, PET, and PU, often blended with additives that enhance performance, including plasticizers, stabilizers, pigments, flame retardants, and antioxidants, but pose toxicological risks upon release from the polymer matrix or undergo environmental transformation, releasing bioactive and potentially hazardous compounds (Khan and Jia, 2023; Thompson et al., 2024; Crosset-Perrotin et al., 2025).

Ultimately, the environmental transformation of plastics into smaller, chemically reactive fragments represents not only a degradation process but also the emergence of novel particulate contaminants with distinctive physicochemical properties, environmental behavior, and potential biological effects.

1.1.3. Properties of Micro- and Nanoplastics that Raise Human-Health Concerns

Once released, MNPLs persist in the environment for extended periods due to their resistance to biological and physicochemical degradation. Their small size and high surface-area-to-volume ratio confer unique properties that enhance uptake, reactivity, and absorption capacity (Avio et al., 2017; Khan and Jia, 2023). Nanoplastics exhibit colloidal behavior and have been found to cross biological barriers, enabling cellular uptake through endocytosis or diffusion (He et al., 2020; Liu et al., 2022). Their reactive surfaces can catalyze the generation of reactive oxygen species (ROS), disrupt redox balance and contribute to oxidative stress and inflammation (Bhattacharya et al., 2009; Das, 2023; Mahmud et al., 2024).

The incorporation of chemical additives, such as phthalates, bisphenols, brominated flame retardants, and inorganic mineral additives, including titanium dioxide (TiO_2), may increase the toxic potential of plastics. These compounds can migrate or leach from the polymer matrix, acting as endocrine disruptors or genotoxic agents (Wagner et al., 2024). Furthermore, the surfaces of MNPLs adsorb and concentrate persistent organic pollutants and metals present in the environment, including complex mixtures containing polycyclic aromatic hydrocarbons, metals, and other reactive compounds, functioning as "vectors" that enhance the bioavailability and transport of these co-contaminants through ecosystems (Browne et al., 2013; Sun et al., 2023). This behavior depends on polymer type, surface chemistry, and degree of ageing; although oxidized or roughened surfaces, for example, have shown higher pollutant affinity (Li et al., 2022; Pradel et al., 2023).

Moreover, characteristics such as surface charge, hydrophobicity, and particle morphology determine cellular interactions and toxicokinetics. Positively charged or amine-functionalized particles interact more easily with negatively charged cell membranes, enhancing uptake and cytotoxicity (Fuchs et al., 2016). In the case of irregularly shaped secondary MNPLs, they can physically damage membranes and promote stronger inflammatory responses than smooth, spherical primary particles (Schröter and Ventura, 2022; Ruggieri et al., 2025).

Collectively, size, shape, surface chemistry, additive content, and interaction with co-pollutants determine how MNPLs behave in biological systems and highlight their potential to affect human health.

1.2. Human Exposure to Micro- and Nanoplastics

1.2.1. Routes of Human Exposure

Accumulated evidence confirms the ubiquity of MNPLs across all environmental compartments. MNPLs have been detected in marine and freshwater ecosystems, atmospheric fallout, soil, and indoor environments (Dris et al., 2016; Avio et al., 2017; Gasperi et al., 2018). Their persistence allows long-range atmospheric transport, facilitating deposition even in remote regions (Le et al., 2023; Yang et al., 2025). Urban air and household dust, for instance, contain substantial concentrations of synthetic fibers and fragments originating from textiles, packaging, and even tire wear (Liu et al., 2019; Materić et al., 2022). Additionally, transfer of MNPLs has been detected across trophic levels in both aquatic and terrestrial food webs, leading to their accumulation in organisms consumed by humans (Cverenkárová et al., 2021). Consequently, humans

are exposed to MNPLs continuously through multiple environmental pathways, with ingestion, inhalation, and dermal deposition being the most relevant routes (Figure 2) (Vethaak and Legler, 2021; Khan and Jia, 2023).

Ingestion represents a primary entry route. MNPLs have been detected in a wide range of food items, including fish, shellfish, fruits, vegetables, honey, and table salt, providing dietary exposure routes for humans (Sendra et al., 2021; Ruggieri et al., 2025). Drinking water, including tap and bottled water, also contains microplastic fragments and fibers (Cox et al., 2019). The consumption of processed foods, plastic packaging, and food-contact materials increases human dietary exposure (Wagner et al., 2024).

Inhalation constitutes another major exposure pathway, particularly in indoor and urban environments contaminated with airborne synthetic fibers and fragments released from textiles, dust, and tire wear (Dris et al., 2016; Gasperi et al., 2018; Le et al., 2023). The aerodynamic behavior of MNPLs allows them to penetrate the lower respiratory tract, where ultrafine particles may deposit in bronchioles and alveoli (Lim et al., 2021; Jenner et al., 2022). This raises occupational concerns for workers involved in plastic manufacturing, waste processing, or textile production, where concentrations are orders of magnitude higher than ambient levels (OECD, 2022).

The dermal route is considered a comparatively minor exposure pathway and is likely to become less relevant over time, as several jurisdictions have restricted the use of intentionally added primary microplastics (microbeads) in personal care products, including cosmetics and skin-care formulations (U.S. Congress., 2015; European Commission, 2023). While intact skin provides an efficient barrier, penetration of nanosized particles over compromised or inflamed epithelia has been discussed (Khan and Jia, 2023).

Beyond the identification of relevant exposure pathways, several studies have attempted to estimate the magnitude of human MNPL exposure. Dietary-based estimates suggest that intake can reach tens of thousands of particles per person per year, with additional contributions from inhalation depending on environment and lifestyle (Cox et al., 2019; Senathirajah et al., 2021). However, the detection, identification, and quantification of MNPLs in environmental and biological matrices remain major technical barriers for exposure assessment and risk evaluation (Materić et al., 2022; Crosset-Perrotin et al., 2025). This challenge is rooted in the particles' nanoscale size, low mass concentrations, and the complexity of matrices such as tissues or soil that mask their signals. As a result, large uncertainty remains across studies due to differences in sampling, size detection

limits, and reporting metrics, and current exposure estimates should therefore be interpreted with caution.

Together, these findings indicate that human exposure is not a sporadic event but rather chronic and continuous, reflecting the ubiquitous environmental presence of MNPLs across air, water, and food matrices. Multiple exposure routes contribute simultaneously, while current estimates suggest that exposure occurs at scales that, despite methodological uncertainty, are recurrent over the human lifespan. Importantly, the ubiquity of MNPLs in environmental compartments and consumer-relevant matrices supports their consideration as emerging, low-dose stressors within complex exposure scenarios, rather than as isolated contaminants. Once internalized, smaller particles may translocate across epithelial barriers and reach secondary organs, emphasizing the need to evaluate their potential health impacts (Jenner et al., 2022; Horvatits et al., 2022).

1.2.2. Systemic Translocation and Tissue Accumulation of MNPLs

A growing body of experimental and biomonitoring evidence demonstrates that MNPLs can translocate across epithelial barriers and accumulate in internal tissues. *In vitro* and *in vivo* studies show that nanoparticles, particularly those below 100 nm, can cross the intestinal and alveolar barriers following similar pathways to other engineered nanomaterials, subsequently entering the lymphatic or circulatory systems, and distributing to secondary organs (Johnston et al., 2010; He et al., 2020; Liu et al., 2022).

In vitro studies using human epithelial monolayers have demonstrated that polystyrene nanoplastics are internalized via endocytosis and transcytosis, localizing within endosomes, lysosomes, and mitochondria (Johnston et al., 2010; He et al., 2020; Liu et al., 2022). In human intestinal Caco-2 and HT29 cell models, particles in the 50-100 nm range were shown to cross the epithelium within hours, with smaller and positively charged particles exhibiting higher transport efficiency (Fuchs et al., 2016). Similarly, alveolar models such as BEAS-2B and Calu-3 cultures have shown nanoplastic penetration, potentially via tight junctions and paracellular diffusion, especially when oxidative stress or inflammation compromises epithelial integrity (Jeon et al., 2022; García-Rodríguez et al., 2024).

In vivo animal studies have confirmed these findings. Following oral administration in rodents, radio-labeled or fluorescent polystyrene nanoparticles were detected in the liver, spleen, and kidneys within 24-48 hours (Yang et al., 2019; Fan et al., 2022). Zebrafish embryos and larvae exposed to PS or PET nanoplastics exhibited systemic uptake through the gut epithelium and subsequent accumulation in the brain and heart (Ji et al.,

2020; Sendra et al., 2021; Zhou et al., 2022). These studies suggest a particle size threshold for efficient barrier translocation of around 100 nm, with smaller and more hydrophilic or oxidized particles showing enhanced bioavailability (Schröter and Ventura, 2022).

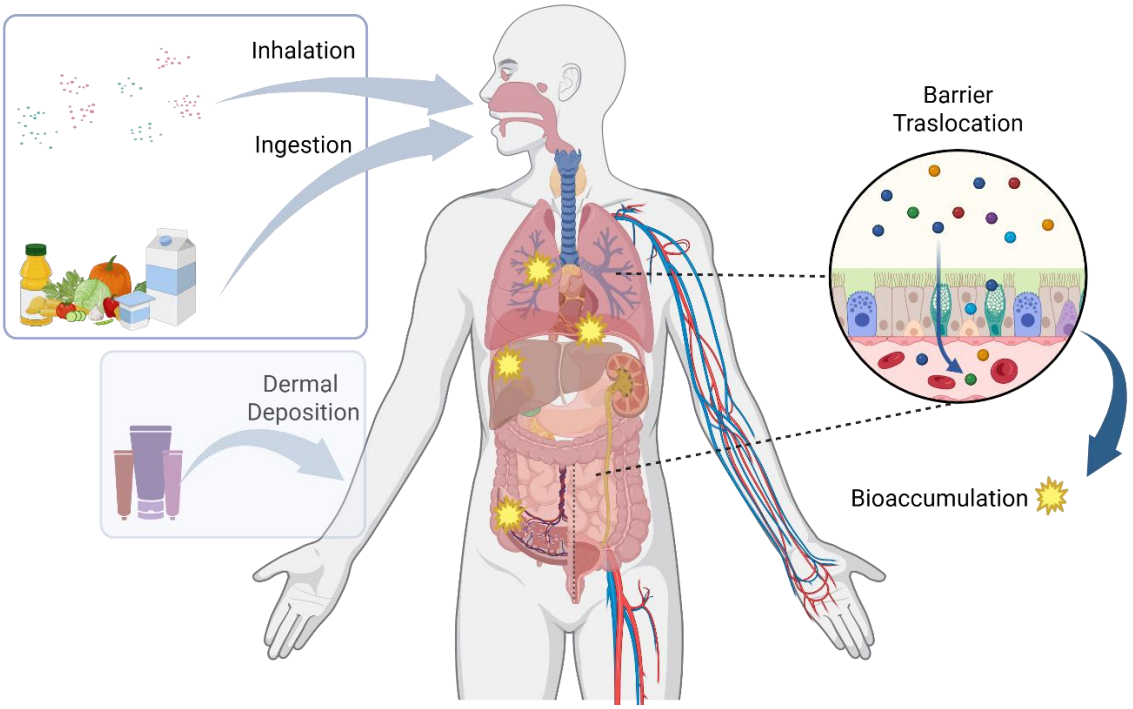

Figure 2: Primary routes of human exposure and systemic translocation of nanoplastics. The main pathways for human contact with nanoplastics include ingestion of contaminated food and beverages, inhalation of airborne particles, and dermal deposition from consumer products. Following exposure, NPLs are capable of barrier translocation crossing epithelial barriers such as the gastrointestinal tract or lungs to enter systemic circulation. This allows for their subsequent distribution and bioaccumulation in secondary organs.

Direct evidence of the accumulation of MNPLs in humans is expanding. These particles have been identified in stool (Ruggieri et al., 2025), urine (Pironti et al., 2022), blood (Vethaak and Legler, 2021; Leslie et al., 2022), placental tissue (Ragusa et al., 2021), lung tissue (Jenner et al., 2022), and cirrhotic liver samples (Horvatits et al., 2022). Although the exposure assessment remains limited by the techniques of quantification of MNPLs in environmental and biological matrices, as exposed in Section 1.2.1, these findings confirm systemic exposure and demonstrate that nanoplastics can cross key biological barriers, including the intestinal epithelium, alveolar membrane, and even the placental interface.

Laboratory and computational studies further indicate that MNPLs interact with plasma proteins to form a “biocorona” which influences biodistribution and cellular uptake (Mahmud et al., 2024). Factors such as particle size, surface charge, and polymer type

modulate internalization efficiency (Fuchs et al., 2016; Schröter and Ventura, 2022). The detection of MNPLs in multiple human compartments thus demonstrates their potential for bioaccumulation and long-term retention, particularly under chronic, low-dose exposure scenarios (Catalan et al., 2025).

1.2.3. Early Evidence of Health Effects

While human epidemiological data specifically for MNPLs remain limited, a convergence of toxicological, mechanistic, and clinical evidence indicates that exposure can trigger biological responses linked to chronic disease. Across *in vitro, in vivo,* and *ex vivo* human studies, MNPLs have been shown to induce oxidative stress, inflammation, fibrosis, metabolic disruption, and processes associated with carcinogenic progression. Thus, in human cell models, MNPL exposure consistently activates oxidative and inflammatory pathways. Studies in bronchial epithelial, hepatic, and immune cells have reported ROS generation, mitochondrial dysfunction, and cytokine release (Weber et al., 2022; Das, 2023; Mahmud et al., 2024). Functionalized NPLs have been shown to alter cytoskeletal organization and induce oxidative stress in endothelial systems, illustrating how surface modifications influence cellular toxicity (Martín-Pérez et al., 2024). In inhalation models, nanoplastic aerosols induced macrophage activation, epithelial damage, and impaired barrier function (Lim et al., 2021; Jeon et al., 2022). Notably, NPLs coming from polylactic acid (PLA), one of the most used bio-based plastics, also resulted in ROS generation and barrier impairment in lung cells, indicating that cytotoxicity is not limited to traditional polymers like polystyrene (García-Rodríguez et al., 2024).

Mammalian *in vivo* studies corroborate these findings. Oral or inhaled nanoplastics have been shown to disrupt intestinal homeostasis, alter glucose and lipid metabolism, and elicit oxidative stress in metabolic organs. Fan et al. (2022) demonstrated that chronic oral exposure to PS nanoplastics perturbed plasma glucose metabolism and hepatic antioxidant capacity in mice. Shen et al. (2022) reported activation of the cyclic GMP-AMP synthase - stimulator of interferon genes (cGAS–STING) pathway and fibrotic remodeling in liver tissue after PS microplastic ingestion, linking immune signaling to tissue damage. The detection of MNPLs in cirrhotic human liver provides clinical corroboration of these pathways (Horvatits et al., 2022).

Recent cardiovascular findings have broadened the scope of concern. Marfella et al. (2024) identified micro- and nanoplastics embedded within human atheromatous plaques, reporting that higher concentrations were associated with increased incidence of acute cardiovascular events. The authors proposed that MNPLs promote endothelial

activation, oxidative stress, and macrophage infiltration, thereby accelerating atherogenesis. That study provides the first direct evidence linking MNPLs bioaccumulation to clinically relevant cardiovascular outcomes in humans.

At the mechanistic level, chronic *in vitro* exposure studies have begun to associate MNPLs with pro-carcinogenic signaling. Gutiérrez-García et al. (2025) showed that long-term exposure of BEAS-2B cells to true-to-life PET nanoplastics promoted anchorage-independent growth, invasive behavior, and activation of NRF2, HSP70, and MMP pathways. Transcriptomic analyses of PET-exposed cells further revealed alterations in redox homeostasis, cell adhesion, and immune modulation, while Yang et al. (2025) demonstrated the involvement of extracellular-matrix remodeling and immune evasion networks consistent with cancer progression.

Together, these studies group evidence that MNPLs are bioactive contaminants capable of crossing physiological barriers, accumulating in tissues, and triggering molecular responses associated with the risk of chronic disease. Continuous low-dose exposure to MNPLs under environmentally relevant scenarios may create progressive molecular and cellular alterations that accumulate over time, posing health risks that remain unquantified.

1.3. Current Research Needs on MNPLs Toxicology

1.3.1. Limitations of Current Test Materials

A primary limitation in nanoplastic toxicology is the prevalent reliance on materials that do not represent environmentally real samples. The absence of certified reference materials compromises reproducibility and cross-study comparisons (Catalan et al., 2025). Although the field is evolving, most available experimental evidence has been obtained using commercially pristine PS nanoparticles. These particles serve as convenient models due to their monodisperse size, surface stability, and ease of modification. While essential for methodological standardization, this approach provides an oversimplified representation of the heterogeneous mix of NPLs found in the environment (Martin et al., 2022; Schröter and Ventura, 2022; Domenech et al., 2024). Consequently, most studies assess biological responses to particles that differ significantly from those relevant to human risk.

The reliance on pristine PS introduces several biases. First, environmental particles are basically secondary NPLs, characterized by irregular, angular, and polydisperse morphologies, whereas primary PS NPLs are spherical and monodisperse (Schröter and

Ventura, 2022). Irregular edges and higher aspect ratios have been shown to increase cellular adhesion and membrane disruption, yet this shape-dependent toxicity remains largely unexplored (Domenech et al., 2023; Le et al., 2023).

Second, this model overlooks the critical role of environmental ageing. Commercial nanoplastics possess smooth, non-oxidized surfaces. In contrast, environmental NPLs undergo photo-oxidation, hydrolysis, and abrasion, processes that introduce oxygenated functional groups and adsorbed biomolecular coronas (Li et al., 2022; Pradel et al., 2023). These aged surfaces alter particle charge and reactivity, modulating bioavailability and toxicity (Thompson et al., 2024). Current models, lacking these features, may underestimate cellular interaction and internalization efficiency.

Furthermore, this focus on a single polymer type is a poor proxy for real-world diversity. Environmental samples contain PE, PP, PVC, PET, PU, and polyamide (PA), not just PS (Thompson et al., 2024; Crosset-Perrotin et al., 2025). These polymers vary widely in density, hydrophobicity, and crystallinity, all of which influence reactivity and cellular interactions, limiting the extrapolation of PS-based findings.

This discrepancy extends to chemical additives. Consumer plastics contain plasticizers, stabilizers, and flame retardants that can leach or remain embedded within secondary fragments. These compounds are often more bioactive than the polymer matrix itself (Khan and Jia, 2023). "Real-life" models generated from degraded consumer products, like from PET bottles, incorporate these chemical mixtures and have shown distinct transcriptomic and functional responses compared to pristine PS (Villacorta et al., 2022, 2023; Gettings et al., 2024; Gutiérrez-García et al., 2025). However, most published datasets still evaluate nanoplastics as chemically inert entities.

These limitations have urged efforts to produce "top-down" or "real-life" nanoplastics via mechanical milling, photo-ageing, or sonication of consumer products (Villacorta et al., 2023, 2024; Domenech et al., 2024; Crosset-Perrotin et al., 2025). While these materials are more representative, such preparations remain labor-intensive, poorly standardized, and incompletely characterized. Harmonized methods to generate and characterize aged, additive-containing, multi-polymer NPLs are therefore essential to bridge the gap between experimental models and environmental reality.

1.3.2. Limitations in Reproducing Realistic Exposure Scenarios

In addition to the lack of representative test materials, nanoplastic toxicology is limited by its reliance on experimental designs that fail to represent the complexity of human

exposure. The field is dominated by acute, high-concentration, and single-pollutant models. While valuable for initial mechanistic insights, these approaches do not capture the chronic, low-dose, and mixed-exposure context relevant to human health.

As explained in Section 1.2.1, real-world exposure is characterized by continuous, low-dose contact throughout life. In contrast, most available studies use high concentrations designed to provoke measurable cytotoxic or oxidative responses within hours or days (Banerjee and Shelver, 2021; Haldar et al., 2023). These acute assays are rapid and standardized but fail to capture the adaptive, cumulative, and transformation-related processes that may arise from persistent exposure to environmentally relevant doses (Liu et al., 2022; Brandts et al., 2023). As a result, acute assays may underestimate long-term biological impacts.

Traditional nanotoxicology has largely relied on short-term assays designed to measure acute endpoints such as cell viability, reactive oxygen species generation, or membrane integrity. While these endpoints provide a preliminary indication of cytotoxicity, they are insufficient to capture the complex and often subtle molecular perturbations that support long-term health outcomes. In the context of nanoplastics, where chronic, low-dose exposure is the most realistic scenario, evaluating disease-relevant endpoints is essential to determine mechanisms of genotoxicity, inflammation, fibrosis, and carcinogenesis (Banerjee and Shelver, 2021; Domenech et al., 2024).

In vivo models for assessing systemic responses, biodistribution, and organism-level outcomes following MNPL exposure remain essential. However, their application to long-term, low-dose, and complex exposure scenarios is restricted by ethical considerations and logistical limitations (Kaplan et al., 2024). These constraints are particularly relevant when investigating chronic exposures or combinatorial scenarios that would require prolonged dosing, large animal cohorts, or extensive experimental replication. As a result, complementary *in vitro* strategies have gained increasing relevance as ethically responsible and mechanistically informative tools to model environmentally realistic exposure conditions.

To approximate chronic exposure, long-term *in vitro* models where cells are cultured for weeks to months with sub-cytotoxic nanoparticle concentrations are emerging. These models allow the evaluation of general toxicological effects that may not be detectable following short-term treatments, including subtle genotoxic responses, low-grade inflammatory signaling, alterations in barrier integrity, or adaptive stress responses that emerge progressively over time (Vales et al., 2015; Choo et al., 2016). In this context, long-term exposure models enable the investigation of cumulative and adaptive cellular

responses rather than acute cytotoxicity, rather than focusing exclusively on acute cytotoxicity. Importantly, such approaches also open the possibility to explore complex downstream outcomes that typically require extended exposure periods to manifest, including cell transformation and carcinogenic-related processes, which are unlikely to be observed following acute or single-dose exposures.

In addition to the limitations in the study of the effects of long-term exposure to MNPLs, these methodological limitations are also compounded by the fact, noted earlier, that realistic exposures involve complex mixtures, not isolated agents. Humans are exposed to NPLs that coexist with a wide array of chemical pollutants, metals, and toxins (Sun et al., 2023). Nanoplastics act as vectors for these co-contaminants, potentially modifying their bioavailability and toxicity (Browne et al., 2013; Sun et al., 2023). Nevertheless, most studies test NPLs in isolation, ignoring the interactive effects that define real-world risk. While some studies have shown synergistic effects (Domenech et al., 2021; Barguilla et al., 2022), the shortage of mixture studies remains a critical gap due to experimental complexity.

Ultimately, integrating duration and complex mixtures is essential. Advancing in the establishment of standardized, chronic co-exposure models, particularly using human-derived cells and environmentally representative NPLs (Villacorta et al., 2022), is necessary to identify the cumulative and interactive effects that determine the long-term biological relevance of nanoplastic exposure.

To sum up these limitations, Figure 3 schematizes the need to move towards more complex exposure scenarios that better reflect real-life conditions.

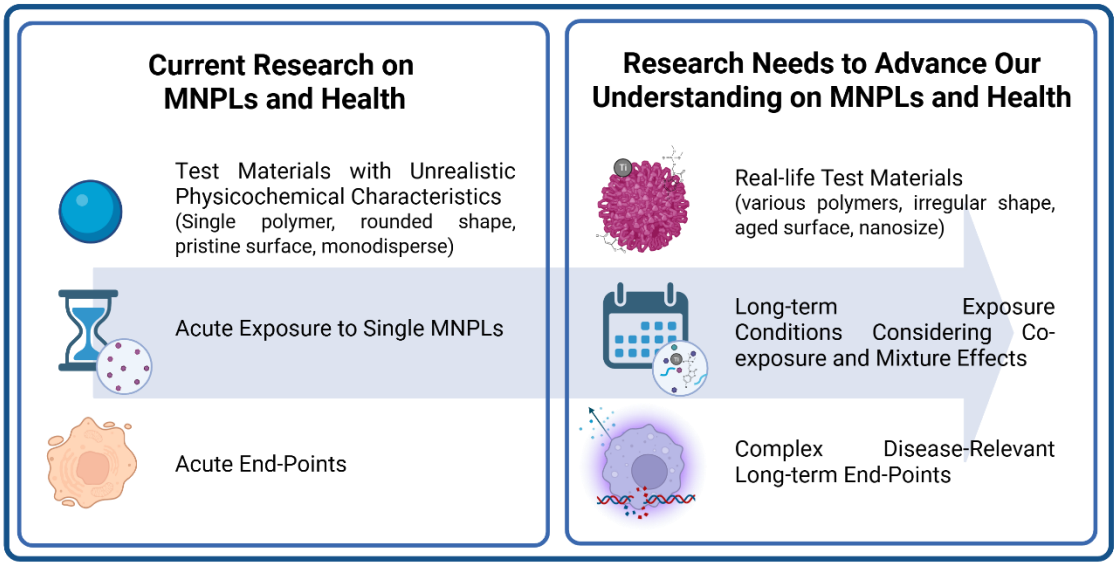

Figure 3. The difference between current research in MNPLs and research priorities to advance MNPLS and health. The diagram contrasts the limitations of current research models with the complexity of real-world human exposure. The current studies (left) are predominantly based on pristine, spherical polystyrene, acute exposure times, and simple, often cytotoxic, endpoints. This contrasts with the real-life exposure scenario (right), which involves real-life aged, irregularly shaped particles of various polymers, co-exposure with additives and pollutants, chronic exposure durations, and the need to measure complex, disease-relevant endpoints such as genotoxicity, inflammation, and transformation.

1.4. The Role of New Approach Methodologies (NAMs) in the Study of MNPLs

1.4.1. The Regulatory and Conceptual Basis of NAMs

Over the past two decades, toxicology has undergone a profound paradigm shift toward mechanistic, human-relevant, and non-animal testing strategies collectively known as New Approach Methodologies (NAMs). NAMs include *in vitro, in silico*, and computational tools designed to evaluate chemical safety based on biological mechanisms of action rather than empirical observation of adverse outcomes in animal models (Carmichael et al., 2022; Hristozov et al., 2024). This transition aligns with the 3Rs principle of “Replacement, Reduction, and Refinement” of animal use, and in the global policy commitment to develop human-relevant, mechanism-driven safety assessment frameworks (Kaplan et al., 2024).

In practice, NAMs are being operationalized through Integrated Approaches to Testing and Assessment (IATA), which combine mechanistic and computational evidence to address specific regulatory questions (Caloni et al., 2022; Carmichael et al., 2022). The

IATA concept supports a modular workflow from problem formulation to data integration to uncertainty analysis, which allows regulators to judge fitness for purpose even when traditional apical data are unavailable. NAMs operate on the premise that toxicological phenomena can be reconstructed as networks of biological perturbations across distinct levels of biological organization. Rather than focusing solely on apical endpoints such as lethality or organ pathology, NAMs emphasize molecular and cellular key events that precede adverse outcomes and can be quantified using standardized assays (Hristozov et al., 2024). This mechanistic orientation allows for integration of multiple data streams into structured decision frameworks such as the Adverse Outcome Pathway (AOP) framework.

Although challenges remain regarding standardization and validation, consensus is growing that the question is no longer whether NAMs will be implemented, but how and when (Schmeisser et al., 2023). Recent reviews highlight increasing regulatory confidence in the reproducibility and predictive capacity of *in vitro* systems and computational models, especially when combined with robust exposure assessment (Paul Friedman et al., 2025).

For emerging contaminants such as MNPLs, the application of NAMs is particularly relevant. Conventional animal studies are poorly suited to capture the low-dose, chronic, and particle-specific mechanisms of MNPL toxicity. In this context, human-relevant mechanistic NAMs, including advanced *in vitro* models, high-content imaging, and omics-based profiling, offer a scientifically robust and ethically responsible path forward. Consortia such as CUSP (Cluster to Understand the Health Impacts of Micro- and Nanoplastics) have identified NAM integration as a priority to align MNPL hazard assessment with Next Generation Risk Assessment (NGRA) principles (Catalan et al., 2025; Foss et al., 2025).

1.4.2. Human Cell-Based *In Vitro* NAM Systems

Human cell-based *in vitro* systems represent one of the most implemented pillars of the NAMs framework. Their use aligns with the ethical and scientific objectives of the 3Rs and addresses the limitations of animal models, which often fail to capture species-specific responses (Zink et al., 2020; Kaplan et al., 2024). By focusing on molecular and cellular events that precede tissue- or organism-level toxicity, these models enable the systematic mapping and connecting of molecular initiating events (MIEs) and key events (KEs) to apical adverse outcomes (AO) within the AOPs framework and provide mechanistic insights into the biological impact of emerging contaminants.

The rationale for using human-derived cells in NAMs lies in their ability to recapitulate tissue-specific biology under controlled conditions (Zink et al., 2020). They allow exposure scenarios to be tailored to realistic human routes and facilitate quantification of cellular uptake, internal dose, and downstream effects at concentrations relevant to human exposure (Caloni et al., 2022; Carmichael et al., 2022). For MNPL research, key *in vitro* models used for this Thesis include:

- BEAS-2B bronchial epithelial cells, a model for the respiratory epithelium that enables investigation of inhalation exposure to airborne MNPLs and cigarette smoke co-pollutants (Yang et al., 2021; Jeon et al., 2022).
- HuH-7 hepatocytes represent the metabolic interface of the liver, involved in biotransformation, oxidative stress, and inflammatory signaling (Almukhlafi et al., 2021).
- THP-1 monocytes and macrophage-like derivatives are key immune models for studying phagocytosis, cytokine secretion, and the inflammasome activation (Chanput et al., 2014).

Additional cell systems, such as HUVEC endothelial cells or placental trophoblasts, are increasingly applied to study vascular or transplacental transfer of MNPLs (Ragusa et al., 2021; Martín-Pérez et al., 2024). Each model provides organ-relevant mechanistic data that can be integrated through IATA frameworks to describe systemic toxicity.

As Zink et al. (2020) emphasize, the predictive power of human *in vitro* systems lies not in single assays but in integrated endpoint profiling. NAM-compatible test batteries combine functional, molecular, and omic-level measurements, directly addressing the research need for disease-relevant endpoints identified in Section 1.3.2. These assays can be linked to defined AOP networks for processes like inflammation or carcinogenesis. Key endpoint categories included in this Thesis are:

- Oxidative Stress and Redox Imbalance: Assessed via ROS quantification, glutathione depletion, and expression of NRF2-responsive genes such as *NQO1* and *HMOX1* (Dinkova-Kostova and Abramov, 2015; Taguchi and Yamamoto, 2020).
- Inflammation and Immune Response: Monitored through cytokine profiling (IL-6, IL-8, TNF-α) and inflammasome activation markers including NLRP3 and IL-1β (Weber et al., 2022; Pratim Das and Medhi, 2023).
- Genotoxicity and DNA Repair: Measured using single-cell comet assays (with lesion-specific enzymes), micronucleus tests, and quantification of γ-H2AX foci (Collins, 2004; Vales et al., 2015).

- Omics-Based Analyses: Transcriptomics, proteomics, and metabolomics used to elucidate pathway-level perturbations and identify MIEs (Zink et al., 2020; Yang et al., 2025).

While valuable for mechanistic screening, 2D *in vitro* models lack tissue-level complexity. Persistent challenges include the need for standardized dosimetry, particle characterization, and robust *in vitro* to *in vivo* extrapolation (IVIVE) to connect concentrations to realistic human exposure levels (Paul Friedman et al., 2025). Efforts are ongoing to standardize these methods within the OECD and CUSP frameworks (Catalan et al., 2025; Mortensen et al., 2025).

1.4.3. Long-Term and Mechanistically Informed *In Vitro* Exposure as the Next Generation of NAMs

A critical gap in toxicology, as highlighted in Section 1.3.2, is the inability of conventional short-term assays to reproduce chronic, low-dose, and cumulative exposures that define human contact with MNPLs. Addressing this requires a shift toward long-term *in vitro* exposure paradigms, an emerging frontier within the NAM and NGRA framework (Hristozov et al., 2024; Paul Friedman et al., 2025).

Real-world exposure is continuous, suggesting that cellular stress, redox imbalance, and low-grade inflammation may progress for weeks or months before overt toxicity is evident (Domenech et al., 2023; Mahmud et al., 2024). As Zink et al. (2020) and Caloni et al. (2022) emphasize, extending *in vitro* models into chronic regimes allows researchers to capture adaptive and maladaptive transitions, such as persistent oxidative stress or epithelial to mesenchymal transition (EMT). These processes often represent KEs linking molecular changes to adverse outcomes like fibrosis or carcinogenesis.

Recent studies have demonstrated the feasibility of these designs. Gutiérrez-García et al. (2025) exposed BEAS-2B cells to true-to-life PET nanoplastics for 30 weeks, documenting the gradual emergence of oxidative stress, cytokine release, and anchorage-independent growth, all hallmarks of cellular transformation. Similarly, Domenech et al. (2024) and Choo et al. (2016) showed that chronic exposure to polymeric or metal-containing nanoparticles induced tumorigenic traits without overt cytotoxicity, emphasizing that long-term adaptation, rather than acute cell death, is a critical endpoint for risk assessment. These studies reveal mechanistic signatures, such as NRF2 activation, mitochondrial stress, and matrix remodeling, that acute assays could miss.

Long-term *in vitro* exposure models provide an ideal platform for AOP-based mechanistic mapping. They allow differentiation between transient adaptive responses and persistent pathological alterations, key for identifying early markers of chronic disease. Furthermore, by measuring pathway-specific markers, these systems generate quantitative data that can populate KEs in relevant AOPs and support WoE evaluations. When coupled with transcriptomic profiling, long-term assays reveal stable shifts in gene expression indicative of epigenetic adaptation or metabolic rewiring, providing molecular anchors for chronic toxicity assessment (Yang et al., 2025). These mechanistic depths, positions chronic exposure NAMs as key tools for bridging the gap between *in vitro* data and regulatory interpretation. However, technical challenges persist. Maintaining cultures for months requires strict control of particle stability, medium composition, and sublethal exposure levels to prevent artifactual stress (Domenech et al., 2024). Ensuring consistent dosimetry, meaning the effective particle dose interacting with cells, remains a limiting factor for reproducibility and inter-laboratory comparison (Paul Friedman et al., 2025). Additionally, chronic *in vitro* models generate complex temporal datasets that necessitate bioinformatics pipelines for trend detection and AOP linkage (Zink et al., 2020).

2. OBJETIVES

2. OBJECTIVES

The main objective of this PhD Thesis is to advance knowledge on the biological effects induced by nanoplastics (NPLs) exposure in human cell models by addressing current research needs related to the use of realistic NPLs materials and biologically relevant exposure conditions, contributing to the evaluation of disease-relevant data for human hazard assessment.

To achieve this goal, this Thesis is structured around the following four specific objectives:

2.1. To assess the influence of nanoplastic physicochemical characteristics on cellular internalization dynamics and short-term biological effects in human hepatocytes, through a comparative analysis of different polymer types (PS, PET, and PLA).
(Chapter 1 – Exploring the impact of nanoplastics on human hepatic cells: dynamics of internalization and harmful effects in HuH-7 cells)

2.2. To evaluate the role of additive-containing nanoplastics in modulating cellular internalization and genotoxicity in human immune cells, by comparing PET nanoplastics and titanium-doped PET nanoplastics (PET-Ti).
(Chapter 2 – Biological Impact of True-to-Life PET and Titanium-Doped PET Nanoplastics on Human-Derived Monocyte (THP-1) Cells)

2.3. To determine whether long-term exposure to titanium-doped PET nanoplastics (PET-Ti) induces persistent cellular alterations and transformation-like phenotypes in lung epithelial cells, through a comparative analysis of acute and chronic exposure scenarios.
(Chapter 3 – Acute and long-term effects of titanium-doped polyethylene terephthalate nanoplastics [PET(Ti)-NPLs] in human bronchial epithelial (BEAS-2B) cells)

2.4. To assess whether long-term co-exposure to PET nanoplastics and cigarette smoke condensate enhances genotoxicity, cellular transformation, and carcinogenesis-related processes in lung epithelial cells, compared to single-agent exposures.

(Chapter 4 – The long-term *in vitro* co-exposure of polyethylene terephthalate (PET) nanoplastics and cigarette smoke condensate exacerbates the induction of carcinogenic traits)

3. RESULTS

3. RESULTS

The results of this Thesis have been organized into four studies that have already been published as four articles in different peer-reviewed journals.

Each chapter is linked to a specific objective of the Thesis and ordered as follows:

3.1 Chapter 1 (Article 1): Exploring the impact of nanoplastics on human hepatic cells: dynamics of internalization and harmful effects in HuH-7 cells**.**

3.2 Chapter 2 (Article 2): Biological Impact of True-to-Life PET and Titanium-Doped PET Nanoplastics on Human-Derived Monocyte (THP-1) Cells.

3.3 Chapter 3 (Article 3): Acute and long-term effects of titanium-doped polyethylene terephthalate nanoplastics in human bronchial epithelial cells.

3.4 Chapter 4 (Article 4): The long-term *in vitro* co-exposure of polyethylene terephthalate (PET) nanoplastics and cigarette smoke condensate exacerbates the induction of carcinogenic traits.

3.1. Chapter 1 (Article 1)

Exploring the impact of nanoplastics on human hepatic cells: dynamics of internalization and harmful effects in HuH-7 cells.

Environmental Science: Nano, 12(11), 4920-4934. (2025)

Doi: 10.1039/d5en00434a

Impact Factor: 5.1 (2024)

Environmental Science Nano

ROYAL SOCIETY OF CHEMISTRY

PAPER

View Article Online
View Journal | View Issue

Cite this: *Environ. Sci.: Nano*, 2025, **12**, 4920

Exploring the impact of nanoplastics on human hepatic cells: dynamics of internalization and harmful effects in HuH-7 cells

Michelle Morataya-Reyes, [a] Aliro Villacorta,[ab] Jessica Arribas Arranz,[a] Joan Martín-Pérez, [a] Juan Francisco Ferrer,[c] Susana Pastor,[a] Raquel Egea, [a] Irene Barguilla, [a] Ricard Marcos [a] and Alba Hernández*[a]

Received 30th April 2025,
Accepted 28th August 2025

DOI: 10.1039/d5en00434a

rsc.li/es-nano

The increasing prevalence of micro- and nanoplastics (MNPLs) in the environment necessitates a detailed examination of their potential health impacts and the factors influencing these responses. Since internalization is a prerequisite for inducing adverse effects, we investigated the roles of surface modifications and polymer composition in human liver cells (HUH-7). Our study compared the internalization and effects of a pristine polystyrene nanoplastic (PS50-NPLs), two carboxylated polystyrenes of different sizes (cPS50-NPLs and cPS100-NPLs), and two environmentally relevant nanoplastics derived from polyethylene terephthalate water bottles (PET-NPLs) and polylactic acid pellets (PLA-NPLs). Significant variations in cell internalization were observed, with cPS50-NPLs and PET-NPLs showing the highest levels, and PS50-NPLs showing the lowest. Interestingly, internalization alone did not correlate directly with the induced effects; only PET-NPLs and PLA-NPLs induced reactive oxygen species (ROS), genotoxicity, and increased cytokine release. These results suggest that while internalization is essential in assessing MNPL toxicity, harmful effects also depend on other particle characteristics. The notable impact of the realistic environmental models PET-NPLs and PLA-NPLs underscores the importance of using environmentally representative MNPLs to better assess the health risks associated with environmental MNPL exposure.

Environmental significance

Micro/nanoplastics, as new emergent environmental contaminants, can affect human health. Since the induced harmful effects can correlate with internalization, it is necessary to understand the internalization mechanisms and the potential correlations between internalization and induced effects. To solve these points, pristine polystyrene nanoplastics and true-to-life nanoplastics, derived from plastic goods and pellets, were evaluated. Results indicate the polymeric nature and surface charge are relevant factors modulating internalization. Furthermore, internalization does not correlate with the induce effects, polyethylene terephthalate (PET) and polylactic acid (PLA) true-to-life nanoplastics inducing stronger effects. This highlights the importance of using environmentally representative MNPLs to better assess the health risks associated with environmental MNPL exposure.

1. Introduction

The exponential increase in plastic production and usage, particularly over the last decade, has brought significant advantages but also serious waste management challenges.[1] When used, improperly disposed of, or recycled plastics degrade in the environment through mechanical wear, photo-oxidation, hydrolysis, and microbial action, leading to the formation of microplastics (MPLs, 1–1000 μm) and nanoplastics (NPLs, 1–1000 nm).[2] This constant degradation results in a range of particle sizes, often referred to as environmental secondary micro/nanoplastics (MNPLs) due to their continuous breakdown in natural environments.

The minute size of NPLs imparts them with unique physicochemical properties, enhancing their mobility and bioavailability across various environmental settings.[3,4] Characteristics such as Brownian motion, high surface reactivity, additive leachate potential, and the ability to traverse physiological barriers make these particles a particular concern for human health researchers.[2] MNPLs have been detected in numerous consumables, including food and water,[5–7] and have even been identified in human excretions, such as stool and urine,[8,9] confirming exposure

[a] *Group of Mutagenesis, Department of Genetics and Microbiology, Faculty of Biosciences, Universitat Autònoma de Barcelona, Campus of Bellaterra, 08193, Cerdanyola del Vallès (Barcelona), Spain. E-mail: alba.hernandez@uab.cat*
[b] *Facultad de Recursos Naturales Renovables, Universidad Arturo Prat, Iquique, Chile*
[c] *AIMPLAS, Plastics Technology Center, Valencia Parc Tecnològic, 46980 Paterna, Spain*

through diet. Their presence in lung tissue also suggests inhalation exposure.[10,11] While the exact internal dose of these particles remains under investigation,[12] studies have shown that MNPLs can migrate into the bloodstream and reach remote organs, including the heart and placenta.[13–15]

The liver, a critical organ for metabolic regulation and detoxification, is particularly vulnerable to NPLs.[16] In human liver samples from individuals with cirrhosis, MNPLs of various polymers have been identified, unlike in healthy individuals where no such particles were detected.[17] Animal models similarly demonstrate MNPL accumulation in the liver, as observed in fish[18] and mice[19] following oral administration of polystyrene nanoplastics (PS-NPLs).

Research using animal models and *in vitro* approaches has revealed the detrimental effects of NPLs on hepatic cells, including internalization, cytotoxicity, oxidative stress, and disturbed cellular homeostasis in various liver cell lines, such as HepG2 (ref. 20) and HL7702.[21] However, the precise mechanisms underlying NPL-induced hepatotoxicity remain unclear. Furthermore, most studies have focused solely on PS-NPLs of similar sizes and characteristics, which may not accurately reflect the diverse composition of secondary MNPLs found in the environment.

For a more comprehensive understanding of the effects and mechanisms of action of MNPLs on human liver cells, toxicological evaluations should use materials closely resembling those found in real-world environments, varying in size, surface properties, polymer type, and shape.[22] These realistic analogs, termed true-to-life MNPLs, serve as models for environmental secondary MNPLs.[23]

In this study, we examined the dynamics of internalization and effects of five distinct NPLs on HUH-7 hepatic cells. The NPLs selected include three commercial PS-NPLs (one pristine, and two carboxylated of varying sizes) and two environmentally representative NPLs derived from polyethylene terephthalate (PET) and polylactic acid (PLA). By incorporating a variety of polymers, sizes, and surface modifications, we aim to elucidate how these factors influence the hepatotoxic potential of MNPLs.

2. Materials and methods

2.1. NPLs characterization

PS-NPLs (Spherotech, PP008-10), cPS50-NPLs (Polysciences, Inc., 15913-10), cPS100-NPLs (Polysciences, Inc., 16688-15), and their respective fluorescent counterparts f-PS-NPLs (Spherotech, FP-00552-2 ex: 460 nm, em: 480 nm), f-cPS50-NPLs (Polysciences, Inc., 16661-10 ex: 441 nm, em: 486 nm), f-cPS100-NPLs (Polysciences, Inc., 16662-10 ex: 441 nm, em: 486 nm) were purchased from the indicated sources. Realistic environmental model NPLs were in-house obtained from plastic water bottles or pellet degradation, as described in Villacorta *et al.*[24] for PET-NPLs and in Alaraby *et al.*[25] for PLA-NPLs. Their fluorescent counterparts were prepared following a labelling protocol based on the use of a regularly used textile dye, iDye polypink (Jacquard Products, Healdsburg, CA, USA)[26,27] and 5(6)-FAM,[25] respectively. After staining, particles were subjected to ultrafiltration and multiple washing steps to remove unbound dye. The absence of fluorescence in the final wash was used to confirm effective dye removal. The cytocompatibility of these labeled particles was previously validated by Villacorta *et al.*,[27] who reported no additional cytotoxic effects from the labeled NPLs, compared to unlabeled controls.

Size and shape were determined by transmission electron microscopy (TEM) using a JEOL JEM 1400 instrument (JEOL LTD, Tokyo, Japan) at 120 kV operation settings. Particles for TEM were prepared by placing a 7 μL drop of particle suspension at a concentration of 200 μg mL^{-1} on a carbon covered cooper grid, let dry overnight inside a covered petri dish. For all particles in suspension the size distribution was determined by dynamic light scattering (DLS), using a Zetasizer® Ultra device from Malvern PANalytical (Cambridge, United Kingdom). Working particle suspensions were prepared at concentration of 100 μg mL^{-1}. Once sonicated, size was determined by transferring 1 mL of particle suspension on independent DTS0012 cuvettes and performing the experiments by triplicate using refractive indexes of 1.59, 1.47, and 1.57 for PS, PLA and, PET respectively. For ζ-potential a similar approach was done but the measurements were carried out on DTS1070 cuvettes. Parallelly, from the same suspensions the particle size was also determined by a combination of light scattering and Brownian movement on a Nanosight NS300 nanotracking analysis from Malvern PANalytical Ltd (Cambridge, United Kingdom). To assess the chemical composition of the true-to-life PET- and PLA-NPLs, FTIR analyses were carried out. To proceed, we used the protocols previously described[24,28] and the previously reported characteristic polymer spectral bands.[29,30]

2.2. Cell culture conditions

HUH-7 cells obtained from JCRB Cell Bank (JCRB0403) were used for the study. Cells were grown in Dulbecco's modified Eagle's medium (DMEM, Life Technologies, NY, USA) supplemented with 10% fetal bovine serum (FBS, Biowest, France), and 2.5 μg mL^{-1} of Plasmocin (InvivoGen, CA, USA). For HUH-7 passage, TrypLE™ Select Enzyme (1×) (Thermo Fisher Scientific, Waltham, MA) was used to detach cells. Cells were maintained in a 5% CO_2 humidified atmosphere at 37 °C.

2.3. Cell viability

To determine the sub-toxic concentrations of the different NPLs in HUH-7 cells, 1×10^5 cells/well were seeded in triplicate in 12-well plates in a final volume of 1 mL of DMEM and treated with NPLs at concentrations from 0 to 200 μg mL^{-1} for 48 h. Cells were detached and cell number was determined using the LUNA-II™ Automated Cell Counter (Biocat, Heidelberg, Germany) in a 1 : 1 dilution with trypan blue (Sigma-Aldrich, St. Louis, MO). Each concentration

average cell number was normalized against the average of the non-treated cells, and fold change was compared.

2.4. Determination of NPLs internalization in HUH-7 by confocal microscopy

To confirm NPLs internalization in HUH-7 cells, 1×10^4 cells per well were seeded in an μ-Slide 8 well chambered coverslip (Ibidi GmbH, Gräfelfing, Germany) and treated with 100 μg mL^{-1} of the fluorescent/labeled NPLs (f-NPLs) for 48 h. Before observation with a Leica TCS SP5 confocal microscope, cells were washed with growth medium and Hoechst 33342 (ex: 405 nm, em: 415–503) and Cellmask (ex: 633 nm, em: 645–786) markers were added to stain the cell nuclei and cell membranes, respectively.

2.5. NPLs internalization in HUH-7 by flow cytometry

To determine the proportion of cells that internalize the different NPLs, 1×10^5 cells per well were seeded in triplicate in 12-well plates in a final volume of DMEM with 100 μg mL^{-1} of the fluorescent/dyed NPLs. After treatment (1, 3, 24, 48, and 72 h), cells were detached and analyzed using a flow cytometer (CytoFLEX FACS from Beckman Coulter, Pasadena, CA, USA). After scoring 10 000 single cells, the percentage of cells that internalized the NPLs (fluorescent cells) and the mean intensity of the fluorescent signal were determined using CytExpert software.

2.6. ROS levels in HUH-7 cells that internalized NPLs

Production of ROS in HUH-7 cells after NPLs internalization was determined by the dihydroethidium (DHE, Calbiochem, USA) assay and measured using a flow cytometer Cytoflex S device (Beckman Coulter CytoFLEX S). A total of 1×10^5 cells per well were seeded in triplicate in 12-well plates in a final 1 mL of DMEM volume and treated with 100 μg mL^{-1} of the different f-NPLs for 1, 3, 24, 48, and 72 h. After detaching, cells were centrifuged at 1200 rpm for 8 min and the medium was removed and replaced with PBS 1×. DHE solution was added to a final concentration of 1 μg mL^{-1} and the cell suspension was incubated for 30 min at 37 °C. DHE signal was determined by flow cytometry using the CytExpert software in 10 000 single cells of the treated population, and in the 10% showing the highest internalization. ROS level in NPLs-treated cells was normalized against non-treated mean, for comparison.

2.7. DNA damage detected by the comet assay

Genotoxic and oxidative DNA damage in HUH-7 cells after 48 h of exposure to NPLs was evaluated using the comet assay, as described.[31] To proceed, 1.5×10^5 cells per well were seeded in duplicate in 12-well plates and treated with the selected NPLs for 48 h. After the exposure time, cells were washed with PBS 1×, trypsinized using TrypLE™ Select Enzyme (1×), collected, and centrifuged at 300 rcf for 8 min at 4 °C. After the supernatant was removed, cells were resuspended in cold PBS at a density of 1×10^6 cells per mL, diluted (1 : 10) in 0.75% low melting point agarose at 37 °C and 7 μL drops of the mix were placed on Gelbond® films (GF, Life Sciences, Vilnius, Lithuania). Every treatment, and its duplicates, was represented with three drops each, and two GF with the same set of samples were processed in parallel. Cell lysis was done by submerging the GF in a cold lysis buffer for 2 h, at 4 °C. GFs were then washed twice for 5 min with cold enzyme buffer and later submerged for 50 min in the same buffer. A second incubation, with previously activated formamidopyrimidine DNA glycosylase (FPG) enzyme, was done at 37 °C for 30 min while the second identical GF was incubated in the same conditions without the enzyme. These GFs were then washed with electrophoresis buffer and then submerged in the same buffer for 25 min, allowing for DNA to unwind before electrophoresis (20 V, 300 mAmp, 25 min). After two washes with cold PBS, the GFs were fixed in absolute ethanol and stained with SYBR Gold (1 : 2500) (TermoFisher Scientitic, Waltham, MA) in TE buffer (10 mM Tris Base, 1 mM EDTA; pH 8). Comets in the films were scored using an Olympus BX50 microscope at 20× magnification and the DNA percentage in the tail was recorded using the Komet 5.5 Image analysis system (Kinetic Imaging Ltd, Liverpool, UK). For genotoxic and oxidative DNA damage, methyl methane sulfonate (MMS) and potassium bromate ($KBrO_3$) were used as positive controls, respectively.

2.8. Cytokine expression

To determine differences in cytokines expression in HUH-7 cells exposed to NPLs (regarding the control), the Proteome Profiler Human Cytokine Array Kit (Bio-Techne R&D Systems, ARY005B. Minneapolis, MO), which detects 36 human cytokines, chemokines, and acute phase proteins simultaneously, was used. A total of 1×10^6 cells were seeded in a 75 cm^2 flask and treated with 100 μg mL^{-1} of different NPLs for 48 h. Cell culture supernatant and cell lysate for each treatment were collected and incubated with the nitrocellulose membrane containing anti-cytokine antibodies, following the manufacturer's instructions. After detecting chemiluminescence from the membrane using ChemiDoc XRS+ System (BioRad, Alcobendas, Spain), the average pixel density of the pair of spots representing each cytokine was determined using the ImageJ program.

To determine the effect of inflammation stimulus, in cells previously exposed to NPLs, cells were exposed to the fluorescent version of PET- and PLA-NPLs for 48 h and cells were sorted using fluorescence-activated cell sorting (FACS) to separate the 50% of the population showing the highest internalization. After seeding these cells, they were treated with lipopolysaccharide (LPS) at 1 μg mL^{-1} for 12 h and differences in cytokines expression were determined using the previously described method. These profiles were compared to those of HUH-7 cells treated with LPS for 12 h after 48 h of incubation without NPLS.

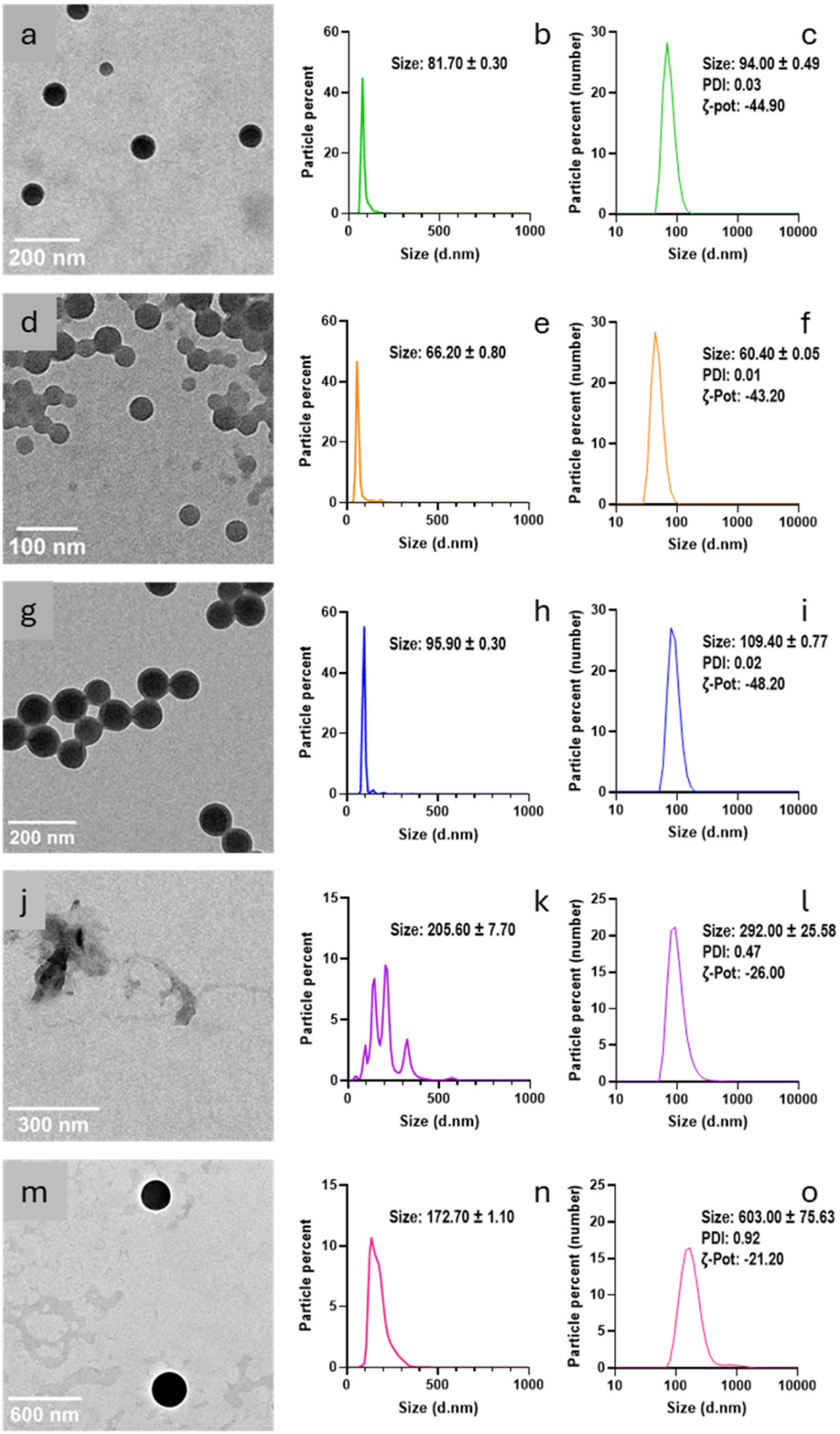

Fig. 1 TEM representative images for PS (a), cPS50 (d), cPS100 (g), PET (j), and PLA (m) NPLs. NTA analysis for the selected NPLs shows a narrow size distribution for PS (b), cPS50 (e), and cPS100 (h), while broader peaks are shown for PET (k) and PLA (n). It is remarkable that multimodal peaks are present for PETNPLs. Hydrodynamic behavior for PS50 (c), cPS50 (f), cPS100 (i), PET (l), and PLA (o) NPLs.

2.9. Statistical analysis

Data was analyzed using the GraphPad Prism Software 7.0 (GraphPad, San Diego, CA). HUH-7 cells after treatment with the different NPLs were compared against non-treated cells using the one-way ANOVA with Dunnett multiple comparisons post-test, and a confidence interval of 95% (n = 3).

3. Results and discussion

3.1. NPL characterization

The maintenance of nanometric-scale characteristics in plastic particle suspensions is crucial for accurately assessing their hazard potential. Therefore, we have adopted an approach aligned with the recommendations of the European Commission,[32] focusing on their size characteristics in the dry state while also evaluating their behavior in suspension. For their dry-state characteristics, we followed previously reported guidelines.[33,34] The shape and size, as assessed by TEM, confirmed a spherical-like morphology for commercially designed particles intended to retain this structure as observed in Fig. 1(a, d and g). Their size distribution was characterized by measuring the Martin diameter of a minimum of 100 nanoparticles, yielding an average size of 76.45 ± 0.02 nm for PS50-NPLs, 46.65 ± 0.01 nm for cPSC50-NPLs, and 97.51 ± 8.64 nm for cPSC100-NPLs. Additionally, the polydispersity index remained consistently low across all samples, recorded at 0.03, 0.04, and 0.01 for PS50-, cPSC50-, and cPSC100-NPLs, respectively. These results are in line with those observed by DLS and NTA, all summarized in Tables S1 and S2, respectively. The little variation in size can be attributed to the high charge of the particles which in all cases for the engineering nanoparticles, the ζ-potentials were higher than −40 mV and therefore the particles in the suspension can be considered stable in terms of electrostatic repulsion.[35] In the electron microscopy analysis, we determined that PET-NPLs exhibit high heterogeneity in terms of particle shape and size (Fig. 1j), which can be considered as a desirable feature when it comes to environmentally representative nanoplastics. However, the submicrometric fraction displays a distribution in which 98.8% of particles are below 500 nm, while the fraction of agglomerates exceeding 1 μm represents only 0.5% of the sample. Consequently, the average particle size in suspension is 176.24 ± 6.52 nm, with hydrodynamic behavior ranging from 200 to 300 nm (Fig. 1j–l). This particle-by-particle behavior, with a small fraction exceeding 500 nm, is evident in Fig. 1k, where the NTA values align with the size description obtained through TEM. This heterogeneity mimics how real-world nanoplastics derived from environmental degradation are unlikely to retain uniform and spherical shapes. Instead, environmental nanoplastics are expected to display a range of irregular forms, surface textures, and sizes due to long-term exposure to mechanical abrasion, photo-oxidation, and chemical weathering.[36,37] Although high-resolution nanoscale characterization of field-collected nanoplastics remains technically limited, emerging studies have documented the presence of polydisperse, non-spherical, and fragmented plastic particles in environmental samples.[38,39] This contrasts with the use of commercially available, monodisperse polystyrene beads, which dominate nanotoxicology literature but may not fully reflect the diversity of particles that organisms are exposed to in real environmental settings.

Regarding suspension stability, the ζ-potential values are near the stability threshold, averaging −26 mV, suggesting that these particles remain relatively stable in suspension. For PLA-NPLs (Fig. 1m–o), the size distribution determined by microscopy is 129.76 ± 1.40 nm, while NTA gives a mean of approximately 172.70 ± 1.10 nm; however, DLS values increase to 603.00 ± 75.63 nm, with a polydispersity index (PDI) that, while low, is the highest among the suspensions analyzed. This discrepancy may be attributed to a reasonably adequate ζ-potential of −21.20 mV which, while relatively good, is not on the range of stability zone (>±30 mV). While excessive agglomeration should not occur, it is well-known that the DLS technique is sensitive to agglomeration occurrences, and their presence can lead to reading errors.[40] The full description of true-to-life PET- and PLA-NPLs for both DLS and NTA values are summarized in Tables S1 and S2, respectively. To confirm the chemical composition of the true-to-life PET- and PLA-NPLs, the obtained FTIR interferograms (Fig. S1) were analysed and contrasted with the representative bands reported in previous studies. The obtained peaks match well with the expected, confirming the PET and PLA nature of the used NPLs.

3.2. NPL toxicity

The human hepatoma-derived HuH-7 cell line is a widely accepted experimental model for studying liver responses, as a substitute for primary hepatocytes.[41] Understanding hepatocyte immune responses to nanoplastics (NPLs) is crucial for clarifying the pathogenesis of NPL-induced liver injury and the broader implications for global health. Hepatocytes play a dual role in immune regulation, acting as both targets and effectors. Recent evidence suggests that NPLs can activate innate immune pathways in hepatocytes, leading to the release of pro-inflammatory cytokines and chemokines. Additionally, NPLs may influence adaptive immune responses through interactions with antigen-presenting cells within the liver microenvironment.[42]

Our findings highlight the notable variation in cellular responses to different nanoplastic types within the same hepatic cell line. Although we observed no direct cytotoxicity (as measured by cell viability), both PLA- and PET-NPLs significantly impacted ROS production, genotoxicity, and cytokine expression in HUH-7 cells, suggesting their potential to induce sub-lethal damage.

Initially, we evaluated HUH-7 cell viability following 48 h exposures to PS-NPLs, carboxylated PS-NPLs (two sizes), PET-NPLs, and PLA-NPLs at concentrations of 50, 100, and 200 μg mL^{-1} (Fig. 2). No significant differences in cell viability were

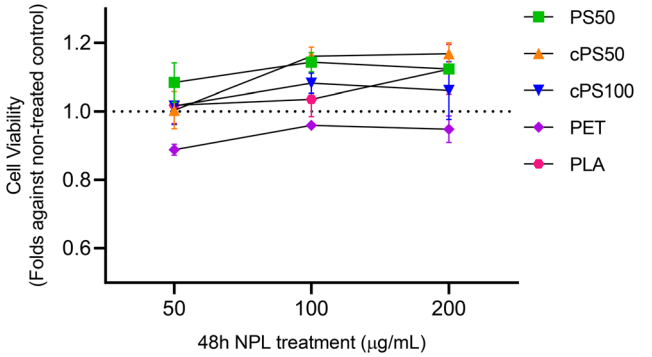

Fig. 2 HUH-7 cell viability after 48 h of treatment with NPLs at 50, 100, and 200 μg mL^{-1}. No significant differences were observed after comparing the fold in cell number of treated cells against the number in the non-treated control when using one-way ANOVA, with Dunnett multiple comparisons post-test and a confidence interval of 95%. Graph represents mean ± SEM fold change against the untreated control (n = 3).

observed across all treatments compared to the control, indicating that short-term exposure to these NPLs does not induce cytotoxicity at the tested concentrations. This lack of an immediate cytotoxic effect could reflect either a resistance specific to this cell line or align with previous studies on nanoplastics, where direct cell death is often absent despite cellular disturbances such as oxidative stress or genotoxicity.[43–45]

While the concentrations of NPLs used in this study are higher than current estimates of environmental exposure levels, this approach is consistent with numerous *in vitro* toxicological studies aimed at uncovering mechanistic insights into cellular responses to these particle exposures. The use of higher concentrations is a well-established strategy to amplify biological signals in a controlled system, and to identify potential pathways of toxicity, especially when investigating emerging contaminants like NPLs, for which standardized exposure metrics and chronic low-dose data are still evolving.[46,47] Moreover, quantifying environmentally relevant internal doses of nanoplastics remains challenging due to variability in particle size, composition, and lack of consensus on exposure metrics.[48] Previous studies have detected MNPLs in human tissues, including lungs, placentas, blood, and even liver samples, confirming human exposure despite low environmental concentrations.[11,13] Given that bioaccumulation, chronic exposure, or co-exposure with other pollutants could enhance toxic effects over time, including these concentrations provides foundational knowledge for risk assessment and helps establish dose–response relationships that may inform future regulatory thresholds.

3.3. NPL internalization

Evaluating NPL internalization is essential when assessing their potential effects. In this study, internalization of NPLs

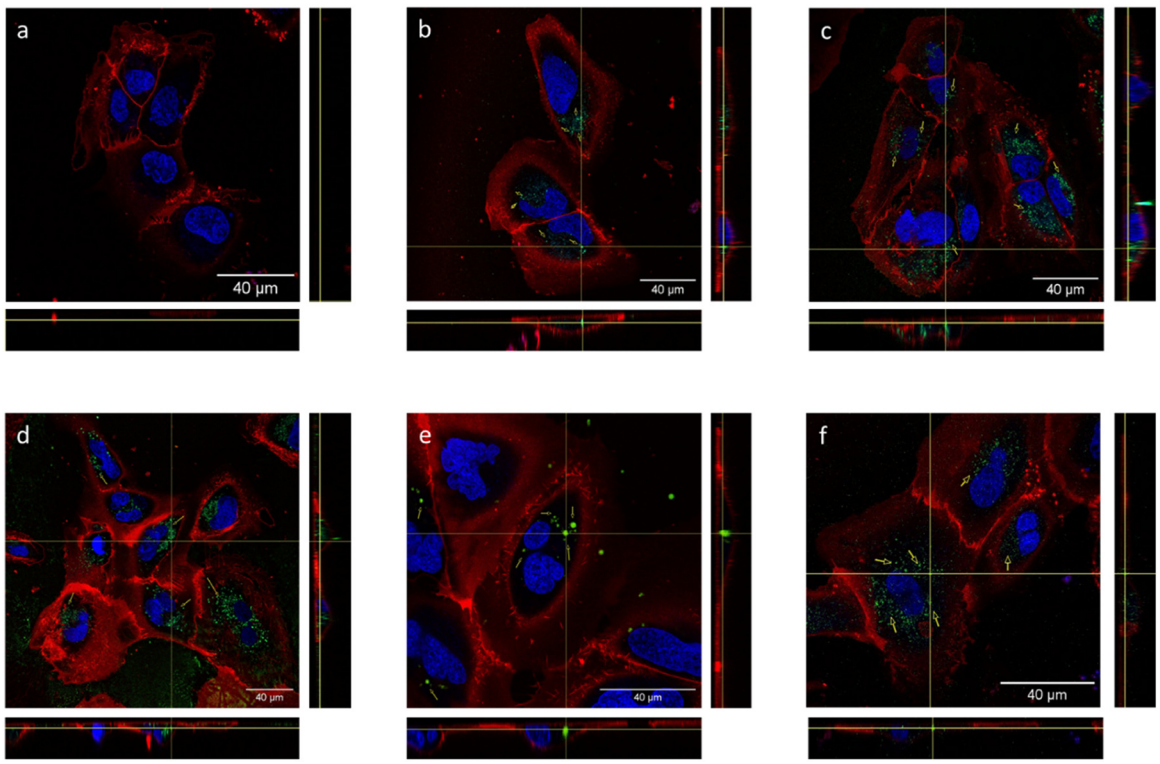

Fig. 3 NPLs internalization in HUH-7 cells after 48 h of treatment using fluorescent/labeled NPLs: a) non-treated control, b) f-PS50-NPLs, c) f-cPS50-NPLs, d) f-cPS100-NPLs, e) f-PET-NPLs, and f) f-PLA-NPLs. Cell nuclei are presented in blue, cell membranes in red, and NPLs in green, annotated with yellow arrows. Orthogonal views are included, showing the different NPLs are inside the cell.

in HUH-7 cells was confirmed using confocal microscopy (Fig. 3) and quantified by flow cytometry (Fig. 4). Confocal microscopy provided visual confirmation of internalization within HUH-7 cells, while flow cytometry allowed quantitative assessment of internalization levels and comparison across different NPL types and exposure times.

The internalization kinetics varied significantly among the NPLs tested. Notably, cPS50-NPLs and PET-NPLs achieved 100% cellular internalization within 1 h, whereas PS50-NPLs took 24 h to reach just 10% internalization. PLA- and cPS100-NPLs exhibited intermediate kinetics, with full internalization observed at 24 and 72 h, respectively. The high internalization rates of the two true-to-life NPLs, representative of secondary environmental NPLs, lend critical insight into their potential relevance. It must be remembered that different fluorophore compounds were used for labelling the different MNPLs and, consequently, differences in detecting the fluorescent signal or intensity could occur. Previous studies have shown that NPL properties such as surface chemistry, size, and functionalization significantly impact cell membrane interactions and uptake efficiency in mammalian cells.[49]

The high internalization rates of PET-NPLs and PLA-NPLs may be linked to their hydrophobicity and chemical composition, as similar findings on cellular uptake have been reported in other studies. Furthermore, the rapid internalization of cPS50-NPLs compared to PS50-NPLs highlights the role of surface characteristics over size in determining internalization efficiency, a finding corroborated by previous studies on other cell types that show enhanced internalization rates of carboxylated PS-NPLs compared to their pristine counterparts. Finally, the delayed but pronounced increase in cPS100-NPL internalization observed at 3 h may be explained by the interplay between their surface carboxylation and size. Carboxyl groups promote stronger electrostatic interactions with the cell membrane, while their diameter around 100 nm corresponds to the optimal size range for clathrin- and caveolae-mediated endocytosis, which typically requires longer vesicle formation times compared to smaller particles. Similar delayed uptake kinetics for carboxylated PS NPLs of this size have been reported in other mammalian cell systems.[49–51]

Internalization was measured in two ways: as the percentage of cells internalizing NPLs and as the amount of NPLs internalized per cell. The latter measurement is especially relevant, as the degree of NPL accumulation has been shown to modulate toxicological responses in cells, such as in mouse macrophages.[52] Accordingly, we assessed accumulation kinetics in HUH-7 cells (Fig. 5). As shown, cPS50-NPLs not only internalized at the highest rate but also reached the highest accumulation per cell over time. Interestingly, the environmentally representative bioplastic model PLA-NPLs also showed significant accumulation over time.

These results support the view that surface characteristics of NPLs significantly influence their internalization kinetics and bioaccumulation potential in cells. Previous studies have found that surface modifications induced by *in vitro* digestion processes can alter PS-NPLs' internalization and toxicological profile in both human liver cells and organisms like zebrafish.[53] Consequently, this study further evaluates whether internalization rates are associated with distinct toxicological profiles in HUH-7 cells.

3.4. ROS induction

Reactive oxygen species (ROS) generation is a well-established mediator of cellular damage and plays a key role in oxidative

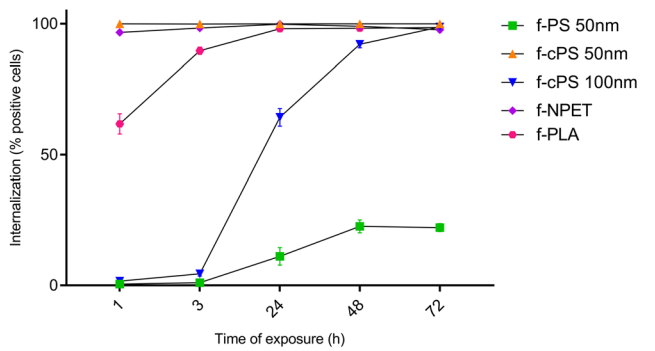

Fig. 4 Cellular internalization of fluorescent/labeled NPLs (f-NPLs) by HUH-7 cells after 1, 3, 24, 48, and 72 h of treatment, using flow cytometry. The dynamic of NPLs internalization is presented as a mean ± SEM percentage of fluorescent cells (n = 3) in a total of 10 000 scored single cells for each point in time.

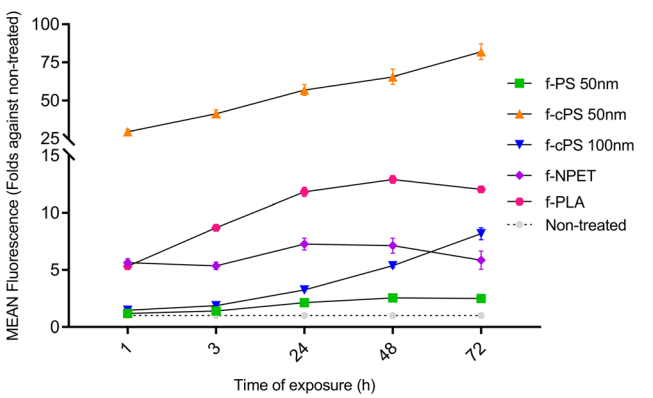

Fig. 5 Mean fluorescence signal of HUH-7 cells with fluorescent-NPLs (f-NPLs) internalization after 1, 3, 24, 48, and 72 h of treatment, using flow cytometry. The average fluorescence signal of the HUH-7 cell population that internalized f-NPLs at each time is taken as an indirect measurement of the amount of NPLs inside each cell and normalized as folds against mean fluorescence of the non-treated control. Significant differences ($p \leq 0.001$) in mean fluorescence compared to the non-treated cells were found at all time points when treated with f-cPS50-, f-PET- and f-PLA-NPLs; and 24, 48 and 72 h when treated with f-PS50- and f-cPS50-NPLs. The one-way ANOVA analysis with Dunnett multiple comparisons post-test and 95% confidence was used for the analysis. The graph shows mean ± SEM of fold change against the non-treated control (n = 3).

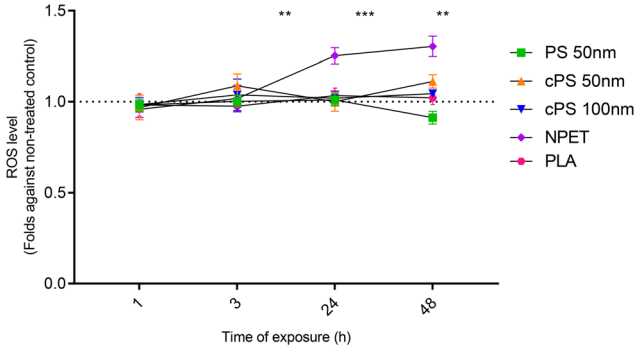

Fig. 6 Determination of ROS levels in HUH-7 cells treated for 1, 3, 24, and 48 h with NPLs. Using flow cytometry sorting, 10% of cells with higher internalization were selected and the average signal in the PE channel for the treated cells was compared to that of the non-treated control. Significant differences in mean fluorescence compared to the non-treated cells were determined using the one-way ANOVA analysis, with Dunnett multiple comparisons post-test and 95% confidence interval (**$p \leq 0.01$, ***$p \leq 0.001$). The graph shows mean ± SEM of fold change against the non-treated control ($n = 3$).

stress-related pathologies, including DNA damage and inflammation, both of which are critical in liver disease progression.[54] ROS levels induced by the selected NPLs are shown in Fig. 6. To better isolate the effects of internalized NPLs, we used cell sorting techniques to select only cells with high levels of internalization.[33] This approach helps prevent the lack of ROS effects in non-internalized cells from masking responses in cells with internalized NPLs.

While overall ROS production did not show a statistically significant increase across all time points and treatments, a marked elevation of ROS levels was observed in cells treated with PET-NPLs, suggesting that the higher internalization rate of these NPLs may lead to localized oxidative stress. The ROS induction in this subpopulation aligns with findings from other studies, which report oxidative stress induction in cells with higher particle uptake.[21,55,56] The pronounced effects of PET observed here are consistent with results from studies in various human cell lines.[24,45,57]

3.5. DNA damage induction

Following the evaluation of oxidative stress potential, we assessed the genotoxic effects of the selected NPLs using the comet assay, which measures both single strand breaks and oxidative DNA base damage. Among the biomarkers for MNPL-induced effects, genotoxicity is especially relevant, given that DNA damage can severely impact cell functionality and, consequently, human health sting.[58] Genotoxicity is crucial in evaluating the potential health impacts of emerging pollutants such as MNPLs. Fig. 7 displays the results from the comet assay.

Among the different NPLs assessed, only PLA exposure produced significant genotoxic damage, evidenced by increased DNA strand breaks in treated cells compared to controls. Notably, none of the NPLs tested induced oxidative damage in DNA bases. Our findings are consistent with previous studies, which have shown PLA-NPLs'

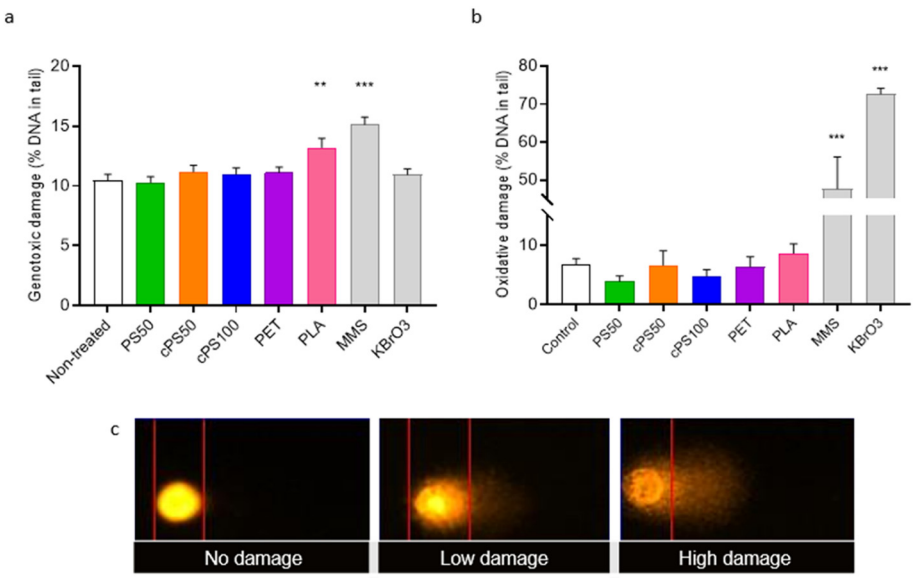

Fig. 7 a) Genotoxic and b) oxidative DNA damage in HUH-7 cells treated with the respective NPL during 48 h. The damage was measured with the comet assay and the percentage of DNA in the tail of the comet used to compare against the non-treated control. After the analysis with the one-way ANOVA tests, Dunnett multiple comparisons post-test, and 95% confidence interval ($n = 3$, **$p \leq 0.01$, ***$p \leq 0.001$), a significative difference was observed for genotoxic damage in the cells treated with PLA when compared to the non-treated control. Methyl methanesulfonate (MMS) and potassium bromate ($KBrO_3$) were used as positive controls for genotoxic damage and oxidative damage, respectively. Graph shows mean ± SEM percentage of DNA in the tail of the comet ($n = 3$). c) Representative images of DNA damage levels scored for the comet assay.

capacity to cause DNA strand breaks in various cell types. For instance, PEG-*b*-PLA exposure has been shown to damage DNA in HT-29 and MCF-7 cells,[59] and PLA induced significant DNA breaks in Calu-3 bronchial epithelial cells, particularly under long-term exposure.[28] Furthermore, *in vivo* studies on *Drosophila* reveal that PLA exposure causes DNA damage in hemocytes, as analogous to lymphocytes in humans.[25]

Though research on the health effects of PLAN-PLs in HUH-7 cells is limited, our findings on their genotoxic potential align with evidence from other cell lines, underscoring the need for further studies into the toxicological profile of this bioplastic degradation product. While the alkaline comet assay used in this case served as a sensitive initial screen for assessing DNA strand breaks and oxidative lesions induced by NPLs exposure in HUH-7 cells, it is important to note that the detection of chromosome loss or breakage and early double-strand breaks would be valuable for future studies.

3.6. Proteome array and cytokine release analysis

The high internalization rates of cPS50-, PLA-, and PET-NPLs can contribute to the induction of cellular damage, which can trigger an inflammatory response. This aligns with the literature suggesting that the surface properties and chemical composition of NPLs strongly dictate their interaction with cellular membranes and their uptake into cells. This interaction type can trigger an immunological response as demonstrated in *ex vivo* studies using human blood cells from healthy donors[33] and in two human cell lines (A549 and THP-1).[60]

To understand the mechanistic of injury susceptibility and damage responses, as well as the discovery of endpoints of effect, the secretome of HUH7cells was analyzed by using the Human XL Cytokine Array Kit, as a fast, sensitive, and economic tool to detect the relative expression levels of 105 soluble human proteins and evaluate changes in cytokine expression between cells exposed to the selected NPLs and the unexposed controls. Growth medium and cell lysates were analyzed to determine differences in cytokine profiles for cells exposed to the different NPLS. Although no significant results were found in the profile after analyzing cell lysates, the cytokines released to the growth medium revealed key insights into the inflammatory responses triggered by the tested NPLs. Fig. 8 presents those cytokines showing important responses to the exposure. As observed, only PET- and PLA-NPLs were able to induce a certain positive release. For PET-NPL-treated cells significant upregulation was observed in ICAM-1, IL-8, MIF, and Serpin E1, indicating a robust pro-inflammatory and tissue-remodeling response. ICAM-1 is a key marker of immune cell adhesion, which suggests that PET-NPLs may facilitate the recruitment of immune cells, potentially amplifying inflammatory responses in the liver. IL-8 further supports this, as it is a potent chemoattractant for neutrophils, linking PET exposure to neutrophil-mediated inflammation, a common feature in liver injury.[61] Additionally, the increase in MIF (macrophage migration inhibitory factor) suggests that PET-NPLs may enhance macrophage activation, contributing to sustained inflammation. Serpin E1, a regulator of extracellular matrix (ECM) degradation, is associated with tissue remodeling and fibrosis, indicating that PET NPLs may induce early fibrotic responses if exposure persists.[17]

It is also important to note that exposure to PS50-NPLs resulted in a general decrease in cytokine expression relative to non-treated controls. This reductive effect is consistent with emerging research showing that PS-NPs can be relatively inert and immunologically silent in hepatic cell models. For instance, Brandts *et al.*[62] demonstrated that PS-NPs largely accumulate in lysosomes of macrophages, as observed also in fish liver cells,[63] but do not trigger significant production of ROS or elevation of inflammatory cytokines such as IL-1β, TNF-α, IL-6, or IL-10.[64] Additionally, tissue slice and *in vitro* studies using PS particles revealed downregulation of IL-1β and IL-10 when corona formation

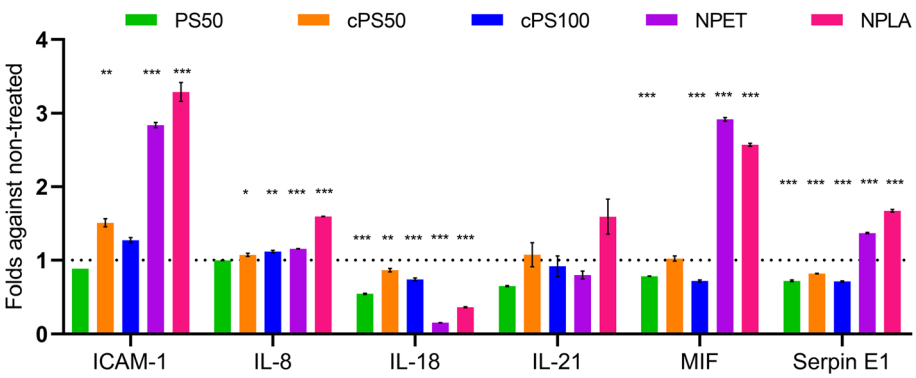

Fig. 8 Analysis of growth factors/cytokines released from HUH-7 cells to the growth medium after 48 h of NPLs treatment using the human cytokine array. Expression is represented as folds against the basal level in non-treated cells, represented by the pointed line in the graph. For the statistical analysis, one-way ANOVA test was used with Dunnett multiple comparisons post-test, and 95% confidence interval (n = 3, *$p \leq 0.05$, **$p \leq 0.01$, ***$p \leq 0.001$).

is allowed by using medium supplemented with serum, indicating that PS exposure can produce a muted inflammatory phenotype rather than a classical upregulated immune response.[65]

The differential cytokine responses observed between PS50-, PET-, and PLA-NPLs further emphasize that nanoplastic characteristics, such as polymer type and surface properties, can distinctly influence cellular behavior and immune modulation. This agrees with findings from previous studies, where PET- and PLA-NPLs have been shown to elicit strong inflammatory responses, but *via* distinct pathways depending on their interaction with cellular receptors and their internalization rates.[28,33] Furthermore, the response induced by PET-NPL and PLA-NPL exposures in liver HUH-7 cells reinforce the view that some characteristics of MNPLs can play pivotal roles in targeting liver as reviewed by different authors.[49,66,67]

To further investigate intracellular responses, cytokine expression was also measured in supernatant and cell lysates of HUH-7 cells exposed to PET- and PLA-NPLs for 48 h, with an additional 12 h LPS treatment to mimic inflammatory stimuli (Fig. 9). Although no significant difference was observed in the supernatant profile, both nanoplastics induced significant upregulation of IL-6, IL-8, IL-18, and Serpin E1 in the lysate of cells exposed under this combination of treatments. This response suggests that PET and PLA not only trigger cytokine secretion but also modulate intracellular signaling pathways involved in immune and inflammatory responses.

Results show that for PET-treated cells, the combination of PET and LPS resulted in significantly elevated levels of IL-6, IL-8, IL-18, and Serpin E1. The sharp increase in IL-6 and IL-8 reflects a potent intracellular inflammatory response, with IL-8 promoting neutrophil chemotaxis and IL-6 driving acute-phase responses.[21] IL-18 further contributes to this inflammatory cascade by promoting the production of IFN-γ, a key cytokine in the immune response to infection.[68] The upregulation of Serpin E1 suggests that PET, especially in combination with LPS, may also stimulate pathways related to extracellular matrix remodeling and fibrosis. Thus, the combined PET-NPLs and LPS treatment appears to exacerbate inflammatory and fibrotic responses, reflecting a synergistic effect between environmental pollutants and microbial stimuli, which could increase the risk of chronic liver inflammation and fibrosis.

For PLA-treated cells, intracellular increases of C5, IL-8, and Serpin E1 were observed after the combined exposure to PLA-NPLs and LPS. The elevation of C5 indicates activation of the complement system, which plays a significant role in inflammation and immune cell recruitment.[69] The increased levels of IL-8 also suggest that neutrophil recruitment is a key response to PLA-NPLs exposure, particularly in the presence of LPS. Interestingly, many other intracellular cytokines were downregulated (below 0.5-fold) compared to the control, suggesting that PLA-NPLs may primarily activate complement and neutrophil-mediated pathways without broadly stimulating other intracellular inflammatory responses. The concurrent increase in Serpin E1 supports the idea that PLA, like PET-NPLs, may induce tissue remodeling and fibrotic changes over time. Interestingly, most of the other cytokines in PLA-treated lysates were expressed at levels significantly below the control, suggesting a suppression of intracellular pro-inflammatory responses for certain cytokines. This could indicate that while PLA-NPLs induces extracellular pro-inflammatory and immune-activating cytokines, its intracellular effects may be more focused on complement activation and neutrophil recruitment, rather than broad pro-inflammatory signaling.

The addition of LPS after 48 h of nanoplastic exposure provides important insights into how environmental

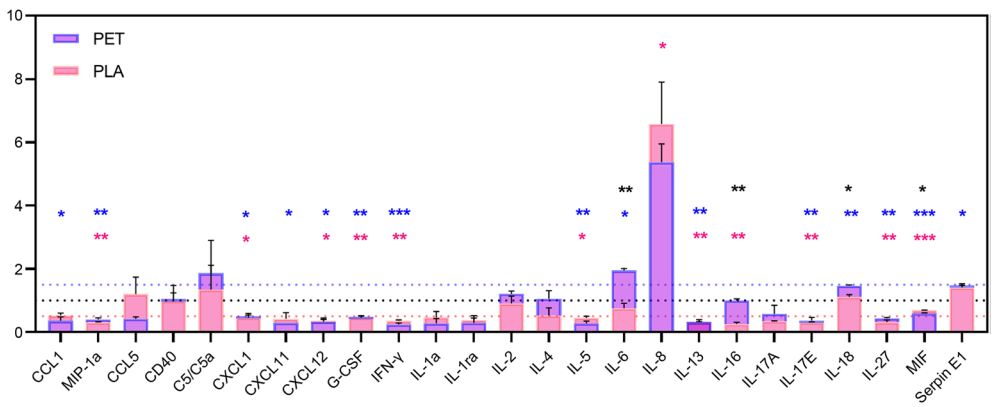

Fig. 9 Analysis of growth factors/cytokines in cell lysis from HUH-7 cells with higher PET and PLA internalization after 48 h and a 12 h treatment with 1 μg mL^{-1} LPS. Expression is represented as folds against the basal level in non-treated cells, represented by the pointed black line in the graph. Cytokines with lower than 0.5 or higher than 1.5 folds compared to the non-treated cells, were included in the analysis. One-way ANOVA analysis, with Dunnett multiple comparisons post-test and 95% confidence interval was used for the analysis (*$p \leq 0.05$, **$p \leq 0.01$, ***$p \leq 0.001$). The graph shows mean ± SEM of fold change against the non-treated control ($n = 3$), with significant differences between NPET and the control in blue *, between the NPLA and the control in red, and between both NPLs in black.

nanoplastics and microbial products can synergize amplifying liver inflammation. LPS is a known activator of the toll-like receptor 4 (TLR4) pathway, which stimulates the release of pro-inflammatory cytokines and chemokines.[70] When combined with nanoplastics like PET or PLA, the presence of LPS appears to amplify inflammatory signaling, resulting in the elevated production of cytokines such as IL-6, IL-8, IL-18, and C5, depending on the nanoplastic type. Thus, the amplified inflammatory response observed after co-treatment with LPS suggests that nanoplastics like PET- and PLA-NPLs could prime hepatocytes for heightened inflammatory sensitivity. This raises concerns about synergistic effects between environmental pollutants and microbial products, which could exacerbate liver inflammation and contribute to the development of chronic liver conditions, including non-alcoholic fatty liver disease (NAFLD) and cirrhosis.[71] The presence of ICAM-1 and IL-6 as key mediators highlights the potential for inflammatory crosstalk between NPL exposure and immune system activation, which could accelerate the progression of liver disease. Moreover, the differential cytokine responses between PLA-NPLs and PET-NPLs suggest that these nanoplastics not only affect oxidative stress pathways but also modulate the immune response in different ways. The strong association between PLA-NPL genotoxicity and IL-18 expression, points toward the activation of pathways involved in cellular damage repair and, possibly, to early fibrotic changes, while PET's induction of IL-6, IL-8, and ICAM-1 suggests a more acute pro-inflammatory response, potentially setting the stage for chronic inflammation if exposure were prolonged.

It is important to address the genotoxic and pro-inflammatory responses in HUH-7 cells after exposure to PLA-NPLs, considering that PLA is widely regarded as a safer and more environmentally friendly bioplastic. However, recent studies have challenged this perception showing these NPLs induce oxidative stress, DNA damage, and inflammatory gene activation *in vivo*, such as in *Drosophila melanogaster* larvae models.[25] *In vitro* studies also demonstrate that UV-aged PLA films release surface-modified nanoplastics with increased reactivity, capable of inducing cytotoxicity and inflammation comparable to that of conventional plastics.[72] The effects have been linked to changes in surface chemistry, such as the appearance of carbonyl or hydroxyl groups, as well as the presence of residual monomers or additives used in commercial PLA formulations. These findings align with the results of the present study and reinforce that bioplastics like PLA can have cytotoxic effects and should be assessed with the same level of scrutiny as conventional petroleum-based plastics when considering potential impacts on human and environmental health. Future studies will be essential to evaluate how environmental degradation, aging, or additive leaching may modulate the toxicity profile of PLA-based materials.

4. Conclusion

This study underscores the importance of evaluating the specific characteristics of nanoplastics (NPLs), such as polymer type, surface charge, and size, when assessing their biological effects. Determining internalization ability and kinetics over time are essential parameters for understanding NPLs' biological impact. Significant differences in cell uptake were observed, notably highlighting the influence of surface charge, as carboxylated PS-NPLs showed high internalization efficiency compared to their pristine counterparts. The robust internalization of PET- and PLA-NPLs may be attributed to surface modifications introduced during their preparation, underscoring the need for realistic environmental analogs in toxicological studies.

Interestingly, efficient internalization alone does not necessarily predict harmful cellular outcomes, as evidenced by pristine PS50-NPLs, which demonstrated high internalization yet minimal adverse effects. This indicates that a specific cell line, such as HUH-7, may exhibit distinct responses to different NPLs, with notable implications for liver health concerning chronic inflammation, fibrosis, and carcinogenesis risk. In our study, PET-NPLs and PLA-NPLs notably induced a range of responses in hepatic cells, including ROS production, genotoxicity, and cytokine release, highlighting the significance of true-to-life MNPLs as representatives of environmentally relevant secondary MNPLs.

Further research is needed to investigate the long-term effects of these nanoplastics, including their internalization kinetics, in hepatic cells and their potential role in liver disease progression.

Author contributions

All authors contributed to the article and approved the submitted version.

Conceptualization: RM and AH; funding acquisition: AH; investigation: MMR, AV, JAA, JMP, SP, RE, and IB; methodology: MMR and AV; resources: JFF; supervision: AH and RM; writing – original draft: MMR; writing – review and editing: RM and AH.

Conflicts of interest

The authors declare that they have no known competing financial interests or personal relationships that could have appeared to influence the work reported in this paper.

Data availability

Supplementary information is available. See DOI: **https://doi.org/10.1039/D5EN00434A**.

Data will be available under request.

Acknowledgements

MMR and JMP hold Ph.D. fellowships from the Generalitat de Catalunya. AV was supported by a Ph.D. fellowship from the National Agency for Research and Development (ANID); Nucleo de Investigación en Ciencias Biológicas., CONICYT PFCHA/DOCTORADO BECAS CHILE/202072210237. IB (Academic record 2023 BP 00212) was granted with a Beatriu de Pinós Postdoctoral Program from the Secretariat of Universities and Research of the Department of Business and Knowledge of the Government of Catalunya. AH was granted an ICREA ACADEMIA award. This project (Plasticheal) has received funding from the European Union's Horizon 2020 research and innovation programme under grant agreement No. 965196. This work was partially supported by the Spanish Ministry of Science and Innovation [PID2020-116789, RB-C43] and the Generalitat de Catalunya (2021-SGR-00731).

References

1 R. Geyer, J. R. Jambeck and K. L. Law, Production, use, and fate of all plastics ever made, *Sci. Adv.*, 2017, **3**(7), e1700782, DOI: **10.1126/sciadv.1700782**.

2 A. Pradel, C. Catrouillet and J. Gigault, The environmental fate of nanoplastics: what we know and what we need to know about aggregation, *NanoImpact*, 2023, **29**, 100453, DOI: **10.1016/j.impact.2023.100453**.

3 D. Materić, R. Holzinger and H. Niemann, Nanoplastics and ultrafine microplastic in the Dutch Wadden Sea—the hidden plastics debris?, *Sci. Total Environ.*, 2022, **846**, 157371, DOI: **10.1016/j.scitotenv.2022.157371**.

4 G. F. Vasse and B. N. Melgert, Microplastic and plastic pollution: impact on respiratory disease and health, *Eur.. Respir. Rev.*, 2024, **33**(172), 230226, DOI: **10.1183/16000617.0226-2023**.

5 S. L. Wright and F. J. Kelly, Plastic and human health: a micro issue?, *Environ. Sci. Technol.*, 2017, **51**(12), 6634–6647, DOI: **10.1021/acs.est.7b00423**.

6 M. B. Paul, V. Stock, J. Cara-Carmona, E. Lisicki, S. Shopova and V. Fessard, *et al.* Micro- and nanoplastics: current state of knowledge with the focus on oral uptake and toxicity, *Nanoscale Adv.*, 2020, **2**(10), 4350–4367, DOI: **10.1039/d0na00539h**.

7 G. Banaei, A. García-Rodríguez, A. Tavakolpournegari, J. Martín-Pérez, A. Villacorta and R. Marcos, *et al.* The release of polylactic acid nanoplastics (PLA-NPLs) from commercial teabags: obtention, characterization, and hazard effects of true-to-life PLA-NPLs, *J. Hazard. Mater.*, 2023, **458**, 131899, DOI: **10.1016/j.jhazmat.2023.131899**.

8 P. Schwabl, S. Köppel, P. Königshofer, T. Bucsics, M. Trauner and T. Reiberger, *et al.* Detection of various microplastics in human stool: a prospective case series, *Ann. Intern. Med.*, 2019, **171**(7), 453–457, DOI: **10.7326/M19-0618**.

9 C. Pironti, V. Notarstefano, M. Ricciardi, O. Motta, E. Giorgini and L. Montano, First evidence of microplastics in human urine: a preliminary study of intake in the human body, *Toxics*, 2022, **11**(1), 40, DOI: **10.3390/toxics11010040**.

10 G. Chen, Q. Feng and J. Wang, Mini-review of microplastics in the atmosphere and their risks to humans, *Sci. Total Environ.*, 2020, **703**, 135504, DOI: **10.1016/j.scitotenv.2019.135504**.

11 L. C. Jenner, J. M. Rotchell, R. T. Bennett, M. Cowen, V. Tentzeris and L. R. Sadofsky, Detection of microplastics in human lung tissue using μFTIR spectroscopy, *Sci. Total Environ.*, 2022, **831**, 154907, DOI: **10.1016/j.scitotenv.2022.154907**.

12 N. Ali, J. Katsouli, E. L. Marczylo, T. W. Gant, S. Wright and J. Bernardino de la Serna, The potential impacts of micro-and-nano plastics on various organ systems in humans, *EBioMedicine*, 2024, **99**, 104901, DOI: **10.1016/j.ebiom.2023.104901**.

13 A. Ragusa, A. Svelato, C. Santacroce, P. Catalano, V. Notarstefano and O. Carnevali, *et al.* Plasticenta: first evidence of microplastics in human placenta, *Environ. Int.*, 2021, **146**, 106274, DOI: **10.1016/j.envint.2020.106274**.

14 S. Alqahtani, S. Alqahtani, Q. Saquib and F. Mohiddin, Toxicological impact of microplastics and nanoplastics on humans: understanding the mechanistic aspect of the interaction, *Front. Toxicol.*, 2023, **5**, 1193386, DOI: **10.3389/ftox.2023.1193386**.

15 R. Marfella, F. Prattichizzo, C. Sardu, G. Fulgenzi, L. Graciotti and T. Spadoni, *et al.* Microplastics and nanoplastics in atheromas and cardiovascular events, *N. Engl. J. Med.*, 2024, **390**(10), 900–910, DOI: **10.1056/nejmoa2309822**.

16 Y. Ge, S. Yang, T. Zhang, X. Wan, Y. Zhu and F. Yang, *et al.* The hepatotoxicity assessment of micro/nanoplastics: a preliminary study to apply the adverse outcome pathways, *Sci. Total Environ.*, 2023, **902**, 165659, DOI: **10.1016/j.scitotenv.2023.165659**.

17 T. Horvatits, M. Tamminga, B. Liu, M. Sebode, A. Carambia and L. Fischer, *et al.* Microplastics detected in cirrhotic liver tissue, *EBioMedicine*, 2022, **82**, 104147, DOI: **10.1016/j.ebiom.2022.104147**.

18 N. Zitouni, N. Bousserrhine, O. Missawi, I. Boughattas, N. Chèvre and R. Santos, *et al.* Uptake, tissue distribution and toxicological effects of environmental microplastics in early juvenile fish Dicentrarchus labrax, *J. Hazard. Mater.*, 2021, **403**, 124055, DOI: **10.1016/j.jhazmat.2020.124055**.

19 X. Fan, X. Wei, H. Hu, B. Zhang, D. Yang and H. Du, *et al.* Effects of oral administration of polystyrene nanoplastics on plasma glucose metabolism in mice, *Chemosphere*, 2022, **288**, 132607, DOI: **10.1016/j.chemosphere.2021.132607**.

20 Y. He, J. Li, J. Chen, X. Miao, G. Li and Q. He, *et al.* Cytotoxic effects of polystyrene nanoplastics with different surface functionalization on human HepG2 cells, *Sci. Total Environ.*, 2020, **723**, 138180, DOI: **10.1016/j.scitotenv.2020.138180**.

21 K. R. Yang, X. Cheng, C. Guo, X. Xing and H. Sun, *et al.* Accumulation of polystyrene microplastics induces liver fibrosis by activating cGAS/STING pathway, *Environ. Pollut.*, 2022, **300**, 118986, DOI: **10.1016/j.envpol.2022.118986**.

22 L. M. Martin, N. Gan, E. Wang, M. Merrill and W. Xu, Materials, surfaces, and interfacial phenomena in nanoplastics toxicology research, *Environ. Pollut.*, 2022, **292**, 118442, DOI: **10.1016/j.envpol.2021.118442**.

23 C. L. Mills, J. Savanagouder, M. de Almeida Monteiro Melo Ferraz and M. J. Noonan, The need for environmentally realistic studies on the health effects of terrestrial microplastics, *Microplast. Nanoplast.*, 2023, **3**(1), 11, DOI: **10.1186/s43591-023-00059-1**.

24 A. Villacorta, L. Rubio, M. Alaraby, M. López-Mesas, V. Fuentes-Cebrian and O. H. Moriones, *et al.* A new source of representative secondary PET nanoplastics: obtention, characterization, and hazard evaluation, *J. Hazard. Mater.*, 2022, **439**, 129593, DOI: **10.1016/j.jhazmat.2022.129593**.

25 M. Alaraby, D. Abass, M. Farre, A. Hernández and R. Marcos, Are bioplastics safe? Hazardous effects of polylactic acid (PLA) nanoplastics in Drosophila, *Sci. Total Environ.*, 2024, **919**, 170592, DOI: **10.1016/j.scitotenv.2024.170592**.

26 A. Villacorta, L. Vela, M. Morataya-Reyes, R. Llorens-Chiralt, L. Rubio and M. Alaraby, *et al.* Titanium-doped PET nanoplastics of environmental origin as a true-to-life model of nanoplastic, *Sci. Total Environ.*, 2023, **880**, 163151, DOI: **10.1016/j.scitotenv.2023.163151**.

27 A. Villacorta, C. Cazorla-Ares, V. Fuentes-Cebrian, I. H. Valido, L. Vela and F. Carrillo-Navarrete, *et al.* Fluorescent labeling of micro/nanoplastics for biological applications with a focus on "true-to-life" tracking, *J. Hazard. Mater.*, 2024, **476**, 135134, DOI: **10.1016/j.jhazmat.2024.135134**.

28 A. García-Rodríguez, J. Gutiérrez, A. Villacorta, J. Arribas Arranz, I. Romero-Andrada and A. Lacoma, *et al.* Polylactic acid nanoplastics (PLA-NPLs) induce adverse effects on an in vitro model of the human lung epithelium: the Calu-3 air-liquid interface (ALI) barrier, *J. Hazard. Mater.*, 2024, **475**, 134900, DOI: **10.1016/j.jhazmat.2024.134900**.

29 A. Nazrin, S. M. Sapuan and M. Y. M. Zuhri, Mechanical, physical and thermal properties of sugar palm nanocellulose reinforced thermoplastic starch (TPS)/poly(lactic acid) (PLA) blend bionanocomposites, *Polymer*, 2020, **12**(10), 2216, DOI: **10.3390/polym12102216**.

30 L. M. Johnson, J. B. Mecham, S. A. Krovi, M. M. Moreno Caffaro, S. Aravamudhan and A. L. Kovach, *et al.* Fabrication of polyethylene terephthalate (PET) nanoparticles with fluorescent tracers for studies in mammalian cells, *Nanoscale Adv.*, 2021, **3**(2), 339–346, DOI: **10.1039/d0na00888e**.

31 A. Collins, P. Møller, G. Gajski, S. Vodenková, A. Abdulwahed and D. Anderson, *et al.* Measuring DNA modifications with the comet assay: a compendium of protocols, *Nat. Protoc.*, 2023, **18**(3), 929–989, DOI: **10.1038/s41596-022-00754-y**.

32 European Commission, Commission recommendation of 10 June 2022 on the definition of nanomaterial [Internet], 2022 Jun 10 [cited 2025 Sep 4]. Available from: **https://eur-lex.europa.eu/legal-content/EN/TXT/PDF/?uri=CELEX:32022H0614(01)**.

33 J. Arribas Arranz, A. Villacorta, L. Rubio, A. García-Rodríguez, G. Sánchez and M. Llorca, *et al.* Kinetics and toxicity of nanoplastics in ex vivo exposed human whole blood as a model to understand their impact on human health, *Sci. Total Environ.*, 2024, **948**, 174725, DOI: **10.1016/j.scitotenv.2024.174725**.

34 J. Domenech, A. Villacorta, J. Ferrer, R. Llorens-Chiralt, R. Marcos and A. Hernández, *et al.* In vitro cell-transforming potential of secondary polyethylene terephthalate and polylactic acid nanoplastics, *J. Hazard. Mater.*, 2024, **469**, 134030, DOI: **10.1016/j.jhazmat.2024.134030**.

35 A. L. Onugwu, C. S. Nwagwu, O. S. Onugwu, A. C. Echezona, C. P. Agbo and S. A. Ihim, *et al.* Nanotechnology-based drug delivery systems for the treatment of anterior segment eye diseases, *J. Controlled Release*, 2023, **354**, 465–488, DOI: **10.1016/j.jconrel.2023.01.018**.

36 Y. Zhang, S. Kang, S. Allen, D. Allen, T. Gao and M. Sillanpää, Atmospheric microplastics: a review on current status and perspectives, *Earth-Sci. Rev.*, 2020, **203**, 103118, DOI: **10.1016/j.earscirev.2020.103118**.

37 M. Enfrin, L. F. Dumée and J. Lee, Nano/microplastics in water and wastewater treatment processes—origin, impact and potential solutions, *Water Res.*, 2019, **161**, 621–638, DOI: **10.1016/j.watres.2019.06.049**.

38 M. Kooi and A. A. Koelmans, Simplifying microplastic via continuous probability distributions for size, shape, and density, *Environ. Sci. Technol. Lett.*, 2019, **6**(9), 551–557, DOI: **10.1021/acs.estlett.9b00379**.

39 A. Catarino, D. Patsiou, S. Summers, G. Everaert, T. Henry and T. Gutierrez, Challenges and recommendations in experimentation and risk assessment of nanoplastics in aquatic organisms, *TrAC, Trends Anal. Chem.*, 2023, **167**, 117262, DOI: **10.1016/j.trac.2023.117262**.

40 S. Bhattacharjee, DLS and zeta potential—what they are and what they are not?, *J. Controlled Release*, 2016, **235**, 337–351, DOI: **10.1016/j.jconrel.2016.06.017**.

41 E. Jouan, M. Le Vée, C. Denizot, Y. Parmentier and O. Fardel, Drug transporter expression and activity in human hepatoma HuH-7 cells, *Pharmaceutics*, 2016, **9**(1), 3, DOI: **10.3390/pharmaceutics9010003**.

42 X. Wang, K. Deng, P. Zhang, Q. Chen, J. T. Magnuson and W. Qiu, *et al.* Microplastic-mediated new mechanism of liver damage: from the perspective of the gut-liver axis, *Sci. Total Environ.*, 2024, **919**, 170962, DOI: **10.1016/j.scitotenv.2024.170962**.

43 Q. Shi, J. Tang, R. Liu and L. Wang, Toxicity in vitro reveals potential impacts of microplastics and nanoplastics on human health: a review, *Crit. Rev. Environ. Sci. Technol.*, 2021, **52**(21), 3863–3895, DOI: **10.1080/10643389.2021.1951528**.

44 A. Khan and Z. Jia, Recent insights into uptake, toxicity, and molecular targets of microplastics and nanoplastics relevant to human health impacts, *iScience*, 2023, **26**(2), 106061, DOI: **10.1016/j.isci.2023.106061**.

45 A. Tavakolpournegari, B. Annangi, A. Villacorta, G. Banaei, J. Martin and S. Pastor, *et al.* Hazard assessment of different-sized polystyrene nanoplastics in hematopoietic human cell

lines, *Chemosphere*, 2023, **325**, 138360, DOI: **10.1016/j.chemosphere.2023.138360**.

46 M. S.-L. Yee, L.-W. Hii, C. K. Looi, W.-M. Lim, S.-F. Wong and Y.-Y. Kok, *et al.* Impact of microplastics and nanoplastics on human health, *Nanomaterials*, 2021, **11**(2), 496, DOI: **10.3390/nano11020496**.

47 M. Sendra, P. Pereiro, M. Yeste, L. Mercado, A. Figueras and B. Novoa, Size matters: zebrafish (Danio rerio) as a model to study toxicity of nanoplastics from cells to the whole organism, *Environ. Pollut.*, 2021, **268**, 115769, DOI: **10.1016/j.envpol.2020.115769**.

48 A. D. Vethaak and J. Legler, Microplastics and human health, *Science*, 2021, **371**(6530), 672–674, DOI: **10.1126/science.abe5041**.

49 A. Banerjee and W. L. Shelver, Micro- and nanoplastic induced cellular toxicity in mammals: a review, *Sci. Total Environ.*, 2021, **755**, 142518, DOI: **10.1016/j.scitotenv.2020.142518**.

50 S. Mazumdar, D. Chitkara and A. Mittal, Exploration and insights into the cellular internalization and intracellular fate of amphiphilic polymeric nanocarriers, *Acta Pharm. Sin. B*, 2021, **11**(4), 903–924, DOI: **10.1016/j.apsb.2021.02.019**.

51 J. Martín-Pérez, A. Villacorta, G. Banaei, M. Morataya-Reyes, A. Tavakolpournegari and R. Marcos, *et al.* Hazard assessment of nanoplastics is driven by their surface-functionalization: effects in human-derived primary endothelial cells, *Sci. Total Environ.*, 2024, **934**, 173236, DOI: **10.1016/j.scitotenv.2024.173236**.

52 V. Collin-Faure, M. Vitipon, A. Torres, O. Tanyeres, B. Dalzon and T. Rabilloud, The internal dose makes the poison: higher internalization of polystyrene particles induce increased perturbation of macrophages, *Front. Immunol.*, 2023, **14**, 1092743, DOI: **10.3389/fimmu.2023.1092743**.

53 N. Yan, Y. Wang, T. Y. Wong, Y. Hu, H. Xu and A. Parodi, *et al.* Surface topography of nanoplastics modulates their internalization and toxicity in liver cells, *Environ. Sci.:Nano*, 2023, **10**, 2685, DOI: **10.1039/D3EN00347G**.

54 H. Sies and D. P. Jones, Reactive oxygen species (ROS) as pleiotropic physiological signalling agents, *Nat. Rev. Mol. Cell Biol.*, 2020, **21**, 363–383, DOI: **10.1038/s41580-020-0230-3**.

55 Y. F. Yang, C. Y. Chen, T. H. Lu and C. M. Liao, Toxicity-based toxicokinetic/toxicodynamic assessment for bioaccumulation of polystyrene microplastics in mice, *J. Hazard. Mater.*, 2019, **366**, 703–713, DOI: **10.1016/j.jhazmat.2018.12.048**.

56 P. Das and S. Medhi, Role of inflammasomes and cytokines in immune dysfunction of liver cirrhosis, *Cytokine*, 2023, **170**, 156347, DOI: **10.1016/j.cyto.2023.156347**.

57 L. Ma, Z. Wu, Z. Lu, L. Yan, X. Dong and Z. Dai, *et al.* Differences in toxicity induced by the various polymer types of nanoplastics on HepG2 cells, *Sci. Total Environ.*, 2024, **918**, 170664, DOI: **10.1016/j.scitotenv.2024.170664**.

58 M. Carbone, S. T. Arron, B. Beutler, A. Bononi, W. Cavenee and J. E. Cleaver, *et al.* Tumour predisposition and cancer syndromes as models to study gene-environment interactions, *Nat. Rev. Cancer*, 2020, **20**(9), 533–549, DOI: **10.1038/s41568-020-0265-y**.

59 K. Koňáriková, G. Girašková, I. Žitňanová, M. Dvořáková, E. Rollerová and S. Scsuková, *et al.* Biological analyses of the effects of TiO2 and PEG-b-PLA nanoparticles on three-dimensional spheroid-based tumor, *Physiol. Res.*, 2023, **72**(S3), S257–S266, DOI: **10.33549/physiolres.935152**.

60 L. Antonio, G. Visalli, A. Facciolà, C. Saija, M. P. Bertuccio and B. Baluce, *et al.* Sterile inflammation induced by respirable micro and nano polystyrene particles in the pathogenesis of pulmonary diseases, *Toxicol. Res.*, 2024, **13**(5), tfae138, DOI: **10.1093/toxres/tfae138**.

61 A. Teijeira, S. Garasa, M. C. Ochoa, A. Cirella, I. Olivera and J. Glez-Vaz, *et al.* Differential interleukin-8 thresholds for chemotaxis and NETosis in human neutrophils, *Eur. J. Immunol.*, 2021, **51**(9), 2274–2280, DOI: **10.1002/eji.202049029**.

62 I. Brandts, R. Solà, M. Garcia-Ordoñez, A. Gella, A. Quintana and B. Martin, *et al.* Polystyrene nanoplastics target lysosomes interfering with lipid metabolism through the PPAR system and affecting macrophage functionalization, *Environ. Sci.:Nano*, 2023, **10**(9), 2245–2258, DOI: **10.1039/d2en01077a**.

63 H. Cheng, Z. Duan, Y. Wu, Y. Wang, H. Zhang and Y. Shi, *et al.* Immunotoxicity responses to polystyrene nanoplastics and their related mechanisms in the liver of zebrafish (Danio rerio) larvae, *Environ. Int.*, 2022, **161**, 107128, DOI: **10.1016/j.envint.2022.107128**.

64 A. Weber, A. Schwiebs, H. Solhaug, J. Stenvik, A. M. Nilsen and M. Wagner, *et al.* Nanoplastics affect the inflammatory cytokine release by primary human monocytes and dendritic cells, *Environ. Int.*, 2022, **163**, 107173, DOI: **10.1016/j.envint.2022.107173**.

65 R. Bartucci, A. Z. van der Meer, Y. L. Boersma, P. Olinga and A. Salvati, Nanoparticle-induced inflammation and fibrosis in ex vivo murine precision-cut liver slices and effects of nanoparticle exposure conditions, *Arch. Toxicol.*, 2021, **95**(4), 1267–1285, DOI: **10.1007/s00204-021-02992-7**.

66 J. Yin, Y. Ju, H. Qian, J. Wang, X. Miao and Y. Zhu, *et al.* Nanoplastics and microplastics may be damaging our livers, *Toxics*, 2022, **10**(10), 586, DOI: **10.3390/toxics10100586**.

67 S. Haldar, N. Yhome, Y. Muralidaran, S. Rajagopal and P. Mishra, Nanoplastics toxicity specific to liver in inducing metabolic dysfunction—a comprehensive review, *Genes*, 2023, **14**(3), 590, DOI: **10.3390/genes14030590**.

68 C. A. Dinarello, D. Novick, S. Kim and G. Kaplanski, Interleukin-18 and IL-18 binding protein, *Front. Immunol.*, 2013, **4**, 289, DOI: **10.3389/fimmu.2013.00289**.

69 C. W. Strey, M. Markiewski, D. Mastellos, R. Tudoran, L. A. Spruce and L. E. Greenbaum, *et al.* The proinflammatory mediators C3a and C5a are essential for liver regeneration, *J. Exp. Med.*, 2003, **198**(6), 913–923, DOI: **10.1084/jem.20030374**.

70 S. Akira, S. Uematsu and O. Takeuchi, Pathogen recognition and innate immunity, *Cell*, 2006, **124**(4), 783–801, DOI: **10.1016/j.cell.2006.02.015**.

71 A. Das, The emerging role of microplastics in systemic toxicity: involvement of reactive oxygen species (ROS), *Sci. Total Environ.*, 2023, **895**, 165076, DOI: **10.1016/j.scitotenv.2023.165076**.

72 X. Wu, H. Zhang, J. Chen, F. Tan, R. Cai and Y. Wang, Photoaging promotes toxic micro/nanoplastics release from PLA/PBAT biodegradable plastic in gastrointestinal condition, *Environ. Health*, 2025, **3**(5), 446–457, DOI: **10.1021/envhealth.4c00209**.

3.2. Chapter 2 (Article 2)

Biological Impact of True-to-Life PET and Titanium-Doped PET Nanoplastics on Human-Derived Monocyte (THP-1) Cells.

Nanomaterials, 15(13), 1040. (2025)

Doi: 10.3390/nano15131040

Impact Factor: 4.3 (2024)

nanomaterials

MDPI

Article

Biological Impact of True-to-Life PET and Titanium-Doped PET Nanoplastics on Human-Derived Monocyte (THP-1) Cells

Aliro Villacorta [1,2,*,†], Michelle Morataya-Reyes [1,†], Lourdes Vela [1,3], Jéssica Arribas Arranz [1], Joan Martín-Perez [1], Irene Barguilla [1], Ricard Marcos [1] and Alba Hernández [1,*]

[1] Group of Mutagenesis, Department of Genetics and Microbiology, Faculty of Biosciences, Universitat Autònoma de Barcelona, 08193 Cerdanyola del Vallès, Spain; herlem.morataya@uab.cat (M.M.-R.); lulis002@hotmail.com (L.V.); jessica.arribas@uab.cat (J.A.A.); juan.martin.perez@uab.cat (J.M.-P.); irene.barguilla@uab.cat (I.B.); ricard.marcos@uab.cat (R.M.)
[2] Facultad de Recursos Naturales Renovables, Universidad Arturo Prat, Iquique 101000, Chile
[3] Faculty of Health Sciences Eugenio Espejo, Universidad UTE, Quito 170508, Ecuador
* Correspondence: avillaco@unap.cl (A.V.); alba.hernandez@uab.cat (A.H.)
† These authors contributed equally to this work.

Abstract

In the environment, plastic waste degrades into small particles known as microplastics and nanoplastics (MNPLs), depending on their size. Given the potential harmful effects associated with MNPL exposure, it is crucial to develop environmentally representative particles for hazard assessment. These so-called true-to-life MNPLs are generated through in-house degradation of real-world plastic products. In this study, we produced titanium-doped nanoplastics (NPLs) from opaque polyethylene terephthalate (PET) milk bottles, which contain titanium dioxide as a filler. The resulting PET(Ti)-NPLs were thoroughly characterized using scanning electron microscopy (SEM), energy-dispersive X-ray spectroscopy (EDS), mass spectrometry (MS), dynamic light scattering (DLS), ζ-potential measurements, transmission electron microscopy (TEM), and Fourier-transform infrared (FTIR) spectroscopy. Human-derived THP-1 monocytes were employed to investigate particle uptake kinetics, dosimetry, and genotoxicity. A combination of flow cytometry and inductively coupled plasma mass spectrometry (ICP-MS) enabled the quantification of internalized particles, while the comet assay assessed DNA damage. The results revealed dose- and time-dependent effects of PET(Ti)-NPLs on THP-1 cells, particularly in terms of internalization. Titanium doping facilitated detection and influenced genotoxic outcomes. This study demonstrates the relevance of using environmentally representative nanoplastic models for evaluating human health risks and underscores the importance of further mechanistic research.

Keywords: nanoplastics; polyethylene terephthalate (PET); tru-to life MNPLs

Academic Editor: Fernanda Cássio

Received: 12 June 2025
Revised: 30 June 2025
Accepted: 1 July 2025
Published: 4 July 2025

Citation: Villacorta, A.; Morataya-Reyes, M.; Vela, L.; Arribas Arranz, J.; Martín-Perez, J.; Barguilla, I.; Marcos, R.; Hernández, A. Biological Impact of True-to-Life PET and Titanium-Doped PET Nanoplastics on Human-Derived Monocyte (THP-1) Cells. *Nanomaterials* **2025**, *15*, 1040. https://doi.org/10.3390/nano15131040

1. Introduction

The growing accumulation of plastic waste in the environment has become a major global concern. Of relevance is the widespread presence of plastic degradation products, broadly termed microplastics (MPLs), which pose potential health risks that remain poorly understood [1]. First introduced by Thompson et al. [2], the term "microplastic" typically refers to plastic fragments smaller than 5 mm. While this definition remains operational, it has been widely debated [3], as it inadequately accounts for the critical role of particle size in biological interactions. Smaller particles have a higher likelihood of being internalized by

living organisms, including humans. To address this, we adopt a size-based classification in which nanoplastics (NPLs) range from 1 to 1000 nm and MPLs from 1 to 1000 µm [4]. Environmental degradation of plastic waste, driven by various abiotic and biotic factors, produces a heterogeneous mixture of micro- and nanoplastic particles (MNPLs). As degradation progresses, the mixture becomes increasingly diverse in size, necessitating the use of the inclusive term micro/nanoplastics (MNPLs) to reflect the continuum of particle sizes found in environmental samples.

Beyond particle size, other features—such as polymer type, additives, and shape—also influence MNPL toxicity. While numerous studies have recently explored the potential adverse effects of MNPLs [5,6], most have used commercially available, pristine polystyrene MNPLs (PS-MNPLs) due to their accessibility. However, for more realistic risk assessments, there is a critical need to evaluate environmentally representative MNPLs generated from actual plastic waste. To address this, true-to-life MNPLs have been proposed [7]. These particles are produced by in-house degradation of consumer plastic items using mechanical methods, resulting in (1) polymeric compositions reflective of real environmental pollutants, (2) diverse morphologies and sizes, (3) the inclusion of additives used in commercial products, and (4) sufficient yields for comprehensive biological testing in vitro and in vivo.

Several studies have applied mechanical sanding using a rotary Dremel tool to produce true-to-life MNPLs from plastic items such as PET water bottles, HDPE containers, PP glasses, and PS utensils [4,8]. Recently, this approach was extended to opaque PET milk bottles, which are pigmented with titanium dioxide (TiO_2) nanoparticles (TiO_2-NPs) to reduce gas permeability and protect UHT milk from light [9]. This process yields titanium-doped PET nanoplastics [PET(Ti)-NPLs], where TiO_2-NPs are embedded within the PET matrix and remain stable over time. These particles hold potential for tracking plastic fate in biological systems, as shown in recent *Drosophila* studies [10].

Initial characterization of PET(Ti)-NPLs revealed no overt toxicity in three human hematopoietic cell lines (THP-1 monocytes, TK6 lymphoblasts, and Raji-B lymphocytes), though THP-1 cells displayed the highest internalization rate [9]. To expand on these findings, we further investigated PET(Ti)-NPLs in THP-1 monocytes, focusing on internalization kinetics and genotoxicity. Titanium doping enables precise quantification of particle uptake via inductively coupled plasma mass spectrometry (ICP-MS). Genotoxicity was assessed using the comet assay to detect DNA strand breaks. For comparison, NPLs derived from PET water bottles [4] and commercial TiO_2-NPs were also tested.

2. Material and Methods

2.1. Particle Source and Characteristics

To obtain environmentally representative PET(Ti)- and PET-NPLs from commercially available sources, diary opaque and regular water PET bottles were used as the source of nanoplastics by following previously published procedures [4,9]. Briefly, in two different procedures, the opaque water and milk bottles were fractioned into smaller pieces of 12 cm^2. These smaller fractions were then sanded with a Dremel 3000 electric multitool with a flexible extension attached to a diamond rotary burr. All components were from Dremel (Robert Bosch Tool Corporation, Mount Prospect, IL, USA). Film-sanded powder was sieved though a 0.20 mm mesh CISA R-92 (Allegion, Dublin, Ireland) until 4 g were obtained. The sieved material was then dispersed for 2 h on a 150 mL beaker containing 40 mL of 60 °C pre-heated 90% v/v trifluoroacetic acid (TFA) (Sigma-Aldrich, St. Louis, MO, USA) for 2 h under constant stirring on a stir heating plate (Heidolph Instruments GmbH & Co. KG, Schwabach, Germany). After 2 h, the temperature was lowered to room temperature and the sample was kept on agitation overnight. On the second day, 40 mL of 20% v/v TFA was added, big aggregates were physically disaggregated or eliminated, and

the generated suspension was then kept on constant stirring for 24 h. Particle suspensions were then passed through the 0.2 mm sieve to eliminate any bigger pieces, and then the collected material was distributed in 10 mL glass tubes and centrifuged at 2500 rcf for 1 h on an Eppendorf 5810 R (Eppendorf AG, Hamburg, Germany). Once the particles were deposited, the TFA acid was eliminated and the particles resuspended in a final volume of 400 mL of 0.5% sodium dodecyl sulfate (SDS) (Merck KGaA, Darmstadt, Germany). The total volume was homogenized by pipetting and distributed in two 250 mL beakers prior to being ultrasonicated in a cold-water bath for 2 min with 9/9 s cycles of 25% amplitude sonication/break on an SSE-1 Branson sonicator (Branson Ultrasonics Co., Brookfield, CT, USA). The sonicated particle suspension was then transferred to a 200 mL graduated cylinder, and bigger particles were then left to sediment for 1 h. The top 100 mL of each cylinder was then collected and distributed in 50 mL tubes and centrifuged under the same conditions as before to eliminate SDS. Particle pellets were then resuspended and transferred to the previously weighed 10 mL glass tubes, and then washed twice with water and twice with ethanol and left to dry for two days under an air laminar flow hood. The particles were then resuspended in Milli-Q water to a final stock concentration of 10 mg/mL and sonicated for 16 min at 10% amplitude in a cold-water bath. One mL of aliquots were then prepared, immediately frozen in liquid nitrogen, and stored at −80 °C. TiO_2 particles were purchased from Chemours™ (Washington, DE, USA). For all biological applications, particles were suspended using the Nanogenotox protocol [11].

Nanoparticle tracking analysis. Size distribution for all particles in suspension was complementarily determined by a combination of both light scattering and Brownian movement using a Nanosight NS300 from Malvern Panalytical Ltd. (Cambridge, United Kingdom). Briefly, a stock solution of 10,000 μg/mL of each nanoplastic/particle suspensions (PET, PET(Ti), and TiO_2) was sonicated for 30 min in an ultrasonic bath (Vevor, Houston, TX, USA). A suspension of 100 μg/mL was prepared in Milli-Q water, and right before the measurement, a 1:50 dilution was carried out using Milli-Q water in an air-pressured cleaned 20 mL glass vial and then vigorously mixed in a SA8 vortex (Merck KGaA, Darmstadt, Germany) operated at 1000 RPM. One mL of the diluted suspension was then transferred to the Nanosight microfluidic system with a syringe. The injection was carried out at decreasing speeds from 1000 to 50 a.u., and three independent measurements were conducted following this procedure. Data were acquired/recorded using a sCMOS detector (Oxford Instruments, Oxford, UK) with a 488 nm laser setup.

Scanning electron microscopy and electron dispersion spectroscopy (SEM-EDS).

PET(Ti)-NPL suspensions were prepared at concentrations of 200 μg/mL from the previously prepared 10,000 μg/mL nanoplastic dispersions. From the diluted aliquot, 10 μL was pipetted on 5 × 5 mm precut silicon chips (Ted Pella, Inc., Altadena, CA, USA) and dried overnight on a Petri dish internally covered with filter paper inside a laminar air flow hood. Particles were then analyzed with a scanning electron microscope (Sem Zeiss, Oberkochen, Germany). Fields were aleatorily selected, and the EDS spectra were obtained with a X-Max 20 mm EDS system (Oxford Instruments, Oxford, UK) and analyzed by INCA Energy software (INCA, Grinnell, IA, USA). Complementary dynamic light scattering (DLS), ζ-Potential, transmission electron microscopy (TEM), and Fourier transform infrared spectroscopy (FTIR) studies are presented in the Supplementary Materials (Section S1 and Figure S1).

2.2. Cell Culture

The human leukemia monocytic THP-1 cell line was used. THP-1 cells were grown in filtered cap T-25 flasks (SPL Life Sciences Co., Pocheon-si, Gyeonggi-do, Republic of Korea) at cell concentrations ranging from 0.5×10^6 to 1×10^6 and at a maximum volume of

5 mL. Cells were grown in suspension in RPMI (Roswell Park Memorial Institute) culture medium supplemented with 10% FBS (fetal bovine serum), 1% glutamine (Biowest, Nuaille, France), and 2.5 µg/mL of Plasmocin® (InvivoGen, San Diego, CA, USA). Cultures were grown at 37 °C in a humidified atmosphere with 5% CO_2 in an ICO150med CO_2 incubator (Memmert GmbH + Co. KG, Schwabach, Germany).

2.3. Cell Viability

To determine the effects of PET(Ti)-NPLs in THP-1 cells, 5×10^5 cells/mL were seeded in U-bottom 96-well plates in a final volume of 0.2 mL of medium and treated with NPLs at concentrations of 0 to 100 µg/mL for 24 h. Exposure to the same concentrations of PET-NPLs and the corresponding TiO_2-NP concentrations was carried out in parallel, as was seeding of non-treated THP-1 control cells. After the exposure time, the cells were mixed and diluted at 1:100 in ISOFLOW, and the cell number was determined using a ZTM Coulter Counter (Beckman Coulter Inc., Brea, CA, USA). The average cell number for each NPL concentration was compared with the average number of non-treated THP-1 cells after 24 h. Data were analyzed using GraphPad Prism 8.0.2. (GraphPad Software Inc., Boston, MA, USA).

2.4. Internalization Studies

2.4.1. Flow Cytometry Fluorescent Particle Detection

THP-1 cells were seeded at an initial concentration of 5×10^5 cells/mL in U-bottom 96-well plates (200 µL/well) and exposed for 24 h to iDye-labeled PET(Ti)-NPLs. The protocol to dye MNPLs using the textile dye iDye PolyPink (Rupert, Gibbon & Spider, Inc., Healdsburg, CA, USA) was recently published [12]. The tested concentrations were 0, 25, 50, and 100 µg/mL. For the flow cytometry analysis, exposed cells were separated by centrifugation (8 min at 300 rcf) using Eppendorf 5810 R tubes (Eppendorf AG, Hamburg, Germany) and rinsed twice with sterilized phosphate-buffered saline (PBS 1×) (Gibco, Thermo Fisher Scientific Inc., Waltham, MA, USA) prepared in distilled water. Cell data were collected on a CytoFLEX LX device (Beckman Coulter, Brea, CA, USA) and analyzed using the CytExpert 2.5 software from the same company. Data were analyzed using GraphPad Prism 8.0.2. (GraphPad Software Inc., Boston, MA, USA), and charts were prepared by using the aforementioned software and the Excel® program (Microsoft, Redmond, WA, USA).

2.4.2. Internalization Kinetics and Cell Complexity Analysis

THP-1 cells, at a cell density of 5×10^5 cells/mL, were grown on 96-well plates at a final volume of 200 µL/well and exposed to a concentration of 100 µg/mL of PET(Ti)-NPLs for a period ranging from 1 to 24 h. Exposed cells were evaluated in static conditions and on a digital Rocker 3D (IKA-Werke GmbH & Co, Staufen, Germany). In parallel, cells were exposed to 3 and 100 µg/mL of TiO_2 nanoparticles. For all timepoints, data were acquired in three independent experiments in triplicate for treated and control groups. Internal cell complexity, as an indicator of internalization, was determined as the percentage of positive cells (more complex) and the increase in internal complexity (how complex) by side scatter analysis using a CytoFLEX LX device (Beckman Coulter, Brea, CA, USA) and analyzed on CytExpert 2.5 from the same company. Data were analyzed and charts were prepared using GraphPad Prism 8.0.2. (GraphPad Software Inc., Boston, MA, USA).

2.4.3. Confocal Microscopic Imaging

THP-1 cells were grown on U-bottom 96-well plates at a total volume of 200 µL/well for 24 h. The experiment used a concentration of 100 µg/mL for iDye PET-NPLs and IDye PET(Ti)-NPLs, while the concentration of 3 µg/mL was used for TiO_2NPs. As for

fluorescence detection by flow cytometry, once exposed, the cells were washed twice using 1x PBS and resuspended in pre-warmed supplemented culture media. A total of 300 µL of the respective suspensions were transferred to each well of a chambered coverslip with 8 wells (ibid GmbH, Gräfelfing, Germany) for confocal microscopy observation. Cell nuclei were labeled using Hoechst 33342 (Sigma-Aldrich, Madrid, Spain) with an excitation wavelength (eWL) of 405 nm and an emission collected wavelength (ecWL) of 415–503. Cell membranes were labeled using Cellmask (eWL 633 nm and ecWL of 645–786). For iDye-labeled PET- and PET(Ti)-NPLs, an eWL of 561 nm and an ecWL of 570–630 were used. For TiO_2 localization, reflection images were obtained in parallel in all samples. The confocal device utilized was a Leica TCS SP5 confocal microscope, and the image process was carried out using ImageJ 1.54f analysis software, version 1.8.0_322 (USA National Institutes of Health, Bethesda, MD, USA).

2.4.4. Scanning and Transmission Electron Microscopy

THP-1 cells at a cell density of 5×10^5 cells/mL were grown in filtered cap T-25 flasks (SPL Life Sciences Co., Pocheon-si, Gyeonggi-do, Republic of Korea) in standard conditions. Exposure to PET(Ti)-NPLs lasted for 24 h at a concentration of 100 µg/mL. This concentration was selected according to previous studies [9]). Exposed and control cells were collected and fixed at 4 °C in aldehyde mix (2% paraformaldehyde and 2.5% glutaraldehyde) and subjected to a post treatment with 1% osmium tetroxide (OsO_4) and 0.8% potassium hexacyanoferrate (II) trihydrate. The following steps included dehydration in successive steps of increasing concentrations of acetone (as detailed in Supplementary Table S1) as a previous step for resin infiltration at room temperature (as detailed in Table S2). The resin sample mixture was then deposited in molds for sample block creation. Thin and ultrathin (70 nm) sections were prepared on a Leica EM UC6 ultramicrotome, and the sections were placed on AMR carbon support film on a copper 200-square mesh with and without carbon covering for scanning electron microscopy (SEM, Zeiss MERLIN FE-SEM, Oberkochen, Germany) and transmission electron microscopy (TEM, JEOL JEM 1400 instrument JEOL LTD, Tokyo, Japan), respectively. SEM visualization was complemented by elemental energy dispersive spectroscopy (EDS) detection using an X-Max 20 mm EDS system (Oxford Instruments, Oxford, UK). TEM was complemented with electron diffraction detection using a CCD GATAN Orius detector (Gatan, Inc., Pleasanton, CA, USA).

2.5. Cell Sorting and Titanium Quantification

Similar to the cell culture maintenance strategy, a final volume of 4 mL of suspension of THP-1 cells at a cell density of 5×10^5 cells/mL were grown in standard conditions for 24 h under an exposition regime of PET(Ti)-NPLs at a concentration of 100 µg/mL in filtered cap T-25 flasks (SPL Life Sciences Co., Pocheon-si, Gyeonggi-do, Republic of Korea). Cells were then collected and transferred to 15 mL tubes. Untreated (control) cells were used to diagram the gates for cell sorting of the treated cells. Exposed cell populations were sorted using a BD FACSJazz™ Cell Sorter and analyzed using the BD FACS Software version 6.0 sorter from the same company (Becton, Dickinson & Co., Franklin Lakes, NJ, USA). Positive and negative cells were collected in 15 mL tubes, and the relative Ti content was determined by ICP-MS. Shortly thereafter, the cell suspensions were kept at −20 °C, and before the measurement they were thawed and vigorously homogenized for approximately 1 min by vortexing. The collected aliquots were subjected to chemical digestion using HNO_3 65% p/v and HF 40% in a 4:1 ratio. Samples were then diluted in HNO_3 1% v/v and analyzed on an ICP-MS Agilent, model 7900 device (Agilent Technologies, Santa Clara, CA, USA).

2.6. Effects on ROS Levels

Reactive oxygen species (ROS) generation in THP-1 cells following nanoplastic (NPL) internalization was assessed using the dihydroethidium (DHE; Calbiochem, San Diego, CA, USA) assay. THP-1 cells were seeded at a density of 5×10^5 cells per well in U-bottom 96-well plates (triplicate) with a final volume of 0.2 mL RPMI medium and subsequently exposed to increasing concentrations (0–100 μg/mL) of PET(Ti)-NPLs and TiO_2-NPs for 24 h. Following exposure, cells were centrifuged at 1200 rpm for 8 min, washed with PBS 1X, and stained with DHE at a final concentration of 1 μg/mL. Samples were incubated at 37 °C for 30 min prior to analysis. ROS production was quantified by flow cytometry (CytoFLEX LX, Beckman Coulter, Brea, CA, USA) using CytExpert software, measuring mean FIT-C fluorescence in 10,000 single-cell events per condition. Average mean fluorescence in the treated cells was compared against that of non-treated THP-1 cells, and data were analyzed using GraphPad Prism 8.0.2 (GraphPad Software, San Diego, CA, USA).

2.7. Genotoxicity

The comet assay. The levels of DNA damage in THP-1 cells exposed for 24 h to PET-NPLs, PET(Ti)-NPLs, and TiO_2NPs were evaluated by using the single-cell gel electrophoresis (comet) assay, which detects mainly single-strand breaks. The cells (exposed/unexposed) were centrifuged at 0.30 RCF for 8 min at 4 °C. Pelletized cells were washed with cold PBS 1x, and the concentration was adjusted to 1×10^6 cell per mL. The cells were then mixed 1:10 with 0.75% previously melted low-melting-point agarose at a stabilized temperature of 37 °C, carefully mixed, and then dropped in triplicate onto GelBond® films (GBFs) (Life Sciences, Vilnius, Lithuania). GBFs with the samples were kept overnight in cold lysis buffer at 4 °C and, finally, washed. An incubation step lasting for 30 min at 4 °C on the electrophoresis buffer was carried out before submission to electrophoresis (20 V, 300 mA, 4 °C, 23 min). GBFs were then recovered and washed twice with cold PBS 1x, fixed in absolute ethanol for at least 1 h, and air-dried overnight at room temperature. A posterior staining with SYBR Gold (Invitrogen, Thermo Fisher Scientific Inc., Waltham, MA, USA) was carried out for 20 min on a Heidolph orbital shaker (Heidolph Instruments GmbH & Co., Schwabach, Germany). GBFs were then mounted and covered on glass and analyzed by epifluorescent microscopy (Olympus BX50, Hamburg, Germany). The levels of DNA damage, determined as percentage of DNA in the tail, were quantified using the Komet 5.5 Image analysis system (Kinetic Imaging Ltd., Liverpool, UK). Data were analyzed and graphics were prepared using GraphPad Prism 8.0.2. (GraphPad Software Inc., San Diego, MA, USA).

3. Results and Discussion

3.1. Nanoparticle Characteristics

The PET- and PET(Ti)-NPLs employed in the present study were exhaustively characterized. One of the implemented methodologies was particle-by-particle tracking, and, as observed in Figure 1, both the sizes and the concentrations were consistent and fell within comparable ranges and concentrations. It should be noted that, in addition to the NPLs, TiO_2NPs were also included in the study to cover as many variables as possible (Figure 1a–c). Moreover, it was observed that TiO_2NPs could be detected within the PET(Ti)-NPLs, and it was feasible to perform compositional mapping. This not only facilitated biological tracking but also enabled particle-level monitoring, thereby confirming the mixed nature of the material under study (Figure 1d–f). Furthermore, analysis of the mapping regions for titanium confirmed its presence via energy-dispersive spectroscopy (EDS), which revealed not only the characteristic peaks for carbon and oxygen from the polymer but also those indicative of titanium (Figure 1g). Additionally, the hydrodynamic

behavior of the particles was examined, revealing a coherent size distribution of 282 ± 3.12 nm for PET- and 320 ± 8.18 nm for PET(Ti)-NPLs, with polydispersity indexes of 0.47 and 0.34, respectively. The correlation curves are also presented (Figure S1b,c,e,f). Transmission electron microscopy, presented in the same figure (Figure S1a,d), further demonstrated the similar nature of the generated nanoplastics and underscores the importance of complementary analytical techniques in characterizing not only the surface but also the internal composition of the particles. Finally, to determine the chemical nature of the polymer, Fourier-transform infrared spectroscopy (FTIR) data show the previously described characteristic peaks for PET [13–16], provided in the Supplementary Materials (Figure S1g).

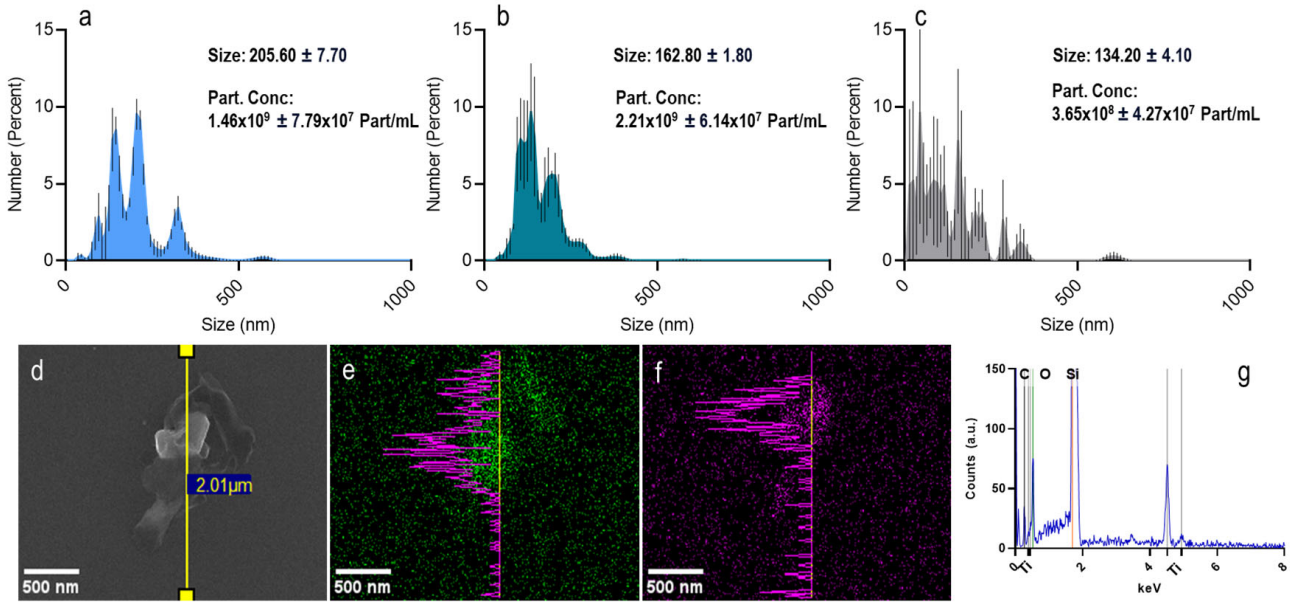

Figure 1. Nano-tracking analysis of PET-NPLs (**a**), PET(Ti)-NPLs (**b**), and TiO_2NPs (**c**) expressed as a percentage with standard error. SEM images of the PET(Ti) composite (**d**) and the mapping for Ti (**e**) and carbon (**f**) along with the EDS spectra (**g**), confirming the presence of Ti inside what at first glimpse seems to be only PET particles.

The above data confirm the usefulness of the presented protocol to obtain true-to-life PET MNPLs, as evidenced by recent publications [10,12,17–21].

3.2. NPL Cytotoxicity

For the selection of the concentrations to be used, a previous cytotoxicity study was required. Our results revealed no distinct cytotoxic patterns between PET- and PET(Ti)-NPLs in THP-1 monocytes, at any of the concentrations studied. The highest concentration (100 µg/mL) of both PET- and PET(Ti)-NPLs caused significant biological observable effects in terms of cell viability (Figure 2a). At the same time, concentrations of TiO_2-NPs at maximum present concentrations in PET(Ti)-NPLs and seriated dilutions revealed no statistically significant cytotoxicity (Figure 2b). The results for these nanoplastics are in line with previous reports for acute exposure in several cell lines studied for both materials [9,18,21,22].

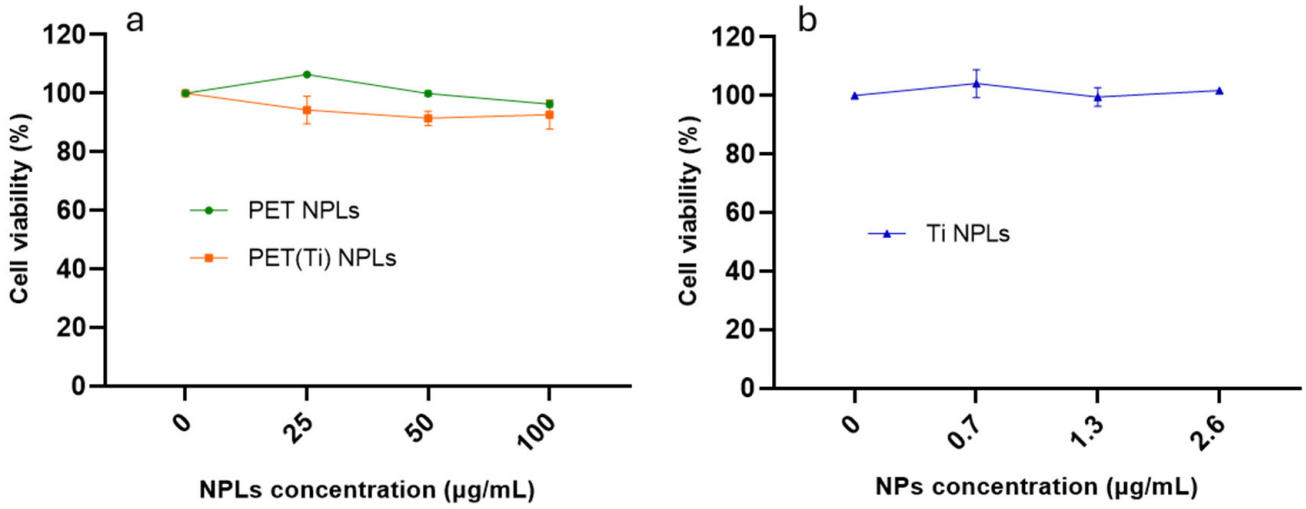

Figure 2. Cell viability after 24 h of THP-1 exposure to 0–100 µg/mL of PET- and PET(Ti)-NPLs (**a**) and the corresponding concentration of TiO_2-NPs in the PET(Ti)-NPLs (0–2.6 µg/mL) (**b**). Values of cell viability were normalized against non-treated THP-1 cell number after 24 h.

3.3. Internalization of PET(Ti)-NPLs

The kinetics of cell uptake of MNPLs is a complex topic since it depends not only on the physicochemical characteristics of the MNPLs but also on the cell used. Using different hematopoietic cell types, a differential cell uptake was observed for the different cells [5,23]. In the same way, using PS-NPLs with different surface functionalization, different dynamics of internalization have been observed [24]. This highlights the relevance of accurately confirming the cell uptake of the used MNPLs, mainly when new true-to-life MNPLs are evaluated.

In this study, we analyzed the dynamic of internalization (cell complexity) by light scattering, as well as the levels of fluorescence intensity within the cells. We chose THP-1 as a suitable cell mode due to its demonstrated MNPL uptake [25] and exposure conditions of 25, 50, and 100 µg/mL lasting for 24 h. The results obtained are indicated in Figure 3. Under these conditions, approximately 60% of the cell population internalized PET(Ti)-NPLs (Figure 3a), which agrees with previous studies [9]. In addition to the percentage of cells with internalized PET(Ti)-NPLs, the amount of internalization was also determined (Figure 3b). It must be noted that within the population of cells that internalized PET(Ti)-NPLs there were subpopulations with higher emission intensities, allowing us to distinguish between cells with more or fewer particles. As observed, the proportion of cells with high levels of internalization was concentration dependent. This approach of measuring exposure is interesting because it has been shown that the levels of internalization correlate with the induced effects [25]. To determine whether exposure conditions affected internalization, the effects of a rocking platform that kept the cells in constant motion were compared with those of static exposure. The results show that both conditions induced similar proportions of cell internalization and similar levels of internalization (Figure 3c,d). Interestingly, this trend remained regardless of the length of exposure to PET(Ti)-NPLs in the cell type evaluated, although the internalization was time dependent.

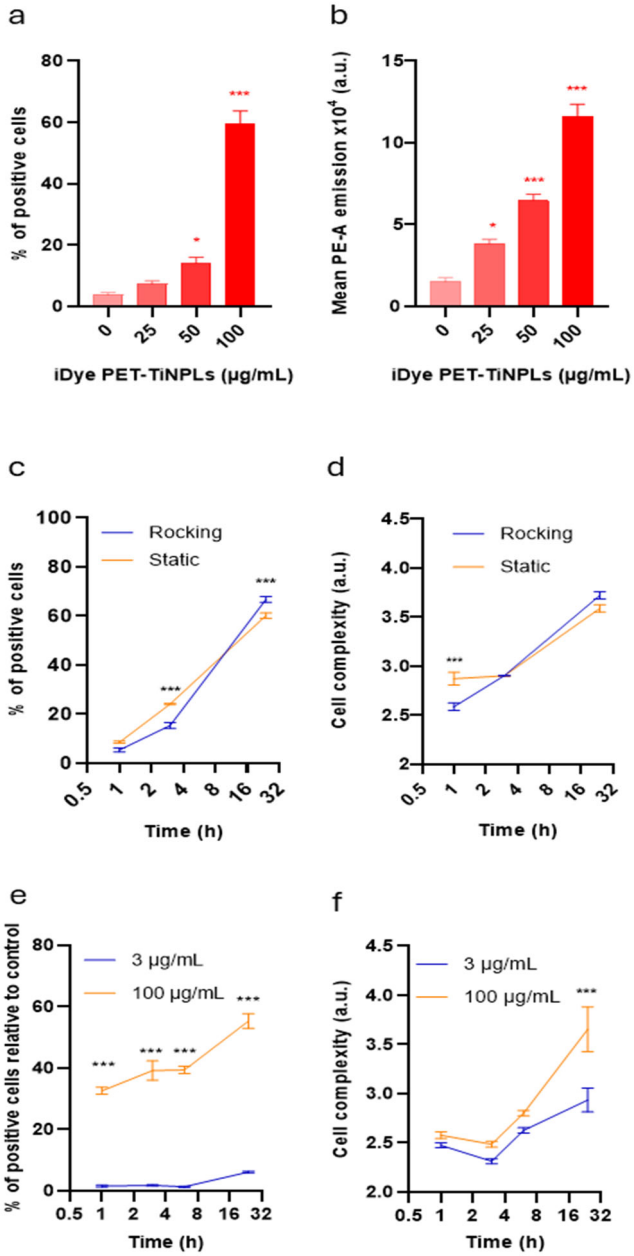

Figure 3. Relative internalization of PET(Ti)-NPLs in THP-1 cells exposed to 25 to 100 µg/mL lasting for 24 h. The percentage of cells that internalized PET(Ti)-NPLs (**a**) and the relative quantity of particles internalized (**b**). The effects of internalization (100 µg/mL) using rocking and static platforms are indicated for the percentage of cells with PET(Ti)-NPLs (**c**) and the quantity of internalized particles (**d**). Differences in internal complexity in terms of percentage of cells that internalized PET(Ti)-NPLs (**e**) and the relative quantity of particles internalized (**f**) of two different concentrations of TiO_2NPs in a time range of exposure of 1 to 24 h. * $p \leq 0.05$; *** $p \leq 0.001$.

An attractive question is whether the presence of titanium in PET(Ti)-NPLs modulates its uptake. Considering that the content of Ti in PET(Ti)-NPLs is approximately 2.6% [9,10], a similar amount (3 µg/mL) of TiO_2-NPs was used to determine its internalization, in comparison with a high concentration (100 µg/mL). As indicated in Figure 3e, the low concentration of TiO_2-NPs showed a very poor uptake, and a high concentration was required to obtain a percentage of cells with internalized TiO_2-NPs, like that observed for PET(Ti)-NPLs. When the number of internalized TiO_2-NPs was determined (Figure 3f), similar results were observed. This indicated that the cell uptake results are not related to the TiO_2-NP content but rather to the composite nature of PET(Ti)-NPLs.

To better visualize the described internalization, complementary methods were also used. Thus, when confocal microscopy was used, the internalization of PET(Ti)-NPLs in THP1 cells exposed to 100 µg/mL for 24 h was observed (Figure 4c). For a better comparison, cells without exposure (Figure 4a), cells exposed to 100 µg/mL of PET-NPLs (Figure 4b), and cells exposed to TiO_2-NPs (Figure 4d) were also included. Scanning electron microscopy (SEM) methodologies were also used to detect internalization thanks to the electron density of Ti (Figure 4e). The confirmation of this internalization was determined by using energy dispersive X-ray spectroscopy tools identifying the presence of Ti (Figure 4f). Transmission electron microscopy (TEM) was also used to confirm the presence of internalization (Figure 4g), and the use of the electron diffraction pattern (Figure 4h) confirmed the crystalline nature of the Ti-doped PET nanoplastic.

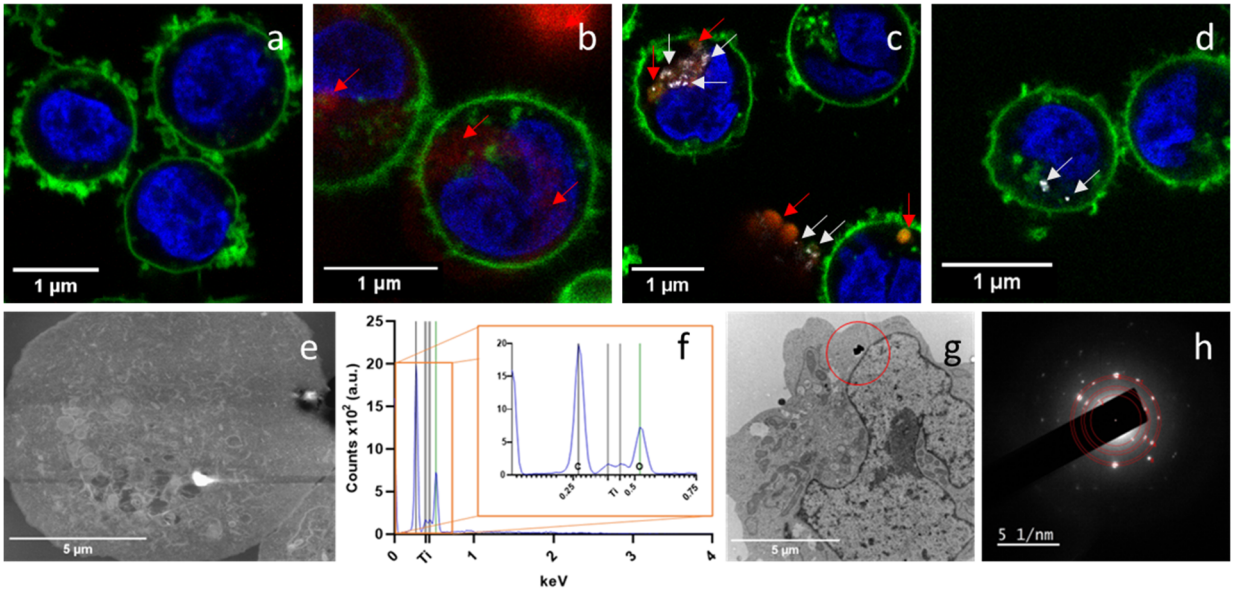

Figure 4. Confocal microscopy images of particle internalization of THP-1 cells using no particles as negative control (**a**), iDye-marked PET-NPLs showing the signal of PET-NPLs in red highlighted with red arrows (**b**), iDye-marked PET(Ti)-NPLs showing the colocalization of signals of Ti as a white signal with white arrows and the PET polymer as a red signal with red arrows (**c**), and TiO_2NPs as observed on a white signal with white arrows (**d**). Scanning electron microscopy images showing an image of PET(Ti)-NPLs internalized by THP-1 cells (**e**) and the signal translated into an energy dispersive diagram (**f**). Internalized PET(Ti)-NPLs by TEM as indicated by a red circle (**g**) and the diffraction pattern of TiO_2 contained in the PET(Ti)-NPLs (**h**).

Our results confirm the internalization of PET(Ti)-NPLs and show the advantages of using a wide range of complementary methodologies for detection. Nevertheless, other techniques can also be useful for detecting cell internalization, and among them, Raman microscopy stands out, as demonstrated in the identification of MNPLs in complex biological matrices, including cells [26–28]. In addition, Raman scattering signals are consistently stronger when the analyzed particles are not perfectly shaped, as is the case of true-to-life MNPLs [29].

3.4. Cell Sorting and Mass Spectroscopy

Dosimetry is a critical factor when evaluating the toxicity of NPLs, especially considering that particulate matter behaves quite differently from chemicals, which always distribute homogeneously in the water column or medium. This makes it essential to describe how the internal dose leads to significant biological changes, since in scavenger cells macrophage alterations in immune-related functions are directly associated with the

dose and size of internalized MNPLs [25]. Therefore, estimating the amount of nanoplastics within cells can provide a comparative advantage in drawing final conclusions about the induced effects. In such a context, the use of metal-doped NPLs, as in our case, can permit them to go further than mere visualization. To quantify the number of particles within the cells, we employed cell sorting to use only cells that had internalized PET(Ti)-NPLs.

Using side light scattering, we successfully separated populations according to their complexity. As shown in Figure 5a, some untreated cells exhibited greater complexity than the rest, which must be considered in further analysis. As expected, when cells were treated with PET(Ti)-NPLs, the number of cells shifting to a more complex region increased considerably because of the exposure (Figure 5b). After performing cell sorting, there was a considerably lower number of complex cells in the control population than in the population that had indeed internalized the nanoplastics (Figure 5c,d, respectively). It was observed that even after cell sorting, some cells were still categorized as negative. This could be due to cells that had released internalized PET(Ti)-NPLs into the surrounding medium.

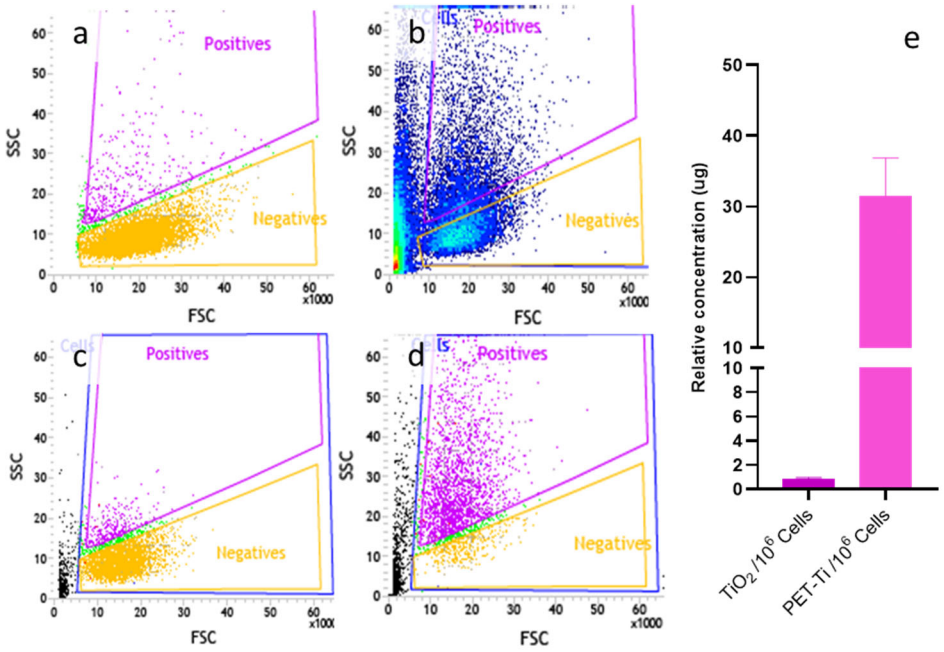

Figure 5. Flow cytometry data on THP-1 of untreated cells (**a**) and cells treated with PET(Ti)NPLs (**b**). After sorting, the number of complex cells is reduced in the negative population of THP-1 cells (**c**), but it is large in THP-1 cells that have internalized PET(Ti)NPLs (**d**). The relative amount of TiO_2NPs and PET(Ti)NPLs, per million cells, is depicted (**e**).

Despite that noise, cell sorting can be a suitable tool to determine the effects associated with MNPL exposure using only those cells that have internalized MNPLs and avoiding the use of cell populations with an undefined percentage of cells with no internalized particles, with a considerable possibility of masking measurable real effects on the truly exposed population. These complex scenarios were observed in whole human blood of healthy donors, where no effects were detectable after MNPL exposure in the complex mixture of blood cell types. Nevertheless, after sorting the different types of white blood cells, significant differences in both internalization and effects were observed between them [19,30]. This type of approach has also been used in mouse alveolar macrophages (MH-S) exposed to PET-NPLs obtained from the degradation of plastic water bottles. That study focused only on the cells that had internalized them as a novel approach capturing the realistic adverse effects only in the cells that have internalized the agent under study, thereby mitigating any biases while assessing the risk of these MNPLs [21].

Interestingly, by determining the amount of titanium in 1 mL of medium containing one million cells, we estimated the presence of approximately 0.82 µg of Ti. Considering that titanium constitutes 2.6% of the used nanoplastics, this value can be estimated at 31.56 µg of PET(Ti)-NPLs per 1×10^6 of THP1 cells, as depicted in Figure 5e. This type of dosimetry only can be carried out using metal-doped NPLs and, although some synthetic metal-doped NPLs have been obtained using different approaches [31,32], our true-to-life PET(Ti)-NPLs can be considered a real representative of the environmental secondary NPLs resulting from the constant degradation of plastic goods.

3.5. Reactive Oxygen Species Related to PET(Ti)-NPL and TiO_2-NP Exposure

The induction of intracellular reactive oxygen species (ROS) is considered a common hazard associated with nanoparticle exposure, and increased ROS levels have been reported in different in vivo and in vitro studies after exposure to MNPLs [33]. In our study, no significant changes in the ROS pattern expression were observed (Figure 6). However, it is important to keep in mind that not only is the cell type used for studies relevant but also the systemic response evaluation, as observed in previous studies conducted on *Drosophila* hemocytes, where relevant increases in oxidative damage induction were observed for PET-NPL, PET(Ti)-NPL, and TiO_2-NP exposure [10,18]. Therefore, a more careful evaluation is needed to unmask possible biological detrimental interactions of the tested NPLs.

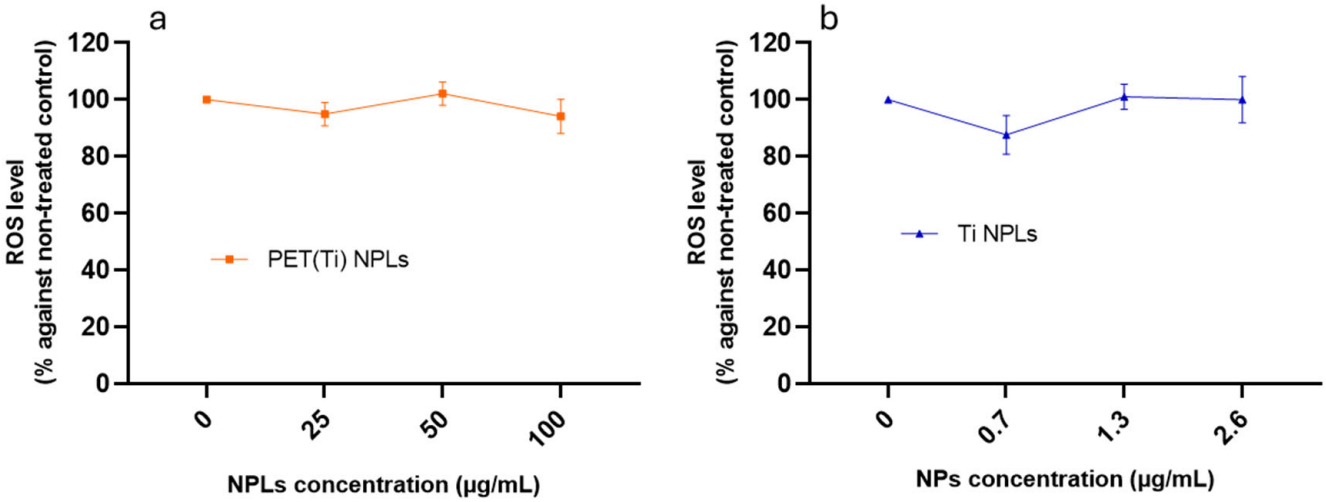

Figure 6. Change in ROS levels after 24 h of THP-1 exposure to 0–100 µg/mL of (**a**) PET(Ti)-NPLs and (**b**) the corresponding concentration of TiO_2-NPs in the NPLs (0–2.6 µg/mL). Values of ROS were normalized against those in non-treated THP-1 after 24 h.

3.6. DNA Damage Induction

Aiming to detect the potential harmful effects of PET(Ti)-NPLs, this work focused on their potential genotoxic effects. This is because some alarms exist about the genotoxicity of TiO_2-NPs. Although titanium compounds, including TiO_2-NPs, were authorized as a food additive (E 171) in the EU a long time ago, the recent position of the European Food Safety Authority (EFSA) announcing that it is not possible to rule out the genotoxicity from titanium dioxide and therefore that it "can no longer be considered as safe when used as a food additive" [34] suggests that the EU has banned its use [35]. In addition, it is well known that there exists a strong association between DNA damage induction and drastic health consequences for humans [36]. Since DNA damage can result from multiple mechanisms, we selected the comet assay as a tool for detecting primary DNA damage. In our study, PET- and PET(Ti)-NPLs not only internalized but also exhibited genotoxic effects, as shown in Figure 7.

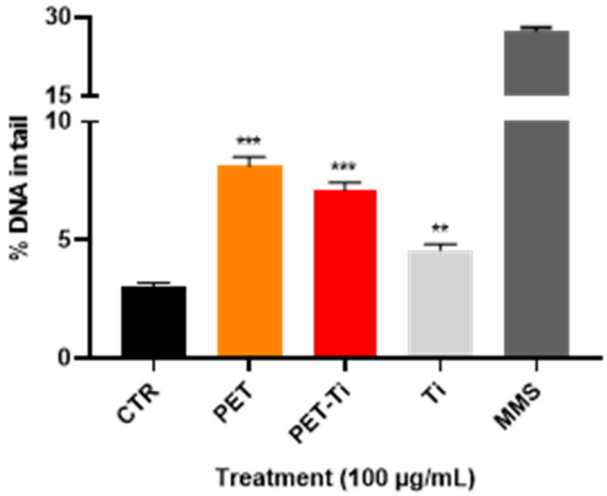

Figure 7. Percentage of DNA on the tail for the comet assay with methyl methanesulfonate (MMS) as a positive control. The effects were induced on THP-1 cells treated for 24 h with 100 µg/mL of PET-NPLs, PET(Ti)-NPLs, and TiO_2 -NPs. CTR refers to untreated cells as a negative control. ** $p \leq 0.01$; *** $p \leq 0.001$.

To determine the relative relevance of the two moieties (TiO_2-NPs and PET-NPLs), THP-1 cells were also exposed to these two components. It is important to note that genotoxic DNA damage was observable in all three cases: PET-NPLs, PET(Ti)-NPLs, and TiO_2-NPs alone. PET-NPLs alone caused the most significant damage, while PET(Ti)-NPLs were right in the middle of the effects exerted by the PET-NPLs and TiO_2-NPs alone. High concentrations of PET nanoplastics have been shown in recent studies to induce cell-transforming biological effects, with the potential to promote tumors. However, this effect was only observed at concentrations above 200 µg/mL [20]. On the other hand, genotoxic damage at the dose investigated here has been reported for PET-NPLs in *Drosophila* [17]. Moreover, both PET(Ti)-NPLs and TiO_2-NPs alone have been shown to effectively alter genotoxic damage pathways in the same model [10]. This, far from being contradictory, may be an indicator of a more systemic reaction than cellular alone. It is important to consider that although both PET-NPLs and TiO_2-NPs alone showed detectable effects in the comet assay, these effects were not exacerbated by their presence together in a nanoplastic composite. Instead, the effect was diminished. While it is challenging to directly attribute this outcome to a specific cause, it is not difficult to understand that the effect generated by PET-NPLs may have been reduced due to the PET mass reduction due to the additional weight contributed by the Ti in the particle. Thus, our results show that genotoxic damage was readily observed in cell populations exposed to PET-NPLs. It is also evident that PET(Ti)-NPLs induced a similar but less pronounced effect, whereas the damage caused by TiO_2 NPs alone was detectable by the comet assay. Overall, our findings highlight that PET-NPLs, specifically true-to-life particles, are significant inducers of primary DNA damage in the human immune cell model presented in this study.

4. Conclusions

The present study demonstrates that both PET and titanium-doped PET nanoplastics are internalized by THP-1 monocytes. Furthermore, we have demonstrated that the dynamic of uptake is significantly influenced by both particle concentration and exposure duration. The titanium additive in PET(Ti)-NPLs facilitates not only tracking but also dosimetry studies. The presence of titanium appears to mitigate the extent of genotoxic damage compared to PET-NPLs alone. These results underscore the importance of using representative NPL models in toxicological assessments and provide information on the

way to future and more complex studies aimed at elucidating the molecular mechanisms underlaying nanoplastic-induced cellular effects.

Supplementary Materials: The following supporting information can be downloaded at: https://www.mdpi.com/article/10.3390/nano15131040/s1, Figure S1: Transmission electron microscopy (TEM) micrographs of PET and PET(Ti) particles are shown (a,d). The hydrodynamic behavior of PET nanoplastics (NPLs) exhibits an average size of 282 nm, a relatively high polydispersity index of 0.47, and a ζ-Potential close to 29 mV (b). Additionally, the correlation coefficient of independent measurements is presented (c). Similarly, PET(Ti) displays an average particle size of approximately 320 nm with a polydispersity index of 0.34 and a ζ-Potential around 18.2 mV. A corresponding correlation curve is provided alongside the graphs (f). Finally, the Fourier-transform infrared spectroscopy (FTIR) spectra of PET and PET(Ti) reveal the characteristic peaks of PET. Interactions of polar ester groups and benzene rings (1), Vibrations of adjacent two aromatic H in p-substituted compound and aromatics bands (2), aromatic rings (3), methylene group aand vibrations of the ester C-O bond (4), Therephtalate group ($OOCC_6H_4$-COO)(5), stretching of the C-O group deformation of the O-H group and bending and wagging vibrational modes of the ethylene glycol segment (6), vibration aromatic skeleton with stretching C=C (7), stretching of C=O of carboxylic acid group (8), axial symmetrical deformation of CO_2 (9), C-H symmetrical stretching (10), symmetrical stretch of CH (11) and OH (hydroxyl) group (12); Table S1: Material for TEM visualization. Dehydration steps of increasing concentrations of acetone; Table S2: Material for TEM visualization. Steps for resin infiltration at room temperature.

Author Contributions: A.V., R.M. and A.H. planned the experiments. A.V., M.M.-R., L.V., J.M.-P., J.A.A. and I.B. carried out the experimental part. A.V., L.V. and M.M.-R. analyzed the data. A.V. was involved in the DLS measurement. A.V. and M.M.-R. prepared tables/figures. A.V., M.M.-R., R.M. and A.H. wrote the final manuscript. All authors have read and agreed to the published version of the manuscript.

Funding: This project has received funding from the European Union's Horizon 2020 Research and Innovation Programme under grant agreement No. 965196. This work was also partially supported by the Spanish Ministry of Science and Innovation [PID2020-116789, RB-C43], and by the Generalitat de Catalunya (2021-SGR-00731).

Data Availability Statement: Data are contained within the article and Supplementary Materials.

Acknowledgments: A. Villacorta was supported by PhD fellowships from the National Agency for Research and Development (ANID) from the CONICYT PFCHA/DOCTORADO BECAS CHILE/2020-72210237, Nucleo de Investigación en Ciencias Biológicas. L. Vela was supported by a PhD fellowship from the Fundación Carolina. M. Morataya-Reyes and J. Martín-Perez were supported by a PhD FI fellowship from the Generalitat de Catalunya. I. Barguilla (academic record 2023-BP-00212) was granted a Beatriu de Pinós Postdoctoral Program from the Secretariat of Universities and Research of the Department of Business and Knowledge of the Government of Catalunya. A. Hernández was granted an ICREA ACADEMIA award.

Conflicts of Interest: The authors declare that they have no known competing financial interests or personal relationships that could have appeared to influence the work reported in this paper.

References

1. Yang, T.; Wang, J. Exposure sources and pathways of micro- and nanoplastics in the environment, with emphasis on potential effects in humans: A systematic review. *Integr. Environ. Assess. Manag.* **2023**, *19*, 1422–1432. [CrossRef] [PubMed]
2. Thompson, R.C.; Olsen, Y.; Mitchell, R.P.; Davis, A.; Rowland, S.J.; John, A.W.G.; Mcgonigle, D.; Russell, A.E. Lost at sea: Where is all the plastic? *Science* **2004**, *304*, 838. [CrossRef]
3. Frias, J.P.G.L.; Nash, R. Microplastics: Finding a consensus on the definition. *Mar. Pollut. Bull.* **2019**, *138*, 145–147. [CrossRef]
4. Villacorta, A.; Rubio, L.; Alaraby, M.; López-Mesas, M.; Fuentes-Cebrian, V.; Moriones, O.H.; Marcos, R.; Hernández, A. A new source of representative secondary PET nanoplastics. Obtention, characterization, and hazard evaluation. *J. Hazard. Mater.* **2022**, *439*, 129593. [CrossRef] [PubMed]

5. Rubio, L.; Barguilla, I.; Domenech, J.; Marcos, R.; Hernández, A. Biological effects, including oxidative stress and genotoxic damage, of polystyrene nanoparticles in different human hematopoietic cell lines. *J. Hazard. Mater.* **2020**, *398*, 122900. [CrossRef]
6. Landrigan, P.J. Plastics, fossil carbon, and the heart. *N. Engl. J. Med.* **2024**, *390*, 948–950. [CrossRef] [PubMed]
7. Mills, C.L.; Savanagouder, J.; de Almeida Monteiro Melo Ferraz, M.; Noonan, M.J. The need for environmentally realistic studies on the health effects of terrestrial microplastics. *Microplast. Nanoplast.* **2023**, *3*, 11. [CrossRef]
8. Marchesi, C.; Rani, M.; Federici, S.; Alessandri, I.; Vassalini, I.; Ducoli, S.; Borgese, L.; Zacco, A.; Núñez-Delgado, A.; Bontempi, E.; et al. Quantification of ternary microplastic mixtures through an ultra-compact near-infrared spectrometer coupled with chemometric tools. *Environ. Res.* **2023**, *216 Pt 3*, 114632. [CrossRef]
9. Villacorta, A.; Vela, L.; Morataya-Reyes, M.; Llorens-Chiralt, R.; Rubio, L.; Alaraby, M.; Marcos, R.; Hernández, A. Titanium-doped PET nanoplastics of environmental origin as a true-to-life model of nanoplastic. *Sci. Total Environ.* **2023**, *880*, 163151. [CrossRef]
10. Alaraby, M.; Villacorta, A.; Abass, D.; Hernández, A.; Marcos, R. Titanium-doped PET nanoplastics, from opaque milk bottle degradation, as a model of environmental true-to-life nanoplastics. Hazardous effects on *Drosophila*. *Environ. Poll.* **2024**, *341*, 122968. [CrossRef]
11. Nanogenotox. 2011. Available online: http://www.nanogenotox.eu/files/PDF/Deliverables/nanogenotox%20%20deliverable%203_%20wp4_%20dispersion%20protocol.pdf (accessed on 4 March 2025).
12. Villacorta, A.; Cazorla-Ares, C.; Fuentes-Cebrian, V.; Valido, I.H.; Vela, L.; Carrillo-Navarrete, F.; Morataya-Reyes, M.; Mejia-Carmona, K.; Pastor, S.; Velázquez, A.; et al. Fluorescent labeling of micro/nanoplastics for biological applications with a focus on "true-to-life" tracking. *J. Hazard. Mater.* **2024**, *476*, 135134. [CrossRef] [PubMed]
13. Andanson, J.M.; Kazarian, S.G. In situ ATR-FTIR spectroscopy of poly(ethylene terephthalate) subjected to high-temperature methanol. *Macromol. Symp.* **2008**, *265*, 195–204. [CrossRef]
14. Chen, Z.; Hay, J.N.; Jenkins, M.J. The thermal analysis of poly(ethylene terephthalate) by FTIR spectroscopy. *Thermochim. Acta* **2013**, *552*, 123–130. [CrossRef]
15. Dos Santos Pereira, A.P.; Da Silva, M.H.P.; Lima, É.P.; Dos Santos Paula, A.; Tommasini, F.J. Processing and characterization of PET composites reinforced with geopolymer concrete waste. *Mater. Res.* **2017**, *20*, 411–420. [CrossRef]
16. Johnson, L.M.; Mecham, J.B.; Krovi, S.A.; Moreno Caffaro, M.M.; Aravamudhan, S.; Kovach, A.L.; Fennell, T.R.; Mortensen, N.P. Fabrication of polyethylene terephthalate (PET) nanoparticles with fluorescent tracers for studies in mammalian cells. *Nanoscale Adv.* **2021**, *3*, 339–346. [CrossRef]
17. Alaraby, M.; Villacorta, A.; Abass, D.; Hernández, A.; Marcos, R. The hazardous impact of true-to-life PET nanoplastics in *Drosophila*. *Sci. Total Environ.* **2023**, *863*, 160954. [CrossRef]
18. Annangi, B.; Villacorta, A.; Vela, L.; Tavakolpournegari, A.; Marcos, R.; Hernández, A. Effects of true-to-life PET nanoplastics using primary human nasal epithelial cells. *Environ. Toxicol. Pharmacol.* **2023**, *100*, 104140. [CrossRef]
19. Arribas Arranz, J.; Villacorta, A.; Rubio, L.; García-Rodríguez, A.; Sánchez, G.; Llorca, M.; Farre, M.; Ferrer, J.F.; Marcos, R.; Hernández, A. Kinetics and toxicity of nanoplastics in ex vivo exposed human whole blood as a model to understand their impact on human health. *Sci. Total Environ.* **2024**, *948*, 174725. [CrossRef]
20. Domenech, J.; Villacorta, A.; Ferrer, J.F.; Llorens-Chiralt, R.; Marcos, R.; Hernández, A.; Catalán, J. In vitro cell-transforming potential of secondary polyethylene terephthalate and polylactic acid nanoplastics. *J. Hazard. Mater.* **2024**, *469*, 134030. [CrossRef]
21. Tavakolpournegari, A.; Villacorta, A.; Morataya-Reyes, M.; Arribas Arranz, J.; Banaei, G.; Pastor, S.; Velázquez, A.; Marcos, R.; Hernández, A.; Annangi, B. Harmful effects of true-to-life nanoplastics derived from PET water bottles in human alveolar macrophages. *Environ. Pollut.* **2024**, *348*, 123823. [CrossRef]
22. Gutiérrez-García, J.; Egea, R.; Barguilla, I.; Nymark, P.; García-Rodríguez, A.; Guyot, B.; Maguer-Satta, V.; Marcos, R.; Rubio, L.; Hernández, A. Long-term exposure to real-life polyethylene terephthalate nanoplastics induces carcinogenesis in vitro. *Environ. Sci. Technol.* **2025**, *59*, 10891–10904. [CrossRef] [PubMed]
23. Tavakolpournegari, A.; Annangi, B.; Villacorta, A.; Banaei, G.; Martin, J.; Pastor, S.; Marcos, R.; Hernández, A. Hazard assessment of different-sized polystyrene nanoplastics in hematopoietic human cell lines. *Chemosphere* **2023**, *325*, 138360. [CrossRef] [PubMed]
24. Martín-Pérez, J.; Villacorta, A.; Banaei, G.; Morataya-Reyes, M.; Tavakolpournegari, A.; Marcos, R.; Hernández, A.; García-Rodriguez, A. Hazard assessment of nanoplastics is driven by their surface-functionalization. Effects in human-derived primary endothelial cells. *Sci. Total Environ.* **2024**, *934*, 173236. [CrossRef]
25. Collin-Faure, V.; Vitipon, M.; Torres, A.; Tanyeres, O.; Dalzon, B.; Rabilloud, T. The internal dose makes the poison: Higher internalization of polystyrene particles induce increased perturbation of macrophages. *Front. Immunol.* **2023**, *14*, 1092743. [CrossRef]
26. Pironti, C.; Notarstefano, V.; Ricciardi, M.; Motta, O.; Giorgini, E.; Montano, L. First evidence of microplastics in human urine, a preliminary study of intake in the human body. *Toxics* **2023**, *11*, 40. [CrossRef]
27. Ragusa, A.; Svelato, A.; Santacroce, C.; Catalano, P.; Notarstefano, V.; Carnevali, O.; Papa, F.; Rongioletti, M.C.A.; Baiocco, F.; Draghi, S.; et al. Plasticenta: First evidence of microplastics in human placenta. *Environ. Int.* **2021**, *146*, 106274. [CrossRef]

28. Ragusa, A.; Notarstefano, V.; Svelato, A.; Belloni, A.; Gioacchini, G.; Blondeel, C.; Zucchelli, E.; De Luca, C.; D'avino, S.; Gulotta, A.; et al. Raman microspectroscopy detection and characterisation of microplastics in human breastmilk. *Polymers* **2022**, *14*, 2700. [CrossRef]
29. Mogha, N.K.; Shin, D. Nanoplastic detection with surface enhanced Raman spectroscopy: Present and future. *TrAC-Trend. Anal. Chem.* **2023**, *158*, 116885. [CrossRef]
30. Ballesteros, S.; Domenech, J.; Barguilla, I.; Cortés, C.; Marcos, R.; Hernández, A. Genotoxic and immunomodulatory effects in human white blood cells after ex vivo exposure to polystyrene nanoplastics. *Environ. Sci. Nano* **2020**, *7*, 3431–3446. [CrossRef]
31. Hendriks, L.; Kissling, V.M.; Buerki-Thurnherr, T.; Mitrano, D.M. Development of single-cell ICP-TOFMS to measure nanoplastics association with human cells. *Environ. Sci. Nano* **2023**, *10*, 3439–3449. [CrossRef]
32. Mitrano, D.M.; Beltzung, A.; Frehland, S.; Schmiedgruber, M.; Cingolani, A.; Schmidt, F. Synthesis of metal-doped nanoplastics and their utility to investigate fate and behaviour in complex environmental systems. *Nat. Nanotech.* **2019**, *14*, 362–368. [CrossRef] [PubMed]
33. Yu, Z.; Li, Q.; Wang, J.; Yu, Y.; Wang, Y.; Zhou, Q.; Li, P. Reactive oxygen species-related nanoparticle toxicity in the biomedical field. *Nanoscale Res. Lett.* **2020**, *15*, 115. [CrossRef] [PubMed]
34. Younes, M.; Aquilina, G.; Castle, L.; Engel, K.H.; Fowler, P.; Frutos Fernandez, M.J.; Fürst, P.; Gundert-Remy, U.; Gürtler, R.; Husøy, T.; et al. Safety assessment of titanium dioxide (E171) as a food additive. *EFSA J.* **2021**, *19*, e06585. [CrossRef] [PubMed]
35. European Union. COMMISSION REGULATION (EU) 2022/63. Amending Annexes II and III to Regulation (EC) No 1333/2008 of the European Parliament and of the Council as Regards the Food Additive Titanium Dioxide (E 171). 2022. Available online: https://eur-lex.europa.eu/legal-content/EN/TXT/?uri=CELEX:32022R0063 (accessed on 4 March 2025).
36. Carbone, M.; Arron, S.T.; Beutler, B.; Bononi, A.; Cavenee, W.; Cleaver, J.E.; Croce, C.M., Jr.; D'aNdrea, A.; Foulkes, W.D.; Gaudino, G.; et al. Tumour predisposition and cancer syndromes as models to study gene-environment interactions. *Nat. Rev. Cancer* **2020**, *20*, 533–549. [CrossRef]

3.3. Chapter 3 (Article 3)

Acute and long-term effects of titanium-doped polyethylene terephthalate nanoplastics in human bronchial epithelial cells bronchial epithelial (BEAS-2B) cells.

Journal of Environmental Sciences. (2026)

Doi: 10.1016/j.jes.2026.03.030

Impact Factor: 6.3 (2024)

Acute and long-term effects of titanium-doped polyethylene terephthalate nanoplastics in human bronchial epithelial cells

Michelle Morataya-Reyes , Aliro Villacorta , Joan Martín-Perez , Irene Barguilla , Laura Rubio , Raquel Egea , Ricard Marcos , Alba Hernández

PII: S1001-0742(26)00195-6
DOI: https://doi.org/10.1016/j.jes.2026.03.030
Reference: JES 5336

To appear in: *Journal of Environmental Sciences*

Received date: 11 December 2025
Revised date: 10 March 2026
Accepted date: 10 March 2026

Please cite this article as: Michelle Morataya-Reyes , Aliro Villacorta , Joan Martín-Perez , Irene Barguilla , Laura Rubio , Raquel Egea , Ricard Marcos , Alba Hernández , Acute and long-term effects of titanium-doped polyethylene terephthalate nanoplastics in human bronchial epithelial cells, *Journal of Environmental Sciences* (2026), doi: https://doi.org/10.1016/j.jes.2026.03.030

Highlights

- True-life PET-nanoplastics containing TiO_2 as additive were produced.
- Short (24-48 h) and long-term exposures (8-15 w) were used.
- Sort exposures caused modest oxidative, inflammatory, and genotoxic effects.
- Long exposure effects induce sustained DNA damage, migration. and invasiveness.
- The relevance of long-term exposures in MNPL risk assessment is remarked.

Acute and long-term effects of titanium-doped polyethylene terephthalate nanoplastics in human bronchial epithelial cells

Michelle Morataya-Reyes[a], Aliro Villacorta[a,b], Joan Martín-Perez[a], Irene Barguilla[a], Laura Rubio[a], Raquel Egea[a], Ricard Marcos[a,*] Alba Hernández[a,*]

a. Group of Mutagenesis, Department of Genetics and Microbiology, Faculty of Biosciences, Universitat Autònoma de Barcelona, Cerdanyola del Vallès 08193, Spain
b. Facultad de Recursos Naturales Renovables, Universidad Arturo Prat, Iquique 110000, Chile

Abstract: Micro/nanoplastics (MNPLs) are widespread airborne pollutants whose potential health risks require urgent investigation. Critical aspects for experimental assessment include MNPL type, exposure scenario, target cells, and relevant biomarkers of effect. Here, we used titanium-doped polyethylene terephthalate (PET) nanoplastics (PET(Ti)-NPLs), derived from the degradation of opaque polyethylene terephthalate bottles containing TiO_2 nanoparticles, as a model of environmentally representative NPLs. To mimic human exposure, both acute (24–48 h) and long-term (8–15 weeks) exposures were evaluated in non-tumorigenic human bronchial epithelial (BEAS-2B) cells, a relevant respiratory model. Biomarkers assessed included oxidative stress, genotoxicity, and cytokine expression after acute exposure, and genotoxicity, cytokine expression, and cell transformation markers (anchorage-independent growth, migration, invasion) after prolonged exposure. Acute exposure caused modest oxidative and inflammatory responses with detectable DNA strand breaks. In contrast, chronic exposure induced persistent genomic instability, altered cytokine and oncogenic signaling, and acquisition of early oncogenic changes. Notably, after 15 weeks, PET(Ti)-NPLs triggered sustained DNA damage, dynamic modulation of phosphorylated H2AX histone, disrupted cytokine and cancer-related protein profiles, and enhanced migratory and invasive behaviors, even without anchorage-independent growth. These findings demonstrate that sub-toxic concentrations of PET(Ti)-NPLs promote time-dependent, early carcinogenic-like phenotypes in human bronchial epithelial cells, underscoring the importance of considering long-term exposure scenarios in MNPL risk assessment.

Keywords:
PET nanoplastics
Beas-2B cells
Acute and long-term exposure
Genotoxicity
Cytokine expression
Hallmark carcinogenesis biomarkers

*Corresponding authors. E-mails: alba.hernandez@uab.cat (A. Hernández) ricard.marcos@uab.cat (R. Marcos).

1 Introduction

Plastic pollution has emerged as a global environmental and public health issue. With annual plastic production increasing from 234 million tons (MT) in 2000 to 460 MT in 2019, global annual plastic waste has also increased from 156 to 353 MT during such period. The ineffective end-of-life disposal of plastics waste has resulted in these materials leaking into the environment, where they degrade from large pieces (macroplastics) to microplastics (< 5 mm) and nanoplastics (< 1 μm). Micro- and nanoplastics (MNPLs) have become ubiquitous environmental contaminants, and those characteristics making plastic popular and durable are the ones that guarantee their long-term presence in the environment. This widespread environmental presence raises concerns about potential human exposure, particularly via inhalation and ingestion, and the associated adverse health effects (Mahmud et al., 2024).

The potential risk of exposure to MNPLs on human health has made this a topic of interest, and many studies have reported the environmental occurrence of these particles in different bodies of water as well as in the atmosphere, where they are detected in outdoor-indoor air and urban areas (Rahman et al., 2021), and their atmospheric deposition has been proved (Wright et al., 2020). These findings highlight inhalation as a relevant exposure route to MNPLs. As expected, MNPLs with higher occurrence in the atmosphere are those more commonly used in human daily life such as polyethylene (PE), polyvinyl chloride (PVC), polypropylene (PP), polystyrene (PS), and polyethylene terephthalate (PET) plastic goods (Dong et al., 2020). However, most of the studies evaluating the potential effect of MNPLs on human health fail in using relevant MNPL types and exposure conditions since they used commercially available MNPLs, such as pristine PE and PS, as models, which are not representative of environmental

MNPLs resulting from the degradation of plastic goods. It must be remembered that during the production of plastic goods, many additives are included for enhancing their functionality. Consequently, its degradation can generate MNPLs functionalized with additives which are of particular concern due to their environmental persistence, bioaccumulation potential, and widespread use in products such as beverage bottles, textiles, and disposable masks (Le et al., 2023). The included plastic additives are multiple and varied, including endocrine disrupting chemicals (such as bisphenol A) and metals (as titanium dioxide) that can be released once MNPLs are inhaled or ingested and translocate across biological barriers, accumulating in tissues, and disrupting cellular homeostasis (Li et al., 2024). Accordingly, the use of representative true-to-life MNPLs obtained from plastic goods is crucial for a correct determination of potential harmful effects of MNPLs (Villacorta et al., 2022).

Another limitation of most studies evaluating the harmful effects of MNPLs, is the exposure scenario. Most of the studies focused on acute exposure, which may overlook long-term cellular responses such as adaptation, cumulative damage, or phenotypic transformation. In lung epithelial cell models, acute PS- or PE-NPLs exposure has been shown to induce oxidative stress, inflammation, autophagy activation, and mitochondrial damage (Schröter and Ventura, 2022), as well as epithelial-mesenchymal transition (EMT) (Traversa et al., 2024). However, using true-to-life MNPLs resulting from the degradation of PET plastic water bottles and chronic exposure lasting for 30 weeks, enhanced markers associated with cell transformation in BEAS-2B cells have been observed (Gutiérrez-García et al., 2025).This phenotype was exacerbated when the same cells were co-exposed to PET-NPLs and cigarette smoke condensate for four additional weeks, compared to the treatment with each of these agents alone, highlighting the importance of investigating chronic exposure effects (Morataya-Reyes et al., 2025a). These results point out exposure duration as a critical factor in the potential effects of MNPLs since acute exposures may primarily trigger stress and inflammation, while chronic exposure may remodel gene expression, cellular phenotypes, and transformation potential.

Despite growing evidence of the hazardous potential of MNPLs, studies determining both acute and long-term exposures are rare. To fill such knowledge gap, human bronchial epithelial (BEAS-2B) cells were acute (24/48 h) and long-term (15 weeks) exposed to titanium-dopped PET nanoplastics [PET(Ti)-NPLs], as a model of representative environmental MNPL. Such MNPLs result from the degradation of PET opaque plastic bottles, containing titanium dioxide nanoparticles (TiO_2-NPs), included as additive during their production. Opaque PET bottles are highly used for packing milk because they provide the light protection that UHT milk requires and minimize gas permeability (Villacorta et al., 2023). Focusing on PET-NPLs, they have

already been found in lung tissues, highlighting inhalation as a relevant exposure route, raising concerns about respiratory health risks (Jenner et al., 2022). For such reason, this study uses human bronchial epithelial (BEAS-2B) cells as a model of targeted cells. Real plastic goods include additives, and the potential hazardous effects of such additives are understudied. Aiming to study real-life NPLs we have obtained PET(Ti)-NPLs from opaque plastic PET bottles, including TiO_2 as a filler. Exposure effects on endpoints such as viability, oxidative stress, inflammation, EMT, and transformation processes provide critical insights into the health risks posed by representative environmental MNPLs useful for regulatory strategies.

2 Materials and methods

2.1 Experimental materials

2.1.1 Preparation and characterization of PET(Ti)-NPLs

PET(Ti)-NPLs were obtained from commercially available opaque PET bottles containing titanium dioxide nanoparticles (TiO_2-NPs) as a filler, using the protocol published by Villacorta et al. (2023). The production process involved mechanical sanding and physicochemical dispersion protocols, followed by physicochemical characterization including transmission and scanning electron microscopy (TEM/SEM), multi-angle light scattering of dispersed particles (DLS-MADLS), zeta potential, nanotracking analysis, FTIR spectroscopy, energy-dispersive X-ray spectroscopy (EDS), and ICP-OES for titanium quantification. For these assays, a stock suspension of 10 mg/mL of PET(Ti)-NPLs was prepared in Milli-Q water and sonicated for 16 min at 10 % amplitude in an ice bath to ensure dispersion. Results of the complete characterization can be found in previous works (Villacorta et al., 2023, 2025) where the hybrid nature of these PET(Ti)-NPLs, with embedded TiO_2-NPs within PET matrices, as well as their size distribution and behavior in aqueous and cell culture media, were comprehensively described. Additionally, for all biological assays, particles were previously resuspended using the Nanogenotox protocol, including controlled sonication to minimize agglomeration and ensure reproducibility between experiments. As previously reported for these PET(Ti)-NPLs, the particles exhibit a heterogeneous size distribution and may undergo dynamic aggregation and protein corona formation when dispersed in serum-containing cell culture medium. Such behavior is characteristic of environmentally derived nanoplastics and was therefore considered intrinsic to the exposure scenario.

Additionally, a fluorescently labeled version of the particles was prepared following the protocols described by Villacorta et al. (2023, 2024). Briefly, the PET(Ti)-NPLs were subjected to a staining procedure using the textile dye iDye PolyPink (Rupert, Gibbon & Spider, Inc.,

Healdsburg, CA, USA), which has been validated as a reliable and biocompatible fluorophore for true-to-life nanoplastics. The dye was incubated with PET(Ti)-NPLs under controlled heating and agitation, and the suspension was subsequently purified by multiple washing and ultrafiltration steps to remove free residues. The absence of fluorescence in the final wash confirmed the complete removal of dye. The labeled particles exhibited excitation and emission at 561 nm and 580–700 nm, respectively, enabling their detection using standard confocal microscopy and cytometry settings. These fluorescently labeled PET(Ti)-NPLs were subsequently used in confocal microscopy and flow cytometry assays to track uptake and intracellular distribution in BEAS-2B cells.

2.1.2 The BEAS-2B cells

Non-tumorigenic bronchial epithelium cells transformed with Ad12-SV40 2B (BEAS-2B) were used for the study. Cells were grown in Dulbecco's modified Eagle's medium (DMEM, Life Technologies, NY, USA) supplemented with 2.5 µg/mL of Plasmocin (InvivoGen, CA, USA) and 10 % fetal bovine serum (FBS, Biowest, France). For cell passage, TrypLE™ Select Enzyme (1X) (Thermo Fisher Scientific, Waltham, MA) was used to detach cells and later inactivated using the same DMEM. Cells were maintained in a 5 % CO_2 humidified atmosphere at 37 °C.

2.2 Experimental groups

2.2.1 Acute exposure

Effects of acute exposure to PET(Ti)-NPLs in BEAS-2B cells were evaluated after 24 and 48 h of exposure to the particles. To proceed, 1×10^5 cells/plate were seeded in triplicate in 12-well plates in a final volume of 1 mL of DMEM containing PET(Ti)-NPLs or the corresponding concentration of TiO_2-NPs only, with parallel non-treated cells, considered as the experimental control. Cell viability was evaluated at 0, 25, 50, 100, and 200 µg/mL of PET(Ti)-NPLs, and the corresponding 0, 0.6, 1.3, 2.6, and 6 µg/mL of TiO_2-NPs. Internalization, ROS levels, cytokine expression profile, and genotoxic damage were evaluated under these acute conditions.

2.2.2 Long-term exposure

To determine the effect of long-term exposure of BEAS-2B cells to PET(Ti)-NPLs, cells were exposed for up to 15 weeks to these NPLs. A total of 2×10^5 cells were seeded in triplicate in 75 cm^2 flasks in a total volume of 10 mL of culture medium and treated with 50 µg/mL of

PET(Ti)-NPLs under the culture conditions previously described. Constant chronic exposure to PET(Ti)-NPLs was ensured by replacing the cell culture medium every 3 days with a fresh medium containing the same concentration of NPLs and doing a weekly cell passage. The effects of continuous cell passaging were evaluated by culturing non-exposed passage-matched cells in triplicate under the same cell culture conditions as the long-term treated cells, based on the description of Barguilla et al. (2023) to determine the potential effects on cellular transformation of environmental pollutants in *in vitro* long-term/low-concentration studies. While standard propagation of BEAS-2B cells is often performed in BEGM or LHC-9 media, this study required an adequate medium for long-term, high-density cultures for transformation assays. Therefore, DMEM-based medium supplemented with 10 % FBS was used, following the same established protocol.

2.3 Detection methods

2.3.1 Cell viability measurement

To determine the sub-toxic concentrations of PET(Ti)-NPLs in BEAS-2B cells, 1×10^5 cells/well were seeded in triplicate in 12-well plates in a final volume of 1 mL of DMEM and treated with the NPLs at concentrations from 0 to 200 µg/mL for 24 and 48 h. Cells were detached and cell number was determined using the LUNA-II™ Automated Cell Counter (Biocat, Heidelberg, Germany) in a 1:1 dilution with trypan blue (Sigma-Aldrich, St. Louis, MO). Each concentration's average cell number was compared with the average of the non-treated cells. Viability of BEAS-2B cells was measured after treatment with the corresponding content of TiO_2-NPs present in each of the PET(Ti)-NPLs concentrations (0 to 6 µg/mL) evaluated, to determine the effects of these particles alone. Data was analyzed for three independent experiments using GraphPad Prism Software 8.0.2 (GraphPad, San Diego, CA).

2.3.2 Nanoparticle internalization by confocal microscopy

Internalization of PET(Ti)-NPLs in BEAS-2B cells was determined by confocal microscopy. To proceed, 1×10^4 cells/well were seeded in an µ-Slide 8 well chambered coverslip (Ibidi GmbH, Gräfelfing, Germany) and treated with 50 µg/mL of the fluorescent/labeled PET(Ti)-NPLs for 48 h. Before observation with a Leica TCS SP5 confocal microscope, cells were washed with growth medium and nuclei marker Hoechst 33342 (ex: 405 nm, em: 415–503 nm) and cell membrane marker Cellmask (ex: 633 nm, em: 645–786 nm) were added. Non-treated cells visualized using the same markers were kept as negative controls.

2.3.3 PET(Ti)-NPLs internalization using cell flow cytometry

The proportion of cells that internalize the PET(Ti)-NPLs was determined using cell flow cytometry. For this, 1×10^5 cells/well were seeded in triplicate in 12-well plates in a final volume of DMEM with 25 and 50 µg/mL of the fluorescent/dyed NPLs. After 24 and 48 h of treatment, cells were detached and resuspended in PBS X1 to be analyzed using a flow cytometer (CytoFLEX FACS from Beckman Coulter, Pasadena, CA, USA). After scoring 10,000 single cells, the percentage of cells that internalized the NPLs (fluorescent cells) and the mean intensity of the fluorescent signal were determined using CytExpert software. Data of three independent experiments was later analyzed using GraphPad Prism Software 8.0.2 (GraphPad, San Diego, CA).

2.3.4 Reactive oxygen species levels determination

Reactive oxygen species (ROS) levels in BEAS-2B cells, after internalization of PET(Ti)-NPLs and TiO_2-NPs, was measured via the dihydroethidium (DHE, Calbiochem, USA) assay using a flow cytometer Cytoflex S device (Beckman Coulter CytoFLEX S). For the assay, 1×10^5 cells/well were seeded in triplicate in 12-well plates in a final volume of 1 mL DMEM and treated with 50 µg/mL of PET(Ti) NPLs and 1.5 µg/mL of TiO_2-NPs for 1, 3, 24, and 48 h. Cells were detached and centrifuged at 1200 r/min for 8 min and the medium was replaced with 1X PBS. DHE solution (1 µg/mL) was added to the cell suspension and then incubated for 30 min at 37 ℃. DHE signal was determined by flow cytometry using the CytExpert software in 10,000 single cells of the treated population and relativized to non-treated control cells. Data was analyzed for all independent experiments (n = 3) using GraphPad Prism Software 8.0.2 (GraphPad, San Diego, CA).

2.3.5 Cytokines and oncology profile measurement

Differences in cytokine expression in BEAS-2B cells after exposure to PET(Ti)-NPLs were determined using the Proteome Profiler Human Cytokine Array Kit (Bio-Techne R&D Systems, ARY005B. Minneapolis, MO), which detects 36 human cytokines, chemokines, and acute phase proteins. For this assay, a total of 1×10^6 cells were seeded in a 75 cm^2 flask and treated with 50 µg/mL of PET(Ti)-NPLs for 24 and 48 h. The cell lysates for each treatment and a non-treated control were collected and incubated with the nitrocellulose membrane containing anti-cytokine antibodies, according to the manufacturer's instructions. The chemiluminescence from the membrane was detected using ChemiDoc XRS+ System (BioRad, Alcobendas, Spain), and the average pixel density of the spots representing each cytokine was determined using ImageJ

software 1.8.0_322. Cytokine expression normalized to the non-treated control was analyzed for each independent experiment ($n = 4$) using GraphPad Prism Software 8.0.2 (GraphPad, San Diego, CA). The cytokine profile of BEAS-2B cells, exposed to PET(Ti)-NPLs for 8 and 15 weeks, was also analyzed using their cell lysate and following the steps previously mentioned, and their expression was normalized against their respective cell-passaging control. Additionally, using the same lysates, the Proteome Profiler Human XL Oncology Array (ARY026, Bio-Techne R&D Systems, Minneapolis, MN, USA) was employed to detect differences between the three replicates of the long-term PET(Ti)-NPLs-treated and their corresponding passaging control in 84 cancer-related proteins.

2.3.6 H2AX histone expression evaluation

Double-strand break DNA damage after exposure to PET(Ti)-NPLs was determined by measuring the expression of H2AX histone after acute and 8 and 15-weeks long-term exposure. For this, 1×10^6 cells were seeded in a 75 cm^2 flask and treated with 50 µg/mL of PET(Ti)-NPLs for 24 and 48 h. After treatment, the cells were washed twice with cold PBS 1X, detached and then centrifuged at 1200 r/min for 8 min, and the medium was replaced with 1X RIPA buffer (50 mmol/L Tris-HCl pH 7.5, 150 mmol/L NaCl, 1 % NP-40, 0.5 % sodium deoxycholate, 0.1 % SDS; Millipore, Germany) supplemented with protease and phosphatase inhibitor (Roche, Mannheim, Germany). Cells were resuspended in the RIPA buffer and incubated for 10 min at 37 °C. Lysates were centrifuged at 13,000 × *g* for 5 min at 4 °C to remove debris, and the supernatants were collected for protein quantification using the Protein Assay Dye Reagent (BioRad, CA, USA). For SDS-PAGE, 20 µg per lane were mixed with 2 × Laemmli sample buffer (Sigma, St. Louis, US) containing 10 % β-mercaptoethanol, boiled at 95 °C for 5 min, and loaded onto 10 % SDS–polyacrylamide gels. Proteins were separated by electrophoresis at 35 mA and transferred onto cellulose membranes using the iBlot™ 2 dry blotting system (Thermo Fisher) for 7 min at 20 V. Membranes were then blocked with 5 % non-fat dry milk in Tris-buffered saline with 0.1 % Tween-20 (TBST) for 1 h at room temperature. Membranes were then incubated overnight at 4°C with H2AX (Invitrogen, MA1-2022, Rockford, IL) and GAPDH (Santa Cruz Biotechnology Inc., sc-32233, Dallas, TX) primary antibodies diluted 1:2000 in blocking solution. After washing with TBST (3 × 10 min), membranes were incubated with appropriate horseradish peroxidase (HRP)-conjugated goat anti-mouse secondary antibody (Santa Cruz Biotechnology Inc., sc-2005, Dallas, TX) for 1 h at room temperature. After final washes (3 × 10 min with TBST), protein bands were visualized covering the membrane with Immobilon® Crescendo Western HRP substrate (Millipore,

Ontario, Canada) and imaged using ChemiDoc XRS+ System (BioRad, Alcobendas, Spain). Band intensity for each independent experiment (n = 3) was quantified using ImageJ software 1.8.0_322, normalized to the GAPDH loading control and expressed relative to non-treated control conditions.

2.3.7 Genotoxic damage using the comet assay

Genotoxic and oxidative DNA damage in BEAS-2B cells after 24 and 48 h of acute exposure, and 8-week and 15-week long-term exposure to PET(Ti)-NPLs, was evaluated using the comet assay as previously described (Morataya-Reyes et al., 2025a). The assay was repeated in three independent experiments (n = 3). Comets were scored using an Olympus BX50 microscope at 20X magnification, and the Komet 5.5 Image analysis system (Kinetic Imaging Ltd, Liverpool, UK) was used to record DNA percentage in the tail. For genotoxic and oxidative DNA damage, methylmethane sulfonate (MMS) and potassium bromate ($KBrO_3$) were used as positive controls, respectively. Non-treated cells were analyzed as baseline negative controls and cells treated with methylmethane sulfonate (MMS) and potassium bromate ($KBrO_3$) were used as positive controls for genotoxic and oxidative DNA damage, respectively. Data was analyzed using GraphPad Prism Software 8.0.2 (GraphPad, San Diego, CA).

2.3.8 Soft-agar assay for anchorage-independent growth

The direct soft-agar assay permits to evaluate the cellular transformation after long-term exposure to NPLs, and it is considered one of the hallmarks of carcinogenesis (Barguilla et al., 2023). The assay was used to measure the cell ability to grow independently of anchorage after 8 and 15-weeks of exposure to PET(Ti)-NPLs. The final plates were scanned at 1200 dpi to count the colonies per well using OpenCFU-3.9.0 software and the numbers were normalized against the passage-control corresponding to the same week. Independent experiments (n = 3) for each of the long-term exposure triplicates and their passage-controls were carried out. Data was analyzed using GraphPad Prism Software 8.0.2 (GraphPad, San Diego, CA).

2.3.9 Migration and invasion potential

Following the reported method to determine different carcinogenic hallmarks (Barguilla et al., 2023), the invasion and migration potential were evaluated as an indirect assessment of the metastatic potential of the cells after 8 and 15 weeks of exposure to PET(Ti)-NPLs. The assay was repeated thrice evaluating the triplicates of each long-term treatment and the corresponding passaging-controls were evaluated for both invasion and migration potential by taking pictures

of five different regions per transwell, using a confocal microscope Olympus FV1000. The area covered by cells was analyzed with ImageJ software 1.8.0_322 and the data was later analyzed using GraphPad Prism Software 8.0.2 (GraphPad, San Diego, CA).

3 Results and discussion

3.1 Particle characterization

The PET(Ti)-NPLs used in this study were derived from the degradation of opaque polyethylene terephthalate (PET) from consumer bottles containing titanium dioxide (TiO_2-NPs) as an additive, resulting in environmentally realistic secondary NPLs. A complete morphological and physicochemical report was comprehensively analyzed in previous works (Villacorta et al., 2023, 2025). Results using scanning electron microscopy (SEM) revealed the heterogeneous surface geometry, with embedded titanium-rich domains visible in the matrix, supporting the incorporation of TiO_2-NPs into the PET polymer structure (**Fig. 1a**). Inductively coupled plasma–optical emission spectrometry (ICP-OES) was used to quantify the titanium content, confirming that TiO_2 constituted approximately 2.6 % of the total mass of the nanoplastic/metal composite suspension, in line with reported concentrations in commercial PET packaging materials. These TiO_2-NPs inclusions were further confirmed by energy-dispersive X-ray spectroscopy (EDS), which showed co-localization of titanium signals within the PET matrix, indicating the hybrid nature of PET(Ti)-NPLs (**Fig. 1b**). Transmission electron microscopy (TEM) confirmed that PET(Ti)-NPLs displayed irregular morphologies typical of environmentally derived MNPLs (Appendix A Fig. S1a), while Fourier-transform infrared spectroscopy (FTIR) confirmed the chemical identity of PET through characteristic ester and aromatic ring stretching bands (Appendix A Fig. S1b).

Size distribution was determined by different approaches. Thus, nanotracking analysis (NTA) revealed the polydispersity nature of the sample with particle size ranging from 25 to 900 nm with a mean size of 159.80 ± 1.80 nm, which in turn implies that the major concentration of the particles is found in the 100-200 nm neighborhood, as indicated in the concentration chart (**Fig. 1c**). Multiangle dynamic light scattering (MADLS) measurements confirmed the multimodal size distribution, with an average size of 352.00 ± 28.30 nm. As expected, larger agglomerates in the range of several hundred nanometers were also present (**Fig. 1d**). The zeta potential of PET(Ti)-NPLs was consistently negative, with an average value of -18.20 ± 0.82 mV, indicating relatively good colloidal stability. The polydispersity index of 0.26 confirmed the wide size range distribution observed in the previously mentioned figures. Importantly, both MADLS and NTA analyses confirmed a multimodal size distribution, with the presence of

distinct particle sub-populations and larger agglomerates, rather than a single monodisperse fraction. This heterogeneity reflects the environmentally derived origin of the PET(Ti)-NPLs, and it is consistent with previous reports using true-to-life nanoplastics.

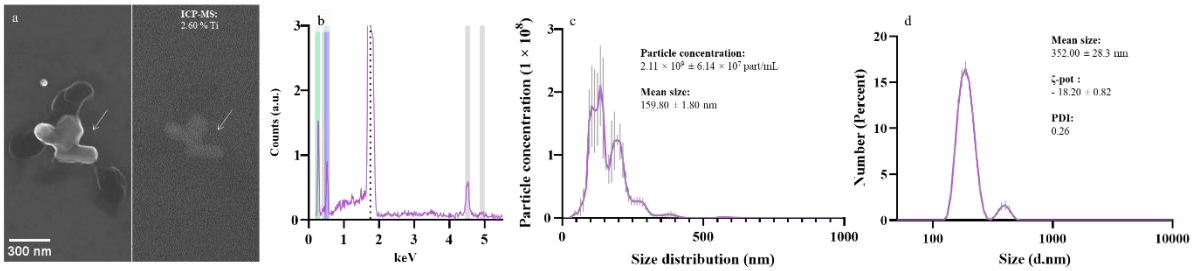

Fig. 1 Characterization of PET(Ti)-NPLs. (a) SEM images of the PET(Ti) nanoplastic showing the irregular geometry of the PET-Ti composite and the Ti internal presence with the TiO_2 percentage indicated as determined by ICP-MS. (b) Electron dispersion spectroscopy (EDS) showing the relevant peaks for Ti in grey the oxygen in blue and carbon in green. (c) Nano-tracking analysis (NTA) shows the particle concentration distribution by size. (d) Multi angle dynamic light scattering (MADLS) confirms the multimodal size distribution of the particles.

Together, these data support that PET(Ti)-NPLs used in the current study represent a true-to-life nanoplastics model, retaining both plastic polymer identity and embedded metal oxide additives, enhancing their relevance as an *in vitro* exposure model that mirrors the complex nanoplastics found in the environment. Their size, charge, and hybrid composition make them particularly relevant for investigating environmental exposure scenarios and potential interactions with biological systems.

3.2 Effects of acute exposure to PET(Ti)-NPLs

3.2.1 Internalization and cytotoxicity

BEAS-2B cells are immortalized non-tumorigenic human bronchial epithelial cells used as a representative model for the human respiratory tract, since they maintain key physiological features of bronchial epithelium, including mucosal integrity and relevant metabolic pathways, which are essential for toxicological studies (Gupta et al., 2021). They are particularly valuable for assessing inhalation exposure risks, as nanoplastics and nanoparticles are prevalent airborne pollutants that can reach the bronchial epithelium (Yang et al., 2021). In this study they were used as an appropriated *in vitro* cell model to study the effects of exposure to PET(Ti)-NPLs.

When evaluating the cytotoxicity of PET(Ti)-NPLs, results showed a reduced viability at concentrations higher than 50 µg/mL (Fig. 2a), while its TiO_2-NPs component did not have any effect in viability when cells were exposed to TiO_2-NPs alone in a range of 0 to 6 µg/mL

concentrations (Fig. 2b), covering the range corresponding to the Ti content present in used PET(Ti)-NPLs concentrations. This observation is aligned with the broader TiO_2-NPs literature in BEAS-2B, where cytotoxicity is often absent at low doses and becomes apparent only at higher mass or surface-area concentrations, depending on the crystal structure and dispersion levels (Vales et al., 2015; Fresegna et al., 2021). Taken together, it is unlikely that the content of TiO_2-NPs alone explains the cytotoxicity observed at higher concentrations of PET(Ti)-NPLs. Instead, the obtained results are in line with current research demonstrating that the biological effects induced by polymer–nanoparticle composites are primarily governed by particle heterogeneity, surface charge (Liang et al., 2022), size, morphology, and protein corona formation, rather than by the bulk composition of the polymer itself (Bilardo et al., 2022). Importantly, although the highest PET(Ti)-NPL concentrations induced a clear reduction in viability, the concentration of 50 µg/mL remained sub-cytotoxic at both 24 and 48 h, supporting its suitability for subsequent long-term exposure experiments.

The internalization of PET(Ti)-NPLs in BEAS-2B after 24 to 48 h of exposure was confirmed with minimal acute cytotoxicity at concentrations of 25 and 50 µg/mL. When using confocal microscopy, no detectable signals were observed in the non-treated BEAS-2B cells (Fig. 2c); whereas the signal of the tested NPLs was observed inside the cell (Fig. 2d). The dynamic of internalization of this particles, from 0 to 48 h, was further determined using flow cytometry, and an dose- and time-dependent increase in particle internalization was observed both as the percentage of cells that had internalized the fluorescent version of the PET(Ti)-NPLs, as well as the amount of particles inside the cell, when measuring the average intensity inside each cell (Fig. 2e and f). The absence of acute toxicity, despite internalization, fits previous results observed with acute exposure in other inhaled-relevant nanoparticles and nanoplastics, such as titanium dioxide nanoparticles (Vales et al., 2015) and silver nanoparticles in BEAS-2B cells. In addition, 50 and 100 nm PS-NPLs were able to internalize BEAS-2B and A549 cells, via energy-dependent endocytosis and traffic to endo-lysosomal compartments (Liu et al., 2022).

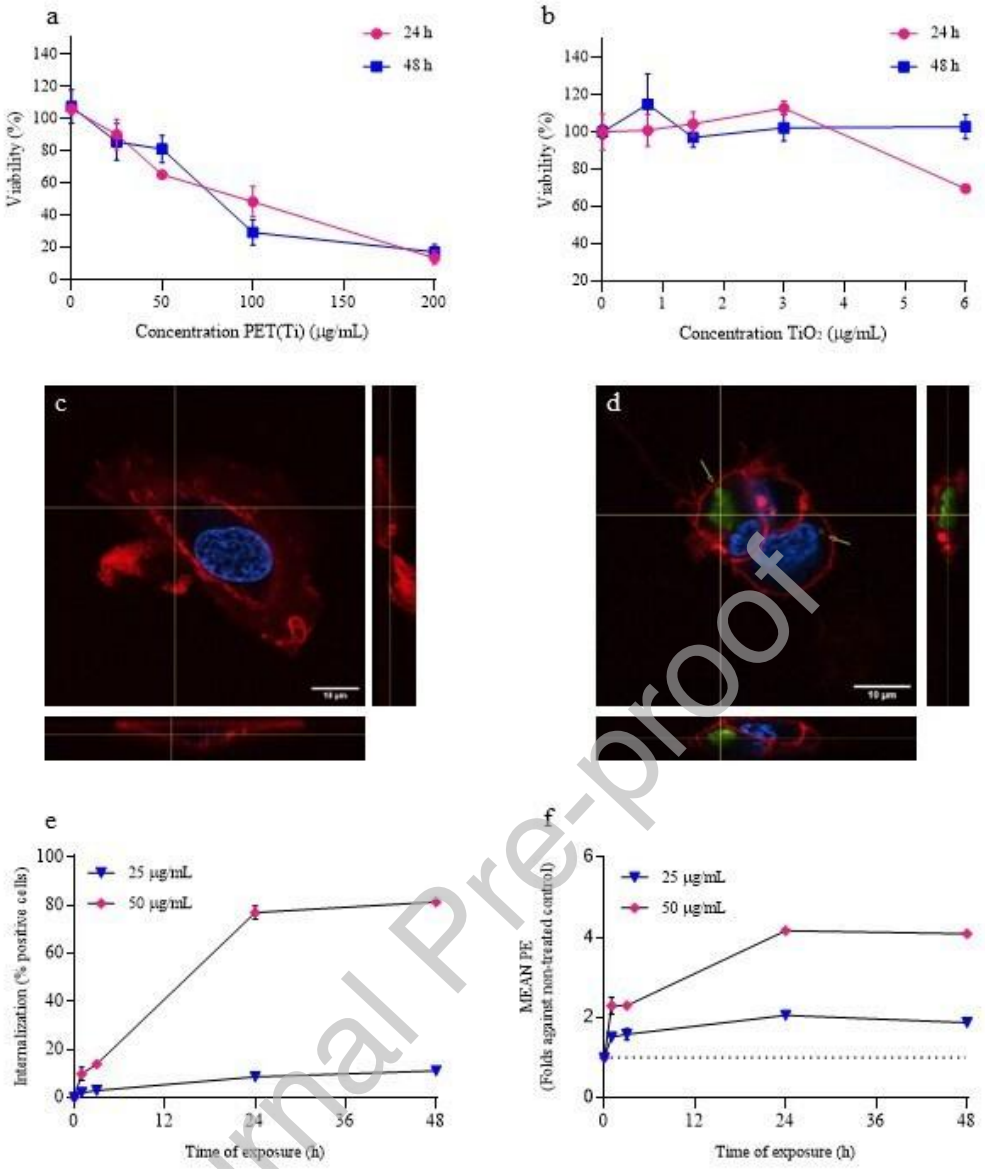

Fig. 2 Internalization and cytotoxicity of PET(Ti)-NPLs in BEAS-2B cells. (a) Viability of BEAS-2B cells after 24 and 48 h treatment with increasing concentrations of PET(Ti)-NPLs (0–200 µg/mL) and (b) after exposure to equivalent TiO_2-NPs concentrations present in PET(Ti)-NPLs (0–6 µg/mL). (d) Confocal microscopy images of BEAS-2B after 48 h of exposure to 50 µg/mL PET(Ti)-NPLs, showing cell membrane (red), nucleus (blue), and internalized particles (green), compared to (c) non-treated controls. Flow cytometry analysis showing percentage of cells with internalized PET(Ti)NPLs at 1–48 h and (f) average fluorescence intensity as an indirect measure for internalized particle load.

3.2.2 Oxidative stress and cytokine expression after acute exposure

Reactive oxygen species (ROS) levels and cytokine expression were measured in BEAS-2B cells after exposure to PET(Ti)-NPLs for 1 to 48 h. In acute NPLs exposure models, ROS and

cytokines can be used as early indicators of cellular stress and inflammatory signaling, providing mechanistic insight into sub-lethal changes in epithelial cellular behavior. Measuring these endpoints allows for initial detection of oxidative damage and immune activation, important contributors to long-term pathological processes associated with inhaled environmental particles (Mahmud et al., 2024).

The results showed a non-significant increase in ROS (Fig. 3a), but an elevation of inflammatory cytokines such as CXCL-12, IL-18, and ICAM-1 at 24 h, with a decline by 48 h (Fig. 3b). These findings suggest an early but controlled oxidative and inflammatory response without causing direct cytotoxicity. The moderate oxidative response is consistent with studies showing that NPLs-induced redox responses are highly dependent on polymer type, dose, exposure configuration, and cell phenotype. In BEAS-2B and other lung epithelial models, strong ROS rises have been reported with commercial polystyrene nanoplastics. However, differences have been reported with positively charged PS microplastics (NH_2-PS-MPLs) that significantly increased the ROS levels and the expression and secretion of the pro-inflammatory cytokine IL-β in mice experiments, while neutral or negatively charged particles did not (Jeon et al., 2023). The contrasting results highlight the influence of surface chemistry on oxidative stress induction, supporting the use of low ROS generation and limited cytokine upregulation as a reflection of moderated nanoparticle-cell interaction that could potentially be modulated by particle charge or surface characteristics.

Additionally, it is important to note that in a study carried out using the same true-to-life PET(Ti)-NPLs, THP-1 monocytes did not significantly change intracellular ROS levels after exposures lasting for 24 h to concentrations rising to 100 µg/mL, although primary DNA damage using the comet assay was detectable (Villacorta et al., 2025). The cited work pointed out how non-internalizing cells dilute the effects of exposure, pointing out how cell heterogeneity can mask early and weak oxidative signals. This masking phenomenon has also been reported with sorted alveolar macrophages exposed to true-to-life PET-NPLs, where it was observed that when the analysis is restricted to cells that internalized the NPLs (selected by cell sorting), significant ROS increases and mitochondrial dysfunction become evident even if no effects were initially observed in the unsorted population (Tavakolpournegari et al., 2024). The results of internalization of PET(Ti)-NPLs in BEAS-2B by confocal microscopy and cell cytometry (Fig. 2) indicate that at the concentrations tested, not all the cells have internalized PET(Ti)-NPLs, even after exposures lasting for 48 h. Consistently, the ROS assay in these conditions of averaging across the entire cell population, could underestimate oxidative stress occurring in the internalizing subpopulation. Although incomplete internalization could be

perceived as a limitation, it is scientifically important to evaluate sub-toxic concentrations that do not saturate uptake pathways or force uniform particle loading.

When evaluating the cytokine profile expression of BEAS-2B after exposures to PET(Ti)-NPLs, at 25 and 50 μg/mL for both 24 and 48 h, increases in CXCL-12, IL-18, ICAM-1, MIF (macrophage migration inhibitory factor), and Serpin-1 were observed, particularly at the 24 h (Fig. 3). The combination of these cytokines reflects an inflammatory response by IL-18 and MIF that stimulates innate and adaptive responses (Chiang et al., 2022), and the activation of migration, proliferation, and tissue damage repair by ICAM-1, Serpin-1, and CXCL-12, as well as the promotion of cell motility by this last one (Chen et al., 2024; Hostler et al., 2024). This pattern of responses suggests a coordinated activation of epithelial defense, barrier modulation, and immune signaling pathways after exposure to PET(Ti)-NPLs, even in the absence of clear cytotoxicity or persistent oxidative stress

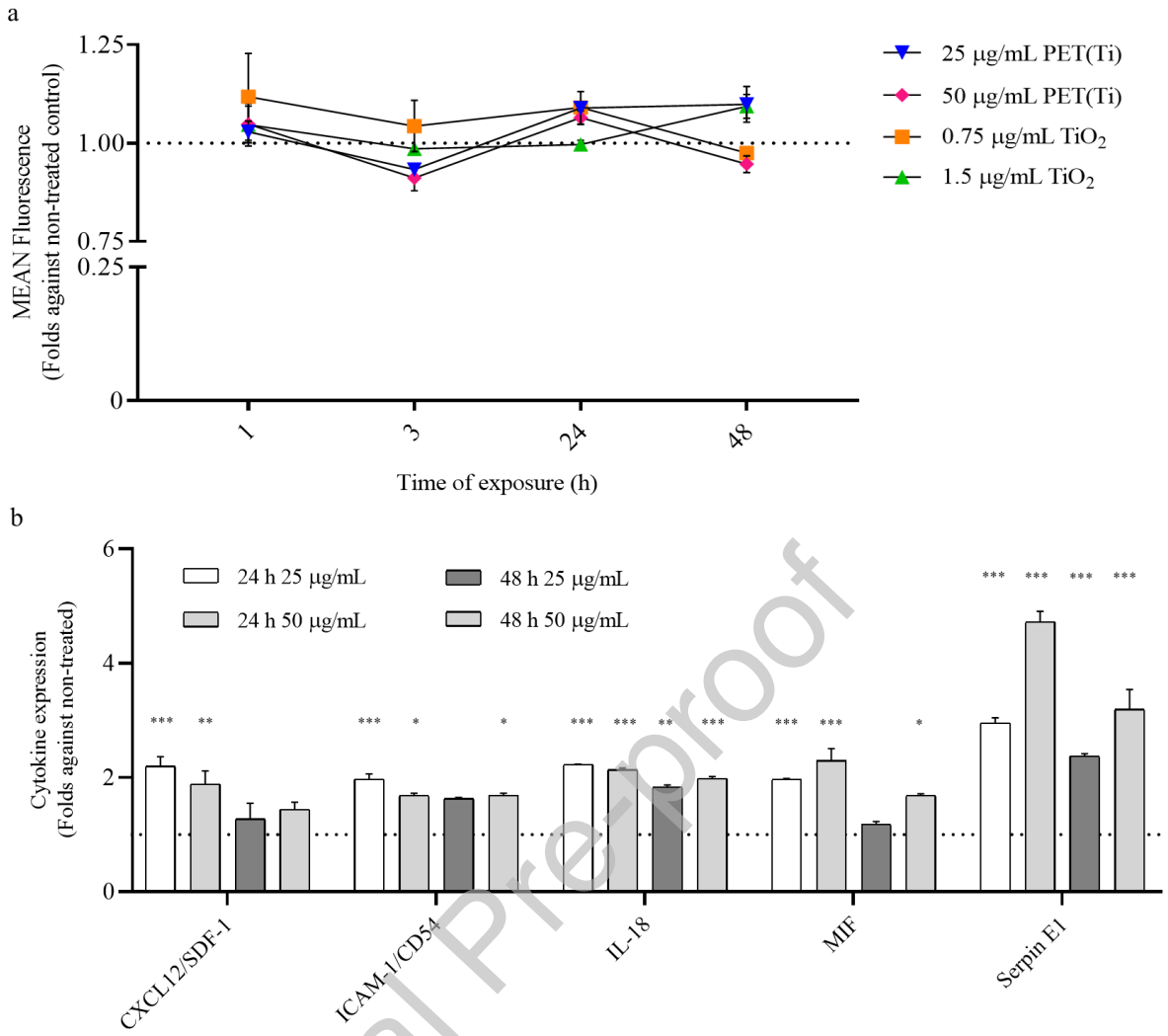

Fig. 3 Stress and inflammatory responses in BEAS-2B cells exposed to PET(Ti)-NPLs. (a) Reactive oxygen species (ROS) levels at 1, 3, 24, and 48 h after exposure to 25 and 50 µg/mL of PET(Ti)-NPLs, and their corresponding TiO_2-NPs concentrations, showing no significant differences compared to controls. (b) Cytokine array analysis after 24 and 48 h exposure. Increased expression of CXCL-12, ICAM-1, IL-18, MIF, and Serpin E1 were observed at 24 h for both concentrations of PET(Ti)-NPLs. Expression of CXCL-12, ICAM, and MIF did not show a difference after 48 h of treatment, compared to non-treated cells. A one-way ANOVA analysis comparing the different treatments against the non-treated cells and 95 % confidence was used for the analysis (*$p \leq 0.05$, **$p \leq 0.01$, ***$p \leq 0.001$).

The sustained increases across concentrations and time points suggests an early inflammatory activation of bronchial epithelial cells, findings previously observed in exposure to other NPLs such as 50 nm PS, increasing IL-6 and CCL3 expression (Breidenbach et al., 2025) and PVC, increasing the levels of IL-6 and IL-10 (Weber et al., 2022). Additionally,

differences in cytokine expression have also been recently reported in HuH-7 hepatic cells after exposure to five different nanoplastics (Morataya-Reyes et al., 2025b), with non-commercial particles of PET- and polylactic acid (PLA)-NPLs showing an increase in pro-inflammatory response like the one observed for PET(Ti)-NPLs in this study. These comparisons indicate that while cytokine responses vary by polymer type and cell context, the detection of CXCL12, IL-18, ICAM-1, MIF, and Serpin-1 reinforces a conserved epithelial strategy, orchestrating immune cell recruitment, inflammation, and tissue repair following a perturbation by the exposure to NPLs.

3.2.3 Genotoxic damage using the comet assay and H2AX expression

Recent research has demonstrated that MNPLs can cause genotoxic effects, including DNA strand breaks, chromosomal aberrations, and oxidative DNA lesions, in both *in vitro* and *in vivo* models across a range of cells/organisms. In our study, significant genotoxic damage was observed using the comet assay after exposure of BEAS-2B cells to PET(Ti)-NPLs at 25 and 50 µg/mL. While at 24 h only the 50 µg/mL concentration exhibited a significant rise in DNA damage, at 48 h both concentrations showed a clear increase in DNA strand breaks compared to non-treated controls (Fig. 4a). In contrast, H2AX expression, a marker of DNA double-strand breaks (DSBs), did not significantly differ across treatments or time points, compared to non-treated control cells (Fig. 4b).

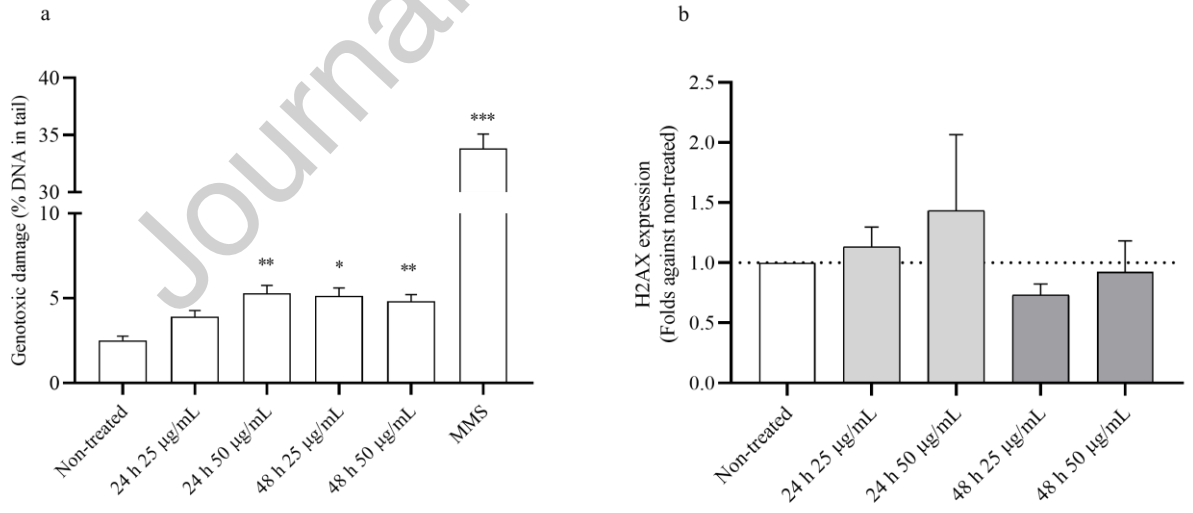

Fig. 4 (a) Genotoxic damage in BEAS-2B after 24 and 48 h of exposure to PET(Ti)-NPLs at concentrations of 25 and 50 µg/mL. A significant increase in genotoxic damage was observed after 48 h of exposure at both concentrations and at 24 h at the highest of 50 µg/mL. MMS was used as positive control for DNA damage (b) Relative expression of H2AX as a measurement of chromosome breakage, using the Western blot technique. No significant change in expression

was observed between the different concentrations of PET(Ti)-NPLs at 24 and 48 h when compared to the non-treated control. A one-way ANOVA analysis comparing the different treatments against the non-treated cells and 95 % confidence was used for the analysis (*$p \leq 0.05$, **$p \leq 0.01$, ***$p \leq 0.001$).

The present study shows that PET(Ti)-NPLs induce moderate DNA strand breaks in BEAS-2B, detectable by the comet assay but they do not initiate a H2AX-mediated DNA damage response high enough to be detected by these acute exposure conditions. It must be remembered that the comet assay is highly sensitive in detecting single- and double-strand breaks, alkali-labile sites, and oxidative lesions, even at low levels of DNA damage and early in the exposure timeline. On the other hand, the detection of H2AX phosphorylation (a known marker of DSBs and crucial for recruiting repair proteins to damage sites) requires a certain threshold of DSBs or replication-associated breaks to activate the DNA damage response pathways (Zhao, et al., 2019). Consequently, the absence of significant changes in H2AX expression could suggest that the observed DNA damage may mainly consist of single strand breaks or subtle lesions that do not reach sufficient severity to trigger γH2AX formation. Additionally, the levels, or type of DNA damage, may be below the sensitivity threshold of H2AX detection for methods such as Western blot, especially when both the internalization of the NPLs and the damage are heterogeneous across the cell population. Moreover, the genotoxic mechanisms of PET(Ti)-NPLs could involve oxidative base damage or replication-associated stress that produce breaks inefficiently signaled via H2AX. Unless DSBs are widespread or replication forks collapse, γH2AX may remain below detection thresholds despite measurable genotoxicity.

As mentioned before, the genotoxic effects of MNPLs have been reported in multiple study models and under exposure to diverse polymers. However, the mechanisms underlying this DNA damage are complex, involving direct physical interactions with DNA molecules, oxidative stress, and interference with DNA repair pathways (Sun et al., 2023; Pujol et al., 2025). Thus, the extent of genotoxicity appears to depend on several factors, including particle size, surface charge, chemical composition, and environmental aging or functionalization of the nanoplastics (Martín-Pérez et al., 2024). While PS-NPLs are the most studied, evidence is emerging for genotoxic effects from other petroleum-based polymer types such PET and PVC, as well as for certain bioplastics like polylactic acid (PLA) (Alaraby et al., 2024; García-Rodríguez et al., 2024; Villacorta et al., 2025). Notably, some studies report minimal or no DNA damage under certain conditions, stressing the complexity of MNPL toxicity and the need for further research to clarify exposure risks (Xu et al., 2022). Finally, the difference in results

highlights the importance of using complementary genotoxic endpoints, especially under sub-cytotoxic low-level exposure scenarios that are environmentally relevant. For this reason, for future work it is recommended to employ complementary techniques such as immunofluorescent γH2AX foci counting, or additional endpoints such as micronucleus formation. All together it may provide deeper resolution of damage types and repair dynamics.

3.3 Long-term exposure to PET(Ti)-NPLs

Chronic exposure to environmental pollutants, including MNPLs, can result in cumulative cellular damage and pathological alterations that are not evident under acute exposure scenarios. Long-term *in vitro* exposure models, spanning weeks or months, are crucial for determining progressive genotoxicity, cell transformation, and bioaccumulation patterns that mimic *in vivo* chronic exposure scenarios and may reflect human health risks associated with prolonged exposures (Vales et al., 2015). For example, chronic exposure to multi-walled carbon nanotubes (MWCNTs) in BEAS-2B cells triggered epithelial-mesenchymal transition (EMT) and the formation of anchorage-independent phenotypes over several weeks (Barthel et al., 2021). In the BEAS-2B model, exposure to PET-NPLs for 30 weeks increased genotoxic damage, anchorage-independent growth, and invasive potential, as well as the upregulation of lung cancer-associated genes (Gutiérrez-García et al., 2025). In addition, the co-exposure to PET-NPLS and cigarette smoke condensate over 4 weeks in BEAS-2B cells induced cell transformation, exacerbated oxidative stress, genotoxicity, and tumorigenic transformation, and produced the upregulation of stress-response genes (Morataya-Reyes et al., 2025a). These studies highlight the significance of time-dependent effects and their potential to report effects in early stages of cell transformation. In this study, after evaluating the short-term effects of PET(Ti)-NPLs, BEAS-2B cells were continuously exposed to these NPLs at a concentration of 50 μg/mL for up to 15 weeks, and biological markers associated with cell transformation and cancer phenotype development were evaluated to determine the long-term effects of this exposure. The dose was intentionally chosen as it was the highest concentration producing nontoxic effects after 48 h of acute exposure (Fig. 2a). Using sub-toxic concentrations is critical for long-term models, as it allows for the investigation of cumulative, adaptive, and transformation-related cellular changes over an extended period without the confounding effects of acute cell death. This concentration is also in line with those used in other *in vitro* nanotoxicology studies investigating cellular transformation pathways and lower/equal than those used in other long-term studies reporting transformation-related outcomes following chronic exposure to poorly soluble particles or nanoplastics. These studies include long-term

exposure to TiO_2-NPs and PET-NPLs in BEAS-2B cells (Vales et al., 2015; Gutiérrez-García et al., 2025), PS-NPLs in Caco-2 cells (Domenech et al., 2021), and co-exposure to arsenic and PS-NPLs in mouse embryonic fibroblasts (Barguilla et al., 2022).

3.3.1 Long-term PET(Ti)-NPLs internalization and genotoxicity

Confocal microscopy was used to determine if, after 8 and 15 weeks of continuous exposure to PET(Ti)-NPLs (50 µg/mL), the cell model could still internalize these particles. As shown in Fig. 5, after exposures lasting for 8 and 15 weeks, PET(Ti)-NPLs are still internalizing into BEAS-2B cells (Fig. 5b, d), in contrast to what is observed in passage-matched controls (Fig. 5a, c). The persistent, but moderated, internalization of these NPLs after prolonged exposure indicates that the cell system has not been saturated after the long-term exposure. This agrees with previous studies noticing the differences between treatments and effective doses, showing that cellular internalization does not necessarily scale linearly with administered concentration, due to the dynamic balance between uptake, intracellular processing, dilution through cell division, and clearance mechanisms (Khanbeigi et al., 2012; Vranic et al., 2013; Lichtenstein et al., 2017; Yin et al., 2021). This allows for the study of long-term effects under conditions that mimic the bioaccumulation in relevant chronic low-dose environmental scenarios, without causing cytotoxicity. As discussed for the internalization after short-term exposure to PET(Ti)-NPLs, this can be a consequence of accumulation in lysosomes after internalization via endocytosis (Liu et al., 2022). Although endocytosis and exocytosis pathways operate simultaneously, intracellular load can increase and, even if exocytosis rises, it is often insufficient to eliminate internalized particles. As a result, a dynamic state with partial long-term intracellular retention rather than continuous accumulation is established, maintaining a relatively constant intracellular particle burden that could explain the biological effects observed after long term exposure to PET(Ti)-NPLs (Liu et al., 2023; Yang and Wang, 2023; Chang and Wang, 2024).

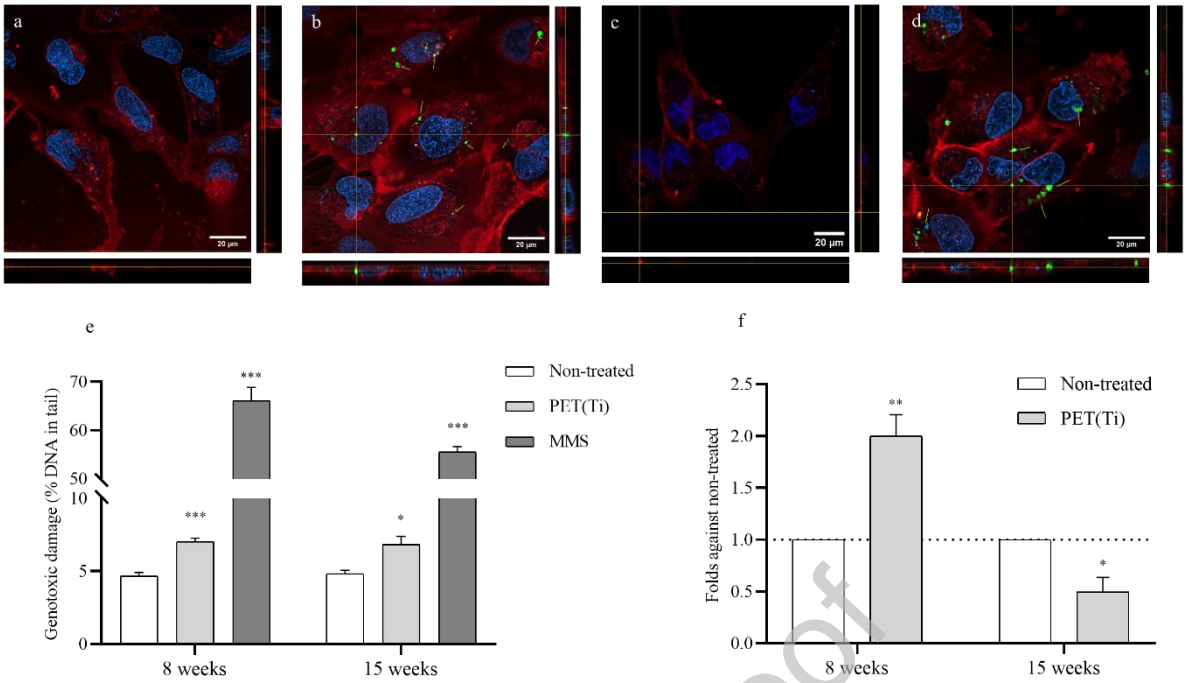

Fig. 5 Internalization and DNA damage in BEAS-2B cells after long-term exposure to PET(Ti)-NPLs. (b, d) Confocal microscopy images of BEAS-2B after 8 and 15 weeks of exposure to 50 µg/mL PET(Ti)-NPLs, showing particle retention, compared to their corresponding (a, c) passage-matched non-treated controls, showing cell membrane (red), nucleus (blue), and internalized particles (green). (e) Comet assay data showing significant DNA damage at both 8 and 15 weeks. MMS was used as positive control. (f) H2AX expression after long-term exposure showed a significant increase at 8 weeks and a significant decrease at 15 weeks compared to passaging controls. A one-way ANOVA analysis comparing the different treatments against the non-treated cells in the comet assay and a *t*-test analysis with 95 % confidence was used to compare the expression of H2AX in treated and non-treated cells (*$p \leq 0.05$, **$p \leq 0.01$, ***$p \leq 0.001$).

The comet assay was used to determine the genotoxic potential of the long-term exposure to PET(Ti)-NPLs. While acute PET(Ti)-NPL exposure induced modest DNA damage at 50 µg/mL after 24 h and at both 25 and 50 µg/mL after 48 h, without a corresponding rise in H2AX expression (Fig. 4a-b), a significant increase in DNA damage was detected in BEAS-2B after 8 and 15 weeks of continuous exposure, compared to the non-treated passage controls (Fig. 5e). This would confirm the potential genotoxic effects of PET(Ti)-NPL exposure. Similarly, a significant increase in H2AX expression at 8 weeks was observed, suggesting activation of the DNA damage response (Fig. 5f). However, after exposures lasting for 15 weeks, H2AX levels significantly decreased compared to the passage controls. This fluctuation suggests a complex

adaptive response and an accumulation of DNA double-strand breaks. The decrease observed at 15 weeks, despite ongoing genotoxic damage resulting from the NPLs exposure (Fig. 5e), may indicate activation of alternative or faulty repair pathways or the cellular adaptation to a new baseline of damage.

These results, compared to those observed in acute exposure at 25 and 50 μg/mL, could indicate ongoing genotoxic stress and activation of DSB-associated repair pathways, whereas its subsequent decrease at 15 weeks could be related to partial repair, checkpoint adaptation, or selection of resistant cell populations. This time-dependent evolution aligns with findings in other long-term exposure studies using other NPL models. Thus, the continuous exposure to PET-NPLs, derived from PET plastic bottles, demonstrated that genotoxic damage, anchorage-independent growth, and invasive behavior emerged only at 30 weeks, not at 15 weeks or earlier, highlighting the sustained nature of transformation processes (Gutiérrez et al., 2025). Additionally, the potential cell transforming effects of PET-MNPL exposure were determined via multi-omics analysis, showing their interaction with proteins critical for cellular proliferation, DNA repair, immune regulation, and apoptosis (Yang et al., 2025). BEAS-2B cells have been used to determine the prolonged effects of other nanoparticles; thus, chronic exposure to multi-walled carbon nanotubes (Barthel et al., 2021) and silver nanoparticles resulted in DNA damage and cell transformation with a required latency period of several weeks or months before the emergence of significant effects.

The temporal mismatch between comet-detectable damage and H2AX signaling highlights the complexity of damage detection and management over time in epithelial cell systems. All together, these data support a model in which acute exposure elicits DNA damage without significant cytotoxicity, and both DNA damage and cellular transformation markers accumulate gradually, reinforcing the importance of extended, realistic exposure models. These parallel effects reinforce how exposure time is a determining factor in the manifestation and repair of genotoxic damage, specifically in a pulmonary epithelial context, while persistent DNA damage and dynamic H2AX response during chronic PET(Ti)-NPL exposure strengthens the potential for progressive genomic instability.

3.3.2 Cytokine and oncology profiles of long-term exposed BEAS-2B cells

The expression of cell cytokines and the oncology profile of long-term exposed BEAS-2B cells were evaluated after 8 and 15 weeks of continuous treatment with PET(Ti)-NPLs at 50 μg/mL (Fig. 6). After 8 weeks of exposure, a significant decrease in ICAM-1 and MMP-3 was detected, alongside a significant increase in progranulin (Fig. 6a). After 15 weeks of exposure

(Fig. 6b), the profile shifted, with a significant increase in MIF, and marked decreases in Cathepsin B, Cathepsin D, CXCL8 (IL-8), and PLAU (urokinase-type plasminogen activator).

Long-term PET(Ti)-NPL exposure in BEAS-2B cells drives dynamic shifts in cytokines and cancer-related protein signatures that appear to transition from early epithelial stress toward a modulated tumor-supportive phenotype. At 8 weeks, elevated progranulin levels are particularly marked, potentially affecting progranulin functions. Progranulin acts as an autocrine growth factor promoting cell proliferation, motility, and tissue repair, and it has been found upregulated across diverse cancers, serving as a prognostic biomarker, especially in lung and epithelial malignancies (Zhou et al., 2021). This increase, next to a reduction in ICAM-1, linked to leukocyte trafficking and barrier integrity (Bui et al., 2020), and MMP-3, central to ECM breakdown and tissue remodeling (Cabral-Pacheco et al., 2020), suggests that long-term exposed epithelial cells may reduce barrier functions and ECM remodeling in favor of proliferative and survival responses.

After exposures lasting for 15 weeks, the expression profile changed and MIF, a multifunctional cytokine involved in inflammation, cell survival, and immune modulation (Sumaiya, et al., 2022), significantly increased. This shift could reflect adaptation toward chronic stress or premalignant behavior (Yan et al., 2024). Simultaneously, drops in Cathepsin B/D, CXCL8, and PLAU (urokinase-type plasminogen activator), all key mediators of proteolysis, chemotaxis, and matrix degradation, could indicate a decrease in immediate inflammatory signaling and invasion-associated behaviors (Repnik et al., 2015; Vizovišek, et al., 2019). Such downregulation might reflect the emergence of a transformed-like state where early defense responses are suppressed in favor of sustained survival and altered cellular communication.

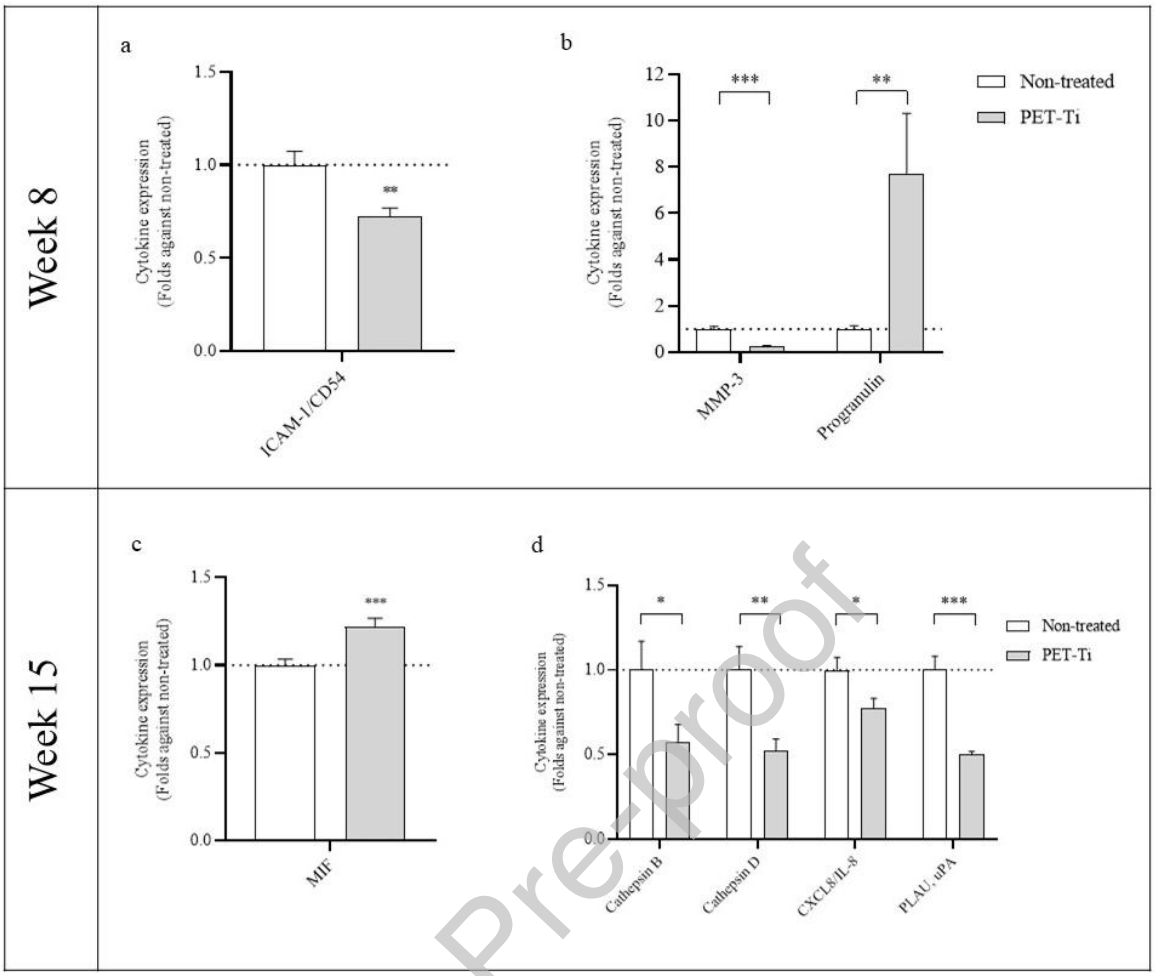

Fig. 6 Cytokine and oncology profile of BEAS-2B cells after 8 and 15 weeks of exposure to PET(Ti)-NPLs at a concentration of 50 µg/mL. A significant decrease in (a) ICAM-1 and (b) MMP-3, as well as an increase in progranulin, cancer-related protein, were observed after 8 weeks of exposure to PET(Ti)-NPLs. For exposures lasting for 15 weeks, (c) an increase in MIF was observed, as well as a (d) significant decrease in Cathepsin B and D, CXCL8, and PLAU, all of them proteins related to the development of an oncologic profile. A *t*-test analysis with 95 % confidence was used to compare the expression of each protein in the non-treated and PET(Ti)-treated cells (*$p \leq 0.05$, **$p \leq 0.01$, ***$p \leq 0.001$).

The comparison between acute and long-term exposures to PET(Ti)-NPLs reveals a notable evolution in epithelial cytokine signaling. During acute exposure, BEAS-2B cells transiently upregulated pro-inflammatory and repair-related cytokines, reflecting a rapid but reversible activation of innate immune and tissue repair pathways. In contrast, long-term exposure leads to a more selective and complex reprogramming towards modulated, oncogenic-like signaling,

reflecting cellular adaptation and potentially pre-malignant remodeling. Similar changes have been documented in lung epithelial models exposed to sub-chronic nanoparticles or pollutant challenges, where initial inflammatory bursts give way to altered secretome landscapes as cells adapt or undergo phenotypic changes (Sanchez-Guzman et al., 2021). These findings reinforce the value of long-term exposure models, since acute studies often miss dynamic and delayed shifts in epithelial function and evidence that persistent nanoplastic retention can rewire cellular signaling toward tumor-associated phenotypes over weeks. In this study, PET(Ti)-NPL exposure stimulated a complex oncogenic signaling profile that unfolds over time, rather than immediately upon contact.

3.3.3 Progression of transformed phenotype after long-term exposure to PET(Ti)-NPLs

Potential cell transforming effects induced by environmental pollutants, such as nanoplastics, appear because of continuous long-term exposure. Following the approach proposed by Barguilla et al. to determine the potential carcinogenic effects of environmental pollutants (Barguilla et al., 2023), intermediate and advanced oncogenic biomarkers such as soft-agar colony formation (Fig. 7a), as a marker of anchorage-independent growth, cell migration (Fig. 7b), and invasion-potential (Fig. 7c) were selected to evaluate exposure to PET(Ti)-NPLs in BEAS-2B for 8 to 15 weeks.

During both 8 and 15 weeks, no significant anchorage-independent growth was observed in BEAS-2B exposed cells, compared to non-treated passage controls. However, cell migration and invasion assays demonstrate significantly enhanced migratory ability and invasive potential in treated cells at both time points.

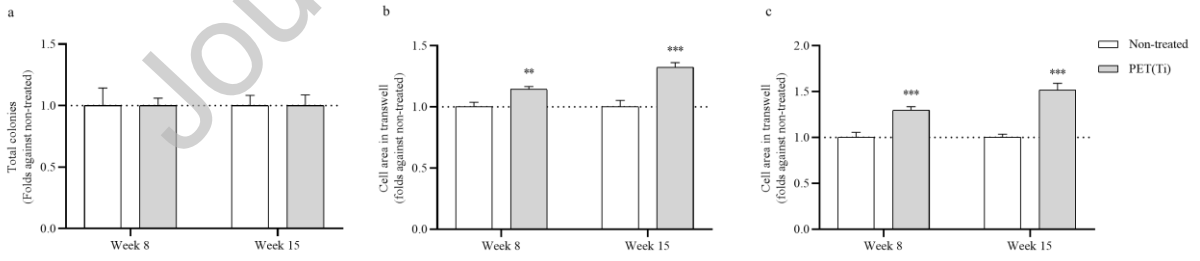

Fig. 7 Anchorage-independent growth and migratory/invasive potential of BEAS-2B cells after long-term exposure to PET(Ti)-NPLs. (a) Soft-agar assay showing no significant difference in anchorage-independent cell growth of BEAS-2B cells between control and PET(Ti)-treated cells after 8 and 15 weeks. (b) Migration assay showing significantly increased migratory ability at 8 and 15 weeks. (c) Invasion assay confirming significantly increased invasive capacity at 8

and 15 weeks. A *t*-test analysis with 95 % confidence was used to compare the results for non-treated and PET(Ti)-NPLs treated cells (**$p \leq 0.01$, ***$p \leq 0.001$).

These results suggest that long-term exposure to a sub-toxic concentration of PET(Ti)-NPLs in BEAS-2B initiates early oncogenic behavior in bronchial epithelial cells, characterized by markedly increased cell motility and invasion, even in the absence of anchorage-independent growth. This phenotypic profile similarly appears in studies of other nanoparticles, for example, chronic treatment of BEAS-2B with silver nanoparticles (Ag-NPs) significantly enhanced anchorage-independent colony formation, migration, invasion, and EMT characteristics, indicating full transformation after prolonged exposure (Choo et al., 2016). In contrast, our PET(Ti)-NPL model appears to correspond to an intermediate transformation stage, wherein migratory and invasive competencies are acquired before anchorage independence. Evidence from PS-NPL studies reinforces this gradual progression with exposure to up to 24 weeks leading to the emergence of several cancer hallmarks, including anchorage-independent growth, showing that nanoplastic-induced transformation changes accumulate over extended periods (Barguilla et al., 2022).

Exposure to TiO_2-NPs was included in the acute assays at concentrations corresponding to the Ti content present in PET(Ti)-NPL samples without cytotoxic or oxidative effects induction. Consequently, and due to the complexity and workload required for chronic studies, the effects of exposure to TiO_2-NPs have not been considered in the long-term study. Instead, comparisons with the previous study of Vales et al. (2015) were taken into consideration since that long-term study included TiO_2-NP exposures at equivalent TiO_2 concentrations as those present in our study. Interestingly, induced anchorage-independent growth without detectable DNA damage was observed, suggesting non-genotoxic pathways to transformation, contrasting with PET(Ti)-NPL effects. These comparisons support a model in which PET(Ti)-NPLs drive progressive acquisition of pre-malignant traits, starting with increased migration and invasion, and potentially culminating in full transformation with longer exposure. The absence of anchorage-independent growth by 15 weeks indicates that this critical oncogenic threshold has not yet been crossed but might emerge with continued exposure. From a mechanistic perspective, migratory and invasive behaviors often reflect cytoskeletal reorganization, ECM receptor modulation, and EMT-like signaling, even absent full transformation (Datta et al., 2021).

While PET(Ti)-NPLs did not trigger colony formation in soft agar, the enhanced motility and invasion could indicate intermediate EMT-like phenotypic shifts consistent with other chronic exposure models to PET-NPLs in lung epithelium (Gutiérrez-García et al., 2025;

Morataya-Reyes et al., 2025a). It is important to notice that in the present study, PET(Ti)-NPLs induced significant migratory and invasive potential at just 8 and 15 weeks (Fig. 7b, c). In contrast, Gutiérrez-García et al. (2025), using the same long-term protocol with PET-NPLs alone, observed these same markers only after 30 weeks of exposure. This suggests that the presence of the TiO_2 additive may significantly accelerate the acquisition of these cell transformation-related phenotypes. These findings could show that, while PET(Ti)-NPL-treated BEAS-2B cells have not acquired full transformation, they exhibit robust acquisition of migration and invasion traits, hallmark behaviors of pre-malignant progression in a time-dependent manner.

Despite the insights provided, the conclusions of this study must be considered in the context of its limitations. It is important to recognize that even if BEAS-2B cells are a standard model for the bronchial epithelium, they cannot capture the full complexity of the human respiratory system, such as the interactions between different cell types or the influence of the *in vivo* microenvironment. There is a research need to move towards more advanced models, including air-liquid interface (ALI), dynamic microfluidic, and 3D/organ-on-chip platforms that better reflect the complexity of the exposure routes as well as the tissue architecture and immune interactions (Forest and Pourchez, 2023; Khan and Jia, 2023; Cho and Kim, 2025). Therefore, while the present findings provide mechanistic insight into the cellular responses and transformation-related phenotypes induced by long-term PET(Ti)-NPL exposure, their extrapolation to the human respiratory system would benefit from further validation in more complex *in vitro* models and future *in vivo* studies.

It should also be considered that, as with other nanomaterials and nanoplastics, the physicochemical state of PET(Ti)-NPLs may evolve once dispersed in serum-containing culture medium due to aggregation and protein corona formation. Such processes can modify the apparent hydrodynamic size and surface properties of the particles, potentially influencing cellular uptake and intracellular trafficking. However, this dynamic behavior is inherent to realistic exposure scenarios and has been widely reported for nanoplastics and other nanoparticles under biological conditions. Importantly, because all experimental conditions were conducted using the same dispersion protocol and medium composition, relative comparisons between treated and control groups remain valid.

Additionally, the long-term experiments were conducted using a single, sub-toxic concentration of 50 µg/mL. As discussed before, this dose was chosen for mechanistic investigation, but the realistic chronic human exposure levels to NPLs remain a topic of debate and could likely be different from the one used here. At present, human chronic exposure to

nanoplastics remains poorly constrained, and direct extrapolation of *in vitro* mass-based concentrations to environmental or occupational exposure scenarios is limited by uncertainties related to particle heterogeneity, dose metrics, deposition efficiency, and internal dose (Forest and Pourchez, 2023; Wright et al., 2024). Accordingly, the concentration used in the present long-term model should be interpreted as a mechanistically informative, sub-cytotoxic dose rather than a direct proxy for environmental exposure levels. Future studies are needed to determine if the observed effects, such as increased migration and genomic instability, also occur at more environmentally representative concentrations. These limitations highlight the need for further research to fully understand the long-term respiratory hazards of hybrid nanoplastics.

4 Conclusions

The present study provides a comprehensive description of the acute and long-term effects of true-to-life PET(Ti)-NPLs in human lung (BEAS-2B) cells, offering novel insights into their potential health risks upon inhalation exposure. Results demonstrate that while acute exposure induces modest oxidative and inflammatory responses and detectable DNA strand breaks without clear cytotoxicity, long-term exposure drives a progressive shift toward sustained genomic instability, altered cytokine and oncogenic signaling, and acquisition of pre-malignant traits. Notably, prolonged exposure for up to 15 weeks led to persistent DNA damage, dynamic modulation of H2AX expression, altered cytokine and cancer-related protein profiles, and significantly increased migratory and invasive behaviors, even in the absence of anchorage-independent growth. Together, these findings highlight that sub-toxic concentrations of PET(Ti)-NPLs can promote early carcinogenic-like phenotypes in human bronchial epithelial cells in a time-dependent manner. The absence of full malignant transformation by 15 weeks underscores the importance of longer-term models to capture the cumulative and progressive nature of nanoplastic-induced effects. Moreover, the observed discrepancies between comet assay outcomes and H2AX dynamics, as well as the evolving cytokine profile, emphasize the complexity of cellular adaptation to chronic nanoparticle stress. Overall, the results obtained strengthens the evidence that inhaled nanoplastics, specifically true-to-life PET(Ti)-NPLs, that combine polymeric and metal oxide components, could pose a potential respiratory hazard, not only by triggering acute stress responses but also by promoting long-term genomic and phenotypic alterations associated with early stages of cell transformation. This supports the need for chronic exposure studies using environmentally relevant nanoplastic models, and it

reinforces the importance of considering nanoplastics as emerging airborne pollutants of toxicological concern in human health risk assessment and regulatory frameworks.

CRediT authorship contribution statement

Morataya-Reyes, Michelle: Methodology, Data curation, Writing-original draft preparation. Villacorta, Aliro: Methodology, Data curation, Reviewing and editing. Martín-Pérez, Joan: Methodology. Barguilla, Irene: Methodology. Rubio, Laura: Methodology. Egea, Raquel: Methodology. Marcos, Ricard: Writing, reviewing, and editing. Hernández, Alba: Writing, reviewing, and editing.

Declaration of competing interest

The authors declare that they have no known competing financial interests or personal relationships that could have appeared to influence the work reported in this paper.

Acknowledgments

This project (PlasticHeal) has received funding from the European Union's Horizon 2020 research and innovation programme under grant agreement No. 965196. This work was partially supported by the Spanish Ministry of Science and Innovation (No. PID2020–116789, RB-C43) and the Generalitat de Catalunya (No. 2021-SGR-00731).

Morataya-Reyes, Michelle holds a FI (2022) Ph.D. fellowship, and Martín-Pérez, Joan holds a FI_SDUR (2021) Ph.D. fellowship, both from the Generalitat de Catalunya. Villacorta, Aliro was supported by a Ph.D. fellowship from the National Agency for Research and Development (ANID), CONICYT PFCHA/DOCTORADO BECAS CHILE/2020–72210237, Núcleo de Investigación en Ciencias Biológicas. Rubio, Laura holds a postdoctoral Juan de la Cierva contract (IJC2020–2686I/AEI/10.13039/501100011033). Barguilla, Irene received funding from the postdoctoral program Beatriu de Pinós (Departament de Recerca i Universitats de la Generalitat de Catalunya, record: 2023-BP-00212). Hernández, Alba was granted an ICREA ACADEMIA award.

Appendix A Supplementary data

Supplementary data associated with this article can be found in the online version at xxxxxx.

References

Alaraby M., Abass D., Farré M., Hernández A., Marcos R., 2024. Are bioplastics safe? Hazardous effects of polylactic acid (PLA) nanoplastics in *Drosophila*. Sci. Total Environ. 919, 170592.

Barguilla I., Domenech J., Rubio L., Marcos R., Hernández A., 2022. Nanoplastics and arsenic co-exposures exacerbate oncogenic biomarkers under an *in vitro* long-term exposure scenario. Int. J. Mol. Sci. 23, 2958.

Barguilla I., Domenech J., Ballesteros S., Rubio L., Marcos R., Hernández A., 2022. Long-term exposure to nanoplastics alters molecular and functional traits related to the carcinogenic process. J. Hazard. Mater. 438, 129470.

Barguilla I., Maguer-Satta V., Guyot B., Pastor S., Marcos R., Hernández A., 2023. *In vitro* approaches to determine the potential carcinogenic risk of environmental pollutants. Int. J. Mol. Sci. 24 (9), 7851.

Barthel H., Darne C., Gaté L., Visvikis A., Seidel C., 2021. Continuous long-term exposure to low concentrations of MWCNTs induces an epithelial-mesenchymal transition in BEAS-2B cells. Nanomaterials 11 (7), 1742.

Bilardo R., Traldi F., Vdovchenko A., Resmini M., 2022. Influence of surface chemistry and morphology of nanoparticles on protein corona formation. Wiley Interdiscip. Rev. Nanomed. Nanobiotechnol. 14 (4), e1788.

Breidenbach J., French B., Shrestha U., Adya Z., Wooten R., Fribley A., et al., 2025. Acute exposure to aerosolized nanoplastics modulates redox-linked immune responses in human airway epithelium. Antioxidants 14 (4), 424.

Cabral-Pacheco G., Garza-Veloz I., La Rosa C., Ramirez-Acuña J., Perez-Romero B., Guerrero-Rodriguez J., et al., 2020. The roles of matrix metalloproteinases and their inhibitors in human diseases. Int. J. Mol. Sci. 21 (24), 9739.

Chang X., Wang W.X., 2024. Differential cellular uptake and trafficking of nanoplastics in two hemocyte subpopulations of mussels *Perna viridis*. J. Hazard. Mater. 471, 134388.

Chen X., Li H., Wei X., Jing N., Qing L., Jiang H., et al., 2024. SERPINA1 promotes the invasion, metastasis, and proliferation of pancreatic ductal adenocarcinoma via the PI3K/Akt/NF-κB pathway. Biochem. Pharmacol. 230 (Pt 2), 116580.

Chiang H., Lu H., Sudhakar J., Chen Y., Shih N., Weng Y., et al., 2022. IL-22 initiates an IL-18-dependent epithelial response circuit to enforce intestinal host defence. Nat. Commun. 13 (1), 874.

Cho Y., Kim H.N., 2025. Organoid-based platforms for investigating microplastic-induced human organ toxicity. Organoid 5, e5.

Choo W.H., Park C.H., Jung S.E., Moon B., Ahn H., Ryu J.S., et al., 2016. Long-term exposures to low doses of silver nanoparticles enhanced *in vitro* malignant cell transformation in non-tumorigenic BEAS-2B cells. Toxicol. in Vitro 37, 41–49.

Datta A., Deng S., Gopal V., Yap K., Halim C., Lye M., et al., 2021. Cytoskeletal dynamics in epithelial-mesenchymal transition: Insights into therapeutic targets for cancer metastasis. Cancers 13 (8), 1882.

Domenech J., De Britto M., Velázquez A., Pastor S., Hernández A., Marcos R., et al., 2021. Long-term effects of polystyrene nanoplastics in human intestinal Caco-2 cells. Biomolecules 11, 1442.

Dong C.D., Chen C.W., Chen Y.C., Chen H.H., Lee J.S., Lin C.H., 2020. Polystyrene microplastic particles: *In vitro* pulmonary toxicity assessment. J. Hazard. Mater. 385, 121575.

Forest V., Pourchez J., 2023. Can the impact of micro- and nanoplastics on human health really be assessed using *in vitro* models? A review of methodological issues. Environ. Int. 178, 108115.

Fresegna A.M., Ursini C.L., Ciervo A., Maiello R., Casciardi S., Iavicoli S., et al., 2021. Assessment of the influence of crystalline form on cyto-genotoxic and inflammatory effects induced by TiO_2 nanoparticles on human bronchial and alveolar cells. Nanomaterials 11 (1), 253.

García-Rodríguez A., Gutiérrez J., Villacorta A., Arranz A., Romero-Andrada I., Lacoma A., et al., 2024. Polylactic acid nanoplastics (PLA-NPLs) induce adverse effects on an *in vitro* model of the human lung epithelium: The Calu-3 air-liquid interface (ALI) barrier. J. Hazard. Mater. 475, 134900.

Gupta G., Vallabani S., Bordes R., Bhattacharya K., Fadeel B., 2021. Development of microfluidic, serum-free bronchial epithelial cells-on-a-chip to facilitate a more realistic *in vitro* testing of nanoplastics. Front. Toxicol. 3, 735331.

Gutiérrez-García J., Egea R., Barguilla I., Nymark P., García-Rodríguez A., Guyot B., et al., 2024. Long-term exposure to real-life polyethylene terephthalate nanoplastics induces carcinogenesis *in vitro.* Environ. Sci. Technol. 59 (22), 10891–10904.

Hostler A., Hahn W., Hu M., Rennert R., Fischer K., Barrera J., et al., 2024. Endothelial-specific CXCL12 regulates neovascularization during tissue repair and tumor progression. FASEB J. 38 (24), e70210.

Jenner L.C., Rotchell J.M., Bennett R.T., Cowen M., Tentzeris V., Sadofsky L.R., 2022. Detection of microplastics in human lung tissue using μFTIR spectroscopy. Sci. Total Environ. 831, 154907.

Jeon M.S., Kim J.W., Han Y.B., Jeong M.H., Kim H.R., Sik Kim H., et al., 2023. Polystyrene microplastic particles induce autophagic cell death in BEAS-2B human bronchial epithelial cells. Environ. Toxicol. 38 (2), 359-367.

Khan A., Jia Z., 2023. Recent insights into uptake, toxicity, and molecular targets of microplastics and nanoplastics relevant to human health impacts. IScience 26 (2), 106061.

Khanbeigi A., Kumar A., Sadouki F., Lorenz C., Forbes B., Dailey L., et al., 2012. The delivered dose: Applying particokinetics to *in vitro* investigations of nanoparticle internalization by macrophages. J. Control. Release 162, 259–266.

Le V.G., Nguyen M.K., Nguyen H.L., Lin C., Hadi M., Hung N.T.Q., et al., 2023. A comprehensive review of micro- and nano-plastics in the atmosphere: Occurrence, fate, toxicity, and strategies for risk reduction. Sci. Total Environ. 904, 166649.

Li Y., Liu C., Yang H., He W., Li B., Zhu X., et al., 2024. Leaching of chemicals from microplastics: review of chemical types, leaching mechanisms and influencing factors. Sci. Total Environ. 906, 167666.

Liang L., Everest-Dass A., Kostyuk A., Khabir Z., Zhang R., Trushina D., et al., 2022. The surface charge of polymer-coated up conversion nanoparticles determines protein corona properties and cell recognition in serum solutions. Cells 11 (22), 3644.

Lichtenstein D., Meyer T., Böhmert L., Juling S., Fahrenson C., Selve S., et al., 2017. Dosimetric quantification of coating-related uptake of silver nanoparticles. Langmuir 33 (45), 13087–13097.

Liu Y.Y., Liu J., Wu H., Zhang Q., Tang X.R., Li D., et al., 2022. Endocytosis, distribution, and exocytosis of polystyrene nanoparticles in human lung cells. Nanomaterials 13 (1), 84.

Liu J., Liu Y.Y., Li C.S., Cao A., Wang H., 2023. Exocytosis of nanoparticles: a comprehensive review. Nanomaterials 13 (15), 2215.

Mahmud F., Sarker D.B., Jocelyn J.A., Sang Q.X.A., 2024. Molecular and cellular effects of microplastics and nanoplastics: Focus on inflammation and senescence. Cells 13 (21), 1788.

Martín-Pérez J., Villacorta A., Banaei G., Morataya-Reyes M., Tavakolpournegari A., Marcos R., et al., 2024. Hazard assessment of nanoplastics is driven by their surface-functionalization. Effects in human-derived primary endothelial cells. Sci. Total Environ. 934, 173236.

Morataya-Reyes M., Villacorta A., Gutiérrez-García J., Egea R., Martín-Pérez J., Barguilla I., et al 2025a.The long-term *in vitro* co-exposure of polyethylene terephthalate (PET) nanoplastics and cigarette smoke condensate exacerbate the induction of carcinogenic traits. J. Hazard. Mater. 493, 138359.

Morataya-Reyes M., Villacorta A., Arribas Arranz J., Martín-Pérez J., Ferrer J.F., Pastor S., et al., 2025b. Exploring the impact of nanoplastics on human hepatic cells: dynamics of internalization and harmful effects in HuH-7 cells. Environ. Sci. Nano 12, 4920.

Pujol G., Marín-Gual L., González-Rodelas L., Álvarez-González L., Chauvigné F., Cerdà J., et al., 2025. Short-term polystyrene nanoplastic exposure alters zebrafish male and female germline and reproductive outcomes, unveiling pollutant-impacted molecular pathways. J. Hazard. Mater. 481, 136529.

Rahman L., Mallach G., Kulka R., Halappanavar S., 2021. Microplastics and nanoplastics science: collecting and characterizing airborne microplastics in fine particulate matter. Nanotoxicology 15 (9), 1253–1278.

Repnik U., Starr A., Overall C., Turk B., 2015. Cysteine cathepsins activate ELR chemokines and inactivate non-ELR chemokines. J. Biol. Chem. 290, 13800-13811.

Sanchez-Guzman D., Boland S., Brookes O., Mc Cord C., Lai Kuen R., Sirri V., et al., 2021. Long-term evolution of the epithelial cell secretome in preclinical 3D models of the human bronchial epithelium. Sci. Rep. 11 (1), 6621.

Schröter L., Ventura N., 2022. Nanoplastic toxicity: Insights and challenges from experimental model systems. Small 18 (31), e2201680.

Sumaiya K., Langford D., Natarajaseenivasan K., Shanmughapriya S., 2022. Macrophage migration inhibitory factor (MIF): A multifaceted cytokine regulated by genetic and physiological strategies. Pharmacol. Ther. 233, 108024.

Sun N., Shi H., Li X., Gao C., Liu R., 2023. Combined toxicity of micro/nanoplastics loaded with environmental pollutants to organisms and cells: Role, effects, and mechanism. Environ. Int. 171, 107711.

Tavakolpournegari A., Villacorta A., Morataya-Reyes M., Arribas Arranz J., Banaei G., Pastor S., et al., 2024. Harmful effects of true-to-life nanoplastics derived from PET water bottles in human alveolar macrophages Environ. Pollut. 349, 123996.

Vales G., Rubio L., Marcos R., 2015. Long-term exposures to low doses of titanium dioxide nanoparticles induce cell transformation, but not genotoxic damage in BEAS-2B cells. Nanotoxicology 9, 568–578.

Villacorta A., Rubio L., Alaraby M., López-Mesas M., Fuentes-Cebrian V., Moriones O.H., et al., 2022. A new source of representative secondary PET nanoplastics. Obtention, characterization, and hazard evaluation. J. Hazard. Mater. 439, 129593.

Villacorta A., Vela L., Morataya-Reyes M., Llorens-Chiralt R., Rubio L., Alaraby M., et al., 2023. Titanium-doped PET nanoplastics of environmental origin as a true-to-life model of nanoplastic. Sci. Total Environ. 880, 163151.

Villacorta A., Cazorla-Ares C., Fuentes-Cebrian V., Valido I.H., Vela L., Carrillo-Navarrete F., et al., 2024. Fluorescent labeling of micro/nanoplastics for biological applications with a focus on “true-to-life" tracking. J. Hazard. Mater. 476, 135134.

Villacorta A., Morataya-Reyes M., Vela L., Arribas Arranz J., Martín-Perez J., Barguilla I., et al., 2025. Biological impact of true-to-life PET and titanium-doped PET nanoplastics on human-derived monocyte (THP-1) cells. Nanomaterials 15 (13), 1040.

Vizovišek M., Fonović M., Turk B., 2019. Cysteine cathepsins in extracellular matrix remodeling: Extracellular matrix degradation and beyond. Matrix Biol. 75, 141-159.

Vranic S., Boggetto N., Contremoulins V., Mornet S., Reinhardt N., Marano F., et al., 2013. Deciphering the mechanisms of cellular uptake of engineered nanoparticles by accurate evaluation of internalization using imaging flow cytometry. Part. Fibre Toxicol. 10, 2.

Weber A., Schwiebs A., Solhaug H., Stenvik J., Nilsen A., Wagner M., et al., 2022. Nanoplastics affect the inflammatory cytokine release by primary human monocytes and dendritic cells. Environ. Int. 163, 107173.

Wright S., Ulke J., Font A., Chan K., Kelly F., 2020. Atmospheric microplastic deposition in an urban environment and an evaluation of transport. Environ. Int. 136, 105411.

Wright S., Cassee F.R., Erdely A., Campen M.J., 2024. Micro- and nanoplastics concepts for particle and fibre toxicologists. Part. Fibre Toxicol. 21 (1), 18.

Xu J., Lin X., Wang J., Gowen A., 2022. A review of potential human health impacts of micro- and nanoplastics exposure. Sci. Total Environ. 851 (Pt1), 158111.

Yan L., Wu M., Wang T., Yuan H., Zhang X., Zhang H., et al., 2024. Breast cancer stem cells secrete *mif* to mediate tumor metabolic reprogramming that drives immune evasion. Cancer Res. 84 (8), 1270–1285.

Yang M., Wang W.X., 2023. Recognition and movement of polystyrene nanoplastics in fish cells. Environ. Pollut. 316, 120627.

Yang S., Cheng Y., Chen Z., Liu T., Yin L., Pu Y., et al., 2021. *In vitro* evaluation of nanoplastics using human lung epithelial cells, microarray analysis and co-culture model. Ecotoxicol. Environ. Safet. 226, 112837.

Yang K., Zhou X., Wu K., Wu J., Huang C., Yang L., 2025. Multi-omics reveals the polyethylene terephthalate carcinogenicity: Cancer progression and immune microenvironment. Ecotox. Environ. Saf. 302, 118522.

Yin Q., Pan A., Chen B., Wang Z., Tang M., Yan Y., et al., 2021. Quantitative imaging of intracellular nanoparticle exposure enables prediction of nanotherapeutic efficacy. Nature Comm. 12 (1), 2385.

Zhao H., Huang X., Halicka H., Darżynkiewicz Z., 2019. Detection of histone H2AX phosphorylation on Ser-139 as an indicator of DNA damage. Curr. Protoc. Cytom. 89, e55.

Zhou C., Huang Y., Wu J., Wei Y., Chen X., Lin Z., et al., 2021. A narrative review of multiple mechanisms of progranulin in cancer: a potential target for anti-cancer therapy. Transl. Cancer Res. 10, 4207–4216.

Graphical Abstract

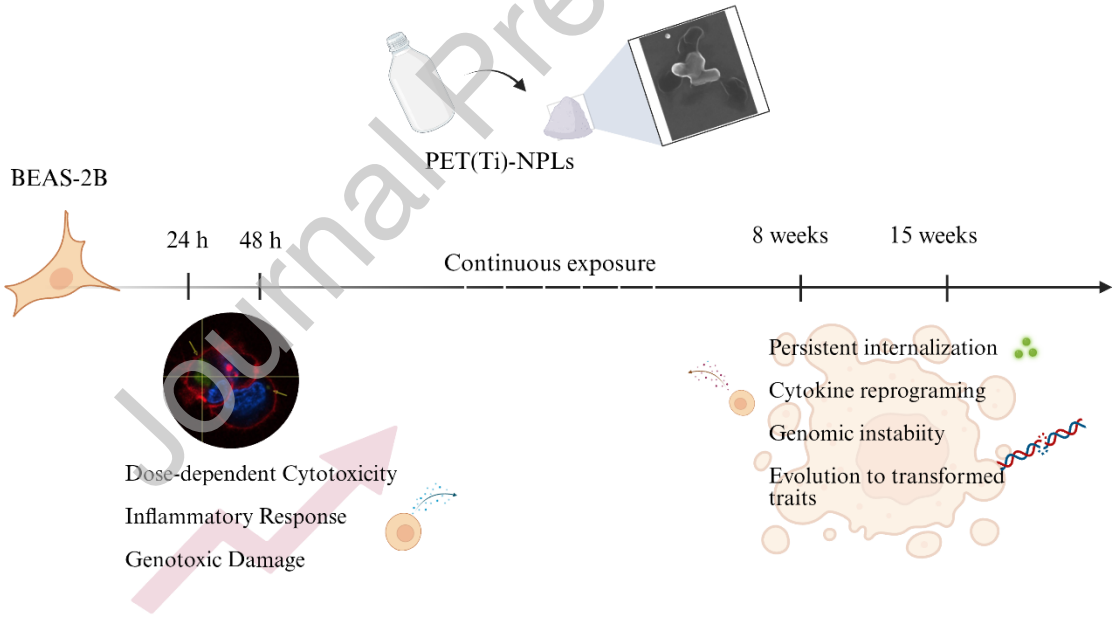

Declaration of Interest Statement

☒ The authors declare that they have no known competing financial interests or personal relationships that could have appeared to influence the work reported in this paper.

☐ The author is an Editorial Board Member/Editor-in-Chief/Associate Editor/Guest Editor for this journal and was not involved in the editorial review or the decision to publish this article.

☒ The authors declare the following financial interests/personal relationships which may be considered as potential competing interests:

3.4. Chapter 4 (Article 4)

The long-term *in vitro* co-exposure of polyethylene terephthalate (PET) nanoplastics and cigarette smoke condensate exacerbates the induction of carcinogenic traits.

Journal of Hazardous Materials, 493, 138359. (2025)

Doi: 10.1016/j.jhazmat.2025.138359

Impact Factor: 11.3 (2024)

Journal of Hazardous Materials 493 (2025) 138359

Contents lists available at ScienceDirect

Journal of Hazardous Materials

journal homepage: www.elsevier.com/locate/jhazmat

The long-term *in vitro* co-exposure of polyethylene terephthalate (PET) nanoplastics and cigarette smoke condensate exacerbates the induction of carcinogenic traits

Michelle Morataya-Reyes [a], Aliro Villacorta [a,b], Javier Gutiérrez-García [a], Raquel Egea [a], Joan Martín-Pérez [a], Irene Barguilla [a], Ricard Marcos [a,*], Alba Hernández [a,*]

[a] Group of Mutagenesis, Department of Genetics and Microbiology, Faculty of Biosciences, Universitat Autònoma de Barcelona, Cerdanyola del Vallès, Barcelona, Spain
[b] Facultad de Recursos Naturales Renovables, Universidad Arturo Prat, Iquique, Chile

HIGHLIGHTS

- The coexposure effects of PET nanoplastics and tobacco condensates were evaluated.
- Long-term and human lung cells was the defined exposure scenario.
- Cancer hallmarks and transcriptomic analysys detect the induced effects.
- Co-exposure exacerbates oxidative stress, genotoxicity, and cell transformation.
- Transcriptomic analysis reveal shifts in cellular stress and key tumor-suppressor genes.

GRAPHICAL ABSTRACT

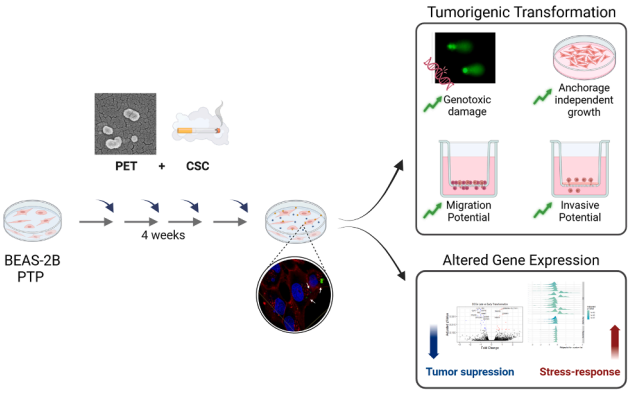

ARTICLE INFO

Keywords:
Nanoplastics
Cigarette smoke condensate
Long-term co-exposure
Beas-2B cells
Carcinogenic traits

ABSTRACT

This study examines the long-term impact of polyethylene terephthalate nanoplastics (PET-NPLs) and cigarette smoke condensate (CSC) on human lung BEAS-2B cells, focusing on key biological hallmarks of carcinogenesis. True-to-life PET-NPLs were generated from plastic water bottles and characterized to simulate environmental exposure conditions; and a comprehensive battery of assays was employed to assess genotoxicity, cellular transformation, and invasiveness. It was observed that, compared to passage control and individual exposures, co-exposure to PET-NPLs and CSC exacerbates oxidative stress, genotoxicity, and tumorigenic transformation, as evidenced by increased DNA damage, colony formation in soft agar, and enhanced cell migration and invasion. Transcriptomic analysis revealed a shift in cellular stress regulation including the upregulation of stress-response genes, including *SLC7A11, NQO1*, and *HSPA1A*, which are linked to oxidative stress adaptation and tumor survival. At the same time, key tumor-suppressor genes, such as *LOX,* and *FN1*, were significantly downregulated, promoting cellular transformation and invasiveness. These results provide compelling evidence that the

* Correspondence to: Group of Mutagenesis, Department of Genetics and Microbiology, Faculty of Biosciences, Universitat Autònoma de Barcelona, Campus of Bellaterra, Cerdanyola del Vallès, Barcelona 08193, Spain.
E-mail addresses: ricard.marcos@uab.cat (R. Marcos), alba.hernandez@uab.cat (A. Hernández).

https://doi.org/10.1016/j.jhazmat.2025.138359
Received 18 February 2025; Received in revised form 3 April 2025; Accepted 19 April 2025
Available online 21 April 2025

combination of PET-NPLs and CSC enhances carcinogenic traits through oxidative stress, genomic instability, and disruption of tumor-suppressive pathways. This study underscores the importance of evaluating the synergistic effects of combined environmental exposures and their implications for human health.

1. Introduction

The pervasive dissemination of plastics in the environment, facilitated by extensive usage and inadequate waste management practices, has emerged as a significant concern for both human health and ecosystem resilience. Particularly interesting is the environmental presence of micro- and nanoplastics (MNPLs). These environmental MNPLs result from both direct manufacturing and the fragmentation of larger plastic entities via processes such as oxidation, hydrolysis, microbial action, and mechanical abrasion [30]. Although under discussion, the present tendency is to define nanoplastics (NPLs) as those measuring 1–1000 nm, and microplastics those in the range 1–1000 mm, associating the definition to the nano/micro range of measure [24,63].

Despite the large amount of information generated during the last three years on the potential hazardous effects of MNPLs, there are four aspects requiring further research. They are i) the use of MNPLs representative (true-to-life) of those secondary MNPLs generated by plastic waste degradation. ii) To explore the effects under long-term exposure regimens, escaping from unrealistic short-time exposures. iii) To move to relevant biological endpoints such as carcinogenesis. iv) To determine the potential interactions between MNPLs and other environmental co-pollutants. Consequently, this work aims to increase our knowledge on these four topics.

Most of the information showing the harmful effects of MNPLs has been obtained using pristine commercial polystyrene MNPLs, which are far from simulating the secondary MNPLs resulting from the environmental degradation of plastic waste. Due to the difficulties of testing environmentally obtained MNPLs, the use of laboratory-made MNPLs, obtained by degrading plastic goods, is considered a good alternative [63]. Although these simulated aged MNPLs can differ from those naturally generated, they represent a step forward in closing the gap of the lack of environmental samples containing specific MNPLs. Currently, there are two main mechanisms to produce true-to-life nanoplastics, using UV-laser ablation [40] and through different mechanical fragmentation procedures, which is the most used (El [19]. By degrading polyethylene terephthalate (PET) plastic containers (including water bottles), PET-MNPLs can be obtained [27,42]; thus, this study uses true-to-life PET-NPLs obtained using such approach [64],

While acute exposure studies provide valuable insights into immediate effects, chronic exposures better capture the cumulative and potentially delayed adverse outcomes associated with NPLs exposure. This is because secondary MNPLs are present everywhere and, consequently, humans are continuously exposed to them by different routes including ingestion, inhalation, and dermal deposition. Therefore, risk assessment approaches evaluating the potential long-term effects of MNPLs exposure are urgently required [5]. Interestingly, chronic exposure studies are crucial for understanding the mechanisms underlying the development and progression of chronic diseases, including cancer. To escape using animals, an *in vitro* battery of assays covering most of the hallmarks of the carcinogenesis process has been proposed [4]. Such assays are classified as early, intermediate, or advanced biomarkers allowing the identification of the cells in the initiation, promotion, or aggressive stages of tumorigenesis. Using a pre-transformed cell model exhibiting a tumor-associated phenotype, long-term (6 months) exposures to polystyrene nanoplastics exacerbated most of the evaluated hallmarks of cancer, independently if they are associated with an early, advanced, or aggressive tumoral phenotype (Barquilla et al., 2022). It should be highlighted that the used cell model presented genetic instability, due to the presence of a mutant *Ogg1* gene. Thus, this approach permits us to identify moderated effects that could go unnoticed in the context of non-transformed cell lines or short exposure conditions, presenting a robust complementary option for assays evaluating tumorigenic potential. More recently, Domenech et al. [16] evaluated the carcinogenic potential of polyethylene terephthalate (PET-), polystyrene (PS-), and polylactic acid (PLA-) NPLs using the *in vitro* Bhas 42 cell transformation assay reporting that all three NPLs were internalized by the cells, PET- and PS-NPLs enhancing cell growth in the initiation assay. The authors also reported that PET-NPLs induced cell transformation when the promotion assay was used, indicating that PET-NPLs could act as non-genotoxic tumor promoters. These data constitute a relevant warning on the potential carcinogenic risk associated with long-term exposures to MNPLs and their potential role as co-carcinogens, when combined with tumor inducers.

Despite their small size, MNPLs exhibit complex physicochemical properties that enable them to adsorb and transport environmental pollutants, traverse biological barriers, and accumulate within living organisms [50]. Thus, the understanding of such interactions between MNPLs and environmental pollutants is of paramount relevance. Recent studies have highlighted the presence of MNPLs in urban air, with concentrations ranging from 0.3 to 1.5 particles per cubic meter, particularly in areas with high vehicular traffic and industrial activities [17]. These airborne MPLs, predominantly fibers, pose inhalation risks to urban populations. Additionally, the potential for bioaccumulation of these particles in respiratory tissues has been shown by studies reporting MPLs in lung tissue samples, with concentrations averaging 1.42 ± 1.50 particles per gram of tissue in healthy individuals [25]. When examining tumor samples, Zhao et al. [77] detected polystyrene (PS), polyethylene (PE), and polyvinyl chloride (PVC) polypropylene MPLs in 80 % of lung tumors. The presence of elevated concentrations of MNPLs in bronchoalveolar lavage fluid of smokers underscore a concerning association between smoking and microplastic inhalation [39]. Despite extensive documentation of the health hazards associated with cigarette smoking, cigarette butts persist as ubiquitous pollutants [54]. In addition to MPLs, cigarette smoke introduces complex mixtures of harmful substances, including polycyclic aromatic hydrocarbons (PAHs) and heavy metals, which can further enhance cellular uptake of microplastics and exacerbate toxic effects. The co-occurrence of MPLs and cigarette smoke in urban environments emphasizes the need to evaluate their combined health effects, as their interaction may lead to enhanced oxidative stress and genotoxicity. Thus, the simultaneous exposure to MNPLs and tobacco smoke components constitutes an expected common exposure scenario. Previous studies have shown interactions between nanoceria and cigarette smoke condensate (CSC), a known carcinogen, showing synergistic effects in different carcinogenic hallmarks in human lung epithelial cells [52], as well as inducing transforming and epigenetic cancer-like features *in vitro* [2].

Hence, the present study aims to explore the long-term carcinogenic effects of PET-NPLs in conjunction with CSC utilizing BEAS-2B cells as a model system. BEAS-2B cells, derived from human bronchial epithelium, serve as a relevant model for studying respiratory health and carcinogenesis [46]. By elucidating the interplay between PET-NPLs, CSC, and cellular responses in a long-term exposure context, this study seeks to advance our understanding of the health risks associated with NPLs pollution and allows the evaluation of PET-NPLs, previously identified as a tumor promoter agent [16], as a co-carcinogen when combined with CSC. The findings from this research may help to take regulatory decisions, risk assessment strategies, and mitigation measures aimed at reducing the adverse effects of NPLs contamination on human health and the environment.

2. Materials and methods

2.1. Particle obtention and labelling

PET-NPLs was obtained following a previously published protocol [63]. Briefly, starting from commercially available PET bottles, nanoparticles were obtained by sanding using a diamond rotary burr. The powder obtained from this process was then sieved through a 0.20 mm mesh. Four grams of the separated material were then placed on a 250 mL beaker containing a 60 ºC pre warmed trifluoroacetic acid (TFA) 90 % for 2 h or until complete dispersion on a stirring hot plate (Heidolph Instruments GmbH & Co. KG. Schwabach, Germany). The temperature was then reduced to 25 ºC, and agitation was maintained overnight. On the second day, an equal volume of TFA 20 % was carefully added to the mixture and bigger agglomerates were removed. After 24 h of stirring, the volume was transferred to glass tubes and volume was centrifuged for 1 h at 2500 rcf. Pellets were resuspended on 0.5 % sodium dodecyl sulfate (SDS) lysis buffer solution and sonicated before transferring to 250 mL graduated cylinders. The bigger fraction was allowed to settle for 1 h and the top 100 mL of each cylinder was recovered and carefully washed twice with water and pure ethanol. Clean and dry particles were then subjected to NanoGenotox protocol [43] for further biological applications.

2.2. Particle labelling

To track nanoparticles inside biological samples, PET-NPLs were labelled following our recently published protocol [62]. To proceed, a working solution of 1 mL of freshly obtained PET-NPLs at a concentration of 5 mg/mL was transferred to a glass vial containing 0.01 g of iDye Poly pink textile dye. The solution was mixed by vortexing and incubated for 2 h on a 70 ºC thermoblock. Immediately after, 9 mL of Milli-Q water were added to the solution and cleaning was carried out to eliminate the excess of dye by centrifuge using an Amicon® Ultra-15 centrifugal Ultracel®-100K filter 1 × 10 5 MWCO (Merck KGaA, Darmstadt, Germany). Shortly, 15-min centrifugations were performed at 3453 rcf, and the process was repeated a minimum of 4 times. A volume ranging from 80 to 160 µL was recovered from the V-shape well and aliquoted to volumes of 1000 µL on Milli-Q water which were maintained covered from light at 4 ºC.

2.3. PET-NPL characterization

The PET-NPLs obtained were submitted to complete analyses to confirm their physicochemical characteristics.

2.3.1. Scanning electron microscopy (SEM)

PET-NPLs were investigated by scanning electron microscopy to determine size and shape. On a sterile and clean environment, a suspension of 100 µg/mL of PET-NPLs was prepared on Milli-Q water and vigorously mixed by vortexing. A single 10 µL drop was then placed on a glass coverslip and allowed to dry overnight on a closed Petri dish. Dried particles were observed, and images were obtained on a SEM Zeiss Merlin system (Oberkochen, Germany). From the acquired images, Martin diameter was measured on 1000 random images using the ImageJ software 1.8.0_322 distribution.

2.3.2. Nanotracking analysis (NTA)

Particle size (in nm), as well as number of particles in suspension (particles per mL) were determined using a Nanosight NS300 particle analyzer from Malvern Panalytical (Cambridge, United Kingdom). Briefly, 1:50 dilutions were prepared on Milli-Q water from 100 µg/mL suspensions. The diluted suspension was mixed using a SA8 Vortex (Merck KGaA) and then 1 mL was collected on a syringe and transferred onto the Nanosight microfluidic collector on decrescent speeds from 1000 to 50 a.u. Three independent measurements were collected on a sCMOS detector using a 488 nm laser.

2.3.3. Dynamic light scattering (DLS) and zeta potential (ζ- Pot)

The particle behaviour in suspension was investigated by measuring the particle size distribution as well as the ζ- potential. Briefly, from 100 µg/mL nanoplastic suspensions the hydrodynamic behaviour or the indicative size of hard spheres that behave equivalent to the PET-NPLs suspension was evaluated by transferring 1 mL to a DTS0012 cuvette and using a dynamic light scattering (DLS) approach. The surface potential was evaluated by transferring a slightly minor volume to a DTS1070 cuvette and in both cases, measurements were carried out on a Zetasizer® Ultra red label apparatus from Malvern Panalytical (Cambridge, United Kingdom).

2.3.4. Fourier transform infrared spectroscopy (FTIR)

Functional groups from PET-NPLs were determined by FTIR. Briefly, a 20 µL drop from 1 mg/mL concentration was placed on a gold mirror and let dry for 5 days on a closed Petri dish. Sample analysis was carried out on a Hyperion 2000 micro-spectrometer (Bruker, MA, USA) using an empty gold mirror as reference. All measurements were carried out at the Molecular Spectroscopy and Optical Microscopy facility at the Institut Català de Nanociència i Nanotecnologia (ICN2). The obtained interferograms were contrasted with standard reports.

2.4. Cigarette smoke condensate (CSC) preparation

A filter pad with cigarette smoke condensate (CSC) was purchased from the University of Kentucky. CSC was prepared by the provider's 3R4F Standard Research Cigarettes on a Federal Trade Commission (FTC) smoke machine. The pad was cut into small pieces, placed in a beaker with 10 mL of DMSO (VWR, Briare, France), and mixed with a magnetic stirrer for 1 h. After removing the pieces of pad, the solution was filtered through an 11 µm-pore Whatman paper filter (GE Healthcare Life Sciences, UK) using a Bucher funnel and vacuum, and later aliquoted in cryotubes and saved at –80 ºC.

2.5. Cell culture conditions

Bronchial epithelium cells transformed with Ad12-SV40 2B (BEAS-2B), previously exposed by 30 weeks to PET-NPLs and showing cell transformation features (including increased genotoxicity, anchorage-independent growth, and deregulation of oncogenes relevant in the lung cancer context) were used as a sensitive pre-transformed cell model. These cells were generated in a study not yet published and, from now on, these cell models will be called prone-to-transformation progress (PTP) BEAS-2B cells (PTP BEAS-2B) [4]. Cells were grown in Dulbecco's modified Eagle's medium (DMEM, Life Technologies, NY, USA) supplemented with 10 % fetal bovine serum (FBS, Biowest, France), and 2.5 µg/mL of Plasmocin (InvivoGen, CA, USA). Cells were maintained in a 5 % CO_2 humidified atmosphere at 37 °C.

2.6. In vitro chronic PET-NPLs and CSC co-exposures

PTP BEAS-2B cells were exposed for 4 weeks to 100 µg/mL PET-NPLs (PTP+PET), 25 µg/mL of CSC (PTP+CSC), or the combination of both (PTP+CSC+PET), next to non-exposed passage-matched cells. A total of 1×10^5 cells were seeded in triplicate in 75 cm^2 flasks, on a total volume of 10 mL of DMEM and treated with the above indicated concentrations. Replicates of exposed cells (PTP + exposure) and non-exposed passage-matched controls (PTB) were maintained in two separate T-25 flasks and grown under the culture conditions previously described. Constant chronic exposure was ensured by replacing the cell culture medium every 3 days with a fresh medium containing the corresponding treatment.

2.7. Determination of PET-NPLs internalization in BEAS-2B cells by confocal microscopy

Confocal microscopy was used to confirm PET-NPLs internalization in PTP BEAS-2B cells using iDye staining, as recently described [62]. To proceed, after the 4 weeks of exposure 7×10^3 cells/well of each condition were seeded in an μ-Slide 8 well chambered coverslip (Ibidi GmbH, Gräfelfing, Germany), and treated with 100 μg/mL of fluorescent-labeled PET-NPLs for 48 h. After washing twice with warm culture medium, cells were observed in a Leica TCS SP5 confocal microscope. Cell nuclei were stained with Hoechst 33342 marker and cell membranes with Cellmask.

2.8. Anchorage-independent growth induction assay (Soft-agar assay)

For the evaluation of cellular transformation, the direct soft-agar assay was used to measure PTP BEAS-2B cell's ability to grow independently of anchorage. A 1:1 mix of previously liquified 1.2 % agar and DMEM 2X (DMEM, 88 mM $NaHCO_3$, 20 % FBS, 2 % non-essential amino acids, 2 % Glutamax, 2 % penicillin-streptomycin) was prepared. 1.5 mL/well of the mix was added to a 6-well plate and left to solidify overnight at 4 °C. The following day the treated cells were trypsinized and centrifuged at 1000 rpm for 8 min before discarding the supernatant and resuspending the cells in 1 mL of PBS. The cell suspension was filtered through a 40 μm mesh filter and cells were counted to determine the volume corresponding to 7.5×10^4 cells. The cells were added to 1.25 mL of DMEM, and this suspension was later mixed with 8 mL of 1:1 mix of previously liquified 1.2 % agar and DMEM 2X mix. 1.5 mL of the cell mix was added to each well with agar on the plates prepared the previous day. The cells were incubated at 37°C in a 5 % CO_2 humidified atmosphere and, after 21 d, 1 mL 1 mg/mL of 2-(4-iodophenyl)-3-(4-nitrophenyl)-5-phenyl-2H-tetrazolium (INT, Sigma-Aldrich, Germany) was added to each well and incubated for one day more. To analyze, the liquid was removed, and the plates were scanned at 1200 dpi to count the colonies per well using OpenCFU-3.9.0 software.

2.9. The comet assay

DNA damage (single strand breaks and oxidized DNA bases), resulting from exposure, was evaluated using the comet assay, with and without formamidopyrimidine DNA glycosylase (FPG) enzyme [11]. Cells were washed with PBS 1X, trypsinized, collected, and centrifuged at 300 rcf for 8 min at 4 °C. The supernatant was removed, and cells were resuspended in cold PBS at 1×10^6 cells/mL density. Cells were diluted (1:10) in 0.75 % low melting point agarose at 37 °C, and 7 μL drops of the mix were placed on Gelbond® films (GBF, Life Sciences, Vilnius, Lithuania). The films were submerged in lysis buffer (2.5 M NaCl, 0.1 M EDTA, 0.01 M Tris Base, 0.2 M NaOH, 1 % Triton X-100, 1 % N-lauroyl sarcosine, 10 % DMSO; pH 10) for 2 h at 4 °C, washed twice with enzyme buffer (0.04 m HEPES, 0.1 m KCl, 0.5 mM EDTA, 0.2 mg/mL; pH 8), and later incubated for 50 min in the same buffer. A second incubation step, with or without previously activated FPG enzyme, was done at 37 °C for 30 min. GBF were then washed with electrophoresis buffer (0.3 M NaOH, 1 mM EDTA; pH 13.4) and submerged in fresh buffer for 25 min for DNA unwinding before starting the electrophoresis (20 V, 300 mAmp, 20 min). After washing twice with cold PBS, the films were fixed in absolute ethanol and stained with 1:2500 SYBR Gold in TE buffer (10 mM Tris Base, 1 mM EDTA; pH 8). Comets were visualized using an Olympus BX50 microscope at 20 × magnification. The DNA percentage in the tail was determined with the Komet 5.5 Image analysis system (Kinetic Imaging Ltd, Liverpool, UK) as a measure of DNA damage in cells. Two samples for each triplicate of exposure treatment and control were analyzed and methyl methane sulfonate (MMS) and potassium bromate ($KBrO_3$) were used as positive controls for genotoxic and oxidative DNA damage, respectively.

2.10. Analysis of cellular senescence

Senescent cells were identified by β-galactosidase staining using the Senescence Cells Histochemical Staining Kit (Sigma-Aldrich, CS0030). Cells were seeded at 3×10^5 cells/well density in 6-well plates and stained according to the manufacturer's recommendations. The number of senescence-associated β-galactosidase-positive cells was counted using a Zeiss Axio Observer A1 microscope ($n = 6$ per treatment).

2.11. Invasion and migration induction

Invasion and migration potential were evaluated as an indirect assessment of the metastatic potential of PTP BEAS-2B after the exposure. Cells grew until the culture reached 60 % confluency before changing to serum-free DMEM for 24 h. For invasion assay, 180 μL of cold Matrigel mix (Matrigel®, 0.1 % BSA, 0.1 M NaOH) were added to each 6-well transwell insert and placed in the incubator at 37 °C and 5 % CO_2 for 1 h. Transwells were placed on a 6-well plate with 2.5 mL/well of chemoattractant medium (DMEM, 15 % FBS, 0.1 % BSA) followed by the addition of 1.5 mL of cell suspension in serum-free medium at a concentration of 2×10^5 cells/mL on top of each transwell. Cells were incubated for 48 h at 37 °C and 5 % CO_2 before fixing them with methanol and 0.2 % crystal violet. Cell invasion was evaluated by taking pictures of five different regions per transwell, using a confocal microscope Olympus FV1000, and analyzing the area covered by cells with ImageJ software 1.8.0_172. For migration assay, the same protocol was followed except for the addition of Matrigel mix to the transwells.

2.12. RNA extraction and RNA seq

After treatments, total RNA was extracted from PTP BEAS-2B cells with TRItidy G™ (AppliChem GmbH) ready-to-use solution for isolation of RNA, following the manufacturer's protocol. RNA from 2×10^6 cells was isolated and quantified for Macrogen (Korea) to perform total RNA sequencing using the Illumina NovaSeq 6000 high- throughput sequencing SBS Technology with a read length of 2×151.

2.13. Transcriptomic analysis

R version 4.3.2 was used for statistical analyses through the R Studio software [59,49]. Raw FASTQ files were quality filtered by Rfastp package [65], including sequence adapters removal, quality trimming and reads filtering below 20 bases in length. Filtered reads were mapped to the human genome GRCh38 from GENCODE and counted by Rsubread package [38,7]. Read counts from PTP cells were included in the dataset. Lowly expressed genes were filtered by the filterByExpr function and normalization between libraries was performed by calcNormFactors function, both from edgeR package [32,8]. Surrogate variants were inferred by sva package and included in the analysis [36]. Differentially expressed genes (DEGs) were obtained through limma [51] and voom [33] by contrasting the co-exposed samples (PTP+CSC+PET) and the single exposed samples. Single exposed samples included PTP and PTP + exposure samples and were combined by computing an average single-exposure value for each gene [34]. DEGs were filtered by the treat function from the limma package setting as 1.1 the minimum fold-change value to be considered meaningful.

To determine the enriched functional terms, DEGs were analyzed by STRING-db [56]. Ten predicted functional partners were added to the network. Clustering was performed by k-means clustering with 7 clusters. All genes were analyzed by gene set enrichment analysis (GSEA) performed by clusterProfiler and ReactomePA packages. Three collections were used as models: Gene Ontology (GO), MSigDB hallmark collection (h) and Reactome [14,76,71]. Parameters were left by default except for maximum gene set size on GSEA with GO which was set up to 800. Data visualization was performed by ggplot2 and ggridges packages [67,68].

2.14. Relative expression of selected DEGs using real-time RT-PCR

Following four weeks of exposure, total RNA was isolated from PTP BEAS-2B cells using TRItidy G® Reagent (Invitrogen, USA), according to the manufacturer's protocol. Residual DNA was removed with Invitrogen™ TURBO DNase™ (Thermo Fisher Scientific Baltics UAB, Lithuania), and cDNA was synthesized from 2 μg of RNA using High-Capacity RNA-to-cDNA™ Kit (Thermo Fisher Scientific Baltics UAB, Lithuania). The resulting cDNA was then analyzed by real-time PCR on a Roche LightCycler 480 to determine the relative expression levels of *SLC7A11, NQO1, HSPA11, LOX,* and *FN1*, with *β-actin* serving as the housekeeping reference. Each 20 μL reaction comprised 4 μL of cDNA (10 ng/μL), 5 μL of 2 × LightCycler 480 SYBR Green I Master (Roche, Manheim, Germany), and 0.5 μL of each primer pair at a final concentration of 500 nM. The thermal cycling conditions were 95 °C for 5 min, followed by 45 cycles of 95 °C for 10 s, 59 °C for 15 s, and 72 °C for 25 s. The primer sets were as follows: SCL7A11 f (5′- CTACTATGGTCAGAAAGCCTGT −3′) and r (5′- CAGCATAAGACAAAGCTCCAAAT −3′); NQO1 f (5′- CGGCTGGGTGTTTCAGTTTG −3′) and r (5′- GGGTGAGTTGTCAAGCCAGT −3′); HSPA11 f (5′- ATAAAAGCCCAGGGGCAAGC −3′) and r (5′- CACAGGTTCGCTCTGGGAAG −3′); LOX f (5′- AATGGAAAATCTGAAGCCCAGC −3′) and r (5′- ACCACCTTGGGCTTGATACA −3′); and FN1 f (5′- CCGCCGAATGTAGGACAAGAA −3′) and r (5′- TCCGTAGGTTGGTTCAAGCC −3′). Cycle threshold (Ct) values were generated using the LightCycler® 480 software and normalized to *β-actin* expression to obtain the fold change (2^−ΔΔCq) relative to the non-treated PTP BEAS-2B cells.

3. Results and discussion

3.1. PET-NPLs characterization

The use of representative MNPLs, that mirror environmentally ones, is a challenge when evaluating the hazards of these materials. To this date, most published studies rely on commercially available or artificially generated MNPLs, which restrict the list of materials to evaluate and may not accurately reflect the physical and chemical properties of particles found in real-life settings. The present study uses PET-NPLs derived from PET plastic water bottles and obtained through a protocol that mimics an environmental degradation process. True-to-life PET-NPLs obtained for this study are not standard materials and, for this reason, a correct characterization of its physicochemical characteristics is needed. As indicated in Fig. 1, PET-NPLs show a spherical-like shape with an average size of around 200 nm, once determined by three different methodological approaches (SEM, DLS, and NTA). Once the chemical nature was confirmed by FTITR, the ability to be properly dyed by iDye was also confirmed.

3.2. PET-NPL internalization by PTP BEAS-2B cells

The internalization of PET-NPLs particles in PTP BEAS-2B cells was visualized using confocal microscopy. As shown in Fig. 2, there were no detectable signals either in the control group (Fig. 2a) nor in the CSC-only treated group (Fig. 2b). In contrast, significant internalization was observed in the groups treated with PET-NPLs (Fig. 2c) and in the combination of CSC and PET-NPLs (Fig. 2d). This indicates that PET-NPLs can penetrate PTP BEAS-2B cells, potentially leading to intracellular accumulation and subsequent biological effects.

The ability of PET-NPLs to cross cellular membranes and accumulate intracellularly is particularly concerning given their potential to

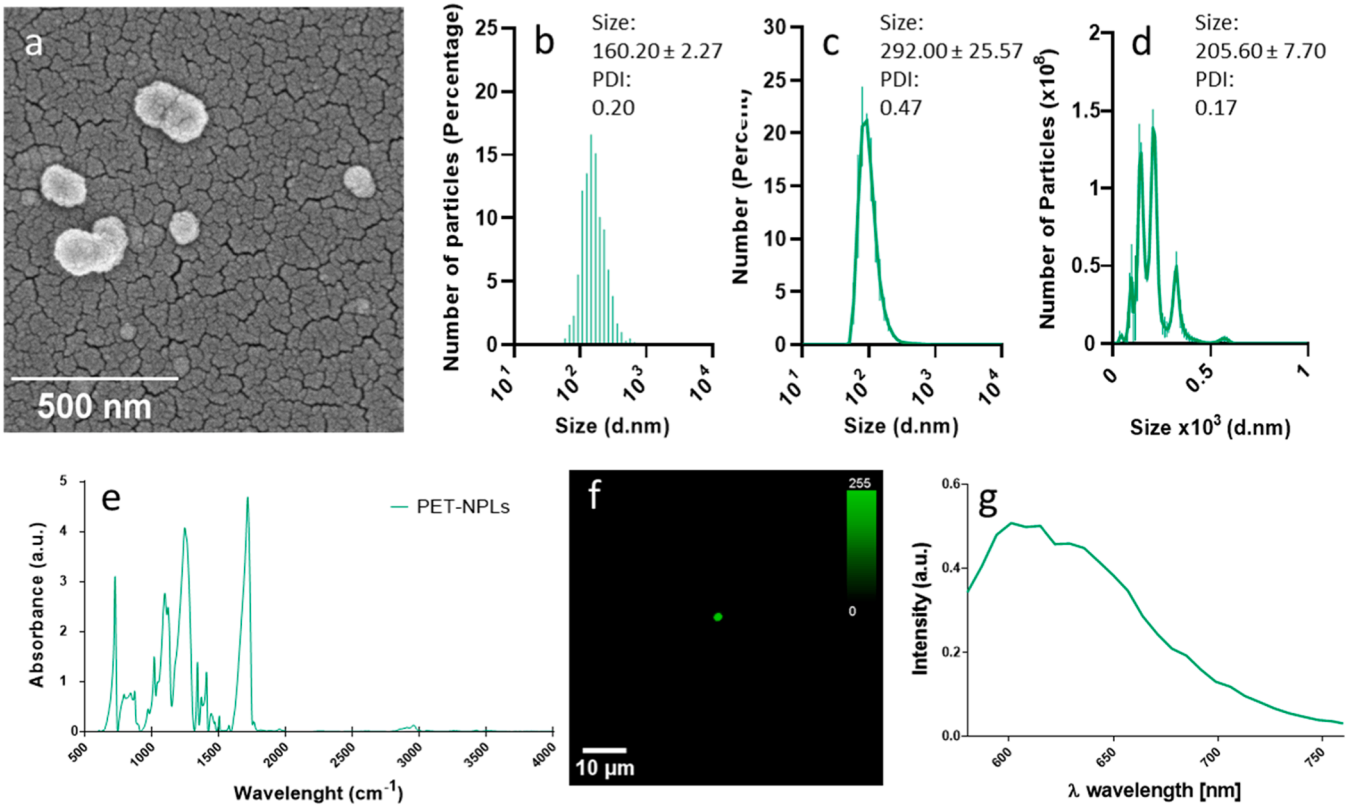

Fig. 1. SEM images of PET NPLs (a), size distribution of nanoplastic was investigated by Martin diameter measurement (b), dynamic light scattering (DLS) (c) and nanotracking analysis (NTA) (d). Chemical identity of functional groups was confirmed by Fourier transformation infrared spectroscopy (FTIR) (e). The lambda scan to detect the dying of the particles was confirmed both visually and in terms of wavelength (f and g, respectively).

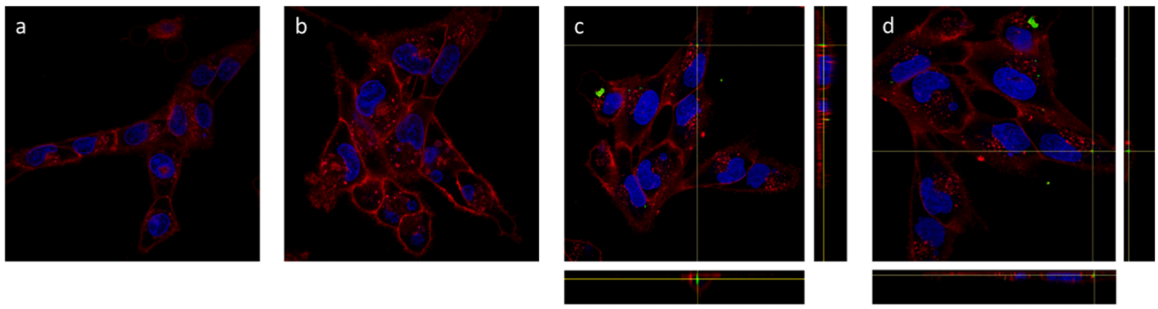

Fig. 2. Visualization of PET-NPL internalization in PTP BEAS-2B cells. a) PTP passage control. b) PTP+CSC. c) PTP+PET. d) PTP+CSC+PET. Orthogonal views of the field confirm the internalization in c) and d) after 48 h of treatment, while no PET-NPL signal is present in a) and b) conditions. Cell nuclei are shown in blue, cell membrane in red, and fluorescent-labeled LMNPET in green.

interfere with cellular processes and induce toxicological effects. Previous studies have demonstrated that the physicochemical properties of nanoplastics, such as size, shape, and surface charge, play crucial roles in their cellular uptake and bioavailability [55]. The fluorescent labeling used in this study allowed for the precise tracking of PET-NPLs particles within the cells, confirming their internalization and raising concerns about their potential to cause subcellular damage. This ability of PET-NPLs to internalize has already been demonstrated in other cell types such as primary human nasal epithelial cells [1] and human alveolar macrophages [58].

The selection of the concentrations to be used is always a conflicting issue, mainly because there is no information regarding the exposure levels of the general population. This lack of information is due to the lack of standardized protocol to quantify such levels [20]. When evaluating the obtained results, it is important to consider the difference between the treatment concentration and the effective cellular concentration. Although the used concentration (100 μg/mL) looks high, the confocal images reveal a moderated intracellular accumulation of fluorescently labeled PET-NPLs, suggesting that the particles reaching the cells are noticeably lower than the total particles treated with. This highlights a key challenge in nanoplastic exposure studies since the inconsistency between treatment and effective doses is well documented in the context of *in vitro* nanotoxicology, where factors such as particle aggregation, sedimentation, and differences in cellular uptake efficiencies influence bioavailability [12,69]. This distinction is important because it allows study bioaccumulation and long-term exposure effects in conditions where cells are not saturated with PET-NPLs, avoiding toxic effects that may accurately reflect chronic low-dose environmental exposure scenarios. By utilizing realistic, bioavailable concentrations, this study provides a relevant model for exposure to NPLs, where accumulation occurs gradually over extended periods.

3.3. Genotoxic effects of PET-NPL

Once it was determined that PET-NPLs were internalized, their potentially hazardous effects were determined. Among the biomarkers of effects genotoxicity stands out since DNA damage can severely impact cell functionality and, consequently, affect human health [6]. The comet assay was used to assess genotoxic and oxidative DNA damage in PTP BEAS-2B cells after 4 weeks of exposure to CSC, PET-NPLs, and their combination. The results, illustrated in Fig. 3, indicate that the (CSC + PET) group had significantly higher levels of DNA damage than the CSC-only and PET-only groups. These synergistic-like effects agree with previous results showing similar effects on the comet assay in co-exposures CSC + nanoceria [52]. Similarly, such co-exposure also enhanced a set of carcinogenesis biomarkers, including the overexpression of microRNAs involved in tumorigenesis [2]. These effects have been associated with the ability of CSC to induce endoplasmic reticulum stress [9]. The observed effect highlights the importance of investigating combined exposures, which may reflect more accurately real-world exposure scenarios.

Despite the effects observed when the induction of single-strand breaks was determined, no significative increases in oxidative DNA damage were found. Oxidative stress is a well-known pathway leading to genotoxicity and carcinogenesis, as it can cause mutations, lipid peroxidation, and protein oxidation [15]. The generation of reactive oxygen species (ROS) by both CSC and PET nanoplastics may lead to a compounded effect, overwhelming the cellular antioxidant defenses and resulting in significant DNA damage.

3.4. Anchorage-independent growth effects induced by PET-NPL

The cells' ability to proliferate without attachment is a key

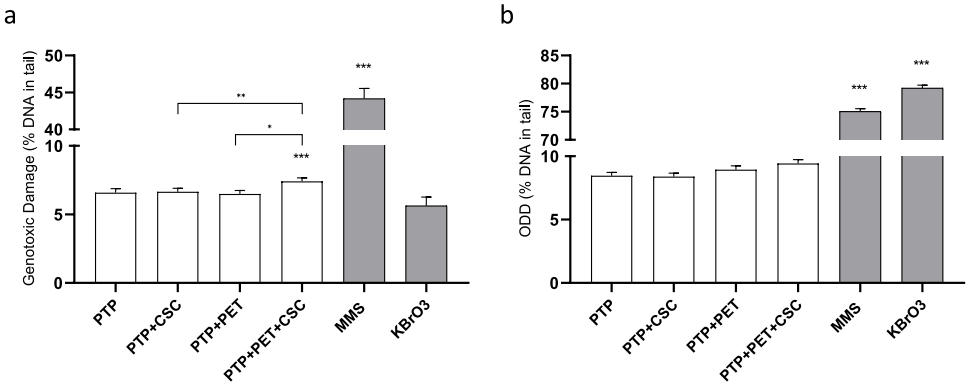

Fig. 3. (A) Genotoxic and (B) oxidative DNA damage after 4 weeks of exposure to CSC, PET, and both PET+CSC compared to PTP BEAS-2B passage control (PTP). The percentage of DNA in the tail of the comet was used to compare the conditions using one-way ANOVA analysis, with Dunnett multiple comparisons post-test and a confidence interval of 95 % (*$P \leq 0.05$; **$P \leq 0.01$, ***$P \leq 0.001$). Methyl methanesulfonate (MMS) was used as a positive control for genotoxic damage and potassium bromate ($KBrO_3$) for oxidative DNA damage.

characteristic of malignant cells, and this was assessed using the soft-agar assay [18]. Fig. 4 shows a significant increase in the total number of colonies formed in the group treated with the combination of CSC and PET-NPLs compared to the control and single treatments (Fig. 4a). The combination treatment resulted in the highest number of colonies, particularly in the smaller size range (<7 dpi), suggesting enhanced cell transformation and anchorage-independent growth (Fig. 4b).

Anchorage-independent growth is considered a hallmark of cellular transformation and is indicative of the tumorigenic potential of the tested agent [61] [4]. Our results with the soft-agar assay align with previous studies reported with silver and polystyrene nanoparticles [10, 3], and with those reporting a synergistic-like effect between CSC and nanoceria [2]. Thus, the effect observed in the co-exposure group suggests that CSC may enhance the tumorigenic properties of PET-NPLs [16] by modulating signaling pathways involved in cell adhesion and proliferation. This result also aligns with the increased genotoxic damage observed, supporting the hypothesis that chronic co-exposure to CSC and PET-NPLs accelerates the transformed phenotype in PTP BEAS-2B cells.

3.5. Migration and invasion effects induced by PET-NPL

Cell migration and invasion abilities are relevant key markers in the carcinogenic process [4]. Thus, further exploration of the potential carcinogenic phenotype using migration and invasion assays revealed significantly enhanced motility and invasive potential in PTP BEAS-2B cells exposed to PET-NPLs alone or in combination with CSC, with the highest levels observed in the co-exposure. As shown in Fig. 5a, there was a significant increase in the proportion of cells able to migrate to the basolateral side of the transwell in the groups treated with PET-NPLs and with its combination with CSC. Nevertheless, regarding the invading ability only in the co-treatments a significant effect was observed. It must be pointed out that invasion has been classified as an advanced biomarker within a battery of biomarkers measuring the progression on the transforming phenotype, while migration is classified as an intermediate biomarker [4].

Our results suggest that chronic co-exposure to CSC and PET-NPLs not only induces cellular transformation, but also enhances the invasive potential of these cells, further underscoring the carcinogenic risk posed by these combined environmental contaminants. The increased migratory and invasive capabilities observed may be attributed to several factors, including changes in the expression of matrix metalloproteinases (MMPs), alterations in the cytoskeleton, and enhanced cellular motility [10]. Thus, the combined exposure to CSC and PET-NPLs may upregulate MMP genes, particularly MMP-14, MMP-2, and MMP-9. Their respective products are key players in extracellular matrix (ECM) degradation and metastasis, facilitating cancer cell dissemination by breaking down ECM components, such as collagen and fibronectin, thereby enabling cells to breach the basement membrane and invade surrounding tissues [21] [44]. This is consistent with the enhanced invasiveness observed in the co-treatment group, where the interaction between CSC and PET-NPLs may upregulate MMP activity, thereby promoting ECM degradation and cell motility. The inflammatory tumor microenvironment induced by CSC exposure likely amplifies the pro-invasive effects of PET-NPLs. Furthermore, it has been described that the exogenously elevated levels of extracellular ATP in the ECM can increase cyclooxygenase-2 (COX-2) expression and subsequent MMP-2 activation, critical for tumor invasion [53]. Consequently, the combined exposure may enhance these pathways, further driving the invasive phenotype and aligning with previous studies showing that the combined activity of MMPs and inflammatory mediators amplifies ECM degradation and cancer cell dissemination [41].

3.6. Cellular senescence effects induced by PET-NPL

Cellular senescence, characterized by permanent cell cycle arrest and altered secretory profiles, was assessed using β-galactosidase staining. As shown in Fig. 6, β-galactosidase staining revealed a notable decrease in senescence-associated cells in the co-treatment group compared to the control and single-treatment groups. This unexpected reduction contrasts with the typical increase in senescence observed under chronic environmental stressors and warrants deeper exploration into the interplay between CSC and PET-NPLs.

The observed reduction in cellular senescence in the CSC+PET-NPLs co-exposure group aligns with emerging perspectives on the dual role of senescence in cancer [75]. While it serves as a tumor-suppressive mechanism by halting cell proliferation, it can also contribute to a pro-tumorigenic microenvironment via the senescence-associated secretory phenotype (SASP). The decreased senescence in the CSC+PET-NPLs group can indicate a suppression of SASP-driven inflammation but it could also be related to oxidative stress, altered proteostasis, or epigenetic silencing of key senescence genes [29]. This background has been observed in cases where insults converge on epigenetic regulators and in co-exposures with nanoparticles in which seemingly unrelated stressors synergize to disable signaling pathways [2,15].

Although the reduction in senescence might seem protective, it could paradoxically enhance tumorigenesis by allowing pre-malignant cells to bypass senescence and continue proliferating. The downregulation of senescence in the CSC+PET-NPLs group may reflect a shift towards other oncogenic pathways, such as those promoting cellular transformation, migration, and invasion, as evidenced by the increased anchorage-independent growth and invasive potential observed in this exposure group. This aligns with previous observations of PET-NPLs being a tumor promoter [16] and could reinforce its potential action as a co-carcinogen when in combination with established carcinogens

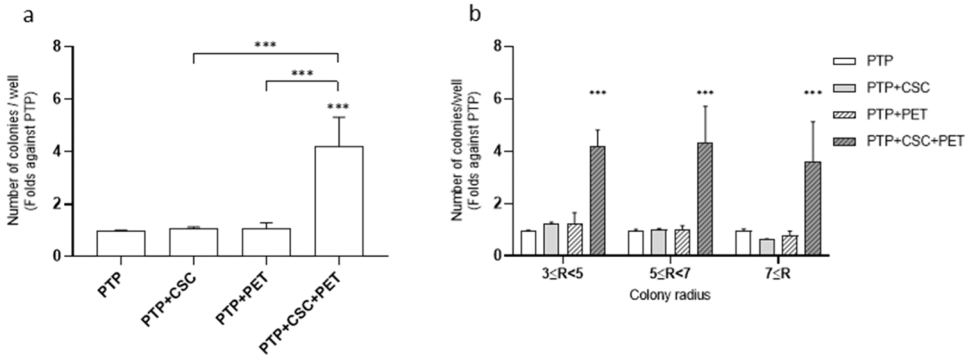

Fig. 4. Comparison of the total number of colonies formed in the anchorage-independent growth assay after treatment with CSC, PET, or the CSC + PET combination. The effects are represented as folds against non-treated PTP BEAS-2B (PTP) cells (a). The number of colonies is significantly higher in PTP BEAS-2B cells co-exposed to CSC + PET even when separating the colonies depending on size (b), represented as dpi colony radius (**$P \leq 0.001$).

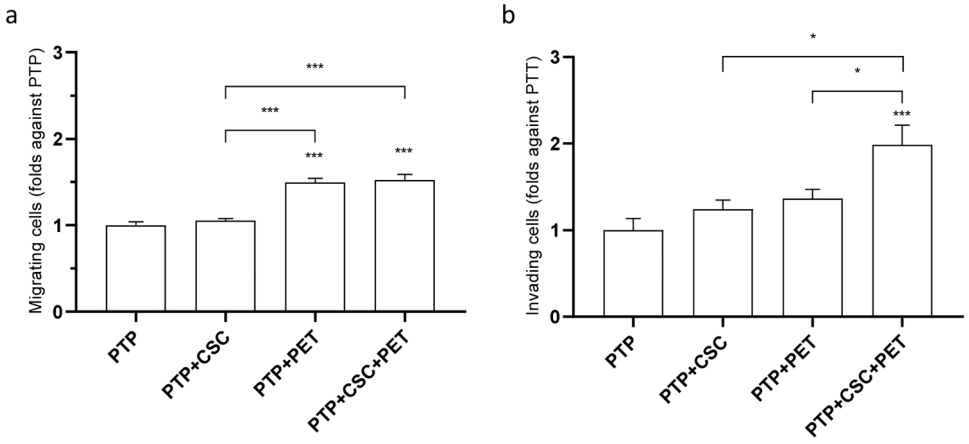

Fig. 5. The proportion of cells that can translocate to the basolateral side of the transwell in the (a) migration, and (b) invasion assays compared to PTP BEAS-2B (PTP) passage control. The folds against the PTP passage control were used to compare the effect of CSC, PET-NPLs (PET) or the combination of both in the assays using a one-way ANOVA test with Dunnett multiple comparisons post-test, having a confidence interval of 95 % (*$P \leq 0.05$; ***$P \leq 0.001$).

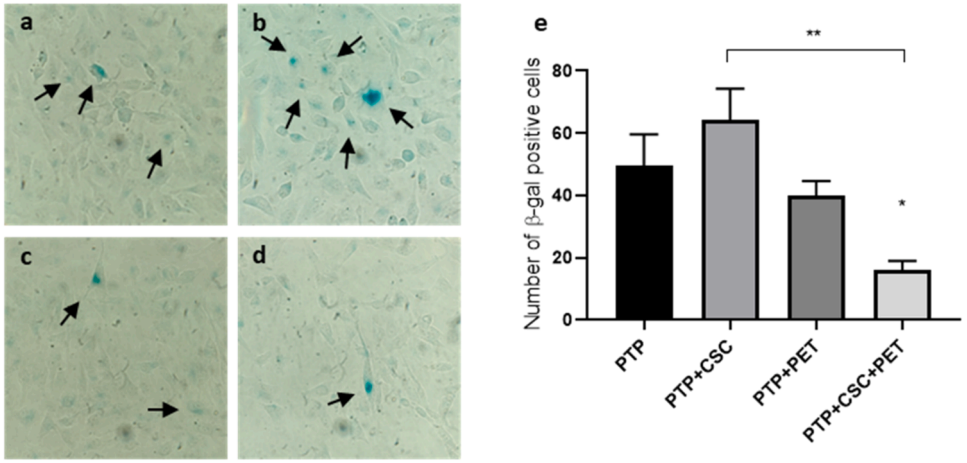

Fig. 6. Effect of CSC and PET-NPLs (PET) cotreatment in PTP BEAS-2B cells (PTP). Representative pictures of senescent cells using β-galactosidase activity in PTP control cells (a) or after 4 weeks of treatment with CSC (b), PET (c) or both CSC and PET (d). The number of β-galactosidase-positive cells (e) was significantly lower in the PTP cells co-exposed to CSC and PET when compared to the non-treated control and CSC or PET treatments alone (*$P \leq 0.05$; **$P \leq 0.01$).

such as CSC. However, further research is necessary on the mechanisms associated with the reduced senescence response examining more senescence markers and incorporating epigenetic modifications.

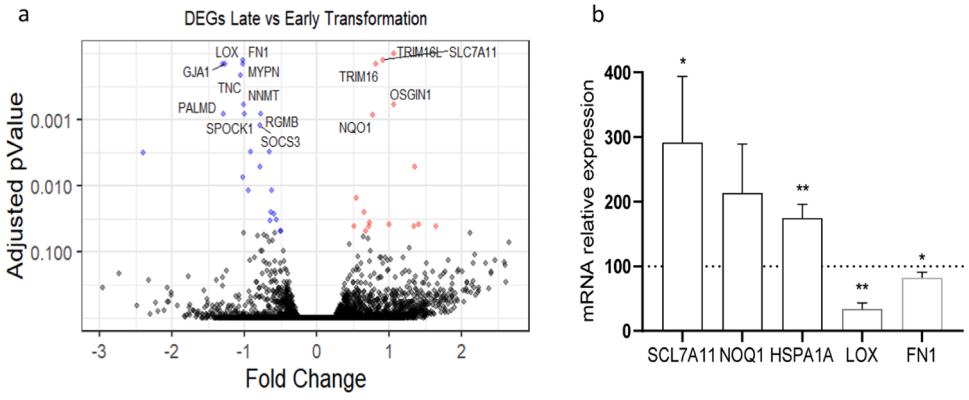

Fig. 7. (a) Volcano plot showing differentially expressed genes (DEGs) significantly up and downregulated when comparing the co-exposure treatment against the single exposure mean. Names of the most significantly expressed genes (*P* value ≤ 0.05) and those appearing in more pathways for the ORA analysis are shown. (b) Relative mRNA expression levels of *SLC7A11, NQO1, HSPA1A, LOX,* and *FN1* measured by RT-qPCR, with *β-actin* as housekeeping gene. Expression is shown as fold change ($2^{-}\Delta\Delta Cq$) relative to non-treated PTP BEAS-2B cells. Bars represent mean ± SEM of four biological replicates. $P \leq 0.05$ compared to control.

3.7. Transcriptomic analysis of the effects induced by PET-NPL and relative mRNA expression levels of DEGs

The gene expression profile of PTP BEAS-2B passage control and with treatments (alone or combined) was studied using total RNA transcriptomic analysis to determine on a broader level other effects of the exposure on PTP BEAS-2B cells. When comparing CSC + PET-NPLs co-exposed samples to single exposed samples, differentially expressed genes (DEGs) could result from differences in culture conditions and treatments. For this reason, all single-exposed samples have been combined to compute an average single-exposure value and compare it to the co-exposure value, as recommended [34].

The transcriptomic analysis revealed significant alterations in gene expression patterns in the co-exposure compared to the single-exposure group. A total of 113 DEGs were identified, with 47 upregulated and 66 downregulated genes (Fig. 7a). Notable upregulated genes include *SLC7A11, NQO1,* and *HSPA1A,* which are heavily implicated in oxidative stress management and tumor survival mechanisms.

The *SLC7A11* gene encodes a cystine-glutamate antiporter crucial for redox homeostasis, with a known role in nutrient dependency and ferroptosis regulation. Its upregulation in the co-exposure treatment presents the possibility of an adaptive response to oxidative stress promoting intracellular glutathione (GSH) synthesis, altering tumor metabolism and could contribute to therapy resistance in cancer cells [31]. This metabolic adaptation not only supports cancer cell proliferation and survival but also confers resistance to ferroptosis, a regulated form of cell death triggered by lipid peroxidation and iron accumulation [35]. Furthermore, high *SLC7A11* expression has been associated with resistance to therapies that rely on oxidative mechanisms, including radiation and certain chemotherapeutics [28]. Given its dual role in maintaining redox homeostasis and promoting therapeutic resistance, *SLC7A11* is increasingly viewed as a promising target for cancer intervention.

The *NQO1* overexpression supports detoxification and anti-oxidative stress mechanisms but also facilitates tumorigenesis in certain contexts [60]. The observed *NQO1* upregulation aligns with its role in promoting cellular proliferation and regulation of cell cycle progression at the G2/M phase related to c-Fos/CKS1 signaling [45]. Its overexpression in cancer cells has been associated with enhanced tumor cell survival under stress conditions, resistance to apoptosis, and evasion of ferroptosis, an iron-dependent form of cell death [48]. Elevated levels of *NQO1* have also been linked to increased tumorigenicity, metabolic reprogramming, and poor prognosis in various cancers, as it facilitates redox homeostasis critical for sustaining rapid cell proliferation [37]. Finally, *HSPA1A* is a member of the heat shock protein family that contributes to tumor cell survival by mitigating apoptosis and enhancing resistance to environmental stressors, was significantly upregulated [23]. Its correlation with poor prognosis in lungs, and other cancers, suggests its involvement in the enhanced malignancy observed in this study.

Conversely, key tumor-suppressor genes, such as *LOX,* and *FN1*, were downregulated in the co-exposure condition. These genes play roles in maintaining cellular adhesion and inhibiting metastatic potential, suggesting that a loss of their regulatory effects contributes to the observed aggressive phenotype. On the other hand, *LOX* and *FN1* downregulation disrupts extracellular matrix stability, favoring tumor metastasis, invasiveness, angiogenesis, and enhancing epithelial-to-mesenchymal transition [47]. As a result, the downregulation of these genes has been linked to poor clinical outcomes in various cancers [66].

To confirm these transcriptomic findings, the expression of the previously mentioned genes (*SLC711A, NQO1, HSPA1A, LOX,* and *FN1*), was validated at the mRNA level using quantitative RT-PCR. The RT-qPCR results confirmed the directionality of expression changes observed in the RNA-Seq data (Fig. 7b), providing additional robustness and biological relevance to the transcriptomic findings. This concordance strengthens the interpretation of the CSC + PET-NPLs co-exposure effects on gene expression.

Based on the identified DEGs, a STRING protein-protein interaction analysis was done with seven clusters, being "NFE2L2 regulating antioxidant/detoxification enzymes" and "Detoxification of Reactive Oxygen Species, and mRNA, protein, and metabolite induction pathway by cyclosporin A" (CsA) pathways the ones involving more DEGs (Fig. 8). It is noted that most of the proteins from the first pathway come from downregulated DEGs while the second one includes only downregulated genes. As a complementary, gene set enrichment analysis (GSEA) demonstrated significant involvement of pathways related to the detoxification of reactive oxygen species (ROS), intercellular communication, extracellular matrix (ECM) remodeling, chemoresistance and ferroptosis (Fig. 9) in CSC+PET-NPLs co-treatment. The findings shown in the ridgeplot provide insights into the complex interplay between compensatory detoxification mechanisms in the presence of combined environmental stressors. However, evaluation at a protein-level and functional assays to determine the extent of the oxidative damage are necessary to confirm its contribution to DNA damage and progression of cell transformation.

The interplay between the downregulation of Nrf2 signaling and the upregulation of CsA-associated detoxification pathways highlights a shift in cellular prioritization from prevention to damage control. While Nrf2 activation generally prevents carcinogenesis by mitigating oxidative stress and maintaining redox homeostasis, the reliance on CsA-associated pathways may reflect a state of chronic stress, wherein cells prioritize immediate survival over long-term genomic stability [13,57]. This shift has significant implications for tumorigenesis. Chronic reliance on compensatory pathways may lead to metabolic and genomic instability, creating a microenvironment conducive to malignant transformation. Furthermore, the activation of CsA-associated pathways has been linked to increased cellular motility and invasive potential, both of which are hallmarks of cancer progression [72]. The dual modulation presented by the transcriptomic analysis aligns with the enhanced cell transformation phenotype observed in the biological assays when the cells are exposed to both CSC and PET-NPLs.

Recent studies have deepened our understanding of the molecular responses of BEAS-2B cells to cigarette smoke and synthetic particles, offering relevant insights into the mechanisms potentially driving the observed phenotypes in our co-exposure model. Xu et al. [74] demonstrated that cigarette smoke extract (CSE) induces inflammation and fibrosis in BEAS-2B cells through dysregulation of the MMP-9/TIMP-1 signaling axis, which plays a critical role in extracellular matrix remodeling, while Wu et al. [70] showed that CSE exposure disrupts cell proliferation and migration via the miR-130a/Wnt1 axis. This supports our findings of deregulated transcriptomic pathways linked to cellular adhesion and communication, further emphasizing the cumulative stress induced by co-exposure. Importantly, polystyrene-based micro- and nanoparticles have also been shown to induce autophagic cell death in BEAS-2B cells [26], highlighting the cytotoxic potential of synthetic particles independently of chemical co-contaminants. Collectively, these studies contextualize our results, supporting the idea that chronic co-exposure to PET-NPLs and CSC can synergistically affect multiple cellular pathways associated with tumor initiation, tissue remodeling, and stress adaptation, reinforcing the carcinogenic potential observed in the present long-term exposure framework.

The present study provides valuable insights into the long-term co-exposure effects of PET-NPLs and cigarette smoke condensate (CSC) on PTP BEAS-2B cells, however, limitations should be acknowledged, starting from the challenge that represents the lack of standardized methods for quantifying human exposure levels to NPLs. Although several studies have detected microplastics in lung tissue and bronchoalveolar lavage fluid, no experimental data exists on the actual concentration of nanoplastics in the human respiratory system due to these analytical limitations. Additionally, while this study proves the importance of *in vitro* models as part of new approach methodologies that complement certified assays, such as the OECD's BHAS-42 assay, it is important to recognize that these models cannot replicate the full

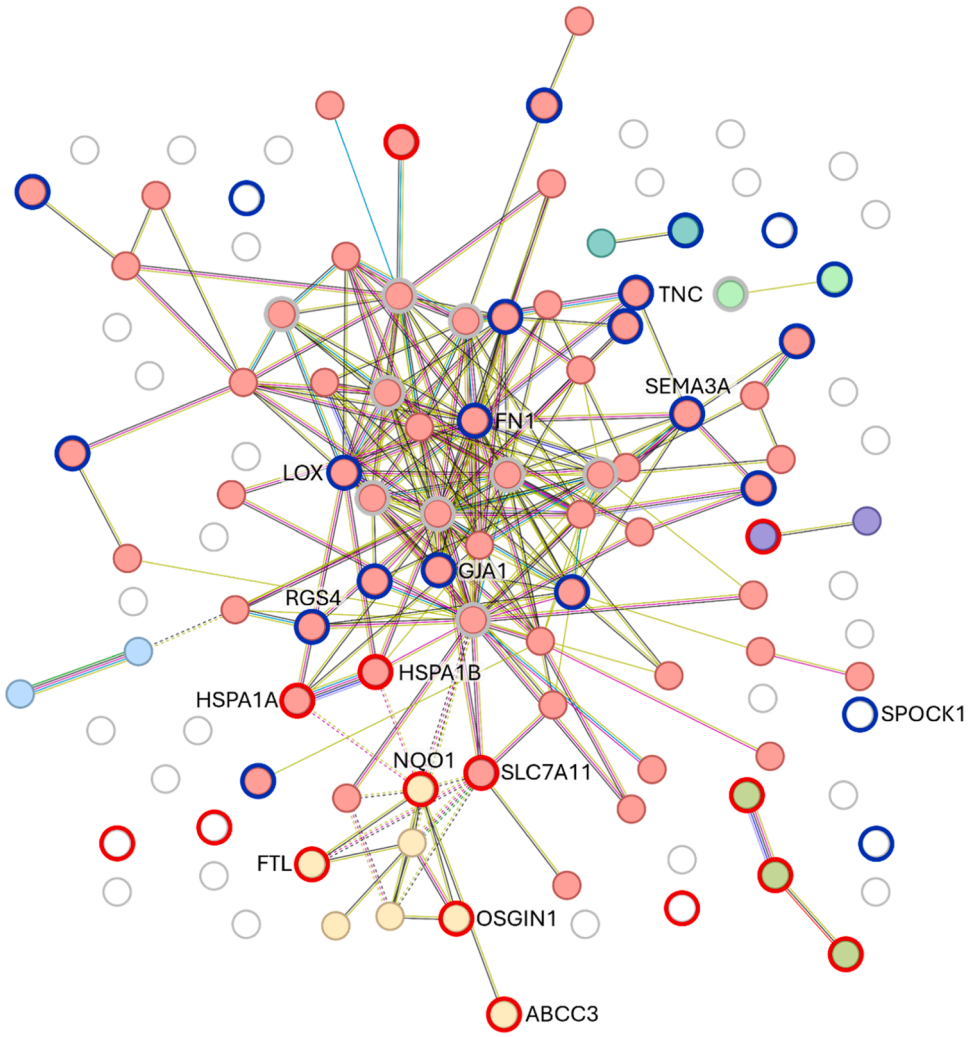

Fig. 8. String analysis of the DEGs up and downregulated in the CSC + PET co-treatment against the single exposure mean. Seven different clusters appear, including "NFE2L2 regulating antioxidant/detoxification enzymes" and "Detoxification of Reactive Oxygen Species, and mRNA, protein, and metabolite induction pathway by cyclosporin A" pathways in yellow. Upregulated and downregulated DEGs from the analysis are highlighted in red, or blue, respectively.

complexity of *in vivo* exposure scenarios, including immune system interactions and physiological clearance mechanisms.

Furthermore, the study uses only a single concentration of PET-NPLs (100 μg/mL) and CSC (25 μg/mL), selected based on prior evidence showing that these doses do not saturate the cells with nanoparticle uptake. Confocal microscopy confirmed that internalization does not occur across the total of the cell population, which supports the relevance of this dose for studying chronic bioaccumulation without inducing artificial toxicity. This scenario confirms that NPLs dosimetry remains a persistent challenge for *in vitro* studies. The effective dose reaching the cells may be significantly lower than the nominal dose due to agglomeration, sedimentation, and heterogeneous particle behavior, highlighting the need for continued efforts to improve present dosimetry models in nanotoxicology.

Another point to be highlighted in this study is the observed synergistic interaction between PET-NPLs and CSC, as indicated by the effects on different biomarkers of cell transformation and by the expression of genes involved in the tumoral response. Synergistic effects of airborne pollutants in BEAS-2B cells have been reported, as in the study of Wu et al. [73] who observed increased effects, such as intracellular ROS and inflammation, in the co-exposure of silica nanoparticles and benzo(α) pyrene after long-term (30 passages) exposure conditions. Similar effects were observed in the co-exposure of cerium NPLs and CSC, where co-exposed cells exhibit cell transforming potential, with significantly increased invasion and tumorsphere formation abilities; in addition of a high impact on a battery of miRNAs [2]. Synergistic effects have also been observed in another type of human bronchial epithelial cells (HBEC3-KT) where combined exposure to diesel exhaust particles and mineral particles induced increases in pro-inflammatory cytokines and expression of genes related to inflammation and redox responses [22]. All this emphasizes the need for further studies focusing on co-exposures to detect potential synergistic effects useful to understanding the potential health effects of such types of exposure, mainly in a long-term exposure scenario.

4. Conclusions

This study provides critical insights into the potential health risks associated with combined exposure to PET-NPLs and CSC, which are likely common in real-world scenarios. Using PTP BEAS-2B cells as a model system, it was demonstrated that long-term co-exposure exacerbates genotoxic damage, and tumorigenic traits, surpassing the effects of individual treatments. The findings are underscored by significant transcriptomic alterations, with upregulation of genes linked to management and downregulation of tumor-suppressor pathways, reflecting the complex molecular interplay induced by combined stressors.

Key results include enhanced DNA damage, anchorage-independent growth, and invasiveness, supported by disrupted antioxidant defenses

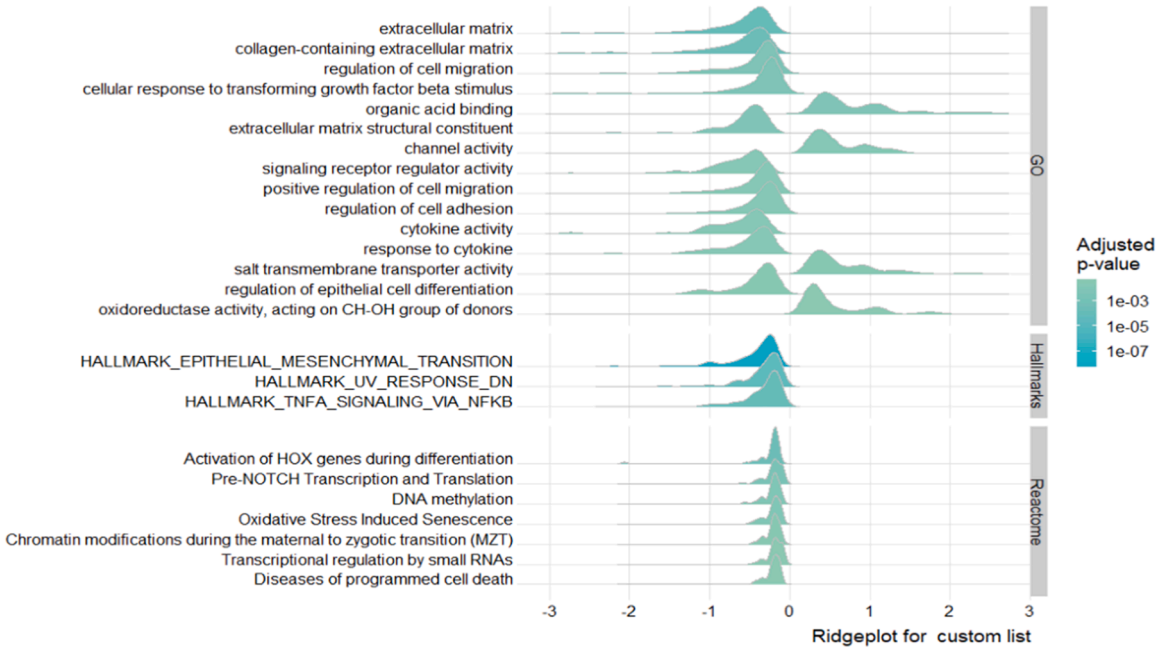

Fig. 9. Ridgeplot for list of significantly up and downregulated pathways from the GSEAs analysis of the co-treatment against the single-exposure treatments. GO, Hallmarks and Reactome databases were used and the pathways with the highest significance were included.

(e.g., *NFE2L2* downregulation) and compensatory mechanisms (e.g., cyclosporin A-mediated detoxification). These outcomes not only advance the understanding of the carcinogenic potential of nanoplastics in the presence of co-pollutants but also highlight the need for regulatory frameworks addressing such contaminants and their combined exposures. This study also becomes a step for future research to focus on elucidating molecular mechanisms further and developing targeted mitigation strategies to protect public health from the compounded effects of MNPLs and other environmental co-pollutants.

These findings underscore the value of *in vitro* long-term exposure studies and contribute to a growing body of evidence supporting the carcinogenic potential of MNPLs under realistic exposure conditions.

Environmental implication

Co-exposures is an understudied field in environmental carcinogenesis. This is especially relevant for micro/nanoplastics, as new emergent environmental contaminants, and tobacco smoke components, as a classical environmental carcinogen. In the environment, exposures last for a long time and, consequently, long-term exposure conditions need to be considered as a realistic exposure scenario. Under such conditions we have demonstrated that this co-exposure exacerbates oxidative stress, genotoxicity, and tumorigenic transformation. In addition, alter the expression of stress-response genes and key tumor-suppressor genes. Our data constitutes a relevant warning on the potential carcinogenic risk of micro/nanoplastics when co-existing with other well-known environmental toxicants.

k of micro/nanoplastics when co-exist with other well-known environmental toxicants.

CRediT authorship contribution statement

Hernández Alba: Writing – review & editing, Supervision, Funding acquisition, Conceptualization. **Marcos Ricard:** Writing – review & editing, Supervision, Conceptualization. **Villacorta Aliro:** Methodology, Investigation. **Morataya-Reyes Michelle:** Writing – original draft, Investigation, Conceptualization. **Egea Raquel:** Methodology, Investigation. **Gutiérrez-García Javier:** Investigation. **Barguilla Irene:** Methodology, Investigation. **Martín-Pérez Joan:** Methodology, Investigation.

Author statement

RM and AH planned the experiments. MMR wrote the first manuscript. MMR, AV, JGG, and JMP carried out the experimental part. MMR, RE, JGG, and IB analyzed the data, carried out the statistical analysis, and prepared tables/figures. MMR, RM, and AH wrote the final manuscript.

Declaration of Competing Interest

The authors declare that they have no known competing financial interests or personal relationships that could have appeared to influence the work reported in this paper.

Acknowledgments

MMR and JMP hold Ph.D. fellowships from the Generalitat de Catalunya. JGG holds a PIF Ph.D. fellowship from the Universitat Autònoma de Barcelona. AV was supported by a Ph.D. fellowship from the National Agency for Research and Development (ANID), CONICYT PFCHA/DOCTORADO BECAS CHILE/2020–72210237. IB (Academic record 2023-BP-00212) was granted with a Beatriu de Pinós Postdoctoral Program from the Secretariat of Universities and Research of the Department of Business and Knowledge of the Government of Catalunya. AH was granted an ICREA ACADEMIA award. This project (PlasticHeal) has received funding from the European Union's Horizon 2020 research and innovation programme under grant agreement No 965196. This work was partially supported by the Spanish Ministry of Science and Innovation [PID2020–116789, RB-C43] and the Generalitat de Catalunya (2021-SGR-00731).

Data availability

Data will be made available on request.

References

[1] Annangi, B., Villacorta, A., Vela, L., Tavakolpournegari, A., Marcos, R., Hernández, A., 2023. Effects of true-to-life PET nanoplastics using primary human nasal epithelial cells. Environ Toxicol Pharm 100, 104140. https://doi.org/10.1016/j.etap.2023.104140.

[2] Ballesteros, S., Barguilla, I., Marcos, R., Hernández, A., 2021. Nanoceria, alone or in combination with cigarette-smoke condensate, induces transforming and epigenetic cancer-like features *in vitro*. Nanomedicine 16 (4), 293–305. https://doi.org/10.2217/nnm-2020-0367.

[3] Barguilla, I., Domenech, J., Ballesteros, S., Rubio, L., Marcos, R., Hernández, A., 2022. Long-term exposure to nanoplastics alters molecular and functional traits related to the carcinogenic process. J Hazard Mater 438, 129470. https://doi.org/10.1016/j.jhazmat.2022.129470.

[4] Barguilla, I., Maguer-Satta, V., Guyot, B., Pastor, S., Marcos, R., Hernández, A., 2023. *In vitro* approaches to determine the potential carcinogenic risk of environmental pollutants. Int J Mol Sci 24 (9), 7851. https://doi.org/10.3390/ijms24097851.

[5] Brachner, A., Fragouli, D., Duarte, I.F., Farias, P.M.A., Dembski, S., Ghosh, M., Barisic, I., Zdzieblo, D., Vanoirbeek, J., Schwabl, P., Neuhaus, W., 2020. Assessment of human health risks posed by nano-and microplastics is currently not feasible. Int J Environ Res Public Health 17 (23), 8832. https://doi.org/10.3390/ijerph17238832.

[6] Carbone, M., Arron, S.T., Beutler, B., Bononi, A., Cavenee, W., Cleaver, J.E., Croce, Jr.C.M., et al., 2020. Tumour predisposition and cancer syndromes as models to study gene-environment interactions. Nat Rev Cancer 20 (9), 533–549. https://doi.org/10.1038/s41568-020-0265-y.

[7] Carlson M. *org.Hs.eg.db:* Genome wide annotation for Human (R package version 3.18.0). 2023. Retrieved from ⟨https://www.bioconductor.org/packages/org.Hs.eg.db⟩.

[8] Chen, Y., Chen, L., Lun, A., Baldoni, P., Smyth, G., 2024. edgeR 4.0: Powerful differential analysis of sequencing data with expanded functionality and improved support for small counts and larger datasets. bioRxiv. https://doi.org/10.1101/2024.01.21.576131.

[9] Chien, C.Y., Chen, Y.C., Lee, C.H., Wu, J.R., Huang, T.W., Huang, R.Y., Cheng, W. C., Hsieh, A.C., Shieh, Y.S., 2021. Dysregulation of the miR-30a/BiP axis by cigarette smoking accelerates oral cancer progression. Cancer Cell Int 21 (1), 578. https://doi.org/10.1186/s12935-021-02276-1.

[10] Choo, W.H., Park, C.H., Jung, S.E., Moon, B., Ahn, H., Ryu, J.S., Kim, K., Lee, Y.H., Yu, I.J., Oh, S.M., 2016. Long-term exposures to low doses of silver nanoparticles enhanced *in vitro* malignant cell transformation in non-tumorigenic BEAS-2B cells. Toxicol Vitr 37, 41–49. https://doi.org/10.1016/j.tiv.2016.09.003.

[11] Collins, A., et al., 2023. Measuring DNA damage with the comet assay: a compendium of protocols. Nat Protoc 18, 929–989. https://doi.org/10.1038/s41596-022-00754-y.

[12] DeLoid, G.M., Cohen, J.M., Pyrgiotakis, G., Demokritou, P., 2017. Preparation, characterization, and *in vitro* dosimetry of dispersed, engineered nanomaterials. Nat Protoc 12 (2), 355–371. https://doi.org/10.1038/nprot.2016.172.

[13] Dinkova-Kostova, A.T., Abramov, A.Y., 2015. The emerging role of Nrf2 in mitochondrial function. Free Radic Biol Med 88, 179–188. https://doi.org/10.1016/j.freeradbiomed.2015.04.036.

[14] Dolgalev, I., 2022. msigdbr: MSigDB Gene Sets Mult Org a Tidy Data Format. Retrieved from. ⟨https://CRAN.R-project.org/package=msigdbr⟩.

[15] Domenech, J., Cortés, C., Vela, L., Marcos, R., Hernández, A., 2021. Polystyrene nanoplastics as carriers of metals. interactions of polystyrene nanoparticles with silver nanoparticles and silver nitrate, and their effects on human intestinal Caco-2 cells. Biomolecules 11 (6), 859. https://doi.org/10.3390/biom11060859.

[16] Domenech, J., Villacorta, A., Ferrer, J.F., Llorens-Chiralt, R., Marcos, R., Hernández, A., Catalán, J., 2024. *In vitro* cell-transforming potential of secondary polyethylene terephthalate and polylactic acid nanoplastics. J Hazard Mater 469, 134030. https://doi.org/10.1016/j.jhazmat.2024.134030.

[17] Dris, R., Gasperi, J., Saad, M., Mirande, C., Tassin, B., 2016. Synthetic fibers in atmospheric fallout: a source of microplastics in the environment? Mar Pollut Bull 104, 290–293. https://doi.org/10.1016/j.marpolbul.2016.01.006.

[18] Du, F., Zhao, X., Fan, D., 2017. Soft agar colony formation assay as a hallmark of carcinogenesis. Bio-Protoc 7 (12), e2351. https://doi.org/10.21769/BioProtoc.2351.

[19] El Hadri, H., Gigault, J., Maxit, B., Grassl, B., Reynaud, S., 2020. Nanoplastic from mechanically degraded primary and secondary microplastics for environmental assessments. NanoImpact 17, 100206. https://doi.org/10.3390/ijerph18062997.

[20] Gigault, J., Davranche, M., 2025. Nanoplastics in focus: exploring interdisciplinary approaches and future directions. NanoImpact 37, 100544. https://doi.org/10.1016/j.impact.2025.100544.

[21] González-Ávila, G., Sommer, B., Mendoza-Posada, D., Ramos, C., Garcia-Hernandez, A., Falfán-Valencia, R., 2019. Matrix metalloproteinases participation in the metastatic process and their diagnostic and therapeutic applications in cancer. Crit Rev Oncol Hematol 137, 57–83. https://doi.org/10.1016/J.CRITREVONC.2019.02.010.

[22] Grytting, V.S., Chand, P., Låg, M., Øvrevik, J., Refsnes, M., 2022. The pro-inflammatory effects of combined exposure to diesel exhaust particles and mineral particles in human bronchial epithelial cells. Part Fibre Toxicol 19 (1), 14. https://doi.org/10.1186/s12989-022-00455-0.

[23] Guan, Y., Zhu, X., Liang, J., Wei, M., Huang, S., Pan, X., 2021. Upregulation of HSPA1A/HSPA1B/HSPA7 and downregulation of HSPA9 were related to poor survival in colon cancer. Front Oncol 11, 749673. https://doi.org/10.3389/fonc.2021.749673.

[24] Hartmann, N.B., Hüffer, T., Thompson, R.C., Hassellöv, M., Verschoor, A., Daugaard, A.E., Rist, S., Karlsson, T., Brennholt, N., Cole, M., Herrling, M.P., Hess, M.C., Ivleva, N.P., Lusher, A.L., Wagner, M., 2019. Are we speaking the same language? Recommendations for a definition and categorization framework for plastic debris. Environ Sci Technol 53 (3), 1039–1047. https://doi.org/10.1021/acs.est.8b05297.

[25] Jenner, L.C., Rotchell, J., Cowen, Benett R., Tentzeris, M., Sadofsky, V., 2022. L. Detection of microplastics in human lung tissue using μFTIR spectroscopy. Sci Total Environ 831, 154907. https://doi.org/10.1016/j.scitotenv.2022.154907.

[26] Jeon, M.S., Kim, J.W., Han, Y.B., Jeong, M.H., Kim, H.R., Sik Kim, H., Park, Y.J., Chung, K.H., 2023. Polystyrene microplastic particles induce autophagic cell death in BEAS-2B human bronchial epithelial cells. Environ Toxicol 38 (2), 359–367. https://doi.org/10.1002/tox.23705.

[27] Ji, Y., Wang, C., Wang, Y., Fu, L., Man, M., Chen, L., 2020. Realistic polyethylene terephthalate nanoplastics and the size-and surface coating-dependent toxicological impacts on zebrafish embryos. Environ Sci Nano 7 (8), 2313–2324. https://doi.org/10.1039/D0EN00464B.

[28] Jiang, Y., Sun, M., 2024. SLC7A11: the Achilles heel of tumor? Front Immunol 15, 1438807 doi: 10.3389/fimmu.2024.1438807.

[29] Jo, H., Shim, K., Jeoung, D., 2023. The potential of senescence as a target for developing anticancer therapy. Int J Mol Sci 24 (4), 3436. https://doi.org/10.3390/ijms24043436.

[30] Johannessen, C., Shetranjiwalla, S., 2021. Role of structural morphology of commodity polymers in microplastics and nanoplastics formation: fragmentation, effects and associated toxicity in the aquatic environment. Rev Environ Contam Toxicol 259, 123–169. https://doi.org/10.1007/398_2021_80.

[31] Koppula, P., Zhang, Y., Zhuang, L., Gan, B., 2018. Amino acid transporter SLC7A11/xCT at the crossroads of regulating redox homeostasis and nutrient dependency of cancer. Cancer Comm 38 (1), 1–13. https://doi.org/10.1186/s40880-018-0288-x.

[32] Law, C., Alhamdoosh, M., Su, S., Dong, X., Tian, L., Smyth, G., Ritchie, M., 2016. RNA-seq analysis is easy as 1-2-3 with limma, Glimma and edgeR. ISCB Comm J-1408 F1000Res 5. https://doi.org/10.12688/f1000research.9005.3.

[33] Law, C., Chen, Y., Shi, W., Smyth, G.K., 2014. voom: Precision weights unlock linear model analysis tools for RNA-seq read counts. Genome Biol 15, R29. https://doi.org/10.1186/gb-2014-15-2-r29.

[34] Law, C., Zeglinski, K., Dong, X., Alhamdoosh, M., Smyth, G.K., Ritchie, M.E., 2020. A guide to creating design matrices for gene expression experiments [Version 1; peer review: 2 approved]. F1000Res 9, 1444. https://doi.org/10.12688/f1000research.27893.1.

[35] Lee, J., Roh, J.-L., 2022. SLC7A11 as a gateway of metabolic perturbation and ferroptosis vulnerability in cancer. Antioxidants 11 (12), 2444. https://doi.org/10.3390/antiox11122444.

[36] Leek, J.T., Johnson, W.E., Parker, H.S., Fertig, E.J., Jaffe, A.E., Zhang, Y., Storey, J. D., Torres, L.C., 2023. sva: surrogate Variable. Anal. https://doi.org/10.18129/B9.bioc.sva. Retrieved from. ⟨https://bioconductor.org/packages/sva⟩.

[37] Li, Z., Zhang, Y., Jin, T., Men, J., Lin, Z., Qi, P., Piao, Y., Yan, G., 2015. NQO1 protein expression predicts poor prognosis of non-small cell lung cancers. BMC Cancer 15 (1), 207. https://doi.org/10.1186/s12885-015-1227-8.

[38] Liao, Y., Smyth, G.K., Shi, W., 2019. The R package Rsubread is easier, faster, cheaper and better for alignment and quantification of RNA sequencing reads. Nucleic Acids Res 47, e47. https://doi.org/10.1093/nar/gkz114.

[39] Lu, W., Li, X., Wang, S., Tu, C., Qiu, L., Zhang, H., Zhong, C., Li, S., Liu, Y., Liu, J., Zhou, Y., 2023. New evidence of microplastics in the lower respiratory tract: inhalation through smoking. Environ Sci Technol 57 (23), 8496–8505. https://doi.org/10.1021/acs.est.3c00716.

[40] Magrì, D., Sánchez-Moreno, P., Caputo, G., Gatto, F., Veronesi, M., Bardi, G., Catelani, T., Guarnieri, D., Athanassiou, A., Pompa, P.P., Fragouli, D., 2018. Laser ablation as a versatile tool to mimic polyethylene terephthalate nanoplastic pollutants: characterization and toxicology assessment. ACS Nano 12 (8), 7690–7700. https://doi.org/10.1021/acsnano.8b01331.

[41] Merchant, N., Nagaraju, G., Rajitha, B., Lammata, S., Jella, K., Buchwald, Z., Lakka, S., Ali, A., 2017. Matrix metalloproteinases: their functional role in lung cancer. Carcinogenesis 38 (8), 766–780. https://doi.org/10.1093/carcin/bgx063.

[42] Najahi, H., Alessio, N., Squillaro, T., Conti, G.O., Ferrante, M., Di Bernardo, G., Galderisi, U., Messaoudi, I., Minucci, S., Banni, M., 2022. Environmental microplastics (EMPs) exposure alter the differentiation potential of mesenchymal stromal cells. Environ Res 214 (Pt 4), 114088. https://doi.org/10.1016/j.envres.2022.114088.

[43] Nanogenotox. 2011. http://www.nanogenotox.eu/files/PDF/Deliverables/nanogenotox%20 deliverable%203_ wp4_%20dispersion%20protocol.pdf.

[44] Niland, S., Riscanevo, A., Eble, J., 2021. Matrix metalloproteinases shape the tumor microenvironment in cancer progression. Int J Mol Sci 23 (1), 146. https://doi.org/10.3390/ijms23010146.

[45] Oh, E., Kim, H., Kim, C., Lee, J., Kim, C., Lee, J., Cho, Y., Park, H., 2023. NQO1 regulates cell cycle progression at the G2/M phase. Theranostics 13, 873–895. https://doi.org/10.7150/thno.77444.

[46] Ou, W.T., Wan, Q.X., Wu, Y.B., Sun, X., Li, Y.L., Tang, D., Zhang, J., Li, S.S., Wang, N.Y., Liu, Z.L., Wu, J.J., 2024. Long noncoding RNA PSMB8-AS1 mediates the tobacco-carcinogen-induced transformation of a human bronchial epithelial cell line by regulating cell cycle. Chem Res Toxicol 37 (6), 957–967. https://doi.org/10.1021/acs.chemrestox.4c00025.

[47] Peng, D., Ungewiss, C., Tong, P., Byers, L., Wang, J., Canales, J., Villalobos, P., Uraoka, N., Mino, B., Behrens, C., Wistuba, I., Han, R., Wanna, C., Fahrenholtz, M., Grande-Allen, K., Creighton, C., Gibbons, D., 2016. ZEB1 induces LOXL2-mediated collagen stabilization and deposition in the extracellular matrix to drive lung

cancer invasion and metastasis. Oncogene 36, 1925–1938. https://doi.org/10.1038/onc.2016.358.
[48] Preethi, S., Arthiga, K., Pati, A.B., Spandana, A., Jain, V., 2022. Review on NAD(P)H dehydrogenase quinone 1 (NQO1) pathway. Mol Biol Rep 49 (9), 8907–8924. https://doi.org/10.1007/s11033-022-07369-2.
[49] R Core Team, 2023. *R: A* Language and Environment for Statistical Computing. R Foundation for Statistical Computing, Vienna, Austria. Retrieved from. ⟨https://www.R-project.org/⟩.
[50] Rafa, N., Ahmed, B., Zohora, F., Bakya, J., Ahmed, S., Ahmed, S.F., Mofijur, M., Chowdhury, A.A., Almomani, F., 2024. Microplastics as carriers of toxic pollutants: source, transport, and toxicological effects. Environ Pollut 343, 123190. https://doi.org/10.1016/j.envpol.2023.123190.
[51] Ritchie, M., Phipson, B., Wu, D., Hu, Y., Law, C., Shi, W., Smyth, G., 2015. limma powers differential expression analyses for RNA-sequencing and microarray studies. Nucleic Acids Res 43 (7), e47. https://doi.org/10.1093/nar/gkv007.
[52] Rubio, L., Bach, J., Marcos, R., Hernández, A., 2017. Synergistic role of nanoceria on the ability of tobacco smoke to induce carcinogenic hallmarks in lung epithelial cells. Nanomedicine 12 (23), 2623–2635. https://doi.org/10.2217/nnm-2017-0205.
[53] Sharma, S., Kalra, H., Akundi, R., 2021. Extracellular ATP mediates cancer cell migration and invasion through increased expression of cyclooxygenase 2. Front Pharm 11, 617211. https://doi.org/10.3389/fphar.2020.617211.
[54] Shen, M., Li, Y., Song, B., Zhou, C., Gong, J., Zeng, G., 2021. Smoked cigarette butts: Unignorable source for environmental microplastic fibers. Sci Total Environ 791, 148384. https://doi.org/10.1016/j.scitotenv.2021.148384.
[55] Stock, V., Böhmert, L., Lisicki, E., Block, R., Cara-Carmona, J., Pack, L.K., Selb, R., Lichtenstein, D., Voss, L., Henderson, C.J., Zabinsky, E., Sieg, H., Braeuning, A., Lampen, A., 2019. Uptake and effects of orally ingested polystyrene microplastic particles *in vitro* and *in vivo*. Arch Toxicol 93 (7), 1817–1833. https://doi.org/10.1007/s00204-019-02478-7.
[56] Szklarczyk, D., Kirsch, R., Koutrouli, M., Nastou, K., Mehryary, F., Hachilif, R., Gable, A., Fang, T., Doncheva, N., Pyysalo, S., Bork, P., Jensen, L., Von Mering, C., 2023. The STRING database in 2023: protein-protein association networks and functional enrichment analyses for any sequenced genome of interest. Nucleic Acids Res 51 (D1), D638–D646. https://doi.org/10.1093/nar/gkac1000.
[57] Taguchi, K., Yamamoto, M., 2020. The KEAP1–NRF2 system as a molecular target of cancer treatment. Cancers 13 (1), 46. https://doi.org/10.3390/cancers13010046.
[58] Tavakolpournegari, A., Villacorta, A., Morataya-Reyes, M., Arribas Arranz, J., Banaei, G., Pastor, S., Velázquez, A., Marcos, R., Hernández, A., Annangi, B., 2024. Harmful effects of true-to-life nanoplastics derived from PET water bottles in human alveolar macrophages. Environ Pollut 348, 123823. https://doi.org/10.1016/j.envpol.2024.123823.
[59] Team, Posit, 2023. *RStudio: Integrated Development Environment for R*. Posit Software. PBC. Retrieved from. ⟨http://www.posit.co/⟩.
[60] Tossetta, G., Fantone, S., Goteri, G., Giannubilo, S.R., Ciavattini, A., Marzioni, D., 2023. The role of NQO1 in ovarian cancer. Int J Mol Sci 24 (9), 7839. https://doi.org/10.3390/ijms24097839.
[61] Vanparys, P., Corvi, R., Aardema, M.J., Gribaldo, L., Hayashi, M., Hoffmann, S., Schechtman, L., 2012. Application of *in vitro* cell transformation assays in regulatory toxicology for pharmaceuticals, chemicals, food products and cosmetics. Mutat Res Genet Toxicol Environ Mutagen 744 (1), 111–116. https://doi.org/10.1016/j.mrgentox.2012.02.001.
[62] Villacorta, A., Cazorla-Ares, C., Fuentes-Cebrian, V., Valido, I.H., Vela, L., Carrillo-Navarrete, F., Morataya, M., Mejia-Carmona, K., Pastor, S., Velázquez, A., Arribas Arranz, J., Marcos, R., López-Mesas, M., Hernández, A., 2024. Fluorescent labeling of nanoplastics for biological applications with a focus on true-to-life MNPLs tracking. J Hazard Mater 476, 135134. https://doi.org/10.1016/j.jhazmat.2024.135134.
[63] Villacorta, A., Rubio, L., Alaraby, M., López-Mesas, M., Fuentes-Cebrian, V., Moriones, O.H., Marcos, R., Hernández, A., 2022. A new source of representative secondary PET. Nanoplastics Obtention, Charact, Hazard Eval J Hazard Mater 439, 129593 doi: 10.10.1016/j.jhazmat.2022.129593.
[64] Villacorta, A., Vela, L., Morataya-Reyes, M., Llorens-Chiralt, R., Rubio, L., Alaraby, M., Marcos, R., Hernández, A., 2023. Titanium-doped PET nanoplastics of environmental origin as a true-to-life model of nanoplastic. Sci Total Environ 880, 163151. https://doi.org/10.1016/j.scitotenv.2023.163151.
[65] Wang, W., & Carroll, T. (2024). Rfastp: An ultra-fast and all-in-one Fastq preprocessor (quality control, adapter, low quality and polyX trimming) and UMI sequence parsing (R package version 1.17.0). Bioconductor. ⟨https://bioconductor.org/packages/Rfastp⟩.
[66] Wang, T.-H., Hsia, S.-M., Shieh, T.-M., 2016. Lysyl oxidase and the tumor microenvironment. Int J Mol Sci 18 (1), 62. Doi: 10.3390/ijms18010062.
[67] Wickham, H., 2016. ggplot2: Elegant Graphics for Data Analysis. Springer-Verlag New York.
[68] Wilke C. ggridges: Ridgeline Plots in 'ggplot2' (R package version 0.5.6). 2024. Retrieved from ⟨https://CRAN.R-project.org/package=ggridges⟩.
[69] Wright, S., Cassee, F.R., Erdely, A., Campen, M.J., 2024. Micro- and nanoplastics concepts for particle and fibre toxicologists. Part Fibre Toxicol 21, 18. https://doi.org/10.1186/s12989-024-00581-x.
[70] Wu, Y., Guan, S., Ge, Y., Yang, Y., Cao, Y., Zhou, J., 2020. Cigarette smoke promotes chronic obstructive pulmonary disease (COPD) through the miR-130a/Wnt1 axis. Toxicol Vitr 65, 104770. https://doi.org/10.1016/j.tiv.2020.104770.
[71] Wu, T., Hu, E., Xu, S., Chen, M., Guo, P., Dai, Z., Feng, T., Zhou, L., Tang, W., Zhan, L., Fu, X., Liu, S., Bo, X., Yu, G., 2021. clusterProfiler 4.0: a universal enrichment tool for interpreting omics data. Innovation 2 (3), 100141.
[72] Wu, Q., Wang, X., Nepovimova, E., Wang, Y., Yang, H., Kuca, K., 2018. Mechanism of cyclosporine A nephrotoxicity: oxidative stress, autophagy, and signalings. Food Chem Toxicol 118, 889–907. https://doi.org/10.1016/j.fct.2018.06.054.
[73] Wu, J., Zhang, J., Nie, J., Duan, J., Shi, Y., Feng, L., Yang, X., An, Y., Sun, Z., 2019. The chronic effect of amorphous silica nanoparticles and benzo[a]pyrene co-exposure at low dose in human bronchial epithelial BEAS-2B cells. Toxicol Res (Camb) 8 (5), 731–740. https://doi.org/10.1039/c9tx00112c.
[74] Xu, W., Li, F., Zhu, L., Cheng, M., Cheng, Y., 2023. Pacenta polypeptide injection alleviates the fibrosis and inflammation in cigarette smoke extracts-induced BEAS-2B cells by modulating MMP-9/TIMP-1 signaling. J Biochem Mol Toxicol 37 (11), e23453. https://doi.org/10.1002/jbt.23453.
[75] Yang, J., Liu, M., Hong, D., Zeng, M., Zhang, X., 2021. The paradoxical role of cellular senescence in cancer. Front Cell Dev Biol 9, 722205. https://doi.org/10.3389/fcell.2021.722205.
[76] Yu, G., He, Q., 2016. ReactomePA: An R/Bioconductor package for reactome pathway analysis and visualization. Mol Biosyst 12 (2), 477–479. https://doi.org/10.1039/c5mb00663e.
[77] Zhao, J., Zhang, H., Shi, L., Jia, Y., Sheng, H., 2024. Detection and quantification of microplastics in various types of human tumor tissues. Ecotoxicol Environ Saf 283, 116818. https://doi.org/10.1016/j.ecoenv.2024.116818.

4. DISCUSSION

4. DISCUSSION

The exponential rise in global plastic production, exceeding 400 Mt annually, has resulted in an unprecedented waste management crisis (Thompson et al., 2024; Landrigan et al., 2025). The environmental degradation of bulk plastics through mechanical, photochemical, and biological processes generates micro- and nanoplastics (MNPLs), the most reactive and biologically accessible fraction of this pollution (Avio et al., 2017). Due to their nanoscale size and physicochemical properties, NPLs are now recognized as ubiquitous contaminants of emerging concern, detected in environmental media and critical human biological samples, including blood, lungs, and placenta (Le et al., 2023; Ruggieri et al., 2025).

The heterogeneity of MNPLs and their prevalence in environmental and consumer-relevant matrices have raised growing concern regarding their potential implications for human health. Current evidence indicates that human exposure to MNPLs is chronic and cumulative, occurring across the lifespan at low doses and in combination with other environmental contaminants (Prüst et al., 2020; Alqahtani et al., 2023). For this reason, assessing these materials under conditions that resemble human real exposures, such as long-term low-dose exposure and co-exposure with other environmental pollutants, is essential for a comprehensive hazard assessment. However, regulatory frameworks and risk assessment strategies for MNPLs remain limited, largely due to insufficient data surrounding exposure levels, material diversity, and the biological relevance of observed effects (Catalan et al., 2025).

Within this context, this Thesis was designed to generate biologically relevant evidence using experimental strategies that better reflect real-life exposure scenarios, focusing on evaluating how variability in physicochemical properties of nanoplastics, mixtures, and exposure duration modulates cellular responses in human-derived models (HuH-7, THP-1, BEAS-2B). By comparing nanoplastics derived from polystyrene (PS), polyethylene terephthalate (PET) from water bottles, and polylactic acid (PLA), and by incorporating titanium-doped PET (PET(Ti)) nanoplastics, this work examines how physicochemical properties, such as polymer identity, source, and additive content, influence cellular internalization and biological effects.

In addition to the use of environmentally relevant materials, this Thesis includes both short-term and long-term exposure conditions, allowing the evaluation of early cellular responses as well as persistent alterations that emerge following prolonged, low-dose exposure. The inclusion of the temporal dimension is crucial for distinguishing acute stress responses from cumulative and potentially adverse biological effects, which are

more representative of continuous human exposure throughout the lifespan. Additionally, this work addresses exposure complexity by incorporating co-exposure scenarios that more closely resemble environmental reality, where humans are rarely exposed to nanoplastics in isolation, but rather in combination with other chemical and particulate contaminants. By evaluating the combined effects of PET nanoplastics and cigarette smoke condensate (CSC), this Thesis explores how nanoplastics may interact with co-contaminants to modulate genotoxicity, cellular stress responses, and transformation-related phenotypes.

By integrating material diversity, exposure duration, and co-exposure complexity within human cell models, this Thesis provides experimental evidence aligned with current research needs in the toxicology field. The findings aim to advance our understanding of how MNPLs' characteristics and exposure conditions influence cellular responses, and to contribute to the generation of disease-relevant data required for human hazard assessment and the development of future regulatory frameworks.

4.1 Biological Effects Following Short-Term Exposure to NPLs

Short-term exposure models provide important insights into the early cellular responses elicited by nanoplastics and represent a necessary first step in characterizing their biological activity (Alqahtani et al., 2023). Acute exposure to nanoplastics across the studies included in this Thesis showed responses of cellular stress, despite the absence of obvious cytotoxicity, with the three primary effects being increased reactive oxygen species (ROS) generation, induction of DNA genotoxic damage, and activation of pro-inflammatory signaling pathways. These responses were observed following exposure to different types of nanoplastics in three human-derived cell models, supporting the idea that nanoplastic-induced effects can occur at sub-lethal concentrations and may precede more persistent alterations observed under prolonged exposure conditions.

Effects of acute exposure to NPLs of different compositions were assessed in the human hepatic cell HuH-7 model, and significant differences were observed in biological outcomes (Chapter 1). Although all particle types were internalized by the cells, pristine and carboxylated polystyrene particles led to no significant toxic effects, despite the relatively high uptake efficiency of cPS50- and cPS100-NPLs. In contrast, exposure to real-life PET- and PLA-NPLs resulted in oxidative stress, DNA strand breaks, and cytokine release. The lack of correlation between internalization and toxicity suggests that the physicochemical characteristics of the polymer are the drivers of adverse biological responses rather than the quantity of NPLs internalized by this cell model.

When compared to existing literature, the acute responses observed across this Thesis are consistent with evidence indicating that oxidative stress, DNA damage, and inflammatory signaling represent early and conserved cellular reactions to MNPLs exposure. Previous *in vitro* studies using commercial polystyrene nanoplastics have reported rapid induction of ROS, oxidative DNA lesions, and pro-inflammatory cytokine release across epithelial, endothelial, and immune models (Rubio et al., 2020; Weber et al., 2022; Milillo et al., 2024). However, comparative analyses increasingly demonstrate that the magnitude and nature of these responses are influenced by polymer identity, surface chemistry, particle morphology, and environmental aging rather than by particle size or uptake alone (Banerjee and Shelver, 2021; Schröter and Ventura, 2022; Martin et al., 2022; Martin-Pérez et al., 2024).

In this context, the significant increase in oxidative and genotoxic responses observed in this Thesis following exposure to realistic PET- and PLA-NPLs compared with polystyrene particles (Chapter 1), despite lower or similar cellular internalization, aligns with evidence that real-life materials have significantly different biological effects than spherical PS models (Annangi et al., 2023; Tavakolpournegari et al., 2024). These findings reinforce the concept that internalization alone is not reliable evidence when assessing MNPLs hazard, and that polymer composition and surface reactivity play dominant roles in shaping early cellular stress responses.

The relevance of realistic material composition was further reinforced when evaluating nanoplastics derived from opaque PET bottles containing embedded titanium dioxide nanoparticles (TiO_2NPs) (Chapter 2), where the role of additives was observed to further modulate the early biological outcome. Comparison between PET- and PET(Ti)-NPLs revealed that the presence of TiO_2NPs influenced the magnitude of genotoxic responses in THP-1 human immune cells, leading to decreased DNA damage relative to additive-free PET-NPLs. Acute exposure experiments in BEAS-2B lung epithelial cells (Chapter 3), however, demonstrated early oxidative and genotoxic stress following acute exposure to PET(Ti)-NPLs. Together, these observations indicate that additives not only contribute to the biological activity of nanoplastics but also represent a key factor for exposure characterization and dosimetry in toxicology studies.

Beyond the early stress responses mentioned before, short-term exposure to realistic nanoplastics led to measurable changes in cytokine secretion profiles, indicating early activation of inflammatory signaling pathways. In Chapter 1, exposure of HuH-7 hepatocytes to PET- and PLA-NPLs resulted in increased release of pro-inflammatory mediators, while polystyrene particles failed to induce a comparable response despite similar cellular internalization in the case of the functionalized particles. This pattern

suggests that cytokine induction is driven primarily by material-specific physicochemical properties rather than by particle uptake alone.

Importantly, the cytokine changes observed under acute exposure conditions were moderate and temporary, consistent with an early, potentially adaptive stress-response profile rather than explicit inflammatory toxicity. In Chapter 3, short-term exposure of BEAS-2B cells to PET(Ti)-NPLs induced only limited alterations in cytokine secretion, with an elevation in CSCL-12, IL-18, and ICAM-1 at 24 h followed by a decrease at 48 h of exposure. This distinction highlights that acute cytokine responses reflect an initial alert or adaptive phase, which may resolve if exposure is limited in time, but could become sustained and pathogenic under chronic exposure scenarios. These findings reinforce the idea that cytokine profiling in short-term assays is valuable for identifying early inflammatory activation, although insufficient on its own to predict long-term inflammatory outcomes.

The results observed after acute exposure to PET(Ti)-NPLs are consistent with the literature, which shows that surface-embedded or co-occurring inorganic constituents can modulate oxidative stress pathways and DNA integrity without necessarily increasing overt cytotoxicity (Jeon et al., 2022; Sun et al., 2023; Thapliyal et al., 2025). Importantly, the ability to quantify titanium content by ICP-MS provided improved confidence in dosimetry, addressing a recurrent limitation in MNPL toxicology where effective-dose concentrations fail to reflect initial treatment concentrations.

One of the primary strengths of this Thesis is the use of real-life nanoplastics generated directly from consumer plastic products, including PET water bottles, PLA pellets, and opaque PET plastic bottles containing a known additive such as TiO_2NPs. This approach allowed the experiments to capture the chemical complexity, irregular surface, and embedded additive content characteristic of environmental MNPLs, traits that pristine commercial nanospheres fail to represent. Next to studies demonstrating variable acute outcomes depending on surface functionalization, particle irregularity, and environmental aging (Martin et al., 2022; Wu et al., 2025), these results highlight how short-term assays remain sensitive tools for identifying early stress responses when applied to materials that realistically reflect environmental MNPLs complexity, as well as to increase our understanding on the role of these MNPLs' properties in their biological effects. Additionally, it demonstrates that acute-evaluation approaches based exclusively on pristine PS-NPLs risk underestimating initial hazards and misrepresenting mechanistic pathways relevant to human exposure, emphasizing the necessity of incorporating more complex, environmentally representative nanoplastics into toxicity assessments.

4.2 Biological Effects Following Long-Term and Multi-Stressor Exposure

As illustrated by Figure 3 of the Introduction, when assessing MNPLs and health, there is a research need to shift from the use of single-agent, short-term and high-dose exposures to a long-term, low-dose, and multi-agent approach that better captures the continuous nature of human contact. Across the work conducted in this Thesis, prolonged exposure scenarios revealed a significantly distinct pattern of biological effects characterized by persistence, accumulation, and phenotypic remodeling, in contrast to the early temporary responses observed following short-term NPLs exposure.

In Chapter 3, long-term exposure of lung epithelial cells to PET(Ti)-NPLs for up to 15 weeks revealed a significantly different biological profile from the one observed after acute exposure (24 and 48 h). While short-term treatment induced modest oxidative stress and mild DNA damage, accompanied by time-limited changes in cytokine secretion, this profile does not reflect the full spectrum of effects relevant to real-world, constant exposures. In contrast, chronic exposure to PET(Ti)-NPLs evaluated at 8 and 15 weeks led to sustained DNA damage, including increased strand breaks and dynamic modulation of DNA damage markers such as the phosphorylation of H2AX histone.

The observations align with previous long-term studies demonstrating that chronic exposure to particulate materials can lead to adaptive transitions, in which initially compensatory responses evolve into persistent dysregulation (Vales et al., 2015; Schröter and Ventura, 2022; Gutiérrez-García et al., 2025). These long-term effects were detectable despite the absence of clear cytotoxicity, illustrating that chronic exposures promote subtle but cumulative alterations that shift epithelial cells toward more aggressive, cancer-associated phenotypes.

A central feature of long-term nanoplastic exposure observed in this Thesis was the establishment of a chronic inflammatory state. In Chapter 3, long-term exposure to NPLs was associated with sustained cytokine signaling and remodeling of the epithelial cellular environment. A dynamic expression of cytokines was observed in BEAS-2B exposed to PET(Ti)-NPLs, with increased ICAM-1 and MMP-3 at 8 weeks, followed by an increase in MIF at 15 weeks and a decrease in Cathepsin B and D, CXCL8, and PLAU oncogenic markers. This profile contrasts with the subtle and often reversible inflammatory responses detected following short-term exposure for the short-term section of the same Chapter and is consistent with literature indicating that continuous low-grade inflammation represents a key mechanism linking chronic environmental exposures to tissue dysfunction (Weber et al., 2022; Mahmud et al., 2024). Similar patterns have been reported in long-term nanoplastic studies using aquatic and mammalian models, where

repeated exposure led to immune dysregulation and tissue-level effects despite limited acute toxicity (Zhou et al., 2022). These findings support the notion that inflammation should be considered a central long-term endpoint in MNPL toxicology rather than a secondary acute response, since signaling following nanoplastic exposure is not necessarily amplified over time, but reorganized from a transient stress response under acute exposure to a persistent inflammatory status under chronic conditions.

Long-term exposure also revealed alterations in cell phenotype and behavior that extend beyond classical toxicity endpoints. In Chapter 3, prolonged exposure to PET(Ti)-NPLs induced changes consistent with epithelial remodeling, pro-oncogenic signaling, and the acquisition of early transformation-like traits, including enhanced cell migration and invasion. These effects were not observed under acute exposure models and reflect observations from other long-term *in vitro* studies where sustained nanoparticle exposure promoted epithelial-mesenchymal transition (EMT)-like features and pro-fibrotic signaling (Vales et al., 2015; Yang et al., 2025; Gutiérrez-García et al., 2025). Such phenotypic remodeling represents a critical biological dimension that cannot be assessed by short-term exposure assays and reiterates the importance of extended exposure models for evaluating disease-relevant processes.

An additional layer of complexity in long-term nanoplastic toxicity arises from the fact that sustained exposure rarely occurs in isolation. Environmental and occupational scenarios typically involve continuous co-exposure to nanoplastics alongside chemical pollutants, combustion-derived particles, and other stressors that come together on shared molecular pathways. Under these conditions, nanoplastics may act not only as stress-inducing agents themselves but also as modulators of cellular responses to co-contaminants (Sun et al., 2023). In this Thesis, this dimension was explicitly addressed in Chapter 4, where incorporating co-exposure of PET-NPLs with cigarette smoke condensate (CSC) in a BEAS-2B cell model presenting transformation features significantly exacerbated biological responses compared to single-agent exposures after only 4 weeks of exposure (Chapter 4). The combined treatment led to an increase in DNA damage, enhanced the ability for colony formation in soft agar, and accelerated both migration and invasion capacity. Additionally, transcriptomic analysis provided a molecular explanation for the synergistic effect observed. The response to co-exposure involved the upregulation of stress-adaptation genes, including *SLC7A11, NQO1,* and *HSPA1A,* linked to oxidative stress and tumor survival, alongside the downregulation of key tumor-suppressor genes such as *LOX* and *FN1*. These outcomes demonstrate that co-exposure generates synergistic interactions that cannot be predicted from single-agent data alone.

The combined long-term treatment evaluated in this Thesis generated a molecular and phenotypic signature consistent with accelerated carcinogenic progression, revealing potential co-carcinogenic properties of nanoplastics in complex, realistic environmental contexts. These findings are consistent with growing evidence that nanoplastics can act as modulators of co-contaminant toxicity, either by altering bioavailability or by converging on shared stress and inflammatory pathways (Barguilla et al., 2021; Sun et al., 2023). Similar synergistic or potentiating effects have been reported in long-term studies using mixture-based NAMs batteries, where combined exposures elicited sustained molecular and phenotypic changes not observed in isolated treatments (Domenech et al., 2021; Thapliyal et al., 2025). In this context, co-exposure models should be viewed as an essential component of long-term NPLs hazard assessment since such approaches better capture the cumulative and interactive processes that define real-life exposure scenarios and provide mechanistic insight into how chronic environmental mixtures may shape adverse biological trajectories over time.

Collectively, the long-term exposure studies presented in this Thesis demonstrate that sustained nanoplastic exposure can drive biological outcomes that differ fundamentally from those observed under single-agent and acute assays alone. While short-term exposure primarily elicited early stress responses, long-term models revealed chronic inflammation, persistent genomic instability, phenotypic remodeling, and transformation-related features that emerge only after prolonged exposure. These findings align with an expanding body of NAMs-based research, which emphasizes the necessity of integrating exposure duration, material realism, and complex mixtures to assess MNPL health effects more accurately (Schröter and Ventura, 2022; Barguilla et al., 2023; Lamoree et al., 2025). Rather than serving as predictors of disease, these long-term results provide mechanistic insight into how continuous exposure to nanoplastics may contribute to adverse biological effects over time.

4.3 Methodological Considerations, Limitations, and Future Research Directions

While the studies included in this Thesis provide biologically relevant insights into the effects of nanoplastic exposure under realistic material and exposure conditions, several methodological considerations should be acknowledged when interpreting the findings. These limitations are necessary to define the factors within which conclusions can be drawn and highlight priorities for future research in nanoplastic toxicology.

A first consideration relates to the use of *in vitro* human cell models as the primary experimental platform. Although human-derived *in vitro* systems offer clear advantages

in terms of mechanistic resolution, reproducibility, and ethical compliance with the principles of the 3Rs, they cannot fully recreate the complexity of whole-organism responses. Processes such as systemic distribution of the particles, tissue–tissue interactions, immune modulation, and clearance dynamics are not captured in isolated cell models. Future studies should incorporate more complex biological systems that could include primary human cells, co-culture or immune-epithelium interaction models, 3D lung and liver organoids, and “organ-on-a-chip” systems. These kinds of platforms could improve biological realism and help validate the mechanistic pathways in more complex systems. Nevertheless, the use of multiple cell types representing distinct target tissues in this Thesis partially mitigates this limitation and aligns with current NAMs-based strategies that prioritize mechanistic, human-relevant data over traditional animal studies based on high-level organismal outcomes.

Although this Thesis already incorporates three materials highly relevant to human exposure, such as PET, PLA, and PET(Ti), future work should evaluate polymer types with different chemical identities and degradation profiles. Additionally, it is important to consider additives such as plasticizers and flame retardants, which may alter particle toxicity and contribute to endocrine disruption or genotoxicity when embedded within the polymer matrix. Environmental-aged particles, subject to UV weathering, oxidation, microbial interaction, and mechanical abrasion, are also critical to better capture the physicochemical complexity characteristic of environmental NPLs. Such work will clarify whether the trends identified here generalize across the spectrum of environmentally relevant materials.

How exposure to NPLs is defined and quantified in *in vitro* systems also represents an additional challenge in nanoplastic research. Despite efforts to use environmentally and consumer-relevant nanoplastics, uncertainties remain regarding the relationship between treatment exposure concentrations and biologically effective doses experienced by the cells, as discussed in Chapters 3 and 4. Factors such as particle agglomeration, sedimentation, protein corona formation, and differential internalization across cell types can influence cellular exposure in ways that are difficult to standardize. The incorporation of PET(Ti)-NPLs and the use of ICP-MS for dosimetry assessment used in Chapter 2 represent a step towards improving exposure quantification. However, harmonized approaches for NPLs dosimetry remain an important area for methodological development. For this reason, future work should focus on refining *in vitro*-to-*in vivo* extrapolation (IVIVE) frameworks to estimate human tissue burdens over years or decades, quantifying NPL accumulation and clearance rates in complex biological systems and integrating real-world exposure data to contextualize *in vitro*

findings. Focusing on these points, next to the progress in dosimetry, will allow more accurate translation of *in vitro* effects to potential human health outcomes.

Another limitation relates to the limited ability of cell models to distinguish between early, temporary responses and persistent biological alterations that develop over prolonged exposure periods. While this Thesis integrates both short-term and long-term exposure approaches across the four Chapters, even extended *in vitro* exposures cannot fully capture lifetime exposure scenarios. Long-term models necessarily involve making compromises related to cell adaptation, culture conditions, and potential clonal selection over time. Nevertheless, the emergence of persistent phenotypic alterations under prolonged exposure, compared to those on passage-control cells, highlights the value of this type of model for identifying biological processes that are not accessible through acute testing alone. Future studies combining long-term *in vitro* exposure with intermittent recovery phases or sequential stressors may further improve the biological relevance of chronic exposure models.

The complexity of real-world exposure scenarios also poses challenges for experimental design. The PET-CSC co-exposure experiments demonstrated synergistic effects on genomic instability, transformation, and transcriptomic disruption. However, CSC represents only one of many real-world inhalation co-pollutants, including airborne particulate matter, heavy metals, and polycyclic aromatic hydrocarbons (PAHs), which frequently co-exist with environmental NPLs. Systematically exploring all possible combinations is neither feasible nor necessary. Instead, future research should prioritize hypothesis-driven mixture studies that focus on shared mechanisms of action, following the principles of the AOP framework, such as oxidative stress, inflammation, and DNA damage, to identify conditions under which combined exposures are most likely to produce biologically meaningful interactions.

From a broader perspective, these considerations emphasize the need for integrative testing strategies that combine functional assays with high-content molecular analyses. The incorporation of transcriptomics and other omics approaches, as employed in Chapter 4 of this Thesis, provides a powerful means of linking early molecular perturbations to phenotypic outcomes and supports interpretation within mechanistic frameworks relevant to NAMs and next-generation risk assessment. In this context, it is important to continue the efforts to standardize such approaches, improve cross-study comparability, and integrate exposure relevance to contribute to advancing the field.

In summary, this Thesis contributes experimental evidence that supports the importance of material realism, exposure duration, and exposure complexity in nanoplastic

toxicology, while also illustrating the inherent limitations of current model systems. Addressing these limitations requires coordinated methodological enhancement rather than isolated experimental advances. Future research integrating long-term, co-exposure, and *in vitro* models with improved exposure characterization and mechanistic profiling is critical for building a robust evidence base that informs human health hazard assessment of nanoplastics.

5. CONCLUSIONS

5. CONCLUSIONS

In the frame of the objectives proposed for this Thesis, and in line with contributing to the advancement in knowledge on the biological effects induced by nanoplastics (NPLs) exposure in human cell models, the following points have been concluded:

1. Internalization of NPLs in the human cell hepatocyte model HuH-7 is influenced by their physicochemical characteristics but does not predict their biological effects. Differences in internalization dynamics were observed in this cellular model, which were dependent on the polymer, size, and surface functionalization. However, efficient cellular uptake alone was not sufficient to be associated with biological effects.
2. Short-term exposure of HuH-7 cells to real-life NPLs induces significant stress responses compared to different models of commercial PS-NPLs. Comparative analysis in this human hepatocyte model showed that exposure to real-life PET- and PLA-NPLs induced significant oxidative stress, genotoxic damage, and cytokine release compared to pristine and functionalized PS-NPLs. These findings demonstrate that the physicochemical properties of nanoplastics are determinants of their effects after acute exposure.
3. Titanium dioxide nanoparticles (TiO_2-NPs), as a plastic additive, modulates the response of THP-1 cells after acute exposure to PET-NPLs. Although no significant changes were observed in viability and ROS-levels, exposure to PET-NPLs in this model of human immune cells induced higher genotoxic damage than PET(Ti)-NPLs and TiO_2-NPs alone, highlighting the role of inorganic additives in NPLs reactivity.
4. Acute exposure to sub-toxic concentrations of PET(Ti)-NPLs cause early stress responses in BEAS-2B lung epithelial cells. After 24-48 h of exposure to PET(Ti)-NPLs, early oxidative, genotoxic stress, and inflammatory signaling were observed in the epithelial model, consistent with an initial stress response rather than disease-relevant effects.
5. Long-term exposure to PET(Ti)-NPLs in BEAS-2B cells reveals relevant biological effects that cannot be assessed after acute exposure to these NPLs. Long-term exposure for up to 15 weeks revealed sustained DNA damage, a chronic inflammatory state, and persistent cellular alterations consistent with an early cell transformation-like phenotype, demonstrating the importance of exposure duration for the assessment of the effects of exposure to NPLs.
6. Long-term co-exposure of PET-NPLs and cigarette smoke condensate (CSC) exacerbates carcinogenic progression in a BEAS-2B model presenting cell transformation traits, after 4 weeks of exposure. Compared to PET-NPLs and CSC

alone, the co-exposure to both contaminants promoted cell transformation-related phenotype and induced transcriptomic changes associated with stress adaptation and carcinogenic-related pathways, indicating that NPLs can act as modulators of co-contaminants' toxicity under realistic exposure scenarios.

7. Nanoplastics are biologically active materials capable of triggering oxidative stress, DNA damage, and inflammatory signaling responses at sub-cytotoxic concentrations across multiple human-derived cell models, supporting their relevance as contaminants of emerging concern.
8. Test material realism is essential for meaningful nanoplastic hazard assessment. The use of environmentally and consumer-relevant nanoplastics, including PET-, PLA-, and PET(Ti)-NPLs, revealed biological effects that were not observed with pristine polystyrene models, highlighting the importance of polymer diversity, surface irregularity, ageing, and additive content in experimental designs.
9. Biological responses to nanoplastics evolve with exposure duration rather than simply increasing in magnitude. Cytokine profiling and genotoxic damage assessment demonstrated that acute exposure elicited moderate and temporal inflammatory signaling, while long-term exposure led to sustained inflammatory reprogramming associated with tissue remodeling and transformation-related processes.
10. By integrating polymer diversity, additive content, long-term exposure, and co-exposure scenarios in human-relevant models, this Thesis advances current research needs of environmentally relevant materials and biologically relevant exposure conditions and informs future strategies for nanoplastic hazard assessment and human health evaluation.

6. REFERENCES

6. REFERENCES

Almukhlafi H, Ali D, Almutairi B, Yaseen K, Alyami N, Almeer R, Alkahtani S, Alarifi S. (2021). Role of oxidative stress in La_2O_3 nanoparticle-induced cytotoxicity and apoptosis in CHANG and HuH-7 Cells. International Journal of Nanomedicine, 16, 3487-3496. https://doi.org/10.2147/ijn.s302478

Alqahtani S, Alqahtani S, Saquib Q, Mohiddin F. (2023). Toxicological impact of microplastics and nanoplastics on humans: understanding the mechanistic aspect of the interaction. Frontiers in Toxicology, 5, 1193386. https://doi.org/10.3389/ftox.2023.1193386

Annangi B, Villacorta A, Vela L, Tavakolpournegari A, Marcos R, Hernández A. (2023). Effects of true-to-life PET nanoplastics using primary human nasal epithelial cells. Environmental Toxicology and Pharmacology, 100, 104140. https://doi.org/10.1016/j.etap.2023.104140

Avio CG, Gorbi S, Regoli F. (2017). Plastics and microplastics in the oceans: From emerging pollutants to emerged threat. Marine Environmental Research, 128, 2-11. https://doi.org/10.1016/j.marenvres.2016.05.012

Banerjee A, Shelver WL. (2021). Micro- and nanoplastic induced cellular toxicity in mammals: A review. Science of The Total Environment, 755, 142518. https://doi.org/10.1016/j.scitotenv.2020.142518

Barguilla I, Domenech J, Rubio L, Marcos R, Hernández A. (2022). Nanoplastics and arsenic co-exposures exacerbate oncogenic biomarkers under an *in vitro* long-term exposure scenario. International Journal of Molecular Sciences, 23(6), 2958. https://doi.org/10.3390/ijms23062958

Barguilla I, Maguer-Satta V, Guyot B, Pastor S, Marcos R, Hernández A. (2023). *In vitro* approaches to determine the potential carcinogenic risk of environmental pollutants. International Journal of Molecular Sciences, 24(9), 7851. https://doi.org/10.3390/ijms2409785

Bhattacharya K, Davoren M, Boertz J, Schins RP, Hoffmann E, Dopp E. (2009). Titanium dioxide nanoparticles induce oxidative stress and DNA-adduct formation but not DNA-breakage in human lung cells. Particle and Fibre Toxicology, 6(1), 17. https://doi.org/10.1186/1743-8977-6-17

Brandts I, Solà R, Garcia-Ordoñez M, Gella A, Quintana A, Martin B, Esteve-Codina A, Teles M, Roher N. (2023). Polystyrene nanoplastics target lysosomes interfering with lipid metabolism through the PPAR system and affecting macrophage functionalization. Environmental Science: Nano, 10(9), 2245-2258. https://doi.org/10.1039/d2en01077a

Browne M, Niven S, Galloway T, Rowland S, Thompson R. (2013). Microplastic moves pollutants and additives to worms, reducing functions linked to health and biodiversity. Current Biology, 23(23), 2388-2392. https://doi.org/10.1016/j.cub.2013.10.012

Caloni F, De Angelis I, Hartung T. (2022). Replacement of animal testing by integrated approaches to testing and assessment (IATA): a call for *in vivitrosi*. Archives of Toxicology, 96(7), 1935-1950. https://doi.org/10.1007/s00204-022-03299-x

Carmichael P, Baltazar M, Cable S, Cochrane S, Dent M, Li H, Middleton A, Muller I, Reynolds G, Westmoreland C, White A. (2022). Ready for regulatory use: NAMs and NGRA for chemical safety assurance. ALTEX, 39(3), 359–366. https://doi.org/10.14573/altex.2204281

Catalan J, Afanou AK, Arribas Arranz J, Ballesteros Riaza A, Banic I, Dirven H, Estrela-Lopis I, Hernández A, Kanerva T, Laforsch C, Lenssen E, Löder MJS, Pastor S, Pulli H, et al. (2025). An integrated approach to assess exposure and early health effects in human populations exposed to micro- and nanoplastics. NanoImpact, 40, 100600. https://doi.org/:10.1016/j.impact.2025.100600

Chanput W, Mes J, Wichers H. (2014). THP-1 cell line: an *in vitro* cell model for immune modulation approach. International Immunopharmacology, 23(1), 37-45. https://doi.org/10.1016/j.intimp.2014.08.002

Choo WH, Park CH, Jung SE, Moon B, Ahn H, Ryu JS, Kim K-S, Lee YH, Yu IJ, Oh SM. (2016). Long-term exposures to low doses of silver nanoparticles enhanced *in vitro* malignant cell transformation in non-tumorigenic BEAS-2B cells. Toxicology in Vitro, 37, 41-49. https://doi.org/10.1016/j.tiv.2016.09.003

Collins AR. (2004). The Comet Assay for DNA damage and repair: principles, applications, and limitations. Molecular Biotechnology, 26(3), 249-261. https://doi.org/10.1385/mb:26:3:249

Cox KD, Covernton GA, Davies HL, Dower JF, Juanes F, Dudas SE. (2019). Human consumption of microplastics. Environmental Science & Technology, 53(12), 7068-7074. https://doi.org/10.1021/acs.est.9b01517

Crosset-Perrotin G, Moraz A, Portela R, Alcolea-Rodriguez V, Burrueco-Subirà D, Smith C, Bañares MA, Foroutan H, Fairbrother DH. (2025). Production, labeling, and applications of micro- and nanoplastic reference and test materials. Environmental Science: Nano, 12(6), 2911-2964. https://doi.org/10.1039/d4en00767k

Cverenkárová K, Valachovičová M, Mackuľak T, Žemlička L, Bírošová L. (2021). Microplastics in the Food Chain. Life, 11(12), 1349. https://doi.org/10.3390/life11121349

Das A. (2023). The emerging role of microplastics in systemic toxicity: Involvement of reactive oxygen species (ROS). Science of The Total Environment, 895, 165076. https://doi.org/10.1016/j.scitotenv.2023.165076

Dinkova-Kostova AT, Abramov AY. (2015). The emerging role of Nrf2 in mitochondrial function. Free Radical Biology and Medicine, 88, 179–188. https://doi.org/10.1016/j.freeradbiomed.2015.04.036.

Domenech J, Cortés C, Vela L, Marcos R, Hernández A. (2021). Polystyrene nanoplastics as carriers of metals. Interactions of polystyrene nanoparticles with

silver nanoparticles and silver nitrate, and their effects on human intestinal Caco-2 cells. Biomolecules, 11(6), 859. https://doi.org/10.3390/biom11060859

Domenech J, Annangi B, Marcos R, Hernández A, Catalán J. (2023). Insights into the potential carcinogenicity of micro- and nano-plastics. Mutation Research - Reviews in Mutation Research, 791, 108453. https://doi.org/10.1016/j.mrrev.2023.108453

Domenech J, Villacorta A, Ferrer JF, Llorens-Chiralt R, Marcos R, Hernández A, Catalán J. (2024). In vitro cell-transforming potential of secondary polyethylene terephthalate and polylactic acid nanoplastics. Journal of Hazardous Materials, 469, 134030. https://doi.org/10.1016/j.jhazmat.2024.134030

Dris R, Gasperi J, Saad M, Mirande C, Tassin B. (2016). Synthetic fibers in atmospheric fallout: A source of microplastics in the environment? Marine Pollution Bulletin, 104(1-2), 290-293. https://doi.org/10.1016/j.marpolbul.2016.01.006

El-Rayes N, Chang A (Jasmine), Shi J. (2023). Plastic Management and Sustainability: A Data-Driven Study. Sustainability, 15(9), 7181. https://doi.org/10.3390/su15097181

European Commission. (2023). Commission Regulation (EU) 2023/2055 of 25 September 2023 amending Annex XVII to Regulation (EC) No 1907/2006 concerning the Registration, Evaluation, Authorisation and Restriction of Chemicals (REACH) as regards synthetic polymer microparticles. Official Journal of the European Union, L238, 67–78. https://eur-lex.europa.eu/eli/reg/2023/2055/oj

Fan X, Wei X, Hu H, Zhang B, Yang D, Du H, Zhu R, Sun X, Oh Y, Gu N. (2022). Effects of oral administration of polystyrene nanoplastics on plasma glucose metabolism in mice. Chemosphere, 288, 132607. https://doi.org/10.1016/j.chemosphere.2021.132607

Foss Hansen S. (2025). CUSP 3rd Policy Brief - Human Health Risks of Micro and Nanoplastics (MNPS). Zenodo. https://doi.org/10.5281/zenodo.15267446

Fuchs A-K, Syrovets T, Haas KA, Loos C, Musyanovych A, Mailänder V, Landfester K, Simmet T. (2016). Carboxyl- and amino-functionalized polystyrene nanoparticles differentially affect the polarization profile of M1 and M2 macrophage subsets. Biomaterials, 85, 78-87. https://doi.org/10.1016/j.biomaterials.2016.01.064

García-Rodríguez A, Gutiérrez J, Villacorta A, Arribas Arranz J, Romero-Andrada I, Lacoma A, Marcos R, Hernández A, Rubio L. (2024). Polylactic acid nanoplastics (PLA-NPLs) induce adverse effects on an in vitro model of the human lung epithelium: The Calu-3 air-liquid interface (ALI) barrier. Journal of Hazardous Materials, 475, 134900. https://doi.org/10.1016/j.jhazmat.2024.13490

Gasperi J, Wright SL, Dris R, Collard F, Mandin C, Guerrouache M, Langlois V, Kelly FJ, Tassin B. (2018). Microplastics in air: Are we breathing it in? Current Opinion in Environmental Science & Health, 1, 1-5. https://doi.org/10.1016/j.coesh.2017.10.002

Gettings SM, Timbury W, Dmochowska A, Sharma R, McGonigle R, MacKenzie LE, Miquelard-Garnier G, Bourbia N. (2024). Polyethylene terephthalate (PET) micro- and nanoplastic particles affect the mitochondrial efficiency of human brain vascular pericytes without inducing oxidative stress. NanoImpact, 34, 100508. https://doi.org/10.1016/j.impact.2024.100508

Geyer R, Jambeck JR, Law KL. (2017). Production, use, and fate of all plastics ever made. Science Advances, 3(7), e1700782. https://doi.org/10.1126/sciadv.1700782

Gutiérrez-García J, Egea R, Barguilla I, Nymark P, García-Rodríguez A, Guyot B, Maguer-Satta V, Marcos R, Rubio L, Hernández A. (2025). Long-term exposure to real-life polyethylene terephthalate nanoplastics induces carcinogenesis in vitro. Environmental Science & Technology, 59(22), 10891-10904. https://doi.org/10.1021/acs.est.5c01628

Haldar S, Yhome N, Muralidaran Y, Rajagopal S, Mishra P. (2023). Nanoplastics toxicity specific to liver in inducing metabolic dysfunction—A comprehensive review. Genes, 14(3), 590. https://doi.org/10.3390/genes14030590

He Y, Li J, Chen J, Miao X, Li G, He Q, Xu H, Li H, Wei Y. (2020). Cytotoxic effects of polystyrene nanoplastics with different surface functionalization on human HepG2 cells. Science of The Total Environment, 723, 138180. https://doi.org/10.1016/j.scitotenv.2020.138180

Horvatits T, Tamminga M, Liu B, Sebode M, Carambia A, Fischer L, Püschel K, Huber S, Fischer EK. (2022). Microplastics detected in cirrhotic liver tissue. EBioMedicine, 82, 104147. https://doi.org/10.1016/j.ebiom.2022.104147

Hristozov D, Badetti E, Bigini P, Brunelli A, Dekkers S, Diomede L, et al. (2024). Next Generation Risk Assessment approaches for advanced nanomaterials: Current status and future perspectives. NanoImpact, 35, 100523. https://doi.org/10.1016/j.impact.2024.100523

Jenner LC, Rotchell JM, Bennett RT, Cowen M, Tentzeris V, Sadofsky LR. (2022). Detection of microplastics in human lung tissue using μFTIR spectroscopy. Science of The Total Environment, 831, 154907. https://doi.org/10.1016/j.scitotenv.2022.154907

Jeon MS, Kim JW, Han YB, Jeong MH, Kim HR, Sik Kim H, Park YJ, Chung KH. (2022). Polystyrene microplastic particles induce autophagic cell death in BEAS-2B human bronchial epithelial cells. Environmental Toxicology, 38(2), 359-367. https://doi.org/10.1002/tox.23705

Ji Y, Wang C, Wang Y, Fu L, Man M, Chen L. (2020). Realistic polyethylene terephthalate nanoplastics and the size- and surface coating-dependent toxicological impacts on zebrafish embryos. Environmental Science: Nano, 7(8), 2313-2324. https://doi.org/10.1039/d0en00464b

Johnston HJ, Semmler-Behnke M, Brown DM, Kreyling W, Tran L, Stone V. (2010). Evaluating the uptake and intracellular fate of polystyrene nanoparticles by primary

and hepatocyte cell lines in vitro. Toxicology and Applied Pharmacology, 242(1), 66-78. https://doi.org/10.1016/j.taap.2009.09.015

Kaplan BL, Hoberman AM, Slikker W, Smith MA, Corsini E, Knudsen TB, Marty MS, Sobrian SK, Fitzpatrick SC, Ratner MH, Mendrick DL. (2024). Protecting human and animal health: The road from animal models to new approach methods. Pharmacological Reviews, 76(2), 251-266. https://doi.org/10.1124/pharmrev.123.000967

Khan A, Jia Z. (2023). Recent insights into uptake, toxicity, and molecular targets of microplastics and nanoplastics relevant to human health impacts. IScience, 26(2), 106061. https://doi.org/10.1016/j.isci.2023.106061

Lamoree MH, van Boxel J, Nardella F, Houthuijs KJ, Brandsma SH, Béen F, van Duursen MBM. (2025). Health impacts of microplastic and nanoplastic exposure. Nature Medicine, 31(9), 2873-2887. https://doi.org/10.1038/s41591-025-03902-5

Landrigan PJ, Dunlop S, Treskova M, RapscH, Symeonides C, Muncke J, Spring M, Stegeman J, Almroth BC, Chiles TC, Cropper M, Deeney M, Fuller L, Geyer R, et al. (2025). The Lancet Countdown on health and plastics. The Lancet, 406(10507), 1044-1062. https://doi.org/10.1016/s0140-6736(25)01447-3

Le V-G, Nguyen M-K, Nguyen H-L, Lin C, Hadi M, Hung NTQ, Hoang H-G, Nguyen KN, Tran H-T, Hou D, Zhang T, Bolan NS. (2023). A comprehensive review of micro- and nano-plastics in the atmosphere: Occurrence, fate, toxicity, and strategies for risk reduction. Science of The Total Environment, 904, 166649. https://doi.org/10.1016/j.scitotenv.2023.166649

Leslie HA, van Velzen MJ, Brandsma SH, Vethaak AD, Garcia-Vallejo JJ, Lamoree MH. (2022). Discovery and quantification of plastic particle pollution in human blood. Environment International, 163, 107199. https://doi.org/10.1016/j.envint.2022.107199

Li Q, Lai Y, Li P, Liu X, Yao Z, Liu J, Yu S. (2022). Evaluating the occurrence of polystyrene nanoparticles in environmental waters by agglomeration with alkylated ferroferric oxide followed by micropore membrane filtration collection and Py-GC/MS analysis. Environmental Science & Technology, 56(12), 8255-8265. https://doi.org/10.1021/acs.est.2c02033

Lim D, Jeong J, Song KS, Sung JH, Oh SM, Choi J. (2021). Inhalation toxicity of polystyrene micro(nano)plastics using modified OECD TG 412. Chemosphere, 262, 128330. https://doi.org/10.1016/j.chemosphere.2020.128330

Liu C, Li J, Zhang Y, Wang L, Deng J, Gao Y, Yu L, Zhang J, Sun H. (2019). Widespread distribution of PET and PC microplastics in dust in urban China and their estimated human exposure. Environment International, 128, 116-124. https://doi.org/10.1016/j.envint.2019.04.024

Liu Y-Y, Liu J, Wu H, Zhang Q, Tang X-R, Li D, Li C-S, Liu Y, Cao A, Wang H. (2022). Endocytosis, distribution, and exocytosis of polystyrene nanoparticles in human lung cells. Nanomaterials, 13(1), 84. https://doi.org/10.3390/nano13010084

Mahmud F, Sarker DB, Jocelyn JA, Sang Q-XA. (2024). Molecular and cellular effects of microplastics and nanoplastics: Focus on inflammation and senescence. Cells, 13(21), 1788. https://doi.org/10.3390/cells13211788

Marfella R, Prattichizzo F, Sardu C, Fulgenzi G, Graciotti L, Spadoni T, D'Onofrio N, Scisciola L, La Grotta R, Frigé C, Pellegrini V, Municinò M, Siniscalchi M, Spinetti F, et al. (2024). Microplastics and Nanoplastics in Atheromas and Cardiovascular Events. New England Journal of Medicine, 390(10), 900-910. https://doi.org/10.1056/nejmoa2309822

Martin LM, Gan N, Wang E, Merrill M, Xu W. (2022). Materials, surfaces, and interfacial phenomena in nanoplastics toxicology research. Environmental Pollution, 292, 118442. https://doi.org/10.1016/j.envpol.2021.118442

Martín-Pérez J, Villacorta A, Banaei G, Morataya-Reyes M, Tavakolpournegari A, Marcos R, Hernández A, García-Rodriguez A. (2024). Hazard assessment of nanoplastics is driven by their surface-functionalization. Effects in human-derived primary endothelial cells. Science of The Total Environment, 934, 173236. https://doi.org/10.1016/j.scitotenv.2024.173236

Materić D, Holzinger R, Niemann H. (2022). Nanoplastics and ultrafine microplastic in the Dutch Wadden Sea – The hidden plastics debris? Science of The Total Environment, 846, 157371. https://doi.org/10.1016/j.scitotenv.2022.157371

Milillo C, Aruffo E, Di Carlo P, Patruno A, Gatta M, Bruno A, Dovizio M, Marinelli L, Dimmito MP, Di Giacomo V, Paolini C, Pesce M, Ballerini P. (2024). Polystyrene nanoplastics mediate oxidative stress, senescence, and apoptosis in a human alveolar epithelial cell line. Frontiers in Public Health, 12, 1385387. https://doi.org/10.3389/fpubh.2024.1385387

Mortensen HM, Gromelski M, Hench G, Martens M, Wittwehr C, Kumar S, Kumar V, Audouze K, Virvilis V, Nymark P, Angrish M, Lynch I, Edwards S, Magagna B, Wojewodzic MW. (2025). The FAIR AOP roadmap for 2025: Advancing findability, accessibility, interoperability, and re-usability of adverse outcome pathways. Computational Toxicology, 35, 100368. https://doi.org/10.1016/j.comtox.2025.100368

OECD (2022). Global Plastics Outlook: Economic Drivers, Environmental Impacts and Policy Options. OECD Publishing, Paris. https://doi.org/10.1787/de747aef-en

Paul Friedman K, Thomas RS, Wambaugh JF, Harrill JA, Judson RS, Shafer TJ, Williams AJ, Lee J-YJ, Loo L-H, Gagné M, Long AS, Barton-Maclaren TS, Whelan M, Bouhifd M, et al. (2025). Integration of new approach methods for the assessment of data-poor chemicals. Toxicological Sciences, 205(1), 74-105. https://doi.org/10.1093/toxsci/kfaf019

Pironti C, Notarstefano V, Ricciardi M, Motta O, Giorgini E, Montano L. (2022). First Evidence of Microplastics in Human Urine, a Preliminary Study of Intake in the Human Body. Toxics, 11(1), 40. https://doi.org/10.3390/toxics11010040

Pradel A, Catrouillet C, Gigault J. (2023). The environmental fate of nanoplastics: What we know and what we need to know about aggregation. NanoImpact, 29, 100453. https://doi.org/10.1016/j.impact.2023.100453

Pratim Das P, Medhi S. (2023). Role of inflammasomes and cytokines in immune dysfunction of liver cirrhosis. Cytokine, 170, 156347. https://doi.org/10.1016/j.cyto.2023.156347

Prüst M, Meijer J, Westerink RHS. (2020). The plastic brain: neurotoxicity of micro- and nanoplastics. Particle and Fibre Toxicology, 17(1), 24. https://doi.org/10.1186/s12989-020-00358-y

Ragusa A, Svelato A, Santacroce C, Catalano P, Notarstefano V, Carnevali O, Papa F, Rongioletti MCA., Baiocco F, Draghi S, D'Amore E, Rinaldo D, Matta M, Giorgini E. (2021). Plasticenta: First evidence of microplastics in human placenta. Environment International, 146, 106274. https://doi.org/10.1016/j.envint.2020.106274

Rubio L, Barguilla I, Domenech J, Marcos R, Hernández A. (2020). Biological effects, including oxidative stress and genotoxic damage, of polystyrene nanoparticles in different human hematopoietic cell lines. Journal of Hazardous Materials, 398, 122900. https://doi.org/10.1016/j.jhazmat.2020.122900

Ruggieri F, Battistini B, Sorbo A, Senofonte M, Leso V, Iavicoli I, Bocca B. (2025). From food-to-human microplastics and nanoplastics exposure and health effects: A review on food, animal and human monitoring data. Food and Chemical Toxicology, 196, 115209. https://doi.org/10.1016/j.fct.2024.115209

Schmeisser S, Miccoli A, von Bergen M, Berggren E, Braeuning A, Busch W, Desaintes C, Gourmelon A, Grafström R, Harrill J, Hartung T, Herzler M, Kass GE, Kleinstreuer N, et al. (2023). New approach methodologies in human regulatory toxicology – Not if, but how and when! Environment International, 178, 108082. https://doi.org/10.1016/j.envint.2023.108082

Schröter L, Ventura N. (2022). Nanoplastic Toxicity: Insights and Challenges from Experimental Model Systems. Small, 18(31), e2201680. https://doi.org/10.1002/smll.202201680

Senathirajah K, Attwood S, Bhagwat G, Carbery M, Wilson S, Palanisami T. (2021). Estimation of the mass of microplastics ingested – A pivotal first step towards human health risk assessment. Journal of Hazardous Materials, 404, 124004. https://doi.org/10.1016/j.jhazmat.2020.124004

Sendra M, Pereiro P, Yeste M, Mercado L, Figueras A, Novoa B. (2021). Size matters: Zebrafish (Danio rerio) as a model to study toxicity of nanoplastics from cells to the whole organism. Environmental Pollution, 268, 115769. https://doi.org/10.1016/j.envpol.2020.115769

Shen,R, Yang K, Cheng X, Guo C, Xing X, Sun H, Liu D, Liu X, Wang D. (2022). Accumulation of polystyrene microplastics induces liver fibrosis by activating

cGAS/STING pathway. Environmental Pollution, 300, 118986. https://doi.org/10.1016/j.envpol.2022.118986

Singh N, Walker TR. (2024). Plastic recycling: A panacea or environmental pollution problem. Npj Materials Sustainability, 2(1), 17. https://doi.org/10.1038/s44296-024-00024-w

Stanley J, Culliton D, Jovani-Sancho A-J, Neves AC. (2025). The Journey of Plastics: Historical Development, Environmental Challenges, and the Emergence of Bioplastics for Single-Use Products. Eng, 6(1), 17. https://doi.org/10.3390/eng6010017

Sun N, Shi H, Li X, Gao C, Liu R. (2023). Combined toxicity of micro/nanoplastics loaded with environmental pollutants to organisms and cells: Role, effects, and mechanism. Environment International, 171, 107711. https://doi.org/10.1016/j.envint.2022.107711

Taguchi K, Yamamoto M. (2020). The KEAP1–NRF2 system as a molecular target of cancer treatment. Cancers, 13(1), 46. https://doi.org/10.3390/cancers13010046

Tavakolpournegari A, Villacorta A, Morataya-Reyes M, Arribas Arranz J, Banaei G, Pastor S, Velázquez A, Marcos R, Hernández A, Annangi B. (2024). Harmful effects of true-to-life nanoplastics derived from PET water bottles in human alveolar macrophages. Environmental Pollution, 348, 123823. https://doi.org/10.1016/j.envpol.2024.123823

Thapliyal C, Negi S, Nagarkoti S, Daverey A. (2025). Mechanistic insight into potential toxic effects of microplastics and nanoplastics on human health. Discover Applied Sciences, 7(6), 645. https://doi.org/10.1007/s42452-025-07214-8

Thompson RC, Courtene-Jones W, Boucher J, Pahl S, Raubenheimer K, Koelmans AA. (2024). Twenty years of microplastic pollution research—what have we learned? Science, 386(6720), eadl2746. https://doi.org/10.1126/science.adl2746

U.S. Congress. (2015). Microbead-Free Waters Act of 2015 (Public Law No. 114–114, 129 Stat. 3129). https://www.congress.gov/bill/114th-congress/house-bill/1321/text

Vales G, Rubio L, Marcos R. (2014). Long-term exposures to low doses of titanium dioxide nanoparticles induce cell transformation, but not genotoxic damage in BEAS-2B cells. Nanotoxicology, 9(5), 568-578. https://doi.org/10.3109/17435390.2014.957252

Vethaak A D, Legler J. (2021). Microplastics and human health. Science, 371(6530), 672-674. https://doi.org/10.1126/science.abe5041

Villacorta A, Rubio L, Alaraby M, López-Mesas M, Fuentes-Cebrian V, Moriones OH, Marcos R, Hernández A. (2022). A new source of representative secondary PET nanoplastics. Obtention, characterization, and hazard evaluation. Journal of Hazardous Materials, 439, 129593. https://doi.org/10.1016/j.jhazmat.2022.129593

Villacorta A, Vela L, Morataya-Reyes M, Llorens-Chiralt R, Rubio L, Alaraby M, Marcos R, Hernández A. (2023). Titanium-doped PET nanoplastics of environmental origin as a true-to-life model of nanoplastic. Science of The Total Environment, 880, 163151. https://doi.org/10.1016/j.scitotenv.2023.163151

Villacorta A, Cazorla-Ares C, Fuentes-Cebrian V, Valido IH, Vela L, Carrillo-Navarrete F, Morataya-Reyes M, Mejia-Carmona K, Pastor S, Velázquez A, Arribas Arranz J, Marcos R, López-Mesas M, Hernández, A. (2024). Fluorescent labeling of micro/nanoplastics for biological applications with a focus on “true-to-life" tracking. Journal of Hazardous Materials, 476, 135134. https://doi.org/10.1016/j.jhazmat.2024.135134

Wagner M, Monclús L, Arp HPH, Groh KJ, Løseth ME, Muncke J, Wang Z, Wolf R, Zimmermann L. (2024). State of the science on plastic chemicals - Identifying and addressing chemicals and polymers of concern. Zenodo. https://doi.org/10.5281/zenodo.10701706

Weber A, Schwiebs A, Solhaug H, Stenvik J, Nilsen AM, Wagner M, Relja B, Radeke HH. (2022). Nanoplastics affect the inflammatory cytokine release by primary human monocytes and dendritic cells. Environment International, 163, 107173. https://doi.org/10.1016/j.envint.2022.107173

Wu X, Zhang H, Chen J, Tan F, Cai R, Wang Y. (2025). Photoaging Promotes Toxic Micro/Nanoplastics Release from PLA/PBAT Biodegradable Plastic in Gastrointestinal Condition. Environment &Amp; Health, 3(5), 446-457. https://doi.org/10.1021/envhealth.4c00209

Yang Y-F, Chen C-Y, Lu T-H, Liao C-M. (2019). Toxicity-based toxicokinetic/toxicodynamic assessment for bioaccumulation of polystyrene microplastics in mice. Journal of Hazardous Materials, 366, 703-713. https://doi.org/10.1016/j.jhazmat.2018.12.048

Yang S, Cheng Y, Chen Z, Liu T, Yin L, Pu Y, Liang G. (2021). In vitro evaluation of nanoplastics using human lung epithelial cells, microarray analysis and co-culture model. Ecotoxicology and Environmental Safety, 226, 112837. https://doi.org/10.1016/j.ecoenv.2021.112837

Yang K, Zhou X, Wu K, Wu J, Huang C, Yang L. (2025). Multi-omics reveals the polyethylene terephthalate carcinogenicity: Cancer progression and immune microenvironment. Ecotoxicology and Environmental Safety, 302, 118522. https://doi.org/10.1016/j.ecoenv.2025.118522

Zhou Y, Zhao L, Xu H, Xu EG, Li M, Wang, Y. (2022). Long-Term Exposure to Polystyrene Nanoplastics Impairs the Liver Health of Medaka. Water, 14(17), 2767. https://doi.org/10.3390/w14172767

Zink D, Chuah JKC, Ying JY. (2020). Assessing Toxicity with Human Cell-Based In Vitro Methods. Trends in Molecular Medicine, 26(6), 570-582. https://doi.org/10.1016/j.molmed.2020.01.008